marine reSEArch@CNR.it

Technologies

National Research Council of Italy

Technologies

Polar Science at the Edge: ERICON Aurora Borealis, the European Icebreaker

A. Bergamasco[1], L. De Santis[2], R. Azzolini[3], F. Falcieri[1]
1, Institute of Marine Sciences, CNR, Venezia, Italy
2, Department of Biological Oceanography, National Institute of Oceanography and Experimental Geophysics, Trieste, Italy
3, Polar Research Coordination Unit, CNR Research Area of Roma "Tor Vergata", Roma, Italy
andrea.bergamasco@ismar.cnr.it

Abstract

The ERICON-AURORA BOREALIS Project represents a comprehensive assemblage of strategic and coordinating activities to prepare the basis for decision making by interested European and international authorities and Funding Agencies in relation to developing a world class Research Infrastructure to be operated in the Polar Regions (Arctic and Antarctic). The ERICON-AURORA BOREALIS project will generate the Strategic, Legal, Financial and Management Frameworks required for interested National Governments to commit financial resources to the construction and running of this proposed unique polar environmental facility. Scientific management frameworks will be assessed including mechanisms to handle dedicated large-scale multi-year or special mission specific research programs will be discussed in parallel with the operational portfolio and requirements. The paper will focus on moving the project from the preparatory phase to the construction phase, showing the ship characteristics and a first portfolio for the italian involvement based on a workshop discussion between several Italian Institutions and the Aurora Borealis team.

1 Introduction

Polar regions play an important role in the Earth System. In fact, polar ocean basins are characterised by large areas, permanently or seasonally covered by sea ice, very low temperatures, pronounced seasonal changes, bordering prominent continental ice sheets, and in the Southern Hemisphere also huge ice shelves. These areas control global climate on a broad range of time scales. Global ocean circulation, sea level change, atmospheric forcing and teleconnections are only some of the topics involved. Again complex interactions between biosphere and hydrosphere-atmosphere-cryosphere and sea ice determine the nature of these unique regions.
In every place of the Earth, long repeated time series observations are critical for understanding the functioning of the climate system, but in the polar regions this importance is critical because both Polar Regions will remain a challange to operate in, due to severe ice and weather conditions.
The polar oceans are potentially most vulnerable to present and future global environmental change, because small shifts

may cause irreversible consequences. Today, even the most sophisticated modelling forecasts, as seen in the IPCC Assessment Report, are limited by insufficient data in space and time coverage especially in high latitudes, and a complete understanding of the small scale processes interacting with global ones. There is a lack of information about natural physical and biological variability of the oceans, long term shifts in the cryosphere and ecosystems due to the extreme technical and logistical efforts involved to operate in these extreme environments.

Aurora Borealis with its unique year round operational capability will allow crucial new process-oriented studies in polar regions. Expeditions can be planned independently of the weather conditions, drifting pack ice even in completely ice covered waters. The advanced scientific drilling capability turns Aurora Borealis icebreaker into an extremely useful platform for scientific deep-sea drilling in regions inaccessible by other conventional drilling platforms.

2 The Consortium

European nations have express a substantial interest in studying polar environments, their potential, processes and changes. The European Research Icebreaker Consortium Aurora Borealis will offer an unique opportunity for European polar and marine scientist to attain a leading position for coming decades. The vessel will facilitate extended expeditions into remote regions. In addition the vessel will be the first platform technically able to operate continuously in these most sensitive parts of the polar regions.

The european research icebreaker Consortium ERICON [1] is managed by the European Science Foundation comprises fifteen partners from ten European nations and associated countries.

The overall aims are to establish strategic, legal, financial and organisational frameworks for this multi-country research facility. The vessel will be operated as a large scale research infrastructure by European Nations and other partner nations. Actually ERICON AB within the EU FP7 will develop the framework for joint ownership and operation of the vessel (www.eri-aurora-borealis.eu). A scientific management frameworks will be established to handle large scale, multi year, mission specific research programs and science & technology co-operations. Figure 1 give the interrelations of the workpackages that build the ERICON AB, EU FP7 project, a 48 months project with end in 2012.

3 Technical Details

The research icebreaker Aurora Borealis will be the most advanced polar research vessel in the world, will be a IACS polar class 1, year-round operations, for all polar waters and multi-year ice. In Figure 2 (side view) and Figure 3 (deck view) we have a first rendering from the technical design. It will be a multi-disciplinary vessel for all polar and marine research, with 120 berthing capacity (science and crew) and 90 days operational endurance. The new technological features will include dynamic positioning in closed sea-ice cover, deployment and operation of remotely operated vehicles (ROV) and autonomous underwater vehicles (AUV) from the twin moon pools. Figure 4 give the bottom view of the vessel, showing the two moon pools and the propellers. In Figure 5 we can see

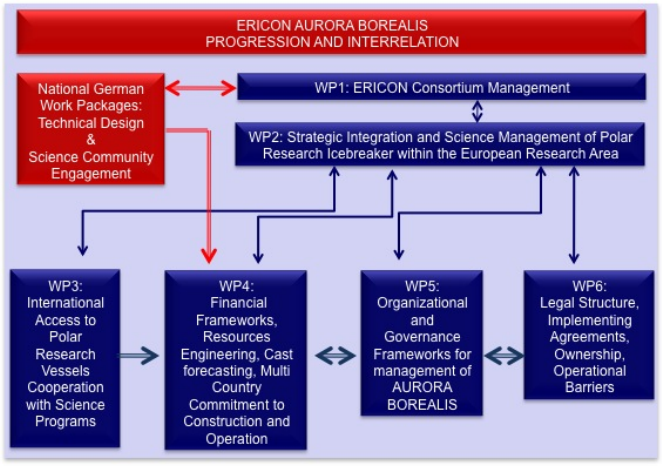

Figure 1: ERICON AB EU FP7 Project , workpackages scheme and interrelation.

a vessel section showing the glass dome roof, retractable with the natural light inside, the direct access to staging hangar and the watertight lower moon pool covers. The vessel will be a powerful icebreaker with approx. 65,000 tons displacement, about 200 m length, 50 m wide and with 90 Megawatt diesel-electric propulsion power. It will have high ice performance to penetrate autonomously, as single ship operation, into the Arctic and Antarctic Ocean with 2.5 m of ice cover, during all seasons of the year. A complete double-hull design, fully redundant engine rooms and safety equipment, full weather protection, combine high ice breaking capability with stable open water performance.
A working deck, see Figure 3, is available for geophysics: an easy use for deployment of 1-4 seismic arrays via built-in ramps for access close to waterline.The most unique feature of the vessel will be the deep drilling rig, which will enable sampling of the ocean floor and sub-sea from 50 m depth up to 5000 m, and 1000 m penetration. Aurora Borealis will be the only vessel worldwide that could undertake the drilling capability on the long run in both Polar regions. Figure 6 give the overview of vessel features.

4 Targets for Polar Research

All of the countries involved in the ERICON Aurora Borealis project have signed the Antarctic Treaty and are members, or observers, of the Arctic Council. Representatives of these countries are active

Figure 2: Aurora Borealis rendering, Side view.

Figure 3: Aurora Borealis rendering, Deck view.

into the SCAR and IASC programmes, that provide independent advice in a variety of fields, particularly on environmental and conservation matters. All countries involved into the ERICON were also members of EUROPOLAR ERA-NET Consortium, participate to many workshops made at national level with the aim to carry out a deep survey on the European polar assets and programmes. These scientific research comprise three major topics: a) climate variability studies: scales and indicators of polar climate change; b) state and stability of the cryosphere: biodiversity and ecosystems in polar environments; c) integrated real-time ice-ocean atmosphere-hydrosphere observations and modeling.
In particular a first italian nation-wide workshop identified a science cluster producing a first stage italian portfolio of possible activities that can be carried out on board of the future AB icebreaker. A cluster of seven main topics was individuated:

1. Geophysics & Geology (Paleoclimate, Bottom current deposits, Slope stability, Sedimentary processes, Fluids as Gas hydrates and mud volcanoes).
2. Polar Oceanography & Climate related processes, (air-sea-ice interactions, brine rejection, turbulent mixing,

Figure 4: Aurora Borealis rendering, Bottom view.

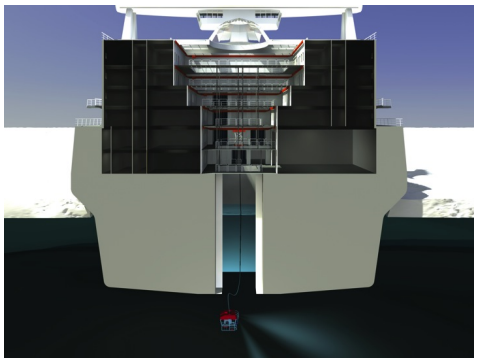

Figure 5: Moon pool section view.

Deep Ocean Ventilation, Benthic Layer Dynamics, Water formation and spreading processes, Abyssal Circulation & Ridge constraints, Ice Cavity dynamics).

3. Ecology, Biogeochemistry & Physics of sea ice (Sea-ice formation and structure, nutrient dynamics inside sea-ice, sea-ice ecosystems, biodiversity associated to the sea ice annual cycle, & related physical processes, role of platelet-ice).

4. Polar Biology & Ecology (Ecology and Biodiversity of deep polar regions, organic matter fluxes and input pathways, quantification and qualification of organic matter in sediment).

5. PaleoOceanography & PaleoEnvironment (carbon burial-sink in the Arctic zone, Retrieve records with the Eocene/Oligocene transition to check for bipolar glaciation, Bipolarity of Climate Change, Ice sheet evolution in Antarctica, Biostratigraphy).

6. Atmospheric physical & Chemistry cluster (Aerosols, Sea-ice-atmosphere interaction processes, Radiation and cloud coverage, Satellite validation ac-

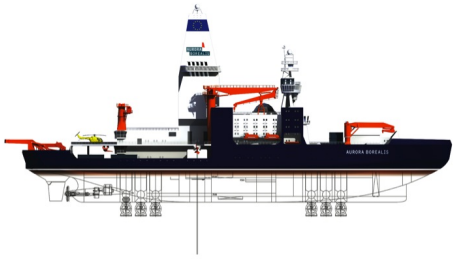

Figure 6: Aurora Borealis scheme.

tivities, Direct measurements of trace gases in remote areas (CO_2, CO, O_3, etc).

7. Polar Chemistry & Biogeochemistry of micronutrients (Trace elements and Organic micro-pollutants dynamics at the sea-ice system and sea-sediment interface, Processes contributing at transport and dispersion of micro-pollutants in polar regions, Effects of climate change on the transport of micro pollutants at global scale).

5 Acknoledgements

This work was realised through the EU FP7 grant.

References

[1] European Polar Research Icebreaker Consortium. European Polar Research Icebreaker Consortium Annex 1° ERICON AB 7th November 2008, Grant Agreement n. 211796. 2008.

Development of a Sediment Washing Technique for the Decontamination of Heavy Metals from Dredged Sediments in the Harbour Area of Taranto

N. Cardellicchio, C. Annicchiarico, M. Buonocore, A. Di Leo, S. Giandomenico, L. Spada
Institute for Coastal Marine Environment, CNR, Taranto, Italy
dileo@iamc.cnr.it

Abstract

Among the research activities of the Institute for Coastal Marine Environment - "UOS" Taranto, the study the anthropic impact on marine ecosystems and the development of innovative technologies for "environmental remediation" have taken particular significance in recent years.
Attention has been paid to the ecological risk analysis for contaminated sites and sustainable management of dredged sediment from coastal areas. The latter issue is of great relevance for the development of harbour areas, especially in Italy.
Concerning dredged and contaminated sediments, the easiest option is often the landfill disposal, even if the problem is considerably complicated in relation to the volumes to be managed and/or treated and the simultaneous presence of different types of pollutants. In order to reuse the dredged sediments both civil and industrial sector, in recent years the development of treatment technologies textitex situ has assumed considerable importance. Among these, the "sediment washing" appears very interesting for the removal of toxic heavy metals from dredged sediments.
For this purpose research has been started aiming to developing a new method of washing with chelating solutions on samples of sediments in the harbour area of Taranto, it's a site remediation of national interest.
Different chelating agents (ethylenediaminetetraacetic acid (EDTA), Ethylenediamine-N,N'-disuccinic acid (EDDS), citric acid) were used at different extraction times. The optimum removal time was found to be 48 h, both with EDTA 0.2 M and EDDS 0.2M. Citric acid was not very efficient for the contamination process. The results suggest that bioavailability and speciation of metals in sediments were the main factors affecting sediment washing. In particular, metal speciation, using sequential extraction technique, were determined before and after washing: this approach was useful to evaluate heavy metals mobility in treated and untreated sediments. The methodology developed could have important implications on industry, also in view of reusing treated material for different purposes (filling, cement production, etc.).

1 Introduction

Heavy metal contamination of sediments is hazardous to benthic organisms and needs more attention in order to prevent accumulation of these metals into the food chain. The interaction of contaminants with sediments is a very complex phenomenon and means are required to understand this matter more fully. In sediments, most of metal compounds are persistent and toxic: so, sediment removal by dredging or excavation is the most frequent cleanup method in marine environment. After dredging, sediment washing is a relatively low cost treatment option when compared to other technologies commonly considered for the remediation. Different chelating solutions have shown the capability to remove heavy metals from sediments. The advantages of using chelating agents in washing process is the high efficiency of metal extraction, high thermodynamic stability of metal complexes and normally low adsorption of the chelating agents and their metals complexes on sediment [1, 2]. The parameters that influence the washing include the type and chelant concentration, pH, Liquid-to-Solid ratio (L/S) and extraction time. For sediment remediation, the very important parameters are pH, particle size distribution, type of metals to be extracted and their concentration, distribution and physicochemical forms in the sediment. The kinetics of metal extraction is also a crucial parameter as it can affect the treatment time and cost. The objective of this research has been to evaluate the performance of particular chelating solutions for removal of heavy metals from sediments taken in a contaminated marine area as Mar Piccolo in Taranto. Experiment for heavy metals removal are showed and discussed. Batch tests of washing with an aqueous solution of three chelating agent were performed at selected liquid/solid (L/S) ratios and different chelant concentrations. The objective of the researches was to investigate metal mobilization and sediment decontamination by washing treatment. In order to determine metal mobilization, speciation techniques of metals using sequential extraction technique have been used. Finally, for each metal removal efficiencies have been evaluated. In addition sediments toxicity tests were used for evaluating the ecotoxicological hazards of contaminated sediments.

2 Materials and methods

The sediment was sampled in the first inlet of the Mar Piccolo in Taranto (Figure 1). Sediment was collected with a Van Veen grab sampler in a station mainly contaminated by heavy metals. The Mar Piccolo is located in the Northern area of the Taranto gulf; it is a semi-enclosed basin (surface area of 20.72 km^2) with lagoon features. The scarce hydrodynamism and the low water exchange with the nearby Mar Grande, determine, mainly in the summer, a high water stratification. The basin is influenced by urbanization, harbour and aquaculture activities. The main problems of environmental impact are nine pipes discharge sewages, the ship-yard of the Italian Navy, the largest mussel farm and small rivers and freshwater springs, which drain in the basin the surrounding agricultural soils.

After collection, sediments were dried, homogenized and stored in a polyethylene container. In sediments the grain size distribution, water content, pH, total organic carbon (TOC), metals and chemical speciations of metals were determined.

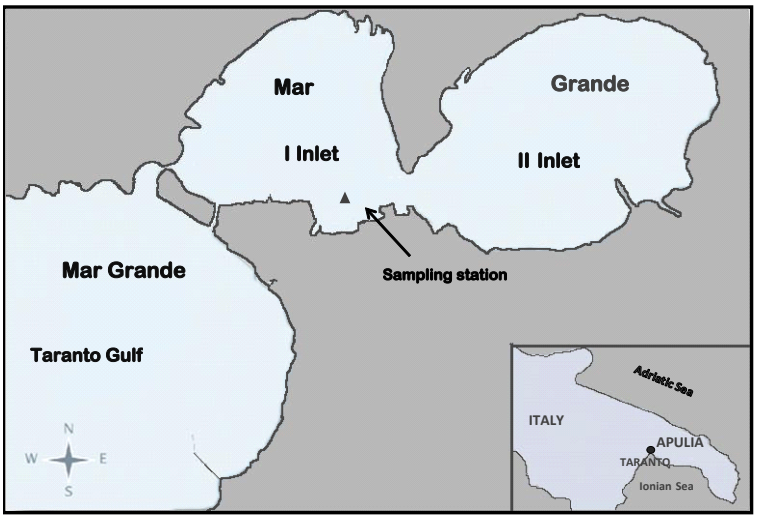

Figure 1: Sampling area in the Mar Piccolo of Taranto.

All the analyses were performed in triplicate. Grain size distribution, water content, and TOC were measured according to the methods prescribed by the APAT & ICRAM [3].

Metal content was determined by atomic absorption spectrophotometry, after sample digestion in a microwave oven at 170°C and 130 psi with 9 ml HNO_3 (J.T.BAKER 69%-70%) and 3 ml HF (J.T.BAKER 60%). Metal concentrations (mg/kg dry weight) before sediment washing are show in Table 1. In this table there are shown also the limit values for sediment remediation referred by ISPRA (Institute for Environmental Protection and Research) in accord to directive 2000/60/EC. and Legislative Decree 152/2006.

Metal speciation in sediments was estimated through extraction procedure according to Tessier et al. [4]. Washing experiments were carried out in a single extraction experiment with EDTA in the sodium salt form, with citric acid (Cit) and with S,S-isomer of the ethylenediaminedisuccinic acid ([S,S]-EDDS) in the form of Na3-N,N′ salt. Dried sediment was treated with each chelant compound, shaking from 0.5 to 48 h; this time has been selected on the basis of previous kinetic experiments [5, 6]. Molar concentration of the chelating agents was 0.2 M, corresponding to a chelant dosage of 10 mol per mol of total trace metals. Since citrate, EDTA, and EDDS usually form 1:1 complexes with most heavy metals, including Zn, Cu and Pb [7], the theoretical minimum amount of chelating agent needed to extract the three metals is equal to the sum of their molar concentrations. In practice, the chelating agent is often applied in several-fold excess to maximize metal extraction [8]. All extractions were carried out at room temperature and pH 5. At the end of the extraction period, the slush was centrifuged at 3000 rpm and supernatant was filtered through 0.45-µm filters and then acidified with HNO_3. The residue from

Concentration		Parameter	Limit Values
mg/Kg d.w.		Metal	mg/Kg d.w.
2.76	PP	Cd	1.0
25.25	PP	Hg	0.8
65.03	P	Ni	40* 100**
219.8	P	Pb	50
172.53		Cu	45

The metals countersigned by Pand PP are respectively the prioritypollutants and priority dangerous pollutants (Decision n° 2455/2001/CE European Parliament, November 20th, 2001)
* for sediment with pelitic fraction < 20%
** for sediment with pelitic fraction > 20%

Table 1: Metal concentrations and limit values for remediation in sediments from the Mar Piccolo of Taranto (contaminated site of national interest).

centrifugation at the end of the extraction experiments was washed two times with 20 ml of distilled water and the wash solutions were discarded. The residual sediment was dried at 60 °C and thereafter subjected to the sequential extraction procedure to evaluate metal speciation. Ecotoxicological evaluations were performed with textitGammarus aequicauda and textitCorophium insidiosum. The general design of toxicity tests was based on the standard guides for acute sediment toxicity tests with marine-estuarine amphipods and isopods, with some modification [9, 10].

3 Results and discussion

The physico-chemical characteristics of the sediment analyzed and used for testing of decontamination process were: % water = 60.7%, pH = 7.85, TOC= 8.5% dry weight. For grain size distribution according to the AASHO classification system, the sediment was found to be composed of 3.98% gravel, 4.77% sand, 91.25% silt and clay, thus belonging to the pelitic fraction.
Ecotoxicological results showed that mortality of the organisms used was very high compared with the control sediment (68.3% for textitG. aequicauda, 34.6% and 40% for textitC. insidiosum) ($p < 0.05$) However, it should be emphasized that the mortality of organisms used in biological tests could be caused by other types of pollutants, not just metals.
Analysis of sediment washing kinetics produced useful information on the relationship between metal extraction yield and contact time. Figure 2 shows the efficiency of washing treatment in terms of percentage of extracted metals as a function of contact time (2, 24 and 48 h). Wide variations in metal removal efficiency were observed depending on both the metal under concern and the chelating agent used.
Among the investigated metals, Ni and V were the most difficult to extract from the sediment matrix after 2 h of washing treatment, as confirmed by kinetics curves (Figures 3,4). According to the Figure 2a the remediation efficiency was 32.9% for Hg

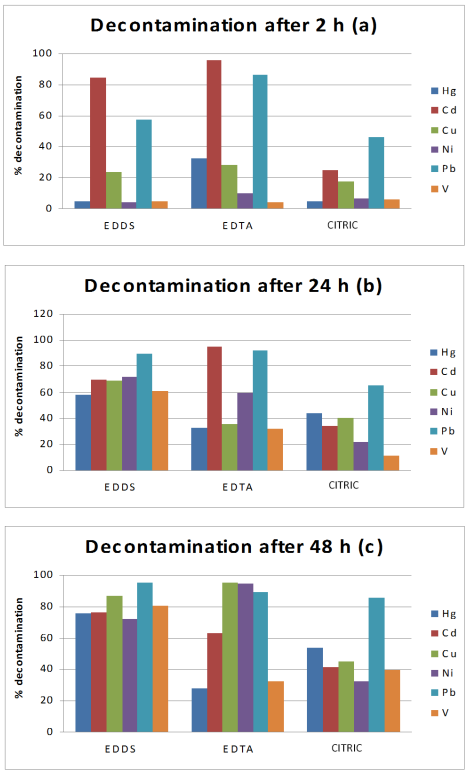

Figure 2: Percentage of metals solubilised by chemical extraction after a) 2 hours, b) 24 hours and c) 48 hours.

(EDTA), 10.2% for Ni (EDTA) and 6.1% for V (Cit). After 24 h of washing (Figure 2b) this percentage increases: 58.4% for Hg (EDDS), 71.8% for Ni (EDDS) and 61.4% for V (EDDS). After 48 h washing, Pb was removed with maximum efficiencies (up the about 95.0 % with EDDS and 89.3% with EDTA). Concerning Cu it was removed until 87.1% with EDDS and until 95.5% with EDTA. After 48 h washing, the removal efficiency increased for all metals. For Pb, the good complexation efficiency with EDDS and EDTA was demonstrated in various studies [11]. In this work, Cu displayed by far a slowest extraction kinetics. It has been proposed [12] that the slower extraction rate may be due to the fact that Cu is usually associated to organic matter or other oxidizable species in soil and sediment. Therefore, the slower extraction kinetics of the copper may be explained by the formation of a low percentage of Cu complexes during washing treatment. Figures 5 and 6 show the different extraction kinetic diagrams for Cu and Pb respectively while Figures 7 and 8 show the speciation analysis of Cu and Pb in the untreated sediment (U.S.) and after extraction with different chelating solutions. In the untreated sediment, Pb and Cu are associ-

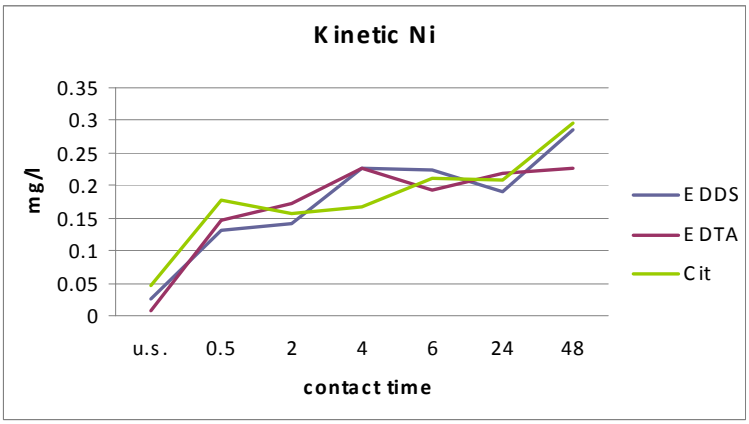

Figure 3: Nickel concentration with time from 0.5 to 48 h in chelating solution (U.S.= untreated sample).

ated to the Fe and Mn oxides fraction (59-55 %).

Concerning Cd, removal was similar for two chelating agents, EDTA, EDDS with 60-75 % removal efficiency after 48 h; low decontamination was obtained after 48 h using citric acid. For Cd a reduction in removal percentage was observed after a time greater than 48 h: in fact, after 24 h of treatment with EDTA, the removal efficiency was 95 %, but after 48 h of treatment the removal efficiency was 63 % (Figures 2b and 2c). The reduction in extraction efficiency after a long contact time with the chelating agents, appeared important and may be attributed either to sorption mechanisms of the newly formed metal-chelant complexes onto the active sites of sediment particles, or metal exchange reactions between metal-chelant complexes. Metal speciation analysis allowed to make some important considerations: the result displays that the chelating agents were capable of extracting, in addition to the easily mobile fraction (exchangeable and carbonate bound), part of other less mobile forms (i.e., Fe oxides and sulphides). In some cases, an increase in the amount of Cu and Pb associated to fraction A (exchangeable) was observed (Figures 7 and 8), most probably as an effect of the presence of residual metal complexes [13]. The amount of Cu and Pb associated to fraction D (bound to organic matter) was in many cases found to increase as a result of treatment. The reasons may be that, in addition to the inability of chelating solutions to solubilize such fractions, re-adsorption of chelant metal complexes or metal ions onto organic matter fraction of the material, may have played a role in the bioavailability and remediation.

As regards the methods of decontamination with chelating agents, metal concentrations in sediments were in some cases below the limits of DM 367/2003, making the treated sediment theoretically be used as beach nourishment. However, the extraction capacity towards various metals depends on the form in which the metal is present and its relationship with the minerals that make up the sediment, ie, the geochemistry of the sediment itself. As a good

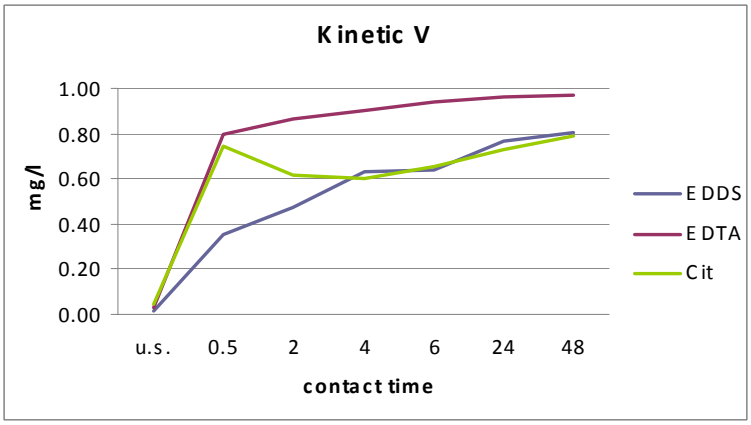

Figure 4: Vanadium concentration with time from 0.5 to 48 h in chelating solution (U.S.= untreated sample).

extraction efficiency was obtained for concentrations of 0.2 M chelating, corresponding to a chelating dosage of 10 mol per mol of total trace metals, it follows that the amount by weight of extractant are considerable, thus presenting problems of cost.

4 Conclusions

The batch washing treatment of 48 h, EDTA and EDDS were effective chelating solutions for removing heavy metals from sediment analysed. The concentration of chelants (0.2 M) and the experimental conditions (pH 5) were found to be useful for achieving high extraction yields. The time of treatment with washing solution of 48 hours gives the best results in the metal extraction. Ni, Cu and V are extracted with high efficiency by EDDS and EDTA. The best extractant for Hg and Cd was found to be the EDDS. For Pb, all three chelants show a high capacity for decontamination. Citric acid did not provide satisfactory results so it is not recommended for remediation of sediments. The possibility of application of the method of sediment washing with chelating agents, such as remediation process of sediment being dredged, is highly dependent on specific properties of the matrices in terms of particle size characteristics, mineralogical composition, nature, and distribution of contamination levels between different fractions. The influence of macro-elements (Ca, Mg, Fe) affect also the efficiency of extraction. In conclusion, the method appear good to remediation of ex situ contaminated sediment in harbour areas. The studies are in progress for optimize a mixture of chelating agents in order to improve the efficiency of extraction.

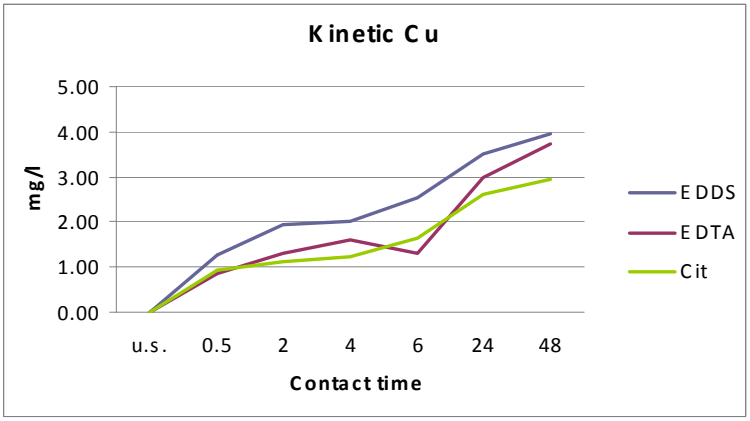

Figure 5: Copper concentration with time from 0.5 to 48 h in chelating solution (U.S.= untreated sample).

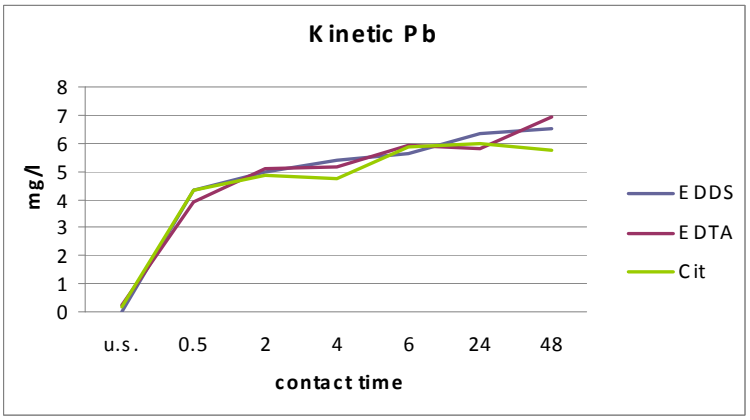

Figure 6: Lead concentration with time from 0.5 to 48 h in chelating solution (U.S.= untreated sample).

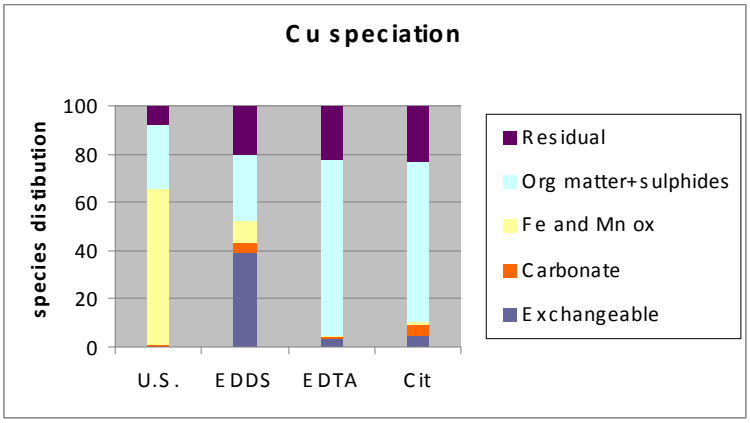

Figure 7: Copper speciation before and after washing (U.S.= untreated sample).

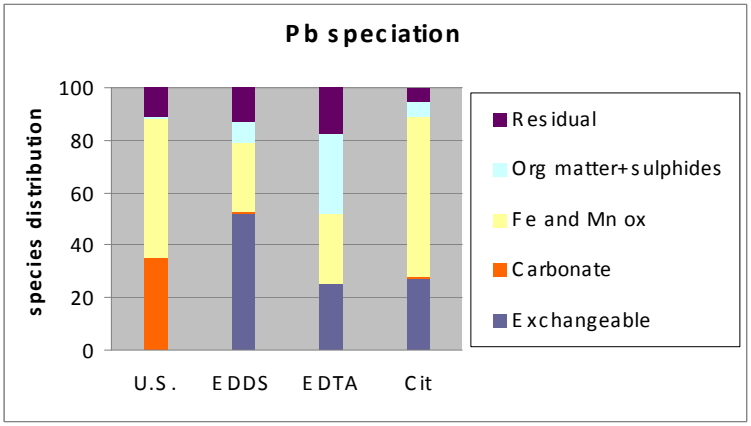

Figure 8: Lead speciation before and after washing (U.S. = untreated sample).

References

[1] R.J. Abumaizar and E.H. Smith. Heavy metal contaminants removal by soil washing. *J. Haz. Mater.*, 66:151–21, 1999.

[2] G.W. Gee and Y.W. Bauder. Particle-Size Analysis In: Methods of soil Analysis. pages 383–411., 1986.

[3] APAT & ICRAM. Manuale per la movimentazione dei sedimenti marini, Ministero della Ambiente e della Tutela del Territorio e del Mare. 2007.

[4] A. Tessier, P.G.L. Cambell, and M. Bisson. Sequential Procedure for the Speciation of Particulate Trace Metals. *Anal. Chem.*, 51:844–850, 1979.

[5] D. Cermigna, A. Polettini, R. Pomi, E. Rolle, L. De Propris, M. Gabellini, and A. Tornato. Comparing sediment washing yelds using traditional and innovative biodegradable chelating agents. pages 24–27, 2005.

[6] A. Polettini, R. Pomi, E. Rolle, D. Cermigna, L. De Propris, M. Gabellini, and A. Tornato. A Kinetic study of chelant-assisted remediation of contaminated dredged sediment. *J. Hazard Mater*, 137:1458–1465, 2006.

[7] A.J. Francis, C. J. Dodge, and J. B. Gillow. Biodegradation of metal citrate complexes and implications for toxic-metal mobility. *Nature*, 356:140–142, 1992.

[8] J.H. Linn and H.A. Elliott. Mobilisation of Cu and Zn in contaminated soil by NTA. *Water, Air, Soil Pollut.*, 37:449–458, 1988.

[9] ASTM. Standard guide for conducting 10-d static sediment toxicity tests with marine and estuarine amphipods. 1993.

[10] SETAC Europe. Guidance document on sediment toxicity assessment for freshwater and marine environments. 1993.

[11] C.N. Neale, R.M., Bricka, and A.C. Chao. Evaluating acids and chelating agents for removing heavy metals from contaminated soils. *Environ. Prog*, 16:274–280, 1997.

[12] P. Vandevivere, F. Hammes, W. Verstraete, T. Feijtel, and D. Schowanek. Metal decontamination of soil, sediment, and sewage sludge by means of transition metal chelant [S,S]-EDDS. *J. Environ. Eng*, 127:802–811, 2001.

[13] B. Sun, F. Zhao, E. Lombi, and S.P. McGrath. Leaching of heavy metals from contaminated soil using EDTA. *Environ. Pollut*, 113:111–120, 2001.

Use of Hydroacoustic Methods for the Identification of Potential Seabed Habitats for Small Pelagic Fish Schools in the Strait of Sicily

B. Patti, M. D'Elia[1], A. Sulli[2], G. Tranchida[1], A. Bonanno[1], G. Basilone[1], G. Giacalone[1], I. Fontana[1], S. Aronica[1], G. Buscaino[1], L. Caruana[1]
1, Institute for Coastal Marine Environment, CNR, Capo Granitola (TP), Italy
2, Department of Geology and Geodesy, University of Palermo, Palermo, Italy
bernardo.patti@cnr.it

Abstract

Contemporary data on both fish distribution and seabed characteristics can be used in ecological studies to investigate the distribution and the behaviour of both demersal and pelagic fish schools in relation to the nature of the sea bottom. In this study we describe a method to classify the sea bottom by a single-beam echosounder used during an echosurvey carried out on the north-western part of Southern Sicilian continental shelf. The study area was divided in two contiguous regions (labelled ZONE 1 and ZONE 2), characterized by different dominant texture, 'sand' for ZONE 1 and 'clayey-silt' for ZONE 2. The acoustic classification evidenced differences in terms of bottom types between the two investigated zones. Though the average bottom depth of the investigated transects is higher in ZONE 1, this area is dominated by substrates having greater backscatter, identifying relatively "harder" bottom types. On the contrary, in ZONE 2 "hard" substrate is confined to the shallower inter-transects regions, with the bulk of seabed deeper than 50 m classified as "soft" bottom. The acoustic classification of the seabed was already used in the context of a recent study, indicating a preference of small pelagic fish schools for soft bottom in ZONE 2, where their occurrence was higher and the bulk of total biomass was concentrated.

1 Introduction

A variety of remote hydroacoustic technologies, which employs a single or a multi-echo, are used to analyze and map seabed characters in term of texture and grain size [1, 2]. The most widespread commercial acoustic bottom classification systems are RoxAnn and QTC-View. They use normal incident echosounders and are based on the measurement, analysis and interpretation of the shape and energy features contained in the bottom acoustic signal [3, 4]. The knowledge of the bottom material and topography is very important in different scientific fields such as geology, offshore industry and fishery, mainly when the activity is focused on demersal fish. Over the last few decades there was a rapid increase in the use of hydroacoustic technologies also for schooling pelagic fish and for the biomass evaluation of pelagic fish populations [5, 6]. Echosounders commonly used to this aim work at fixed fre-

quencies and are able to acquire information from both the fish distribution along the water column and the bottom seabed. Despite this, information from the sea bottom is usually discarded because the acoustic signal is used exclusively to obtain data about pelagic fish biomass and the structure of the fish schools, to the aims of the sustainable management of fisheries resources. However, the consensus that single species stock assessment alone is not sufficient to manage fisheries sustainably has been constantly increasing over the last two decades. Specifically, it has been argued the importance of the so-called ecosystem approach for the effective and sustainable management of fish populations [7, 8, 9, 10, 11]. For instance, the quality of scientific advice on exploited fish populations can be significantly improved by the knowledge of the effects of environmental conditions on the recruitment or fish populations. In this context, the contemporary collection of information on fish distribution and seabed characteristics could be greatly useful in multidisciplinary studies. To this aim, the use of a single beam echosounder was firstly investigated by D'Elia et al. [12], who also demonstrated the preference of small pelagic fish schools for softer (and finer) subtrates. In this study we describe the rationale of method therein used to classify the sea bottom by a single-beam echosounder (SIMRAD EK 500), based on the comparison between hydroacoustic bottom data and granulometric analysis of sediment samples.

2 Materials and methods

2.1 Study area and acoustic survey

Bottom acoustic information were obtained from hydro-acoustic survey conducted over the continental shelf of the Sicily Strait aboard the N/O Salvatore Lo Bianco in June 1998. The surveyed area was divided in two sectors, labeled 'ZONE 1' (north-western sector, over the Adventure Bank) and 'ZONE 2' (south-eastern sector, continental shelf off the central part of the Southern Sicilian coast) (Figure 1). These two sectors are characterized by different dominant seabed conditions, harder (and coarser) in ZONE 1, softer (and finer) in ZONE 2.

2.2 Backscattering signal by the seabed and bottom samples collection

The split-beam echosounder SIMRAD EK 500, originally designed for biological resources, was used to measure the backscattering signal from the seabed, using a transducer operating at the frequency of 38 kHz. The choice of this frequency is linked to its more frequent availability due to its common use in acoustic surveys aimed at biomass evaluations of small pelagic fish species. Raw data from the bottom (Sv) were analyzed using the post –processing software Echoview v.3 by Sonar Data and Matlab scripts. A GPS system, interfaced to the echosounder, was used to record the position of the bottom signal. The method of extracting bottom type information is based on the following considerations. First, there is a direct relationship between the mean diameter of the seabed material and bottom surface (and volume)

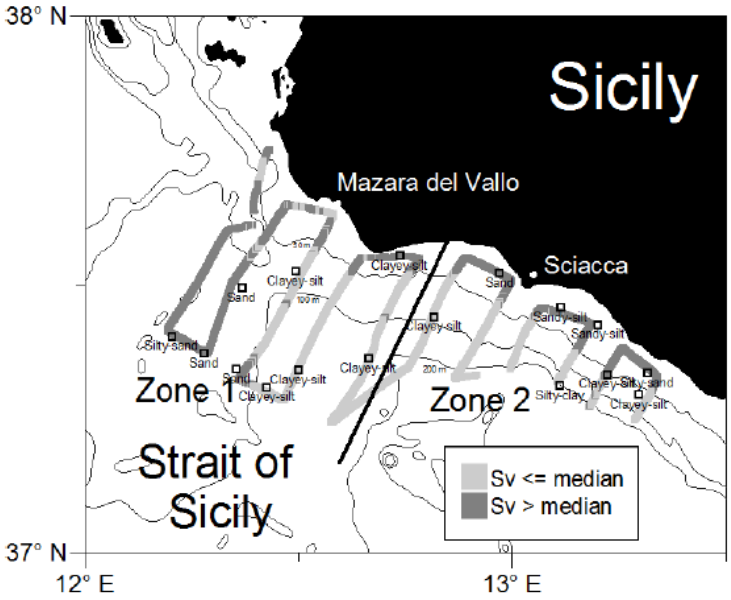

Figure 1: Study area, with Zone 1 (western sector) and Zone 2 (eastern sector) evidenced. Along the transects the acoustic classification of seabed based on bottom Sv is shown. "Hard" seabeds (Sv $>$ median value) is displayed in dark grey, "soft" seabeds (Sv $\leq$ median value) in light grey. The sediment sample sites are also shown with white. Shepard's and Folk's sediment classification labels are also given under the symbols.

backscattering value for normal incident echosounder [13]. It means that to a larger grain size corresponds a greater backscattering surface or volume coefficient. The reason for this is related to the bulk density of the sediment, which mainly depends on porosity. Clayey-silt and Silty-clay sediments have a higher porosity values than sand [14], so they bind more water and have lower density than sandy sediments. The bulk density is in relation to the acoustic impedance of a sediment: the higher sediment density, the higher acoustic impedance and the greater backscattering coefficient [15, 16]. The intensity of the energy scattered back to the instrument is also a function of the bottom roughness, due to the grain size of the particles. Gravel is rougher than sand which in turn is rougher than silt and clay [17]. Starting from this consideration, for each acoustic transect of Figure 1 the Sv volume backscattering values of the seabed line were extracted by means of Echoview software, using the maximum Sv algorithm. Then, a moving average to 50 terms (= acoustic pings), corresponding to about 200–250 m, was calculated to reduce variability in the Sv bottom values. The median value of these averaged Sv bottom data was used to classify the bottom type (0 for Sv bottom values $\leq$ median value, identifying 'soft' seabed areas, and 1 for Sv bottom value $>$ median value,

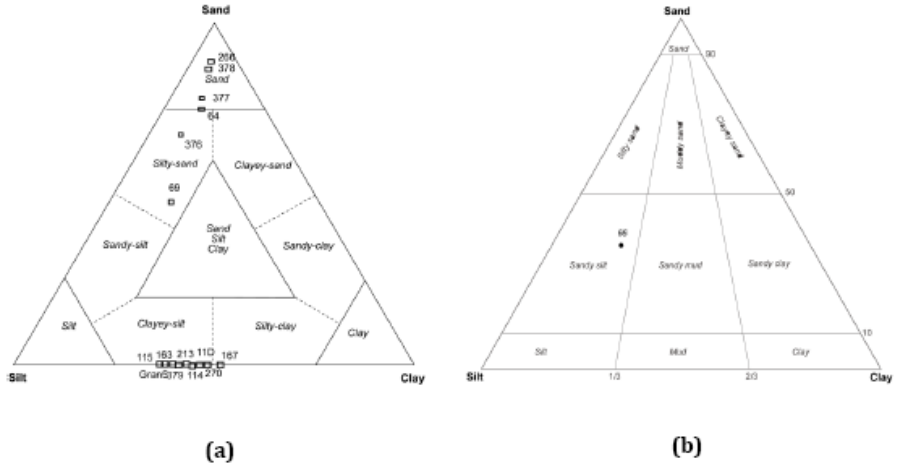

Figure 2: Shepard's (a) and Folk's (b) diagram, showing the classification into grain size for the analyzed samples.

identifying 'hard' seabed areas). In order to verify the results, physical sampling of the bottom was accomplished with grab and box-corer, in proximity of the acoustic prospected transects and a grain size analysis was conducted on the collected samples. The analysis of the particle size of sediment samples required a phase of sample pre-treatment, which included digestion with hydrogen peroxide, washing, separation of particles with a diameter lower than 500 μm and drying and subsequent analysis by a laser diffraction instrument (Fritsch model Analysette 22). The coarse sand-gravel fraction ($>$ 500 μm) was dried and divided in 2 fractions using a sieve with a 2 mm mesh size. Finally, the sieved particles were weighted by a simple balance. A final normalization process of the fraction, analyzed by the laser instrument, was necessary in order to obtain the correct compositional data. The analysis of particle size distribution were conducted using the Wentworth scale, and the classification into grain size class was based on the Shepard's method [18] for samples containing silt, clay and sand. The Folk's method [19] was used for the classification into grain size of sediment samples containing a fraction coarser than sand (diameter$>$2mm, little pebble or bioclastic granules).

3 Results and discussion

The results of the acoustic-based bottom type classification are displayed in Figure 1, together with information obtained from the analysis of sediment samples collected over all the investigated area. The acoustic classification shows the differences in terms of bottom types between the two zones along the investigated transects. ZONE 1 seabeds, at depth less than 100 m (the western sector, over the Adventure Bank) are dominated by substrates with greater scattering strength, indicating rela-

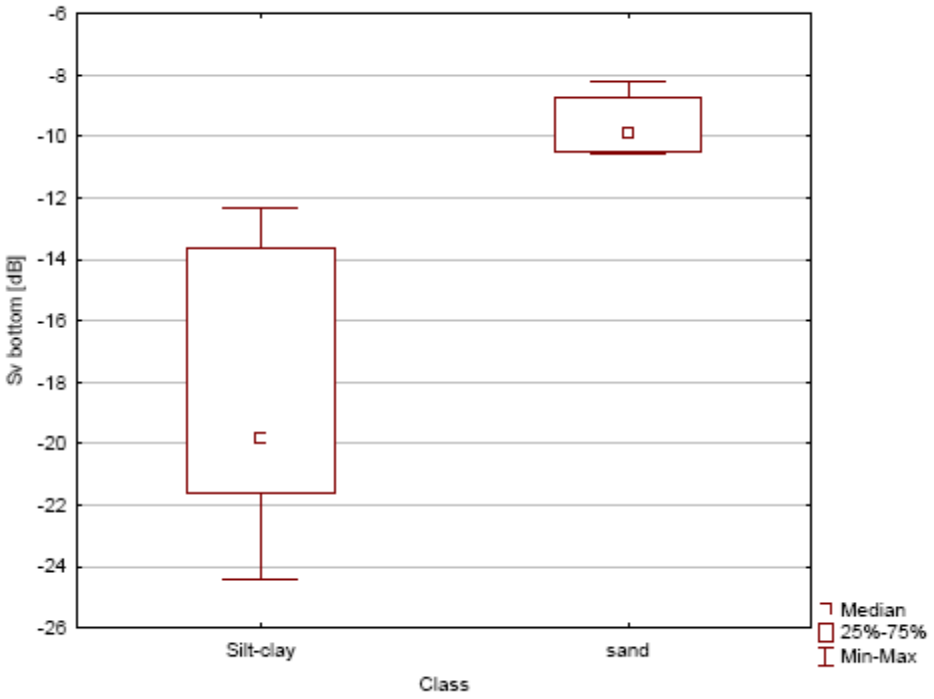

Figure 3: Box plots of bottom Sv for the sediment facies named “Silt-clay” (including sediment samples classified as clayey-silt) and “Sand” (including sediment samples classified as sandy-silt, silty-sand and sand).

tively ‘harder’ (and coarser) bottom types. In contrast, in ZONE 2 the ‘hard’ substrate is confined to the shallower inter-transect regions, with the bulk of the seabed deeper than 50 m classified as ‘soft’ bottom. The granulometric analysis of sediment samples is consistent with the results of the acoustic classification of the seabed (Figure 2 and Table 1). Although the sediment sample sites were available only in proximity of the acoustically prospected transects, it is worth noting that the use of the median value (-17.65 dB re m-1) of bottom backscattering volume strength permitted us to approximately separate finer (and softer) substrate locations (classified as clayey-silt and silty-clay), corresponding at bottom Sv values lower than the global median value, from coarser (and harder) sediment sites (facies: silty-sand, sandy-silt, and sand) matching with higher bottom Sv values (Mann–Whitney U-test, $p = 0.0055$; Figure 3). This paper highlights some important aspect in the application of echosounder data for seabed characterization. If the fisheries oriented instrument such as SIMRAD EK 500 echosounder is contemporarily used both for fisheries data and for bottom classification, its use in ecological studies could be very efficient and cost saving.

Table 1. Compositional data from the granulometric analysis of the collected samples.

Station	Latitude Nord (decimal)	Longitude East (decimal)	Depth (m)	% Clay	% Silt	% Sand	% Gravel	Grain size classification
114	37.33	13.22	57	46.1	53.9	0	0	Clayey-silt
163	37.44	12.82	96	38.8	61.2	0	0	Clayey-silt
270	37.36	12.66	186	49.4	50.6	0	0	Clayey-silt
11D	37.34	12.50	150	45.9	54.1	0	0	Clayey-silt
Gran5	37.55	12.74	29	34.5	52.2	13.5	0.0	Clayey-silt
379	37.31	12.43	136	42.1	57.9	0	0	Clayey-silt
213	37.53	12.49	96	40.8	58.7	0	0	Clayey-silt
63	37.55	12.90	28	42.7	57.3	0	0	Clayey-silt
66	37.46	13.11	28	18.0	47.0	17.2	17.4	Sandy-silt
376	37.40	12.20	68	9.2	19.8	71.0	0	Silty-sand
69	37.34	13.32	24	16.5	36.0	47.5	0	Silty-sand
377	37.37	12.28	73	7.0	17.0	76.0	0	Sand
64	37.52	12.97	30	8.0	17.0	75.0	0	Sand

Table 1: Compositional data from the granulometric analysis of the collected samples.

References

[1] R. Freitas, S. Silva, V. Quintino, A.M. Rodrigues, et al. Acoustic seabed classification of marine habitats: studies in the western coastal-shelf area of Portugal. *ICES Journal of Marine Science*, 60:599–608, 2003.

[2] J.T. Anderson, D.V. Holliday, R. Kloser, D.G. Reid, and Y. Simard. Acoustic seabed classification: current practice and future directions. *ICES Journal of Marine Science*, pages 1004–1011, 2008.

[3] B.T. Prager, D.A. Caughey, and R.H. Poeckert. Bottom classification: operational results from QTC view. *OCEANS '95 - Challenges of our changing global environment conference, San Diego, California*, 1995.

[4] S.P.R. Greenstreet, I.D. Tuck, G.N. Grewar, and E. Armstrong. An assessment of the acoustic survey technique, RoxAnn, as a means of mapping seabed habitat. *ICES J. Mar. Sci.*, (54):939–959, 1997.

[5] R. Muiño, P. Carrera, and M. Iglesias. The characterization of sardine (Sardina pilchardus Walbaum) schools off the Spanish-Atlantic coast. *ICES Journal of Marine Science*, (60):1361–1372, 2003.

[6] B. Patti, A. Bonanno, G. Basilone, Goncharov S., S. Mazzola, et al. Interannual fluctuations in acoustic biomass estimates and in landings of small pelagic fish populations in relation to hydrology in the Strait of Sicily. *Chem. Ecol.*, (20):365–375, 2004.

[7] P.A Larkin. Concepts and issues in marine ecosystem management. *Reviews in Fish Biology and Fisheries*, (6):139–164, 1996.

[8] S. Jennings, M.J. Kaiser, and J.D. Reynolds. Marine Fisheries Ecology. *Blackwell Science*, 2001.

[9] S.M. Garcia, A. Zerbi, C. Aliaume, T. Do Chi, and G. Lasserre. The ecosystem approach to fisheries. Issues, terminology, principles, institutional foundations, implementation and outlook. *FAO Fisheries Technical Paper*, (443), 2003.

[10] E. Pikitch, C. Santora, E.A. Babcock, A. Bakun, et al. Ecosystem-based fishery management. *Science*, (305):346–347, 2004.

[11] G.H. Kruse, Y. Ishida, and C.I. Zhang. Rebuilding of depleted fish stocks through an ecosystem approach to fisheries. *Fisheries Research*, (100):1–5, 2009.

[12] M. D'Elia, Patti B., A. Sulli, G. Tranchida, A. Bonanno, et al. Distribution and spatial structure of pelagic fish schools in relation to the nature of the seabed in the Sicily Channel (Central Mediterranean). *Marine Ecology*, (30):151–160, 2009.

[13] M. Manik, H.M.and Furusawa and Amakasu K. Measurement of the sea bottom surface backscattering strength by quantitative echo sounder. *Fisheries Science*, (72):503–512, 2006.

[14] A.W. Nolle, W.A. Hoyer, J.F. Mifsud, W.R. Runyan, and M.B. Ward. Acoustical properties of water filled sands. *Journal of the Acoustical Society of America*, (35):1394–1408, 1963.

[15] E.L. Hamilton and T.B. Richard. Sound velocity and related properties of marine sediments. *Journal of the Acoustical Society of America*, (72):1891–1904, 1982.

[16] M.D. Richardson. In-situ, shallow water sediment geoacoustic properties. *Proceedings International Conference on Shallow-Water Acoustics, Beijing, China, 21–25 April. China Ocean Press*, page 163–170, 1997.

[17] C. Mazel. Side Scan Sonar Record Interpretation. Training Manual. *Klein Assoc.*, pages 14–16, 1985.

[18] F.P. Shepard. Nomenclature based on sand-silt-clay ratios. *Journal of Sedimentary Petrology*, (24):151–158, 1954.

[19] R.L. Folk. The distinction between grain size and mineral composition in sedimentary rocks nomenclature. *Jour. Geol.*, 62:344–359, 1954.

Benthic Chamber for Metabolic Measurements of Underwater Flora: a New Realization

G. Fasano, A. Materassi, F. Benincasa
Institute for Biometeorology, CNR, Sassari, Italy
g.fasano@ibimet.cnr.it

Abstract

Benthic chambers are widely used in studies concerning both marine sediments and flow of solutes through them up to high depth. Benthic chambers were used also for studies on metabolism of coral reefs and vegetable biomasses; these studies can be carried out for use up to a few meters of depth because the data acquisition instruments can be placed above the water surface. Difficulties arise when these measurements have to be made to depths of several tens of meters. In these cases, the instruments should be waterproof for pressures up to several bar. For a study, in collaboration with the Department of Biology - University of Pisa, a benthic chamber was designed and built. The chamber is able to carry out metabolic measurements of underwater flora at depths between 0 and 50 m. The chamber is large enough to contain several plants and provides a reasonable compromise with chamber handling. Parameters which can be measured are underwater solar radiation (global, red, green, blue), depth, temperature, pH, conductivity, dissolved oxygen. In the Chamber there are two operation phases: measurement of water physical-chemical parameters, altered by biological activity of plants and a water exchange with external water. A pump system avoids the water stratification and allows the water renewal. Results of several tests confirm full compliance of the benthic chamber with respect to the requirements of marine biologists and to the project data.

1 Introduction

Benthic chambers are widely used in studies concerning both marine sediments and the flow of solutes through them (in presence or absence of subterranean megafauna) up to a depth of several thousands of meters [1, 2, 3, 4]. So, benthic chamber technique was used to establish the chemical reactions that occur in the bottom water and the top layer of the sediments [5]. Benthic chambers were used also for studies on metabolism (primary production, respiration, etc.) of coral reefs and vegetable biomasses [6, 7]. These studies concerned the air-water interface or, at most, a few meters below the sea surface [8, 9]. Structures carried out for the first type of studies are elementary, usually small, and use a few simple instruments of detection (individual sensors, or assembled in multiparameter probes, samplers, etc.) that do not require support and management hardware and software [10]. Structures to conduct studies of the second kind are, usually, more complex. These, however, can be easily carried out for use up to a few meters of depth because the instruments (for data acquisition, management and power supplies) can be placed above the water surface. Technological difficul-

ties arise when these measurements have to be made to depths of several tens of meters (10 to 50 m). In these cases, the instruments should be waterproof for pressures up to several bar (1 ÷ 5).

2 Realization

For a study, funded by the Ministry of Education, University and Research (VECTOR Project Line 7: VulnErability of the Italian coastal area and marine Ecosystems to Climatic changes and Their rOle in the Mediterranean caRbon cycles), in collaboration with the Department of Biology of the University of Pisa, a plexiglas benthic chamber was designed and built. The chamber is able to carry out metabolic measurements of underwater flora at depths between zero and 50 meters. The chamber is large enough (diameter 900 mm, height 1000 mm, volume 0.5m^3) to contain several plants and provides a reasonable compromise with chamber handling. The instrument, by monitoring physical parameters related to metabolic activity of plants, makes it possible to deduce the "health" of marine waters in the euphotic zone. The parameters which can be measured are:

- solar radiation that reaches the chamber in the ranges: global (400 ÷ 1100nm), red (500 ÷ 700nm), green (480 ÷ 600nm), blue (450 ÷ 540nm). The instrument, a SuMaRad (SubMarine Radiometer) [11], indicates the quantities as a percentage of the corresponding solar radiation at the sea surface;
- and, by means of a multiparameter probe [12]:
  - depth: 0 ÷ 61m ± 0.12m, resolution 0.001m;
  - temperature: -5 ÷ 45°C ± 0.15°C, resolution 0.01°C;
  - pH: 0 ÷ 14 ± 0.2, resolution 0.01;
  - conductivity: 0 ÷ 100mS·cm^{-1} ± 0.5 % of reading, resolution 0.1 mS·cm^{-1};
  - dissolved oxygen (in two ranges): 0 ÷ 20mg·l^{-1} ± 0.1mg·l^{-1} or 1 %, of reading, (whichever is greater), 20 ÷ 50mg·l^{-1} ± 15 % of reading resolution (in both ranges) 0.01mg·l^{-1}.

Figure 1 shows the benthic chamber, on its trolley, with its measuring instruments: A) SuMaRad, B) multiparameter probe, C) control electronics with battery pack, D) internal circulating pump. In the picture, the charging pump which replaces the water inside the chamber is not visible. Figure 2 shows the front panel of the control electronics within the waterproof case (marked C in Figure 1), which also contains the battery pack. In the picture, A is the magnetic key that allows the programming of the control system, B is the keyboard for entering commands, C is the display, D is the connector for charging batteries. The control electronics is based on an Atmel microcontroller ATMega168 and was developed using Arduino [13], an open-source electronics prototyping platform. Figure 3 shows the block diagram of the control unit.

The control unit allows two modes of pump operation, selectable by the user (Figure 4). **Alternating mode**. The two pumps cannot operate simultaneously and the time in which a pump is working corresponds to the interval time when the other is off. The working phase of the pump can alternate periods of activity and inactivity, without affecting the off pump. The user can set the ratio (in %) between periods of activity and inactivity (duty cycle) during the work-

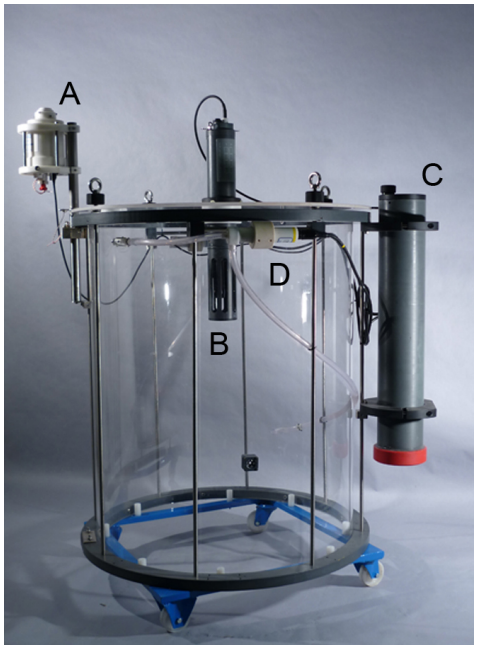

Figure 1: Benthic chamber on its trolley with annexed measuring instruments: A) SuMaRad (SubMarine Radiometer), B) Multiparametric probe, C) Control electronics with battery pack, D) Internal circulating pump. The charging pump is not visible in this picture.

ing time.

Independent mode. The pumps operate in a completely independent mode and for each one the user can set: on time, off time and the delay to their starting after power up of the control unit. Each pump also can always be set on or off. The control unit generates a signal whose amplitude depends on the working state of the pumps. This signal can be sent to a separate input of the multiparameter probe, thus allowing monitoring of the pumps. These pumps are specific for oceanographic applications and are centrifugal type with magnetically coupled impeller and adjustable flow rate [14]. Flow rate was set at 7.5 $\mathrm{l{\cdot}min^{-1}}$ to optimize electrical power consumption.

In alternating mode, there are two operation phases in the Chamber: measurement of water physical-chemical parameters, altered by biological activity of plants (circulating pump on); water exchange: water inside the chamber is replaced by external water to set new initial conditions (charging pump on). The power supply is provided by a pack of sealed lead acid batteries (36 V, 8 Ah). The battery life is more than 30 h (in alternating mode: circulating pump 4 h, 50 % duty cycle, charging pump 1 h, duty cycle 100 %). Diving and surfacing operations are facilitated by a valve system that allows, in the first case, the complete expulsion of air and, in the second case, water discharge.

Figure 2: Front panel of the electronics control within the waterproof case (C in Figure 1), which also contains the battery pack. A) magnetic key for programming the control system, B) keyboard for entering commands, C) display, D) connector for charging batteries.

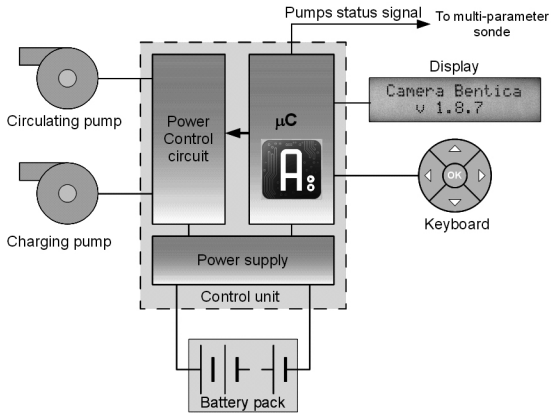

Figure 3: Block diagram of the management system of the benthic chamber. The Block diagram of the control unit is within the dashed rectangle.

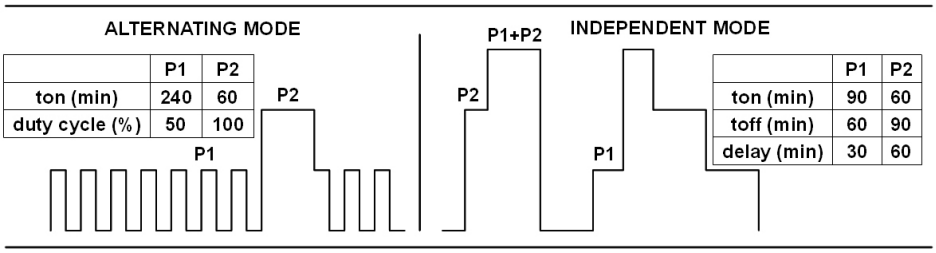

Figure 4: Scheme for the two modes of operation: on the left, Alternating mode: the on and off sequence of the circulation pump, programmed with a duty cycle of 50 %, is visible. The charging pump is running continuously during its operation phase (duty cycle of 100 %). On the right, Independent mode: the two pumps can be both on or off at the same time, and for each one the on time, off time and the delay to their starting after power up of the control unit can be set. Each pump also can be set always on or always off.

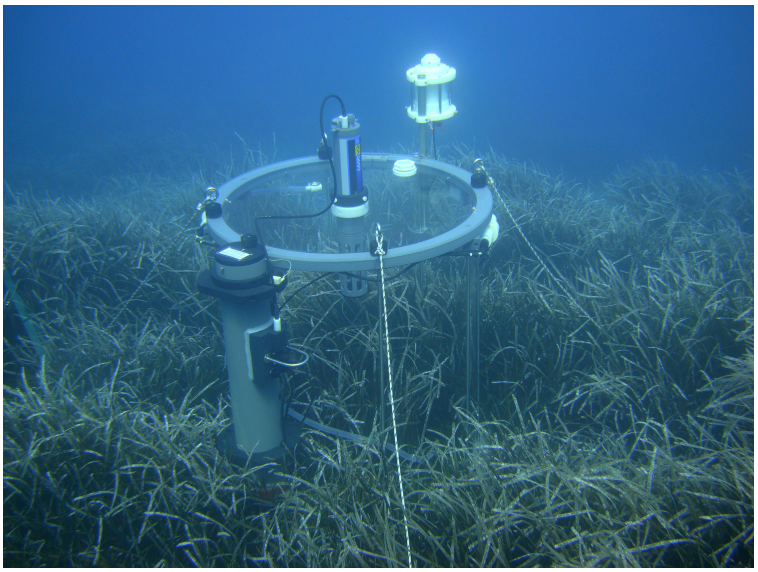

Figure 5: A test to verify the functionality of the Chamber was conducted in the Cala Villamarina (Santo Stefano Island, Archipelago of Maddalena, northern Sardinia) on a Posidonia Oceanica meadow at a depth of 9 m in July 2009.

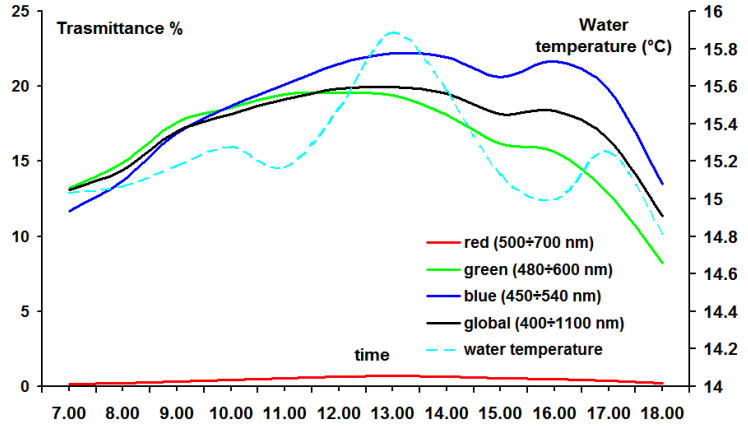

Figure 6: A typical July day: percentage transmittance of the water, the ratio between underwater radiation and outside water radiation in the indicated spectral bands (left ordinate). Dashed line (right ordinate) shows the plot vs. time of the water temperature.

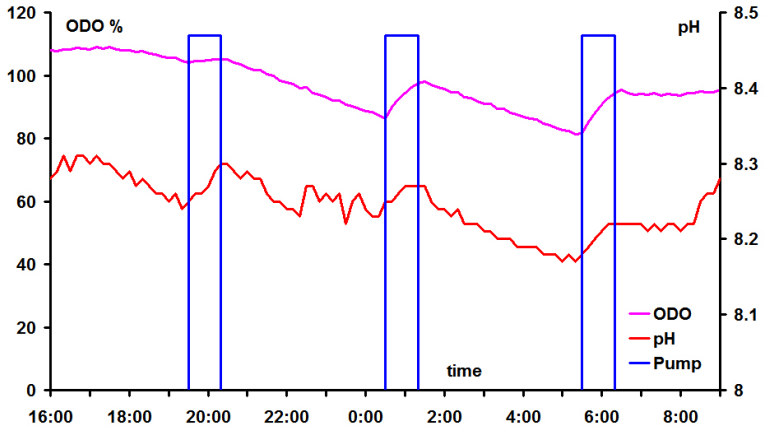

Figure 7: A typical July day: the plot vs. time of dissolved oxygen (upper line, left ordinate) and pH (lower line, right ordinate). Rectangles indicate the time intervals when the water inside the benthic chamber was replaced with external water.

3 Results and Conclusions

In order to verify Chamber functionality, a test was conducted in Cala Villamarina (Santo Stefano Island, Archipelago of Maddalena, northern Sardinia) on a Posidonia Oceanica meadow at a depth of 9 m in July 2009 (Figure 5). Figure 6 shows as an example the plot vs. time of the percent transmittance of the water, the ratio between underwater radiation and outside water radiation in the indicated spectral bands (left ordinate). The dashed line (right ordinate) shows the plot vs. time of the water temperature. Figure 7 illustrates the plot vs. time of two other measured parameters: dissolved oxygen (upper line, left ordinate) and pH (lower line, right ordinate). Rectangles indicate the time intervals (adjustable from 10 minutes to 24 hours) in which the water inside the benthic chamber was replaced with external water. When the charging pump is off the circulating pump is activated to prevent stratification of the water in the chamber. It is possible to observe how, at night, plant respiration reduces dissolved oxygen in sea water and gives off carbon dioxide, lowering the pH (in Figure 7, approximately from 8:00 pm to 5:30 am); vice versa with the return of sunlight, plants absorb carbon dioxide (pH increases) and emit oxygen. The measurement cycle is repeated with each water renewal. The acquired data are stored in internal memory of the multiparameter probe and of the SuMaRad. The results obtained confirm full compliance of the benthic chamber with respect to the requirements of marine biologists and to the project data. This benthic chamber is one of the most versatile for measuring the metabolic activity of marine flora in the euphotic zone due to its size, instrumental equipment, automatic operation, operative autonomy, and low construction cost.

References

[1] W. Dickinson and F.L. Sayles. A benthic chamber with electric stirrer mixing. *Technical Report of WHOI, Massachusetts USA*, 1992.

[2] D.J. Hughes, R.J.A. Atkinson, and A.D. Ansell. A field test of the effects of megafaunal burrows on benthic chamber measurements of sediment-water solute fluxes. *Marine Ecol. Prog. Ser. - Wiley-Blackwell*, 195:189 – 199, 2000.

[3] A.P. Webb and B.D. Eyre. The effects of two benthic chamber stirring systems on the diffusive boundary layer, oxygen flux, and passive flow through model macrofauna burrows. *Eustuaries*, 27(2):353–362, 2004.

[4] S. Sommer, M. Türk, S. Kriwanek, and O. Pfannkuche. Gas exchange system for extended in situ benthic chamber fluxe measurements under controlled oxygen conditions: first application - sea bed methane emission measurements at Captain Arutyunov mud volcano. *American Society of Limnology and Oceanographic: methods*, 6:26 – 33, 2008.

[5] D. Dyrssen, P. Hall, and S. Westerlund. Benthic chamber chemistry. *Anal. Chem.*, 317:380–382, 1984.

[6] L.B. Cahoon and J.E. Cooke. Benthic microalgal production in Onslow Bay, North Carolina, USA. *Mar. Ecol. Prog. Ser.*, 84:185–196, 1992.

[7] L.B. Cahoon, G.R. Beretich, C.J. Thomas, and A.M. McDonald. Benthic microalgal production at Stellwagen Bank, Massachusetts Bay, USA. *Mar. Ecol. Prog. Ser.*, 102:179–185, 1993.

[8] J.P. Gattuso, M. Pichon, B. Delesalle, and M. Frankignoulle. Community metabolism and air-sea CO_2 fluxes in a coral reef ecosystem. *Mar. ecol. Prog. Ser.- Wiley-Blackwell*, 96:259 – 267, 1993.

[9] J.P. Gattuso, C.E. Payri, M. Pichon, B. Delesalle, and M. Frankignoulle. Primary production, calcification, and air - sea CO_2 fluxes of a macroalgal-dominated coral reef community. *Journal of Phicology- John Wiley & Sons Ltd UK*, 33:259 – 267, 1997.

[10] L.B. Cahoon. An instrumented lander for measurement of benthic respiration and production. *The Diving for Science archive.rubicon-foundation.org*, pages 45–51, 1996.

[11] G. Fasano and A. Materassi. Progetto e realizzazione di uno strumento per la misura dell'assorbimento radiativo dell'acqua marina: SuMaRad. *Rivista di Ingegneria Agraria - Ed. ETS Pisa*, 4:1–7, 2003.

[12] YSI. Multiparametric Sonde YSI 6600 V2. *https://www.ysi.com*, 2009.

[13] Anonymous. Arduino: an open-source electronics prototyping platform. *www.arduino.cc*, 2009.

[14] Sea Birds Electronics. Submersible Pump SBE 5P. *http://www.seabird.com*, 2009.

A Multidisciplinary Approach for Paleoenvironmental Reconstruction in Ultra-Shallow Water through Acoustics and Core Sampling

F. Madricardo[1], S. Donnici[1], A. Lezziero[2], F. De Carli[2], J.A. De Souza[3], B. Bertani[4]
1, Institute of Marine Sciences, CNR, Venezia, Italy
2, PHAROS s.a.s. di Alberto Lezziero e C., Venezia, Italy
3, Center Of Studies in Coastal and Oceanic Geology, UFRGS, Porto Alegre, Brazil
4, Information Service of the Water Authority of Venice, Venezia, Italy
fantina.madricardo@ismar.cnr.it

Abstract

The lagoon of Venice represents a very peculiar environment resulting from combined natural and anthropic action. It began to form during the last marine transgression about 5500 years ago. Since then, its morphological aspect has drastically changed. The changes are due, on one hand, to natural causes like tributary river sediment supply, eustatic variations and natural subsidence. On the other hand, the anthropic action had a strong impact on the lagoon evolution. The first anthropic settlements go back in time to the roman age, but big engineering and dredging works started about the 14th century AD and are still ongoing. All these interventions contributed to radical changes in the lagoon hydrodynamics. The consequent change in the lagoon morphology can be established by studying the content of the lagoonal sediments. For this purpose, a multidisciplinary research project has been carried out over a large area (about 50 km^2) of the lagoon. An extensive high space resolution acoustic survey in ultra-shallow water (up to a depth 0.5 m) together with geological analysis from 60 cores extracted in the explored area revealed the Holocene sediment architecture. In particular a complex network of buried palaeochannels was reconstructed thanks to the acoustic techniques that allowed a detailed mapping of the lagoonal sedimentary feature.

1 Introduction

The Lagoon of Venice is the result of a complex interplay of natural and anthropogenic factors. Many studies were carried out to investigate and to reconstruct its origin and its development over time and space up to its current morphological and hydrographic state. The lagoon began to form about 5500 years ago during the late Holocene marine transgression [1]. Since then, a sediment succession of lagoon environments with various morphologies and hydrological regimes overlaid the earliest marine deposits [2]. In historical times, the anthropogenic action had a strong impact on the lagoon evolution. The first settlements go back in time to the roman age, but big engineering and dredging works (major river diversion, construction

of outer jetties of port harbours and industrial area, reclamation works, digging out of large artificial channels) started about the 14th century AD and are still ongoing [3, 4]. The actual lagoon morphologies, like salt-marshes, tidal meanders and their properties and the present tidal network, had been object of very detailed field and laboratory observations and hydrodynamics modelling studies [5, 6, 7, 8, 9]. The ancient lagoon morphologies, on the other hand, were reconstructed thanks to geological investigation based on core sampling (see for example [10, 11, 12] and references therein). In particular, the position of ancient coastal strips and the presence during the Roman age of large emerged areas were discovered [13, 14, 15]. However, the core sampling gives information on discrete points, whereas the extreme spatial and temporal variability of these lagoon morphologies makes it sometimes very difficult to correlate sedimentary facies. The extremely shallow waters (less than 1 m depth) of the Lagoon of Venice had prevented for long time the use of conventional geophysical survey methods. The first field trials with acoustic methods in the lagoon were restricted to few survey lines [16, 17]. Other recent works are focused more on the stratigraphic sequence of the Pleistocene and Holocene sediments than on geomorphological reconstruction and they concern to the southern lagoon [18, 19]. In this context, since 1999, a joint research programme between the CNR Institute of Marine Science (Venice) and the CNR Institute of Acoustics (Rome) together with the PHAROS sas was carried out: extremely shallow zones in the lagoon were explored with a multidisciplinary approach [20]. Within this research project, an extensive high spatial resolution acoustic survey was carried out [21]. The Holocene sediments had been systematically investigated using a single beam echosounder in extremely shallow water, with water levels ranging from about 0.5 m to about 5 m. More than 50 km^2 in the central and northern part of the lagoon for a total of 2000 km of survey lines were explored. The acoustics gave indications of the subbottom layer content over wide areas and provided an extremely useful guide for selection of sample sites for coring. In particular, this geophysical investigation allowed the detailed reconstruction of buried channel paths, internal stratifications and meandering behaviour.

2 Study area and experimental method

The investigated area of about 50 km^2 is located in the Lagoon of Venice (Northeastern Italy), which has a total surface of 550 km^2 and a average depth of 1.05 m for shallow flats and 5.5 for channels (data of year 2000, [9]. It is connected to the Adriatic sea by the inlets of Lido, Malamocco and Chioggia (Figure 1a). The surveyed area is subdivided in two parts: the area A in northern lagoon subbasin (of about 2 km^2) close to the islands of Burano, Mazzorbo and S. Erasmo (Figure 1b) and the area B between the lagoon margin around the city of Venice to the Lido (Figure 1c). The area A is relatively protected from the currents and waves coming from the open sea into the lagoon through the Lido inlet. It is a submerged mudflat with water depth below 1 m. In this area we conducted a very detailed acoustic survey along parallel lines with 2-3 m spacing. This detail was necessary to find buried archaeological structures, of which the northern lagoon

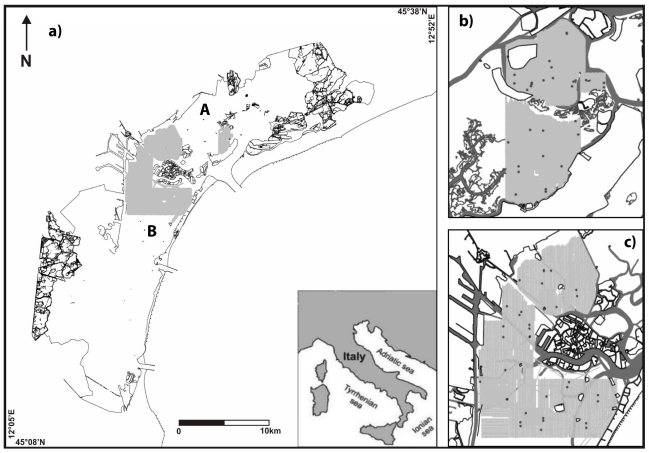

Figure 1: Map of the Venice Lagoon (a) and an enlargement of the survey areas (b,c): The dark grey points indicate the position of the 60 cores extracted in the two areas.

is rich (see for example [22]). In this area, 30 sediment cores were extracted (Figure 1b) to verify the nature of noticeble acoustic features identified during the survey. The area B develops all around the city of Venice and interests both an area of semi-enclosed and of open lagoon, less protected from currents and waves, with an evident tendency to evolve into a bay environment [23]. Main navigation channels are present because of the proximity to the city and to the industrial area. Here, we wanted to identify the main geological structures around the city of Venice. Therefore, the survey was carried out along parallel lines with a 50 m spacing. In addiction, also in this area, 30 truth samples were extracted (Figure 1c). The modified ELAC LAZ 72 single beam echosounder equipped with a 30 kHz LSE 131 transducer was used for the acoustic survey. The echosounder was mounted on a small boat along with a co-located DGPS system Trimble DSM12, which allows a positioning accuracy within one meter. The flat bottom boat was just 7 m long with a 30 cm draft.Thus it was possible to operate under extreme shallow water conditions (down to 50 cm depth). All the survey echograms were processed and interpreted (see [21] for more details). The acoustic anomalies were stored in a database with indications about their form and their depth for comparison with the other data. The geological data presented here for comparison with the results of the acoustic survey were obtained from 5 boreholes: SA4, SA5, SA8, SA9 drilled in the area A and SG25 in the area B. Their geographic positions were determined through a DGPS system, while their lengths varied between 8 and 9.1 m, for all the structures identified by the acoustics to be intersected. They were sampled in September 2004, October 2005 and April 2006 with the help of a rotation method with water circulation. The corer diameter was 101 mm. The lithology and sedimentary structures of all extracted materials were described, using as altitude reference the mean sea level (m.s.l.) of 1897, 23.5 cm

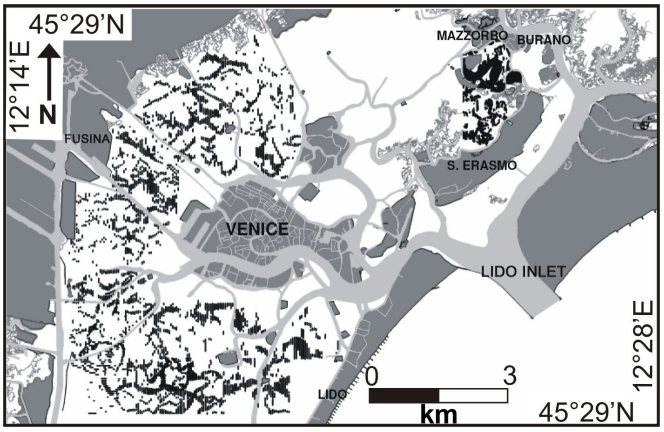

Figure 2: Acoustical anomalies identified as buried palaeochannels: the black lines represent the spatial extension of the palaeochannels along the acoustic survey; in light and dark are shown the actual channel network and the emerged morphologies, respectively.

below the mean present-day level. In particular, the bottom depth with respect to the m.s.l. was 0.54 m for SA4, 0.58 m for SA5, 0.83 m for SA8, 0.7 m for SA9, and 1.19 m for SG25, respectively. The sediment cores were sampled for micropalaeontological and radiometric investigations. Micropalaeontological analyses were carried out on sediment samples, where the organic content was composed of crushed mollusk shells mixed with abundant tests of benthic foraminifera. From each sample at least 150 foraminiferal specimens were classified according to the taxonomic order of Loeblich and Tappan [24]. Their percentage abundance was used for statistical data processing. Radiocarbon ages were calculated on four samples of shells at the Beta Analytic Inc. and at the CEDAD laboratories. The samples were analyzed using the Accelerator Mass Spectrometry (AMS) technique to determine the amount of ^{14}C content. The conventional ^{14}C age before present (BP), i.e. AD 1950, contain the $^{13}C/^{12}C$ corrections to the measured age. The ^{14}C ages were calibrated using the Calib 501 program [25, 26].

3 Results and Discussion

In the surveyed areas a complex network of buried channels was identified both through acoustic and geological data. The peculiar acoustic response of palaeochannels helped us in their recognition and classification. They generally show dipping acoustic reflectors interpretable as inclined deposits due to the channel migration. This interpretation was later confirmed by the accurate inspection of core sedimentary records. As a result of data processing, interpretation and classification, in Figure 2 we mapped the position of the acoustic features corresponding to buried channels. The detected palaeochannels belong to different stages of the lagoon development, as was shown by the radiocarbon dating on our cores. Observing Figure 2, however, one can say that the lagoon has

certainly been the theatre of channel forming, migrating and disappearing, as a consequence of the complex hydrological and sedimentological regime in the area. As observed in many studies, the channel network within the tidal basin is strongly related to its hydrodynamics and sediment exchanges. Whereas the present tidal network, the tidal meanders and their properties, are known and studied from different perspectives, the network of buried, and therefore disappeared, morphologies was never mapped before in such a detail. This map give a first indication of how much the geomorphology of the lagoon have changed since its origin until present. However, the mapped buried morphologies need to be deeply understood, since the acoustic echograms show a general picture referring to different times and hydrodynamic conditions. In the following sections, we present the study of two main buried geomorphological features identified in the acoustic profiles. The first lies in the northern lagoon closer to the Lido inlet (in the A area), while the second one is located in the central lagoon closer to the mainland (in the B area).

3.1 Palaeochannel in the Northern Lagoon (area A)

Acoustic sections intersect a wide palaeochannel that developed with a large meander in an area that now is a submerged mudflat with a mean water depth of about 0.7 m. The 2-D reconstruction of the buried palaeochannel path for a length of 2.7 km is depicted in Figure 3. Two examples of the acoustic anomalies relative to this buried morphology are shown in Figure 4. In Figure 4a, the reflection pattern shows a typical prograded fill of erosional channels [27]. The reflecting horizons correspond to changes in lithology (velocity and density) in the sediment. The related layers are inclined, dipping in a northern direction. This configuration is interpreted as the result of the active lateral accretion of the palaeochannel through point bar migration. In Figure 4b, a survey profile of the same palaeochannel is depicted. It was recorded 550 m to the west of the one shown in Figure 4a. Here, as well, one can see a prograded fill. In this case, the seismic reflectors dip in the southern direction, being a section of a consecutive loop of the same meander pointing in the opposite direction. This is clear also from the full path reconstruction given in Figure 3. The vertical lines in Figure 4 represent the ground-truth samples (cores) extracted to verify the nature of the acoustic anomalies. In Figure 4a the locations of cores SA4 and SA5 are shown. The core SA4 was drilled in the centre of the supposed palaeochannel. The core SA5 was located immediately outside this buried morphology in order to clearly discriminate the sedimentary characteristics given by the presence of the acoustic anomaly. In Figure 4b the locations of the cores SA9 and SA8 are shown. The geological investigation (SA4, SA8, SA9) confirmed the presence of the buried channel. From the depth of -9 m below m.s.l., medium to fine silty laminated sand and sandy silt with frequent millimetric sand layers are present. The emplacement of these layers is related to the changing of energy levels, linked to the tidal phases and sediment transport. These sediments are representative of channel facies and contain a typical foraminiferal association of the outer lagoon environment. This settlements can be explained by proximity of this area to a lagoon inlet up to 500-400 years BP, when the S. Erasmo island (Fig-

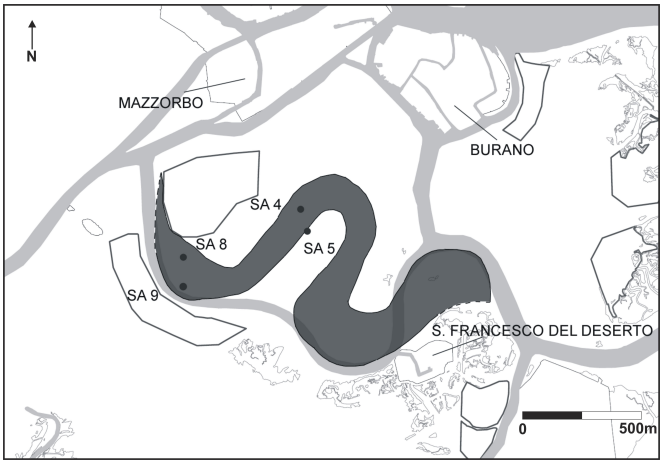

Figure 3: Reconstruction map of the path of a buried palaeochannel with the locations of the cores SA4, SA5, SA8, SA9.

ure 2) was a littoral strip. (see [28]). The radiometric ages of the shells found at the bottom of the channel deposits in cores SA4 and SA9, respectively 4276 $\pm$ 93 and 4341 $\pm$ 82 calibrated years BP, are in very good agreement. They indicate that they belong to the same channel active 4500 years BP at least. Finally, core SA5, coherently with acoustic data, did not reveal the presence of a channel. The undisturbed stratigraphic sequence revealed subtidal lagoon sediments, whose bottom radiometric age is 4531$\pm$87 calibrated years BP. They are mainly clayey or sandy silts, containing mollusc shells and characterized by a high bioturbation level. Foraminiferal analyses suggest the occurrence of freshwater inputs in the lagoon environment. This indication can be explained by the fact that the river inputs were important into this area before the artificial river diversion between the 14th and the 17th century.

3.2 Paleochannel in the Central Lagoon (area B)

Acoustic sections, in this case as well, intersect a palaeochannel that developed between Fusina and Venice with a meander buried in a actual submerged mudflat with mean water depth of about 1-1.5 m. The 2-D reconstruction of the buried palaeochannel path for a length of 2.2 km is shown in Figure 5. An example of the acoustic anomaly relative to this buried morphology is shown in Figure 6. In this case, two different fill patterns are visible. First, one has a prograded fill up to the grey line. Here, the inclined reflectors, dipping into the northern correspond to the palaeochannel point bar migration. Then, the buried channel presents a divergent fill. Therefore, the grey line seems to separate two different phases: an earlier high energetic regime with sand deposition and channel migration and a later low energetic regime with a finer filling and apparently no migration. The palaeochannel was in-

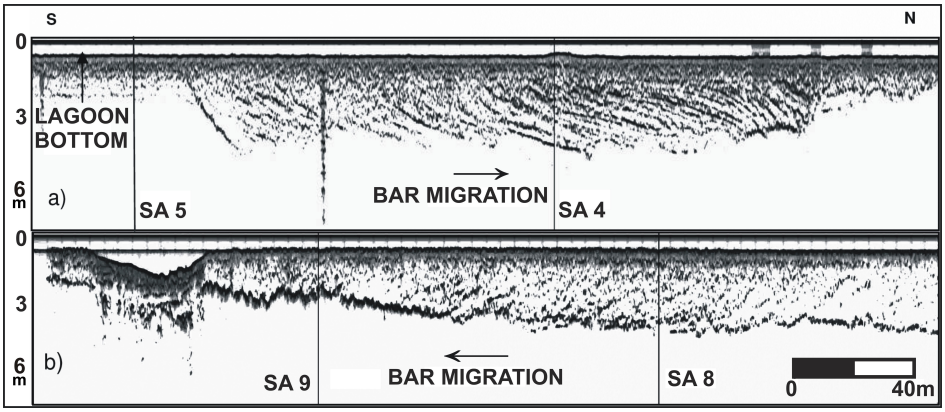

Figure 4: Reflection profiles of a palaeochannel in different points. The straight vertical lines indicate the location of the cores sampled. Horizontal and vertical scales are 300 and 7.5 m, respectively.

tersected by the core SG25, whose location is indicated by the black vertical line in fig.6. The stratigraphic record (Figure 6 right) presents mainly clayey-silty sediments from -1.2 to -5.2 m and sandy sediments from -5.2 to -6.60 m above m.s.l. The radiometric age of the shell found at -5.2 m between the two facies set the energetic regime change about 1600 $\pm$ 90 cal yrs BP (grey line in fig.6). The two phases can possibly be related to a variation of the area hydrodynamics due to the climate worsening between the IV and VI century AD (see [29]).

4 Conclusions

The multidisciplinary approach allows for the first time a very detailed reconstruction of paleochannel paths and internal structures, their meandering behaviour and their evolution related to possible change of the lagoon hydrology. In particular a complex network of palaeochannels was reconstructed thanks to the acoustic techniques that allowed a detail mapping of the buried lagoonal morphology. In this paper, we illustrate two examples of two distinct cases of geomorphological reconstruction: one in the northern and the other in the central Lagoon. The paths and the internal structures of two palaeochannels were mapped and studied, respectively, by correlating the acoustic and geological data. In the first case, the acoustic data show a dense stratification within the palaeochannel due to the meander bar migration testifying a certain constancy of the hydrological conditions until its complete fill. In the second case, instead, the acoustics allowed one to identify a sudden passage from a more energetic environment to one less energetic, possibly related to a rapid change of the hydrodynamic conditions.

5 Acknowledgements

The authors would like to thank the SIN for all the Lagoon of Venice background maps of the figures we presented. Moreover, we

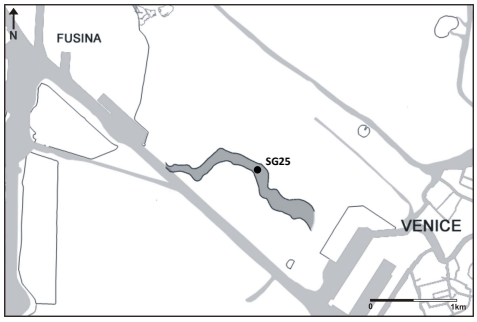

Figure 5: Reconstruction map of the path of the buried palaeochannel intersected by the core SG25.

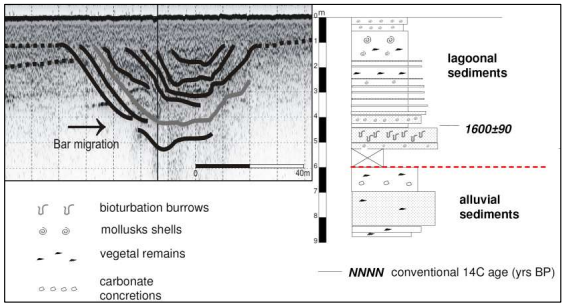

Figure 6: To the left: Buried palaeochannel intersected by the core SG25 (black vertical line). The thick black lines show the channel point bar migration and stratification, while the dashed lines indicate paleosurfaces. The grey line corresponds to the channel's shape about 1600 ± 90 cal yrs BP. To the right: SG25 Core Log. The depth scale is with respect to the lagoon bottom which was 1.19 m below m.s.l.

are very grateful to the referee of this paper, whose suggestions were very useful to improve the paper. This research was supported technically and financially by the Ministero delle Infrastrutture e Trasporti, Magistrato alle Acque di Venezia.

References

[1] P. Gatto and L. Carbognin. The Lagoon of Venice: natural environment trend and man-induced modification. *Hydrological Sciences Bulletin*, 26:379–391, 1981.

[2] R. Serandrei-Barbero, R. Bertoldi, G. Canali, S. Donnici, and A. Lezziero. Paleoclimatic record of the past 22,000 years in Venice (Northern Italy): Biostratigraphic evidence and chronology. *Quaternary International*, 140:37–52, 2005.

[3] L. Carbognin. Evoluzione naturale e antropica della Laguna di Venezia. *Mem. Descr. Carta Geol. Ital*, 42:123–134, 1992.

[4] L. Carbognin, G. Cecconi, and V. Ardone. Interventions to safeguard the environment of the Venice Lagoon (Italy) against the effects of land elevation loss, volume 1 of *Land Subsidence*. La Garangola, Ravenna (Italy), 2000.

[5] S. Fagherazzi, A. Bortoluzzi, W.E. Dietrich, A. Adami, S. Lanzoni, M. Marani, and A. Rinaldo. Tidal networks 1. Automatic network extraction and preliminary scaling features from digital terrain maps. *Water Resources Research*, 35(12):3891–3904, 1999.

[6] S. Lanzoni and G. Seminara. Long-term evolution and morphodynamic equilibrium of tidal channels. *Journal of Geophysical Research-Oceans*, 107(C1), 2002.

[7] M. Marani, S. Lanzoni, and D. Zandolin. Tidal meanders. *Water Resources Research*, 38(11):1125, 2002.

[8] L. Carniello, A. Defina, and L. D'Alpaos. Morphological evolution of the Venice lagoon: evidence from the past and trend for the future. *Journal of Geophysical Research*, 114(F04002), 2009.

[9] E. Molinaroli, S. Guerzoni, A. Sarretta, M. Masiol, and M. Pistolato. Thirty-year changes (1970 to 2000) in bathymetry and sediment texture recorded in the Lagoon of Venice sub-basins, Italy. *Marine Geology*, 258(1-4):115–125, 2009.

[10] L. Alberotanza, R. Serandrei-Barbero, and V. Favero. I sedimenti olocenici della Laguna di Venezia. *Bollettino della Società Geologica Italiana*, 96:243–265, 1977.

[11] A. Bondesan and M. Meneghel. Geomorfologia della Laguna di Venezia. Note illustrative della Carta geomorfologica della provincia di Venezia. Esedra editrice, Padova, 2004.

[12] R. Serandrei-Barbero, A. Albani, S. Donnici, and F. Rizzetto. Past and recent sedimentation rates in the Lagoon of Venice (Northern Italy). *Estuarine Coastal and Shelf Science*, 69(1-2):255–269, 2006.

[13] V. Favero and R. Serandrei-Barbero. Evoluzione paleoambientale della Laguna di Venezia nell' area archeologica tra Burano e il Canale S.Felice. *Lavori Società Veneziana di Scienze Naturali*, 6:119–134, 1981.

[14] R. Serandrei-Barbero, A. D. Albani, and S. Zecchetto. Palaeoenvironmental significance of a benthic foraminiferal fauna from an archaeological excavation in the Lagoon of Venice, Italy. *Palaeogeography Palaeoclimatology Palaeoecology*, 136(1-4):41–52, 1997.

[15] A. Lezziero, S. Donnici, and R. Serandrei-Barbero. Evoluzione paleoambientale dell'area archeologica sommersa di S. Leonardo in Fossa Mala (Laguna di Venezia). *Geografia Fisica e Dinamica Quaternaria Suppl*, 7:201–210, 2005.

[16] C.E. McClennen, A.J. Ammerman, and S.G. Schock. Framework stratigraphy for the lagoon of Venice, Italy: Revealed in new seismic-reflection profiles and cores. *Journal of Coastal Research*, 13(3):745–759, 1997.

[17] C.E. McClennen and R.A. Housley. Late-Holocene channel meander migration and mudflat accumulation rates, lagoon of Venice, Italy. *Journal of Coastal Research*, 22(4):930–945, 2006.

[18] M. Zecchin, L. Baradello, G. Brancolini, F. Donda, F. Rizzetto, and L. Tosi. Sequence stratigraphy based on high-resolution seismic profiles in the late Pleistocene and Holocene deposits of the Venice area. *Marine Geology*, 253(3-4):185–198, 2008.

[19] M. Zecchin, G. Brancolini, L. Tosi, F. Rizzetto, M. Caffau, and L. Baradello. Anatomy of the Holocene succession of the southern Venice lagoon revealed by very high-resolution seismic data. *Continental Shelf Research*, 29:1343–1359, 2009.

[20] S. Buogo, E. Canal, G.B. Cannelli, S. Cavazzoni, S. Donnici, and A. Lezziero. Geoarchaeology in the Lagoon of Venice: palaeoenvironmental changes, ancient sea-level oscillation and geophysical surveys by acoustic techniques. Cambridge University Press, Cambridge, 2005.

[21] F. Madricardo, S. Donnici, A. Lezziero, F. De Carli, S. Buogo, P. Calicchia, and E. Boccardi. Palaeoenvironment reconstruction in the Lagoon of Venice through wide-area acoustic surveys and core sampling. *Estuarine Coastal and Shelf Science*, 75(1-2):205–213, 2007.

[22] E. Canal. Testimonianze archeologiche nella Laguna di Venezia. Edizioni del Vento, Venezia, 1998.

[23] A. Sarretta, S. Pillon, E. Molinaroli, S. Guerzoni, and G. Fontolan. Sediment budget in the Lagoon of Venice, Italy. *Continental Shelf Research*, 30-8:934–949, 2010.

[24] A.R. Loeblich and H. Tappan. Foraminiferal Genera and their Classification. 1987.

[25] M. Stuiver, P. J. Reimer, E. Bard, J. W. Beck, G. S. Burr, K. A. Hughen, B. Kromer, G. McCormac, J. Van der Plicht, and M. Spurk. INTCAL98 radiocarbon age calibration, 24,000-0 cal BP. *Radiocarbon*, 40(3):1041–1083, 1998.

[26] M. Stuiver, P. J. Reimer, and R. Reimer. CALIB 5.0. page http://calib.qub.ac.uk/calib/ program and documentation, 2005.

[27] R.M. Mitchum, P.R. Vail, and J.B. Sangree. Seismic stratigraphy and global changes of sea level, Part 6: Stratigraphic interpretation of seismic reflection patterns in depositional sequences. American Association of Petroleum Geologists Memoir. Tulsa, 1977.

[28] M. Bonardi, E. Canal, S. Cavazzoni, R. Serandrei-Barbero, L. Tosi, A. Galgaro, and M. Giada. Sedimentological, archaeological and historical evidences of palaeoclimatic changes during the Holocene in the Lagoon of Venice (Italy). *World Resource Review*, 9:435–446, 1997.

[29] A. Veggiani. I deterioramenti climatici dell'Età del Ferro e dell'alto Medioevo. *Bollettino della Società Torricelliana di Scienze e lettere*, 45:3–80, 1994.

Innovative Approaches to Retrieve Water Optically Active Parameters from Hyperspectral Data: *in situ* Measurements and Image Processing

F. Santini[3], L. Alberotanza[2], F. Braga[2], R.M. Cavalli[1], S. Pignatti[3]
1, Institute for Atmospheric Pollution, CNR, Roma, Italy
2, Institute of Marine Sciences, CNR, Venezia, Italy
3, Institute of Methodologies for Environmental Analysis, CNR, Potenza, Italy
federico.santini@lara.rm.cnr.it

Abstract

This paper describes the research activities carried out to enhance the performances of the application of remote sensing techniques on water bodies. In order to provide an inexpensive way to gather information linked to the water clarity and quality, several approaches for remotely sensed data interpretation, devoted to produce water optical property parameters, were tested. These approaches range from simple empirical relations to complex physical models. As regards the latest, a method for the retrieve of Chl (chlorophyll), CDOM (coloured dissolved organic matter) and a class taking into account the particulate material (TSM, TSS or Tripton), was assessed. At the purpose, a bio-optical model, based on radiative transfer theory, and an inverse procedure were implemented. The method was applied on spectral data collected during on purpose performed *in situ* campaigns by means of two spectroradiometers (OceanOptics and SpectraScan) following the SeaWiFS protocols. Water samples were collected for validation purposes. Laboratory analysis were performed on the water samples to provide water compound concentrations. The good results obtained by applying the model to *in situ* data encouraged the application to remote sensor data. Various pre-processing steps were carried out on remotely sensed images to make them feasible for the model application.

1 Introduction

Over the past 30 years, many satellite borne sensors have been exploited to gather information on land cover and insight into the biological activity occurring within the water bodies. Remote sensing products offer many new capabilities in a wide variety of applications, including the management of natural resources, inventory assessment (e.g. invasive weeds), environmental hazard, wildlife habitat characterization, and water quality monitoring. The study of the water colour (optical characterization in the visible spectral range) can be carried out by using several sensors like: ENVISAT/MERIS sensor (412-1050 nm) with a spatial resolution of 250 m/pixel; OCEANSAT-1/OCM (Ocean Colour Monitoring) with a spatial resolution of 350 m/pixel and a spectral coverage between 402 and 885 nm; TERRA/MODIS (405-14,382 nm) with a spatial resolution of 1000 m/pixel, Hyperion with a spatial res-

olution of 30 m/pixel and SeaWiFS (402-885 nm) with a spatial resolution of 1000 m/pixel. All the above sensors present a revisiting time suitable to study the seasonal/annual evolution of weed distribution and water clarity time degradation. The launch of new satellites with an increased spectral and spatial resolution (PRISMA, EnMap) will further enhance the utility of remotely sensed information for a water resource management support system. In order to extract water quality information, the optical data can be interpreted using different methods. Simplest methods are based on empirically derived relationships between the measured reflectance ratio and the chlorophyll concentration. These methods are suitable only for those water bodies (like open ocean) where CDOM and particulate material are of autochthonous origin and are strictly linked to phytoplankton abundance. These waters are referred to as Case I waters. Coastal and inland waters are generally much more complex. Because of detritus due to coast erosion or brought from the wind or from rivers, in fact, correlations between compounds fall down. To completely describe these water bodies, known as Case II waters, it is necessary to develop more complex algorithms. This complexity has been reached also through the definition of models which link the spectral behaviour radiometric field to the optical properties of water compounds. This kind of algorithms is named physically based algorithms and relate to the radiative transfer (RT) theory. Several models have been suggested (an exhaustive reference list can be found in [1]) with varying degrees of complexity. In this paper we present the work carried out in different study area to enhances the performances of the application of remote sensing techniques on water bodies. In particular we describe the data and procedure followed to define a physically based model approach. The study areas token into consideration relate to the Montenegrin and Albanian coasts, to the Venice lagoon and to the Kisumu bay (Victoria Lake - Kenya), which, although not being a case of inland water, represents a case of very optically complex water body characteristic of some coastal areas. In the Kisumu bay a field campaign was carried out on January 2004 onboard a small boat. During the field campaign 17 measure stations were devoted to the acquisition of spectral signature of the water surface and emerged vegetation. In 9 of these stations water samples for laboratory analysis were also collected. The data collected for the Albanian and the Montenegrin coastal areas were obtained from R/V G. Dallaporta (ISMAR-CNR, Italy) during two sea campaigns carried out on May 9-21 and on June 24-29, 2008. As regards the Venice lagoon study area, four field campaigns were conducted over the lagoon and the open sea on June-July 2001, June 2004 and May 2005.

2 Field data

Remote sensing measurements require a good field sampling strategy to calibrate and validate the data by-products. Water bodies were characterized, according to Ocean Optics Protocols for Satellite Ocean Colour Sensor Validation [2, 3, 4], by spectral measurements and collecting samples for laboratory analyses. Spectral signatures of the water column were derived from the radiance measurements of the sky and the water.

2.1 Spectral measurements

The optical measurement above water were devoted to the retrieve of the Rrs (Remote sensing reflectance), defined as:

$$Rrs = \frac{L_u(0^-)}{E_d}, \qquad (1)$$

where $L_u(0^-)$ is the upwelling signal coming from just below the water surface (also known as the in-water leaving radiance) and E_d is the irradiance incident (downwelling) on the water surface. The need to define an ad hoc physical quantity for water characterization originates from the fact that standard reflectance (defined as the radiance coming from the target divided by the incident irradiance) includes the surface reflectance contribution, that depends on illumination geometry. Rrs, on the contrary, is independent from illumination condition and is, therefore, functional to characterize water targets. What is directly acquired is $L_u(0^+)$, that is the signal just above the water surface. This can be expressed as

$$L_u(0^+) = L_u(0^-) + aL_{sky}, \qquad (2)$$

where the last term represents the surface reflectance and is supposed to be proportional to the sky radiance (L_{sky}) a depends on the acquisition geometry. To correctly assess Rrs three different set of measures were carried out for E_d, $L_u(0^+)$ and L_{sky} estimates following the SeaWiFS protocol [3].

2.2 Water samples

During all the field campaigns, several measure stations were devoted to the collection of water samples for laboratory analysis. During the field campaigns carried out in the framework of the Hypad.COM project along the Albanian and Montenegrin coastal areas (June-July 2005) samples of CDOM, TSM (Total Suspended Matter) and Chl a at the surface and 10 m depth were collected in 30 suitable stations. As regards the Venice lagoon study area, the first two campaigns (June and July 2001) supplied only water surface radiometric data to validate the remotely sensed data preprocessing chain. The second two field campaigns (June 2004 and May 2005) included water body optical property measurements and water samples for laboratory analysis. In this case study the particulate class was represented by Tripton, which includes only the inorganic material. Finally, during the field campaigns related to the Kisumu bay case study (May 2004), water samples were collected on nine stations and analyzed in the KMFRI laboratory for the assessment of Chl a, (with fluorescence analysis), CDOM and TSS (Total Suspended Solids). All measure and laboratory analysis were performed following the Ocean Optics Protocols For Satellite Ocean Color Sensor Validation [2, 3, 4].

3 Remote images

During the diverse field campaigns some images were acquired for model applications. During the Montenegrin and Albanian field campaigns a MIVIS sensor, onboard an airborne platform, acquired images along the coastline and along one of the measure transects. As regards the Venice lagoon, the first campaign was carried out in concomitance to a Hyperion overpass, while the second and the fourth campaigns were supported by airborne platforms equipped respectively with a MIVIS and a CASI sensor. Finally,

although the Kisumu bay field campaign wasn't programmed in concomitance with any satellite or airborne acquisition, few days after the field campaign took place, a MERIS Image was cloud free and adequate for the model application. Remote image data were pre-processed, analogously to *in situ* data, to obtain the Rrs images.

Noise reduction. A global de-striping procedure was applied to pushbroom sensor data (Hyperion, CASI), in order to reduce the spectral effects of column-to-column noise.

Atmospheric correction. The atmospheric correction were performed by applying the MODTRAN code. Path radiance, transmittance and incoming irradiance were simulated by using standard urban areas aerosol concentration profiles a visibility matching the acquisition condition and illumination geometry corresponding to image acquisition time.

Surface effects correction. Reflected signal was simulated through Hydrolight software (Sequoia Scientific, Inc.), given an illumination geometry corresponding to image acquisition time and a wind speed lower than 5 m/s. The signal over the surface was determined excluding path radiance from remote sensors signal and dividing by the transmittance. Then Rrs, according to its definition, was obtained subtracting surface reflected signal and dividing by incoming surface irradiance.

Geometric correction. The whole reflectance dataset was geocoded according to navigational data available for each platform, in the Gauss-Boaga reference system.

4 Methods

The proposed method includes a bio-optical-model (that defines the optical properties of the main water compounds and connects them to the optical properties of the water body) and a radiative transfer model (that links the optical properties of the water to the radiometric field). The junction of the two models allows estimating radiometric quantity in relation to the abundance of water compounds and their properties of light absorption and scattering. Then, by means of an appropriate inversion procedure, it is possible to retrieve compound concentrations starting from observable radiometric quantities (Rrs).

4.1 Bio-optical model

At a first step, the set of compounds that characterize the water body has to be established, and their specific optical properties have to be defined. The elements taken into account are: pure water, phytoplankton (associated to chl a, that represents its main pigment), CDOM, and a class of particulate (TSM, TSS or Tripton). The main assumption concerning the optical characterization of the whole water body is the linear composition of the single constituent absorption and back-scattering spectra:

$$a = a_0 + \sum_{j=1}^{n} a_j^* C_j; b_b = b_{b0} + \sum_{j=1}^{n} b_{bj}^* C_j, \tag{3}$$

where a_0 and b_{b0} refer to the pure water absorption and back-scattering; C_j represents the concentration of the $j-th$ constituent (chl, CDOM and TSS); a_j^* and b_{bj}^* are the optical properties per unit of concentration for the i-th constituent. The optical characterization of the constituents was obtained on the basis of literature data (Kisumu bay)

or by integrating literature data with laboratory optical profiles (Venice lagoon). For the Venice lagoon case study, chlorophyll and CDOM optical profiles were obtained by laboratory analysis, while in the other case studies they were token respectively from Prieur and Sathyendranath [5], and from Morel [6]. For the backscattering of phytoplankton and TSS/TSM/Tripton a profile based on the scattering phase function of large and small particles, as defined in Kopelevich [7], was utilized. The pure water absorption and back-scattering coefficients are those elaborated in Pope and Fry [8] and in Smith and Baker [9].

4.2 Radiative transfer model

The interactions between light and matter within a water body are well represented by the RT equations. A software (Hydrolight v4, Sequoia Scientific, Inc.) which implements a numerical solution of these equations was used for this study. This software maintains a high physical rigour and allows the computations of radiance distributions and related quantities (reflectance, irradiance) within the water body and upon the surface as a function of the water compound concentrations, the water compound optical properties, the water surface state, the illumination geometry and other boundary conditions. However, this software allows to retrieve water compound abundance only through a time consuming iterative procedure, and it is not suitable for processing large amount of data. If we consider that a remote image normally involves tens of thousands of pixels in different spectral bands, it is understandable that a simplified analytical and invertible formulation of the radiative transfer equations would be precious. Simplified analytical formulations can be derived directly from the RT theory under restrictive conditions [10]. Many treatments [11, 12], in the case of a optically deep and vertically homogeneous water body, agree on solutions similar to the one reported here:

$$\overline{R}rs = F \cdot \frac{b_b}{a + b_b}, \tag{4}$$

where a and b_b are given by the Eq. 3 and F is a parameter related to the illumination fields and the optical properties of the water surface. The F parameter was established for each image through quadratic regressions on the basis of data simulated with Hydrolight software. In this way it was possible to define an analytical formulation that is invertible and, at the same time, coherent with the RT equations. The regression involved several hundreds of simulations, which were carried out using the optical model defined above, considering the illumination geometry related to the remote images acquisition time and varying the abundance of the compounds within the *in situ* measured ranges.

4.3 Inversion procedure

Using Eq. 3 in Eq. 4 and defining the quantities it is possible to obtain a linear relation of the following form [13]

$$Rrs = \sum_{j=1}^{n} S_j C_j. \tag{5}$$

This equation, if applied to the spectral bands of a specified sensor (with m number of bands), corresponds to a linear system of m equations with n unknowns (n = number of compounds). Since m is generally greater than n, many authors define some criteria for band exclusion in order to solve the system. In view of an utilization of hyperspectral sensors, this approach can

result in a loss of information. Therefore, it is proposed to resolve the system through a least square method that allow to fully deploy hyperspectral data [13]. To practically carry out the inversion, a suitable software was developed in IDL language. This software takes as input the bio-optical model and the remote sensed data and starts a cycle on the image pixels. On each step the Eq. 4 is computes and the system of Eq. 5 is inverted. The outputs of the IDL procedure consist of the water compound concentration maps [13]. In the Venice lagoon case study a different inversion procedure was taken into consideration to improve the results. In fact, the solution found for the linearized formulation of Eq. 5 doesn't match exactly the optimal solution of the original non-linear problem. They differ as much as the modeled Rrs differs from the observed Rrs [14]. In the Venice lagoon case study a two-step procedure was presented for the inversion of the model: the solutions of the linearized formulation were used as a starting point for an iteration procedure based on a first order Taylor series expansion. For a detailed description of the two-step procedure see [14]. The solutions of the linearized formulation have been demonstrated to be an optimal starting point, as no divergence occurred for the whole processed dataset. The iteration was stopped when a refinement of less than 0.1% was reached for each parameter.

5 Results and Discussion

Physically based model, differently from the empirical ones, has the great advantage that does not necessitate of large amounts of *in situ* data for parameter refinement. In fact, the F parameter is assessed on the base of a model that solves the RT equations rather than by means of empirical data. This doesn't imply that no field data are needed for model validation. In any case, the quantity of data collected *in situ* is much less crucial than for empirical approaches. A set based on a limited number of stations may be behind the definition of rigorous procedure of error quantifications, but, if supported by historical data and by a regional knowledge, it can be adequate for a preliminary assessment of models and methods and to quantify their usefulness. The different steps of data processing (atmospheric corrections and other pre-processing procedures, bio-optical model definitions, *in situ* data analysis, model parameterization etc.) make it difficult to develop a general aprioristic procedure for final products uncertainty estimation. Therefore, a series of single validation steps which involve a preprocessing, a bio-optical and a thematic product validation has to be carried out.

5.1 Pre-processing validation

Atmospheric correction on remote images and the other pre-processing steps were validated comparing Rrs images with *in situ* measured Rrs spectra. For this comparison, we extracted from the remote sensing data the average value of a square of diverse pixels centred at the location of the *in situ* measurement to take into account possible local water mixing. The gap between field campaign and remote sensor overpass can be partially responsible for the not perfect alignment between compared spectra. Anyway, the fit was appreciable presenting an RMS (Root Mean Squares) value generally lower than 15% of the Rrs signal. As an example, in Figure 1, it is reported the comparison between the CASI spectra and the *in situ* ASD spectra

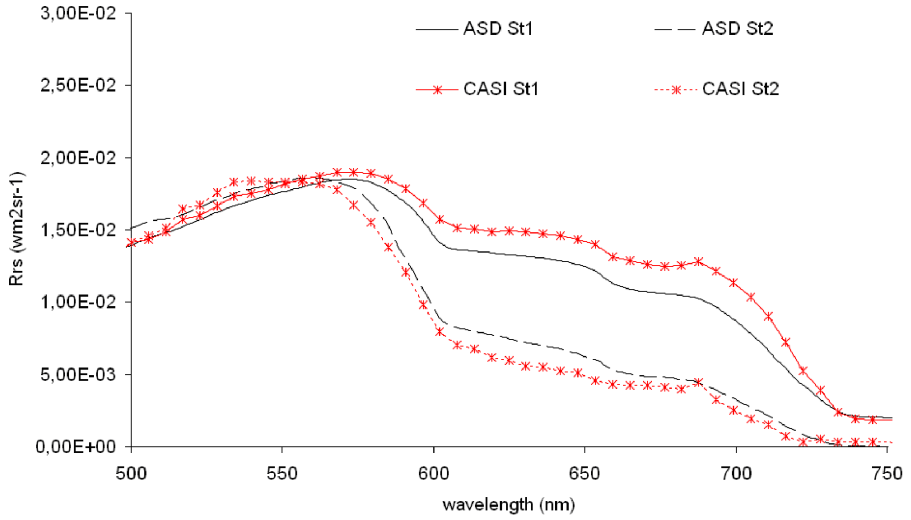

Figure 1: Comparison between CASI and ASD Rrs spectra acquired in two measure stations located in the proximity of a navigable channel of the southern basin (upper spectra) and near the Malamocco inlet (lower spectra) during the 2005 Venice lagoon field campaign.

as acquired in two measure station during the 2005 Venice lagoon campaign.

5.2 Model validation

The model validation was performed by simulating Rrs with Hydrolight software using as input the water compound optical properties and laboratory concentrations. Simulated spectra have been compared with *in situ* measurements of Rrs. An analogous indirect validation was carried out applying the inverse model to the *in situ* measured Rrs spectra and comparing the retrieved compound concentrations with the results of the laboratory analysis. Table 1 report the comparison related to the Kisumu bay, Table 2 reports the comparison related to Venice lagoon. The two-step procedure performed on the Venice lagoon case study allowed an improvement of the results of up to 10 % with respect to the laboratory water compound concentrations [14].

5.3 Remote data applications

The good results obtained by the application of the inverse physical model to the *in situ* Rrs spectra encouraged the application to the pre-processed remote images. The model was thus applied to the MIVIS, CASI and the Hyperion Images acquired close to the time the *in situ* campaigns took place. These applications allowed the production of synoptic images of the water compound concentrations related to the different study areas. As regards the Kisumu bay case study, these products were used to analyze the precon-

station	laboratory analysis			model application		
	Chl	CDOM	TSS	Chl	CDOM	TSS
#	mg/m3	m-1	g/m3	mg/m3	m-1	g/m3
1	15.6	1.9	118	15.2	8.1	87
2	21.1	1.3	65	10.8	1.2	246
3	13.3	1.9	56	17.2	2.7	246
5	24.8	3.1	159	9.9	2.3	200
8	17.6	1.1	78	15.8	-	93
10	29.2	3.1	188	29.1	-	433
11	18.3	1	46	6.6	3.2	-
12	11.6	0.9	42	8.1	1.3	-
15	22.7	0.2	129	6.6	-	-

Table 1: Kisumu bay water constituent concentrations obtained by laboratory analysis (column 2-4) and by the model application to the ASD *in situ* Rrs spectra (column 5-7).

dition for the anomalous proliferation of water weed that affects the area [13]. As the model doesn't take into consideration the bottom contribution, the application to the Venice lagoon was limited to the open sea and the deeper navigable channel. As regards the Montenegrin and the Albanian coasts, no remote images have already been processed. Nevertheless, a large set of MIVIS images covering the whole coastline is appropriate for the model application and will be soon elaborated. Related results and products will be presented in a feature work. In Figure 2 the results obtained for the Venice lagoon case study are showed.

6 Conclusions

This paper showed the potentiality of innovative approaches, based on the radiative transfer theory in water body and atmosphere, to retrieve water optically active parameters from hyperspectral data. A physically based method for the retrieve of water quality parameters in optically complex waters was presented. The model was validated through comparison with *in situ* collected data and applied to remote images acquired close to field campaigns. This allowed to generate synoptic images of the water compound concentrations. The comparison of these information with the results provided by the analysis of the water samples collected during the campaign showed a general good agreement and demonstrated the usefulness of the physical model approach in estimating water quality in coastal and internal water bodies.

station	laboratory analysis			model application		
	Chl	CDOM	Trp	Chl	CDOM	Trp
#	mg/m3	m-1	g/m3	mg/m3	m-1	g/m3
1	3.46	0.27	6.16	4.4	0.22	7.4
2	2.99	0.36	6.69	1.9	0.38	7.3
3	10.11	0.54	20.17	7.4	0.43	14
4	0.8	0.37	11.01	1.9	0.34	13
5	0.41	0.2	5.97	2.3	0.27	8.8
6	1.6	0.31	6.19	2	0.33	7.2
7	4.25	0.32	5.3	5	0.29	7.1
8	4.03	0.32	5.12	5	0.29	5.9
9	3.47	0.41	6.33	3.5	0.33	5.5
10	4.9	0.22	6.66	5.5	0.24	7.5
11	2.17	0.19	2.72	1.5	0.21	1.7

Table 2: Venice lagoon water constituent concentrations obtained by laboratory analysis (column 2-4) and by the model application to the ASD *in situ* Rrs spectra (column 5-7).

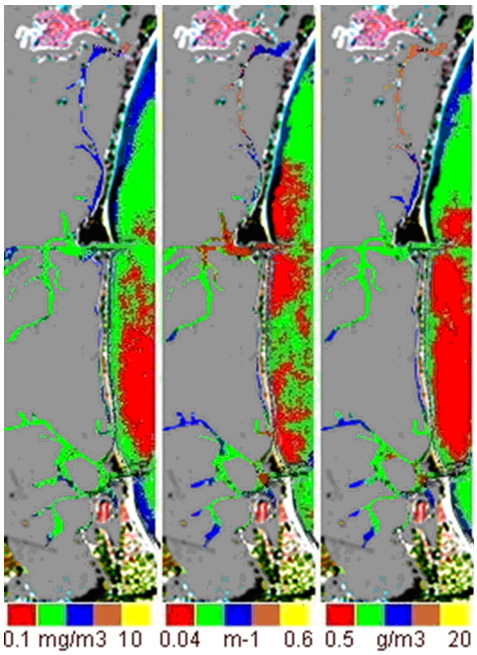

Figure 2: Water compound concentrations obtained from Hyperion data on open sea and navigable channels of the Venice lagoon. From left to right, the maps of Chl, CDOM and Tripton.

References

[1] Z. Lee, K.L. Carder, and R.A. Arnone. Deriving inherent optical properties from water color: a multiband quasi-analytical algorithm for optically deep waters. *Applied Optics*, 41:5755–5772, 2002.

[2] B.G Mitchell, M. Kahru, J. Wieland, and M. Stramska. Determination of spectral absorption coefficient of particles, dissolved material and phytoplankton for discrete water samples. *Ocean Optics Protocols for Satellite Ocean Color Sensor Validation*, pages 39–64, 2003.

[3] J.L. Muller, C. Davis, R. Arnone, R. Frouin, K. Carder, Z.P. Lee, R.G. Steward, S. Hooker, C.D. Mobley, and S. McLean. Above-water radiance and remote sensing reflectance measurement and analysis protocols. *Ocean Optics Protocols for Satellite Ocean-Color Sensor Validation*, pages 21–31, 2003.

[4] C.C. Trees, R.R. Bidigare, D.M. Karl, L.V. Heukelem, and J. Dore. Fluorometric chlorophyll a: sampling, laboratory methods, and data analysis protocols. *Ocean Optics Protocols for Satellite Ocean-Color Sensor Validation*, pages 15–18, 2003.

[5] L. Prieur and S. Sathyendranath. An optical classification of coastal and oceanic waters based on the specific spectral absorption curves of phytoplankton pigments, dissolved organic matter, and other particulate materials. *Limnol. Oceanogr*, 26(4):671–689, 1981.

[6] A. Morel. Light and marine phtosynthesis: a spectral model with geochemical and climatological implications. *Prog. Oceanog.*, 26(6):263–306, 1991.

[7] O.V. Kopelevich. Small-parameter model of optical properties of sea water. *Ocean Optics, I: Physical Ocean Optics*, 1:208–234, 1983.

[8] R.M. Pope and E.S. Fry. Integrating cavity measurements. *Applied Optics*, 36:8710–8723, 1997.

[9] R.C. Smith and K. Baker. Optical Properties for the clearest natural waters. *Applied Optics*, 20(2):177–184, 1981.

[10] C.D. Mobley. Light and Water: Radiative Transfer in Natural Waters. 1994.

[11] C. Giardino, V.E. Brando, A.G. Dekker, N. Strömbeck, and C. Candiani. Assessment of water quality in Lake Garda (Italy) using Hyperion. *Remote Sensing of Environment*, 109:183–195, 2007.

[12] V.E. Brando and A.G. Dekker. Satellite hyperspectral remote sensing for estimating estuarine and coastal water quality. *IEEE transactions on geoscience and remote sensing*, 41(6):1378–1387, 2003.

[13] R.M. Cavalli, G. Laneve, L. Fusilli, S. Pignatti, and F. Santini. Remote Sensing water observation for supporting lake Victoria weed management. *Journal of Environmental Management*, 90:2199–2211, 2009.

[14] F. Santini, L. Alberotanza, R.M. Cavalli, and S. Pignatti. A two-step optimization procedure for assessing water constituent concentrations by hyperspectral remote sensing techniques: An application to the highly turbid Venice lagoon waters. *Remote Sensing of Environment*, 114(4):887–898, 2010.

Integration of Earth Observation Data to Improve the Knowledge of Upwelling Phenomenon in the Strait of Messina

F. Azzaro[1], C. Bassani[2], R.M. Cavalli[2], S. Pignatti[3], F. Santini[3]
1, Institute for Coastal Marine Environment, CNR, Messina, Italy
2, Institute for Atmospheric Pollution, CNR, Roma, Italy
3, Institute of Methodologies for Environmental Analysis, CNR, Potenza, Italy
filippo.azzaro@iamc.cnr.it

Abstract

The work focuses on the data Earth Observation (EO) integration with different spatial and temporal resolution according to the Group on EO Working Plan 2009-2011. In particular, the "Ecosystem observations will be better harmonized and shared, spatial and topical gaps will be filled, and *in situ* data will be better integrated with spacebased observations" (GEOSS Societal Benefit Areas) is the main challenge applied to the Strait of Messina. The area is a coastal site with a remarkable economic and environmental role addressable to the complex dynamic of the water body. The strait is located in the centre of the Mediterranean Sea with strong current and vortex due to the morphology of the site. In this area, the upwelling is a hydrological phenomenon that strongly impacts the marine ecosystem. The upwelling systems are characterized by increased 'biological richness'. The principal indicator of upwelling is low sea surface temperature (SST). Since 1994, SST and phytoplankton were measured by continuous underway surface measurements onboard dedicated research boats. During 1999-2002, these in-situ measurements have been integrated with remote sensing image acquired by MIVIS airborne sensor. The integration meets the requirements to validate the empirical algorithm applied to remotely data in order to retrieve the phytoplankton and, the remote sensing provides a synoptic view of upwelling phenomenon by mapping the SST and the phytoplankton into the water body of the strait.

1 Introduction

The Earth Observations system constitutes a critical input for advancing the understanding and monitoring the Earth system, such as climate, oceans, atmosphere, water, land, natural resources, natural and human-induced hazards and for protecting the global environment, reducing disaster losses and achieving sustainable development [1]. In order to ensure comprehensive and sustained Earth observations, a coordination of the efforts, articulated in the GEOSS 10-Year Implementation Plan, has been built on to add value to existing Earth observation systems, filling critical gaps and supporting their interoperability. Over the next decade, the global scientific community has been expected to join the pivotal GEOSS Plan. The GEOSS will provide an important scientific basis to clearly identify the planning and decision making

in the complexity of the everyday life including public health, agriculture, transportation and numerous other areas to keep abreast of the rapid changes occurring in the society today. In less than two years, the number of participating countries has nearly doubled, and over 40 international organizations also support the emerging global network. The Messina monitoring projects take place at this strategic moment, when the Earth Observation has become an essential component of the global effort to deal with global challenges. The purpose of these projects is to promote capacity building in Earth observation, on existing local, regional and international initiatives and sector-specific needs, like GEOSS planned, in order to achieve comprehensive, coordinated and sustained *in situ*, airborne, and space-based observations of the Messina coastal area. The activities of these projects meet the need for timely, quality local scientific information as a basis for sound decision making, and will enhance delivery of benefits to society especially in the following initial areas, recognized in the GEOSS 10-Year Implementation Plan: "Improving the management and protection of terrestrial, coastal, and marine ecosystems" [2]. Hydrodynamical processes affect the spatial distribution and temporal development of phytoplankton biomass on the world's oceans and seas. Among the hydrological events, the divergent current bring nutrients into the upper layer of the water column and modulates the chlorophyll−a distribution [3]. Upwelling is a hydrological phenomenon that strongly impacts the marine ecosystem. In fact, upwelling systems belong to the most productive marine environments, and are characterized by increased 'biological richness' in all levels of the trophic chain. Low water temperature is one of the indicators of upwelling, and the difference of sea-surface temperatures between an upwelling zone and the surrounding waters is a parameter for defining upwelling intensity [4]. In these environments, phytoplankton growth is primarily regulated by the availability of allochthon nutrients, primarily nitrates, which stimulate the production of phytoplankton [5].

2 Study area

The Straits of Messina (Figure 1), at the center of the Mediterranean Sea, is an area where strong currents determine fast changes in the oceanographic conditions. This system, separating the Italian peninsula from Sicily, is an amphidromic point for the tides of the Tyrrhenian in the northwest and the Ionian seas in the southeast. Morphologically, the Strait resembles a funnel-shaped geometry with a northsouth length of 40 km and a west-east width ranging from 3 km near the Tyrrhenian edge, to about 25 km at the Ionian open boundary. The narrowest section (Ganzirri–Punta Pezzo), which coincides with the sill region, has a depth of about 80m and divides the area into northern and southern sectors. The sea bottom slopes steeply downward to a depth of 1000m at 19 km south of the sill. The northern sector has a gentler slope, and the 400m isobath is located 15 km north of the sill toward the Tyrrhenian Sea. The Straits exhibits strong tidal currents driven by both barotropic and baroclinic processes, due to strong bathymetric constraints exerted by the sill and coastal morphology [6]. Large gradients of tidal displacements are encountered in the Straits of Messina, because the predominantly semidiurnal north and south tides are approximately in phase opposition. Due to both

Figure 1: Study area.

phase opposition and topographic constrictions, the current velocities can attain values as high as 3.0ms^{-1} in the sill region, and are related to the position of the sun, the phase of the moon, the wind speed and direction, and the air pressure distribution [7]. Surface water turbulence in the Straits is mainly influenced by two types of circulation, a steady surface current and a turbulent mixing, both of which generate discontinuity of the thermo–haline distribution in the surface layer. The steady current has a maximum speed of 2m·s^{-1} and a prevalently north to south direction at the surface (0–30m). Water turbulence is caused both by internal waves and by tidal currents [8]. Internal waves are caused by differences in water mass densities of the two basins that are facing in the Straits. Tidal currents are caused by opposite tidal oscillations of the two basins (max 27 cm) with almost the same amplitude and period (about 6 1/4 h). These conditions lead to the upwelling of deeper water of Levantine Intermediate Water origin, which is colder, more salty and more nutrient-rich compared to the Tyrrhenian Surface Waters (Atlantic Water origin). Harmonic oscillations of the current flowing from the Tyrrhenian Sea waters into the Ionian Sea (high tide current), and from the Ionian water into the Tyrrhenian Sea (low tide current) are encountered, with a brief slack water interval (balancing flow). Because of these particular environmental features, the Straits have been studied by many researchers in order to define forcing factors that determine its current regimen [9]. Many hydrobiological studies have been conducted over the last few decades to describe the influence of complex hydrodynamic conditions on biological parameters [10, 11].

Figure 2: MIVIS surveys with superimposed the cruise tracks followed by the R/B "Delfo".

3 Instruments and methods

Since 1994, the IAMC-CNR (Institute for coastal marine environment) measures temperature, salinity, and phytoplankton by continuous underway surface measurements during the dedicated oceanographic cruises. During 1999-2002, remote sensing surveys were performed with MIVIS airborne sensor and specific in-situ measurements. Specific in-situ measurements meet the requirements to validate the empirical algorithm applied to remotely data in order to retrieve the phytoplankton and, the remote sensing provides a synoptic view of upwelling phenomenon by mapping the SST and the phytoplankton into the water body of the strait.

3.1 Oceanographic cruises

Spatial and temporal distribution patterns of physicochemical (temperature, salinity, and nutrient concentrations) and biological (chlorophyll−a measured by *in situ* fluorescence emission), data are presently available for the central-northern side of the Straits of Messina. Discrete water samples (nutrients, chlorophyll−a, etc.) based on conventional methods were collected

during the surveys. The wind, air temperature and pressure were measured during each hydrographic cruise. Automatic real-time data were obtained by monthly surface tracking in the area between Capo Peloro (Sicily) to the north and Reggio Calabria to the south. This area was covered on the R/B "Delfo" using zigzag cruise tracks between the Calabrian and Sicilian coasts, adopting the lagrangian method in order to follow the wave of tide in the Strait. The location of the area and the track followed by the boat in each survey is displayed in Figure 2. It iswell known that the maximum intensity (> 3 $\mathrm{m{\cdot}s^{-1}}$) of the tidal currents occur during spring tides, corresponding to syzygy lunar phases. Measurements were carried out when the water slackens during the spring tide period to individuate the upwelling of deeper waters. Prior to taking measurements, the current forecast from "Tide tables of the Istituto Idrografico della Marina, Genova" was used in order to seize the quasi-stationary situations following the dynamic phases of high (high tide current, 3 h/cruise) and low (low tide current, 3 h/cruise) tides. Parameters taken into consideration in the present work are temperature and fluorescence, continuously (each 30 seconds) measured by means of a multiparameter probe (Meerestechnich Elekronik) and a fluorometer (Haardt-Mod1101LP).

3.2 Remote sensing surveys

3.2.1 Hyperspectral instrument

In situ: The ground-based acquisition have been performed by means of the FieldSpec Pro FR spectroradiometer (ASD). The ASD is a portable instrument covering the spectral domain between 350 nm and 2500 nm, sampled to 1 nm. Remote: The hyperspectral data have been acquired by the airborne MIVIS (Multispectral Infrared and Visibile Imaging Spectrometer) sensor. The MIVIS is a whiskbroom scanner composed of 4 spectrometers covering the spectral domain from 420 to 12700 nm by 102 channels. The scanner geometry is characterized by a Field of View of 90°.

3.2.2 Methods

In situ: During the remote sensing surveys, field measurements were collected to investigate spatial variability of physical, chemical and biological parameters, in particular in each station were collected water samples and performed Optical Measurement. The sampling stations were collocated between Sicily and Calabria coasts. Samples of water for the retrieve of CDOM, TSM (Total Suspended Matter) and chlorophyll-a at the surface and at 25 m depth were collected. At the same time the radiance upwelling from the sea surface and downwelling from the sky was recorded. All acquisition and elaboration procedures followed the Ocean Optics Protocols [12, 13]. The procedure for hyperspectral sea surface reflectance measurement is based on the acquisition of the upwelling and downwelling radiance according to SeaWifs Protocol [14]. Whereas, the reflectance measurements over land are directly the outputs of the instrument. The reflectance is obtained from the relative radiative measurements achieved by a fast double acquisition (target and reference panel) fixed in a nadir pointing configuration. During acquisition time some roles were respected in order to facilitate Rrs estimation and avoid other undesirable effects. At the same time of the remote sensing survey, reflectance spectra of some ma-

terials situated in land over Sicily and Calabria coastal areas, necessary for the atmospheric correction of the MIVIS images, were measured. Remote: The joint MIVIS (CNR LARA) and sailing vessel (CNR IST) campaign were carried out on 25th September 1999 at 2:00 p.m., on 2nd July 2000 at 12:00 a.m. and on 15th May 2002 at 11:30 a.m. in correspondence of the syzygy moon phase, when tidal currents reach maximum intensity. The MIVIS remote sensed 3 scenes with a NNE-SSW and SSW-NNE direction at the altitude of 4000 meters and a scanning speed of 16.5 Hz (Figure 2). A further scene was recorded over Messina at the altitude of 1500m (resolution at ground of about 3m). Preprocessing (sun glint effect): To assess the suspended and dissolved matter in water in the visible and near infrared spectral regions it is necessary to estimate with adequate accuracy the water leaving radiance [15]. Consequently radiance measured by a remote sensor has to be corrected from the atmospheric and the sea surface effects consisting in the path radiance and the sun and sky glitter radiance contributions. This paper describes the application of the sun glint correction scheme on to airborne hyperspectral MIVIS measurements acquired on the area of the Straits of Messina during the campaign in July 2000. In the Messina case study data have been corrected for the atmospheric effects and for the sun-glitter contribution evaluated following the method proposed by Cox and Munk [16]. Comparison between glitter contaminated and glitter free data has been made taking into account the radiance profiles relevant to selected scan lines and the spectra of different pixels belonging to the same scan line and located outside and inside the sun glitter area (Figure 3). The results show that spectra after correction have the same profile as the contaminated ones, although, at this stage, free glint data have not yet been used in water constituent retrieval and consequently the reliability of such correction cannot be completely evaluated [17].

4 Discussion and conclusions

The MIVIS has moreover stressed upwelling areas of the Straits of Messina, previously only hypothesised though never ascertained by the continuous traditional monitoring. As a matter of fact, because of the great space-time variability of the physical-chemical and biological parameters, the monitoring of the Straits by means of the vessel sailing was restricted both from time and space points of view. Therefore, monitoring techniques offered by the MIVIS hyperspectral data have provided for an instantaneous global view of the Straits integrating measures taken continuously by the sailing vessel. Then, the monitoring the Straits of Messina by means of the combined MIVIS and sailing vessel campaigns during the entire yearly cycle, could allow in the future a better vision of the sea circulation and its effects on the biological activity of the system during the seasonal variations.

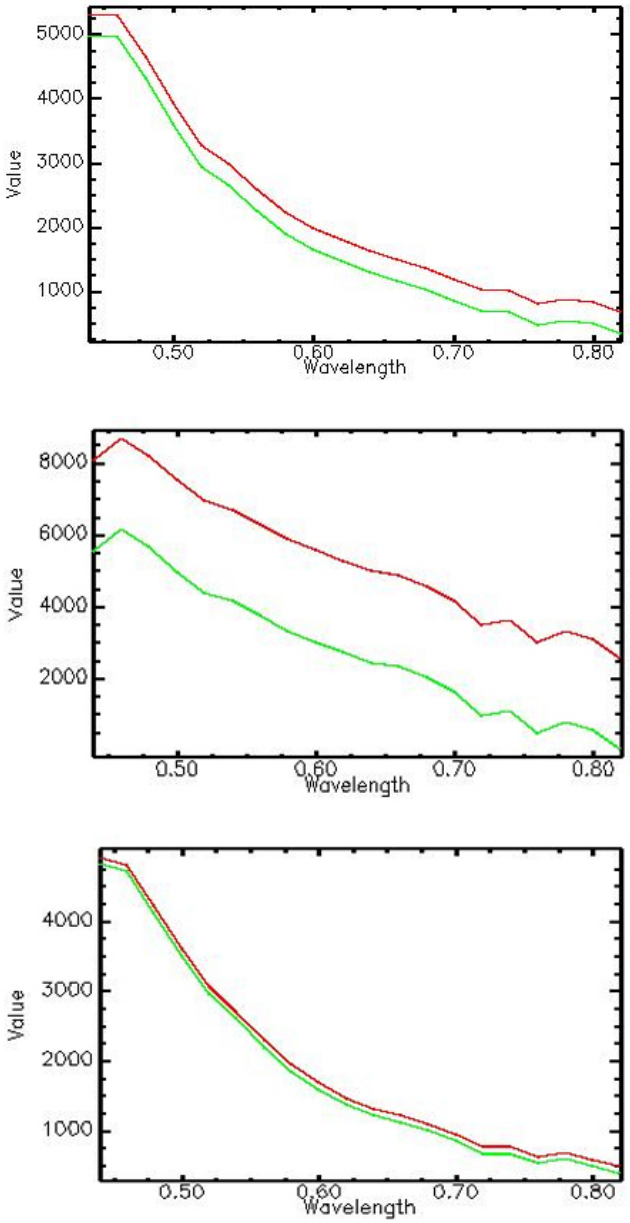

Figure 3: Comparison between spectra before (in red) and after (in green) the sun glint correction, relevant to three different pixels located outside (top and bottom) and inside (central graph) the sun glitter area.

References

[1] GEOSS. 10-Year Plan Reference Document. 2005.

[2] C. Bassani, C. Cattaneo, R.M. Cavalli, L. Fusilli, S. Pascucci, and S. Pignatti. The HYPerspectral for Adriatic Coastal Monitoring (HYPAD.COM) project. *ISRSE 33rd International Symposium on Remote Sensing of Environment. Sustaining the Millenium Development Goals*, 2009.

[3] F. Gomez, G. Gorsky, E. Garcia-Gorriz, and M. Picheral. Control of the phytoplankton distribution in the Straits of Gibraltar by wind and fortnightly tides. *Estuarine, Coastal and Shelf Science*, 59:485–497, 2004.

[4] A. Reul, V. Rodriguez, F. Jimenez-Gomez, J.M. Blanco, B. Bautista, T. Sarhan, F. Guerrero, J. Ruiz, and J. Garcia-Lafuente. Variability in the spatio-temporal distribution and size-structure of phytoplankton across an upwelling area in the NW-Alboran Sea, (W-Mediterranean). page 589–608, 2005.

[5] C.T.A. Chen, L.Y. Hsing, C.L. Liu, and S.L. Wang. Degree of nutrient consumption of upwelled water in the Taiwan Strait based on dissolved organic phosphorus or nitrogen. *Mar. Chem.*, 87(3-4):73–86, 2004.

[6] T.S. Hopkins, E. Salusti, and D. Settimi. Tidal forcing of the water mass interface in the Straits of Messina. *J. Geophys. Res.*, 89:2013–2024, 1984.

[7] A. Defant. Physical Oceanography. 2, 1961.

[8] N. Alpers and E. Salusti. Scylla and Charybdis observed from space. *J. Geophys. Res.*, 88(3):1800–1808, 1983.

[9] E. Bohm, G. Magazzu, L. Wald, and M.L. Zoccoletti. Coastal currents on the Sicilian shelf south of Messina. *Oceanologica Acta*, 10:137–142, 1987.

[10] F. Azzaro, F. Decembrini, F. Raffa, and E. Crisafi. Seasonal variability of phytoplankton fluorescence in relation to the Straits of Messina (Sicily) tidal upwelling. *Ocean Science*, 3:451–460, 2007.

[11] F. Azzaro, R.M. Cavalli, F. Decembrini, S. Pignatti, and C. Santella. Bio-Chemical and Dynamical Characteristics of the Messina Straits Water by Means of Hyperspectral Data. *SPIE Proceedings Series*, 4154(240-248), 2000.

[12] B.G. Mitchell, M. Kahru, J. Wieland, and M. Stramska. Determination of spectral absorption coefficients of particles, dissolved material and phytoplankton for discrete water samples. In: J.L. Mueller, G.S. Fargion, and C.R. McClain (Ed.). *Ocean Optics Protocols for Satellite Ocean-Color Sensor Validation. NASA Tech. Memo. NASA Goddard Space Flight Center, Greenbelt, MD.*, 4(Rev4):39–54, 2003.

[13] J.L. Muller. In-water radiometric profile measurements and data analysis protocols. In: J.L. Mueller, G.S. Fargion, and C.R. McClain (Ed.). *Ocean Optics Protocols for Satellite Ocean-Color Sensor Validation. NASA Tech. Memo. NASA Goddard Space Flight Center, Greenbelt, MD.*, 3(Rev4):39–54, 2003.

[14] G.S. Fargion and J.L. Mueller. Ocean Optics Protocols for Satellite Ocean Color Sensor Validation: Revision 2. *NASA Tech. Memo*, pages 2000–2096, 2000.

[15] F. Santini, L. Alberotanza, R.M. Cavalli, and S. Pignatti. A two-step optimization procedure for assessing water constituent concentrations by hyperspectral remote sensing techniques: An application to the highly turbid Venice lagoon waters. *Remote Sensing of Environment*, 2010.

[16] C. Cox and W. Munk. Measurements of the roughness of the sea surface from photographs of the sun's glitter. *J. Opt. Soc. Am.*, 44:838–850, 1954.

[17] R.M. Cavalli, S. Pignatti, and E. Zappitelli. Correction of sun glint effect on MIVIS dataof the Sicily campaign in July 2000. *Annals of Geophysics*, 49(1), 2006.

Modular Multiparametric Analyser for Automatic Vessel Monitoring of Nutrients in Sea-Water

F. Azzaro
Institute for Coastal Marine Environment, CNR, Messina, Italy
filippo.azzaro@iamc.cnr.it

Abstract

This paper describes the characteristics of a prototype of a modular multiparametric analyser (MicroMAC FAST MP3) for automatic monitoring of sea water and analytical methods for nutrients. The MicroMAC FAST reactor is an evolution of the basic LFA (Loop Flow Analysis) reactor. It has been conceived to assay ammonium, nitrate-nitrite and orthophosphate at low concentration in sea water samples. A sample analysis is 3-4 times faster than that obtainable with a standard LFA reactor. With respect to the previous analyser a temperature control (30-52 °C) on the measurement cell has been added (NH_4, PO_4), while the colorimeter and the related links for transporting the sample have been moved beyond the Loop and form a hydraulic-optical set almost completely independent from the main LFA. All the steps of a wet-chemical colorimetric analysis method are carried out in an analysis cycle sequentially. This new technique allows the preparation of two products of reaction which can be introduced at intervals of 150 seconds in the measurement cell. The statistical test show that the results of automated and manual analyses agree for all the examined parameters ($\leq$4 % RSD). Multiparametric online analyzer: it is possible to connect the analytical modules to a data logger with analogue and digital signals, in order to have online simultaneous analysis of the sample. A typical application is used during research at sea which vessel does not require an operator.

1 Introduction

In the last thirty years an ever increasing number of automatic tools for Colorimetric analysis, principally using "Continuous Flow Analysis" [1, 2] and "Flow Injection Analysis" [3, 4, 5] have been devised. The analysers of this kind, employed for the determination of phosphorus and nitrogen salts, generally have detection limitations, insufficient to satisfy the analytical demands concerning sea-water, generally characterized by poor nutrients.
The need to have automatic monitoring operations during real-time determination of some chemical parameters (such as nutrients) in environments at risk, has made the realization of an automatic chemical analyser suitable for onboard installation.
The MicroMac Fast MP3 (MultiParametric) is an automatic chemical analyser for rapid measurement of seawater (Figure 1), based on analytical technology developed by Systea (an Italian company) and named LFA (Loop Flow Analysis). LFA has permitted levels never reached before in analytical automation and in analyser miniaturization. All the steps of a wet-chemical colorimetric analytic method are carried out in an analysis cycle sequen-

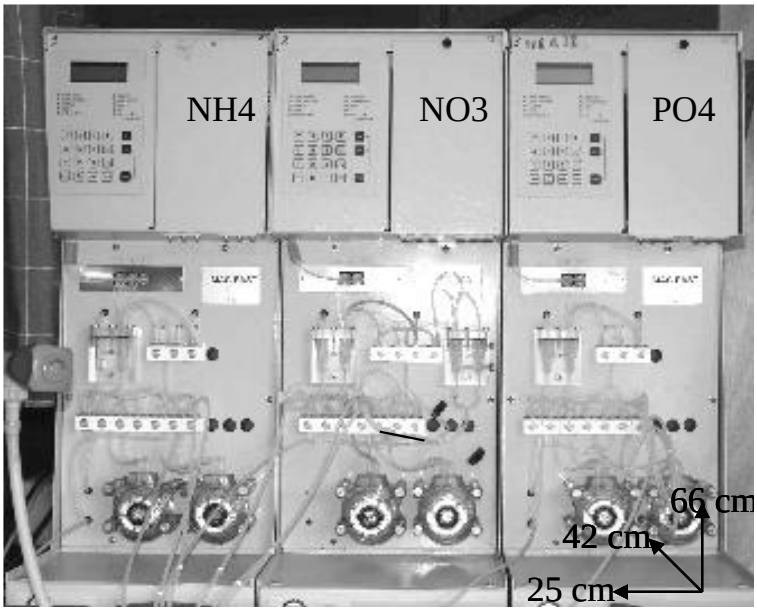

Figure 1: Module ammonia, nitrate and orthophosphate.

tially. The LFR reactor components are sequentially connected to form a Loop, that can be opened (sampling position) or closed (analysis position) by means of 2x3 ways valve. The hermetic closed Loop provides full protection against background interference, a basic requirement for stable trace analysis. At the beginning of a cycle the loop is washed and filled with a sample. The sample color is measured for compensation. Small amounts of concentrated reagents are added and vigorously mixed.

2 Materials and methods

2.1 MicroMac Fast description

The MicroMac Fast is an evolution of the basic reactor LFA and has been conceived for the fast determination of nutrients in seawater. In fact, the frequency of the measurements is 4 times faster than that achieved with previous versions of the instrument μMAC 1000 [6].

With respect to the LFA standard reactor, the colorimeter and the circuit hydraulic connections to bring the sample and the wash of the flowcell, has been shifted outside the loop and make an hydraulic-optical assembly independent from the normal dosing loop (Figure 2). In the Fast system, the LFA standard reactor can make normal and maximum speed, sampling and reagent dosing, similar to the normal LFA reactor. To speed up the reaction, a heating bath (30–52 °C) has been inserted in the circuit, which is made of a teflon tube coiled around an aluminium heater (only for modules NH_4 and PO_4). As in the normal LFA reactor, a SAMPLE/LOOP valve positioned in sample S and the peristaltic pump P1 is activated in direct to draw the

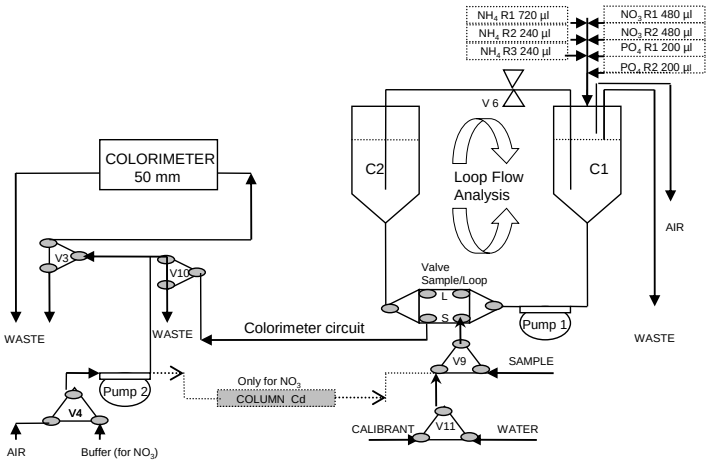

Figure 2: Hydraulic schematic diagram for determination of ammonia, nitrate and orthophosphate.

sample. The sample is drawn up through the V9, starts to flow inside the Loop, washing out the liquid present here. At the end of the sampling, the S/L valve is placed in the Loop and the reagents are injected and mixed as in the normal LFA reactor. At the end of the mixing, the S/L valve is positioned in Sample, the valves V10 and V3 are activated realising a link between LFA base and the colorimeter circuit. The pump P1 is activated in direct for a convenient time to transfer the product of reaction inside the colorimeter. The V10 and V3 are deactivated, disconnecting the colorimeter circuit from the LFA base, which is connected to the waste line through of V10 valve. An extra prolonged activation of the P1 pump, with V9 connected to the sample, allows for complete disposal of the product. A part of this has been transferred to the colorimeter to fill the LFA base circuit with the next sample. The steps required for sampling are the dosing of reagents and their mixing with the sample just aspirated, the product of reaction of the previous sample which is still left inside the colorimeter. This allows sufficient time to for complete color development, that reaches maximum efficiency during the mixing and heating phases in the LFA part of the reactor.

Before transferring the product of the reaction into the colorimeter, the raw optical density of the sample is read and stored. The following wash cycle of the flowcell occurs: activation of V3 valve, activation of V4, activation of P2 (to allow the aspiration of a small portion of air to increase the cleaning efficiency of the flowcell), deactivation of V4 and activation of P2 (to better clean the flowcell), deactivation of P2 and V3 and measuring of the sample blank. As previously said, the new product of reaction can be transferred to the flowcell by the modality described above. This new technique allows the preparation of two products of reaction which can be introduced at 150 second intervals in the measurement cell. The analytical time from

introducing a sample to having a result is 300 seconds. The intensity of the color of the reaction product is measured on the colorimeter using a monochromatic light beam of specific wavelength.
The Fast MP3 is a modular analyser and each analytical module is independent. Numeric results are stored in a system memory together with analytical graphics for further evaluation. The results are given in concentration units.
On line monitor: each module can be used as a stand alone on line monitor or portable analyzer with IP65 protection, the built-in software includes all the functions needed for on line analysis (16-key keyboard): results on display (2x16 row LCD), internal memory up to 100 results, remote printout of stored results, analog output for recorder connection, RS232 serial port. The PC software, expressly developed under Win 95/98 OS, allows a simple and complete management of all the analyzer functions, from autocalibration to results presentation.

2.2 Reaction and OD reading

The reaction takes place in all points of the reactor and therefore in the colorimeter flow cell, thus allowing the monitoring of the reaction from time 0 (reagents injection) to the end point.
If methods require heating, to speed up the colour development (i.e. for NH_4, PO_4) only the colorimeter flow cell will be heated at the requested temperature.
At the reaction end point, measured OD (optical density) is stored.

2.3 Calculations

Reagent Blank OD: stored and used to calculate the calibration factor.
Calibrant OD: stored and used to calculate the calibration factor.
Sample OD: stored together Sample Blank OD and used to calculate Sample concentration.
Sample concentration = (Sample OD – Sample Blank OD – Reagent Blank OD) x Calibration factor.
The wet chemistries used in Fast MP3 are those recommended by international standards [7].

2.4 Determination of ammonia in seawater

In this automated method, the ammonia ions present in the sample react with phenol and hypochlorite in an alkaline medium according to Bethelot's reaction. The trisodium citrate and EDTA are added to the sample to avoid the precipitation of alkaline hydroxides, while nitroprusside acts as a catalyst. The indophenol blue is measured at 630 nm.
Ammonia reagents. The complexing agent for seawater was trisodium citrate, dihydrate 25 g, EDTA, disodium salt 2 g, sodium nitroprusside 0.4 g, deionized water (DIW) q.s. 100 ml. The phenol reagent was phenol, solid and colorless 6.4 g, sodium hydroxide 2.75 g, DIW q.s. 100 ml. The Chlorine reagent was dichloroisocianuric acid (D.I.C.), sodium salt 1 g, sodium hydroxide 4 g, DIW q.s. 100 ml.
Ammonia standard solutions. The standard stock 1000 $mg \cdot l^{-1}$ NH_3 as N (solution A) was ammonium sulphate anhydrous 4.714 g, chloroform 10 drops, DIW q.s. 1000 ml. One ml of solution A when diluted to 100 ml of water gives a working standard of 10 $mg \cdot l^{-1}$ ammonia (solution B). 5 ml of solution B when diluted to 500 ml of natural low nutrient seawater

(LNSW) gives a working standard of 100 ppb NH_3 as N. That is actually introduced into the analyzer for calibration.

2.5 Determination of nitrate-nitrite in seawater

In this automated method, the nitrate present in the sample is reduced to nitrite in a coppered cadmium column, in a buffered medium. The nitrites formed and the ones already present in the sample, react with sulphanilamide and N-(1-naphtyl) ethylendiamine in acid medium to give a colored diazonium salt, which is measured at 550 nm.

Nitrate reagents. The washing water was deionized water. The sulphanilamide (SAA) reagent was sulphanilamide 2.5 g, concentrated hydrochloric acid 25 ml, DIW q.s. 250 ml. The naphtylethylendiamine (NED) reagent was N-(1-naphtyl) ethylendiamine x 2 HCl 0.375 g, DIW q.s. 250 ml. Buffer solution was imidazole 4 g, concentrated hydrochloric acid 1 ml, DIW q.s. 1000 ml.

Nitrate standard solutions. The standard stock 1000 $mg{\cdot}l^{-1}$ NO_3 as N (solution A) was sodium nitrate anhydrous 6.068 g, chloroform 10 drops, DIW q.s. 1000 ml. One ml of solution A when diluted to 100 ml of water gives a working standard of 10 $mg{\cdot}l^{-1}$ nitrate (solution B). 5 ml of solution B when diluted to 500 ml of LNSW gives a working standard of 100 ppb NO_3 as N. That is actually introduced into the analyzer for calibration.

2.6 Determination of phosphate in seawater

In this automated method, the orthophosphate present in the sample reacts with molybdate in an acid medium to form phosphomolybdate, and then with ascorbic acid to form molybdenum blue, whose intensity is measured at 880 nm. The antymonium catalyzes the reaction.

Phosphate Reagents. The molybdate reagent was antimony potassium tartrate 120 mg, ammonium heptamolybdate tetrahydrate 4.3 g, concentrated sulphuric acid 27 ml, DIW q.s. 250 ml. The ascorbic acid reagent was ascorbic acid 10 g, DIW q.s. 100 ml.

Phosphate standard solutions. The standard stock 1000 $mg{\cdot}l^{-1}$ PO_4 as P (solution A) was potassium hydrogen phosphate anhydrous 4.394 g, chloroform 10 drops, DIW q.s. 1000 ml. One ml of solution A when diluted to 100 ml of water gives a working standard of standard 10 $mg{\cdot}l^{-1}$ phosphate (solution B). 5 ml of solution B when diluted to 500 ml LNSW gives a working standard of 100 ppb PO_4 as P. That is actually introduced into the analyzer for calibration.

3 Results and analyses

The colorimetric methods examined have different reaction rates reaching the maximum value of optical density for ammonia after 60 minutes, nitrate after 8 minutes and phosphate after 25 minutes [8]. The difference between the value of optical density read at time T2 and that recorded at time T1 is proportional to the nutrient concentration under examination. The Fast MP3 is a sensitive instrument, also able to detect variations in optical density in the order of a tenth of mAU; therefore, it is not necessary for the colorimetric dose to wait for the complete development of the color (Figure 3). The value of the time T2 usually results from the compromise between

Figure 3: Recorder traces - Orthophosphate product of reaction in 300 seconds, frequency samples each 150 seconds.

the need for the maximum development of color and the number of analysed samples per unit of time.
An important aspect of the system concerns the possibility sample blank measurement and colorimeter zeroing, measuring the optical density immediately after the addition of reagents and the aspiration in the cell, making the approximation that at T1 the colorimetric reaction has not yet occurred. With this stratagem it is possible to correct the value of the optical density, compensating for variations linked to the instability of the lamp, salinity or torbidity of the matrix [9], without resorting to dual ray systems. In Table 1 the analytical protocols for the three considered parameters in sea water are summarised. The calibration of the analysers may be done either with a reading of a standard (100 ppb) located in the reaction chamber or the factor may be set from a series of standard readings at various concentrations, aspirated as samples.

3.1 Accuracy and precision

The precision of the analysis was evaluated by analysing a series of standard solutions (15, 10, 7, 5 and 2.5 ppb) 15 times for all the methods and calculating the relative standard deviation % (RSD) of the measurements (Table 2). The analysis precision proves satisfactory with a % RSD average of 2.5 for the ammonia, 4.0 for the nitrates and 2.7 for the phosphates.

3.2 Comparison of manual and automated chemical analyses

Intercalibration of manual and automated procedures is necessary to detect systematic bias in either method, and to ensure that data from automated analyses are compatible with data from manual analyses. Stock Standards (15, 10, 7, 5, 2.5, 2 ppb prepared in low-nutrient seawater) were used to test the agreement between the Fast MP3 (lightpath 50 mm) and the spectrophotometer determinations Varian Mod. Cary 50 (lightpath 50 mm).

Test	1	2	3
Name	ammonia	nitrate+nitrite	phosphate
sample introduction	Aspiration	Aspiration	Aspiration
first reagent	Citr. Hypoch.	SAA	Ammon. Molyb.
second reagent	Phen.alk + DIC	NED	Ascorbic acid
mixing conditions		Turbulent	
colorimeter	630 nm	550 nm	880 nm
light path	50 mm	50 mm	50 mm
range		0.001 ÷ 1.3 absorbtion units	
kind of measurem.	end point	end point	end point
uses blank	yes	yes	yes
sample blank		automatic zeroing at the end of sampling	
calibration		automatic preparation of the working calibrant	
units	ppb	ppb	ppb
decimal digits	4	4	4
calib. ratio mode	factor	factor	factor

Table 1: Analytical protocol for the ammonia, nitrate+nitrite and phosphate determinations.

3.3 Correlation coefficient

Results indicate good agreement of the two methods with a correlation coefficient R^2= 0.94 for NH_4, 0.98 for NO_3 and 0.96 for PO_4, calculated on n= 86 (Figure 4). The determinable minimal concentration for methods nitrate and orthophosphate is 2.5 ppb while for ammonium it is 5 ppb, considering that the readings below that value were not perfectly repeatable as they were for other concentrations. If the values of 2 ppb were removed then the correlation coefficient would be R^2= 0.99 for NH_4, 0.99 for NO_3 and 0.99 for PO_4, calculated on n= 71

3.4 Instrumental drift

A standard solution (15 ppb) for each method in seawater was analyzed, every 150 seconds, per two hours. The solutions were prepared in a 5 liters container and stirred with a magnetic stirred. The results, shown in Figure 5 do not reveal any instrumental drift.

3.5 Carryover studies

The effects of carry-over which may be present when solutions at highly varied concentrations are sequentially analysed have been evaluated. The Broughton carryover percentage (K) was calculated according to the equation: carryover (%) = [(L1 - L3)/(H3 - L3)] x 100 [10]. Three consecutive samples with high (H) concentrations (ex 500 ppb of NH_4) were measured, followed by three samples with low (L) concentrations (ex 10 ppb of NH_4), and this sequence was repeated five times. All the measurements made as well as for the three analysed parameters, a carry-over coefficient superior than 0.3 % has not been highlighted.

Nutrient Species		Known Concentration (ppb)				
		15	10	7.5	5	2.5
Ammonia	Mean Concentrat.	15.01	9.64	7.30	4.68	2.10
	Stand. Deviation	0.13	0.16	0.10	0.20	0.10
	% RSD	0.84	1.68	1.37	4.13	4.55
Nitrate	Mean Concentrat.	15.07	10.01	7.46	5.01	2.47
	Stand. Deviation	0.37	0.32	0.18	0.29	0.15
	% RSD	2.36	3.18	2.45	5.85	6.23
Phosphate	Mean Concentrat.	15.00	10.00	7.52	4.97	2.46
	Stand. Deviation	0.11	0.23	0.15	0.18	0.13
	% RSD	0.74	2.35	2.01	3.54	5.11

Table 2: Accuracy and precision for each method.

Parameter	detect. limit (ppb)	time analys. (second)	analysis rate Samples/h	vol. samp (ml)	vol. reag (µl)
ammonia	5	300	24	10	1200
nitrate-nitrite	2.5	240	30	11	960
phosphate	2.5	240	30	10	400

Table 3: Main characteristics for each method.

The three chemical parameters examined have different analysis times. The main characteristics of the devised automatic methods are summarised in Table 3.

Anomalous values were recorded occasionally during the various experiments, probably due to air bubbles in the circuit that created errors in reading the sample; these determinations were not included in the elaborations.

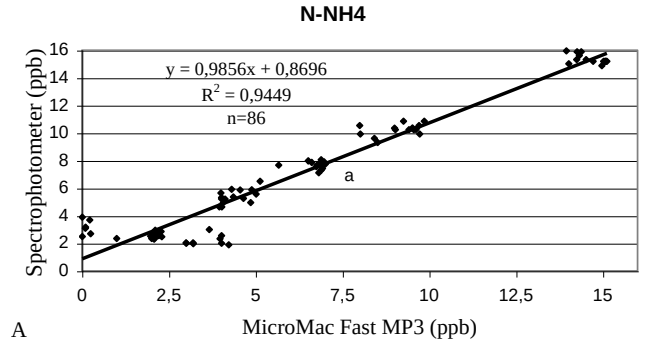

A

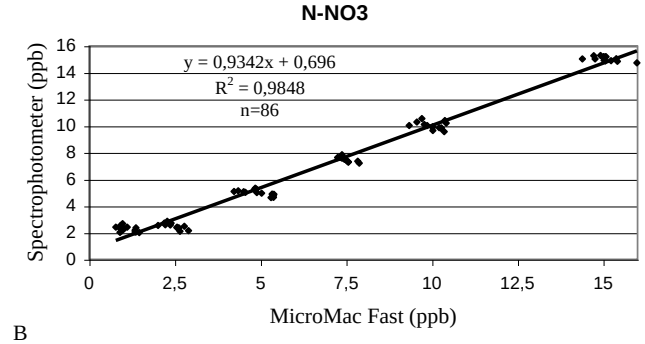

B

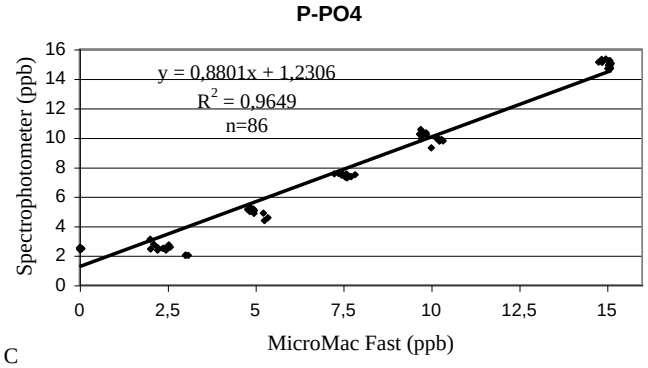

C

Figure 4: Linear regression analysis relationship between automated and manual determinations of ammonia (A), nitrate (B) and orthophosphate (C).

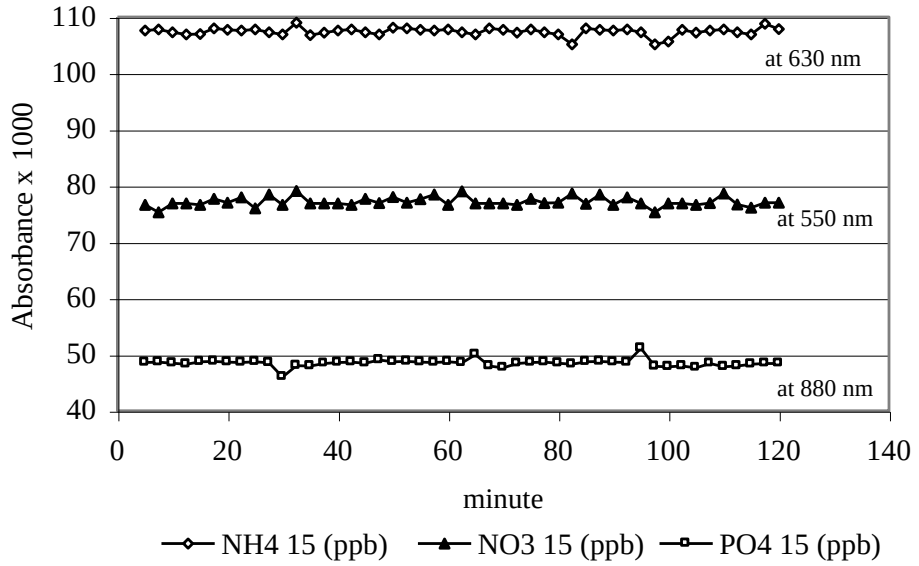

Figure 5: Instrument drift - A standard solution (15 ppb) for ammonia, nitrate and orthophosphate in seawater was analyzed, every 150 seconds.

4 Conclusions

The results obtained suggest that the MicroMac Fast MP3 autoanalyzer is reliable for the automatic performing of chemical analyses of ammonium, nitrate-nitrite and phosphates in sea water. The correlation with traditional methods is optimal, also considering the other positive experiments such as the repeatability of data and the absence of drift. In fact, the cleaning of the loops and the colorimeter is a very important feature for the seawater analysis. Indeed, in flow instrumentation the drift is a limiting factor especially for the orthophosphate analysis.
In the future, with regard to the analysis rate, it would be better that all the modules had the same analysis time in such a way to achieve coastal monitoring with the same analysis rate (every 150 seconds).
In conclusion, the μMAC-FAST MP3 meets the required characteristics for repeatability, accuracy and reading speed, with universally recognised analytical methods. Analysis of nutrients on an equipped boat is the typical application of MicroMAC Fast MP3 that can run a fully automated analysis of nutrients in seawater. Near real-time results, the possibility of connection with the boat positioning system and georeferencing, are the main features of the application.

5 Acknowledgements

The study was carried out within MURST (Italian Ministry for University and Scien-

tific Research) Cluster 10-SAM (Sistemi Avanzati Monitoraggio) Project. The author is grateful to A. Marini and M. Galletta for assistance with the analyses.

References

[1] J. Barwell-Clarke and F. Whitney. Institute of Ocean Sciences Nutrient Methods and Analysis. *Can. Tech. Rep. Hydrogr. Ocean Sci.*, 182:vi – 43, 1996.

[2] X.A. Alvarez-Salgado, F. Fraga, and F.F. Perez. Determination of nutrient salts by automatic methods both in seawater and brackish water: the phosphate blank. *Marine Chemistry*, 39:311–319, 1992.

[3] Y. Hiray, N. Yoza, and S. Ohashi. Flow injection analysis of inorganic ortho and poly-phosphate using ascorbic acid as reductant of molybdophosphate. *Chem. Lett.*, 5:499–502, 1980.

[4] C.B. Ranger. Flow Injection Analysis. *Anal. Chem.*, 53:20A, 1981.

[5] K.S. Johnson and R.L. Petty. Determination of nitrate and nitrite in seawater by flow injection analisis. *Oceanogr. Limnol.*, 28:1260–1266, 1983.

[6] F. Azzaro, E. Crisafi, G. Magazzù, F. Oliva, and A. Puglisi. Un nuovo fotometro automatico per la determinazione di nutrienti da boa Oceanografica. pages 213–226, 1994.

[7] J.D.H. Strickland and T.R. Parsons. A practical handbook of seawate analysis. *Bull. Fish. Res. Ed. Can.*, 167:1–311, 1972.

[8] N. Cardellicchio and M. Luzzana. Messa a punto di un prototipo di analizzatore colorimetrico programmabile per la determinazione automatica dei nutrienti in acqua di mare. *Atti del Seminario Tecnico Scientifico del Progetto Strategico "Monitoraggio automatico dell'Inquinamento Marino nel Mezzogiorno" Lecce Italy*, pages 137–158, 1993.

[9] P.N. Trodelich and M.F.Q. Pilson. Systematic absorbance errors with Technicon Autoanalyzer II colorimeters. *Water Reserch*, 12:599–603, 1978.

[10] P.M.G. Broughton, A.H. Gowenlock, J.J. McCormack, and D.W. Neill. A revised scheme for the evaluation of automatic instruments for use in clinical chemistry. *Ann. Clin. Biochem.*, 11:207–218, 1974.

R/V Luigi Sanzo: A Fifteen Meters Fully Equipped Boat for Coastal Monitoring

F. Azzaro, G. Zappalà, E. Crisafi
Institute for Coastal Marine Environment, CNR, Messina, Italy
filippo.azzaro@iamc.cnr

Abstract

Funded in the frame of the PI-CNR project (Cluster 10 MIUR), a coastal monitoring boat was designed and built to be used by the Ist. Talassografico of Messina (now CNR-IAMC). Launched in 2002, the boat is named after the first director of the Istitute, Prof. Luigi Sanzo, a world-wide known ichthyologist. The boat contains one wet (8 m^2) and one dry (10 m^2) laboratory equipped with refrigerators and freezers. Fresh and salt water lines are available in the lower deck, in the wet laboratory and astern. Deck instruments include one 2000 kg hydraulic crane, one hydraulic winch with 300 m of 6 mm armoured cable, one hydraulic winch with 200 m of 8 mm steel wire rope. A 1,5 m^3 afterpeak is available to hold oceanographic instrumentation under the 13 m^2 wide stern. Instruments for biological, coastal oceanography and monitoring researches are installed on the boat. A rosette equipped with 12-8 litres bottles and one CTDO probe with altimeter, fluorometer and turbidimeter enable to profile the water column. Continuous monitoring on surface water is obtained by a water line feeding both a measurement chamber in which a CTDO probe with integrated fluorometer-turbidimeter is fitted and a group of automatic colorimetric analyzers measuring NH_4, NO_3, PO_4. Meteorological data are measured by a station equipped with barometer, thermometer, anemometer, pyranometer. A data acquisition computer integrates data measured by the scientific instruments with navigation data coming from the GPS.

1 Introduction

Funded in the frame of the PI-CNR project (Cluster 10 MIUR), a coastal monitoring boat was designed and built to be used by the Ist. Talassografico of Messina (now CNR-IAMC). Launched in 2002, by the shipyard "NAVALTECNICA" in Rometta Marea (ME). The boat, owned and operated by IAMC, is designed for research in the coastal zone and instruments testing. It provides quick access to local coastal areas, but can work further offshore and closer inshore than is customary for a boat of its size. It also provides a special capability for the Institution's education program through support of student projects and training [1, 2, 3, 4, 5, 6, 7, 8, 9, 10]. This coastal monitoring boat remembers with its name the first director of the Istituto Talassografico in Messina, Prof. Luigi Sanzo, a world-wide known ichthyologist.

2 Ship specifications

The research vessel (R/V) L. Sanzo is able to operate in the coastal zone, along water column, to perform both basic and applied

Figure 1: The boat R/V Luigi Sanzo.

scientific research programmes, survey activities and monitoring (Figure 1). The R/V L. Sanzo has a cruising range of 350 nautical miles with a typical endurance 1 day, occasionally 2-3 days. Its crew includes a captain and a mate, one officer, and up to 11 scientists on one-day trips. The lower deck hosts a bow cabin with four berths and a fully equipped bathroom. Over that cabin, a flying bridge is available. To obtain the maximum ease of use, three steering and engine command sites are available: in the cockpit, on the upper deck, and astern, near the crane (Figure 2a, 2b, 2c). The main features of the boat are as follows:

- overall lenght 15 m;
- beam 4,3 m;
- max draft 1,2 m;
- max speed 30 knots;
- cruise speed 25 knots;
- propulsion 2 Caterpillar 570 Hp engines;
- electrical supply 8 kW - 220 V diesel generator;
- fuel tanks 3000 l;
- water reservoirs 2000 l;
- electrical bow-prop to maintain bearings during samplings;
- mobile wing system to trim attitude;
- fully air conditioned.

Navigation and safety instruments: Radar, echosounder, VHF, magnetic compass, autopilot, GPS plotter. Control instruments: Engine tachometer, attitude and helm angle indicators. Crane/winches: Hydraulic crane max load 2000 kg (6 m straddle and 360° rotation), Hydrological winch with ≪slip ring≫ double-drum with 300 m of 6 mm armoured cable for rosette system and 200 m cable of 8 mm iron rope for Side-Scan-Sonar, Sub-Bottom-Profiler, etc. (Figure 2d).

The main deck offers a wide open afterdeck and a cabin hosting (from stern to bow) the “wet laboratory” (8 sqm), the “common room-dry laboratory” (10 sqm) including a kitchenette, the cockpit (Figure 3). Laboratories are equipped with refrigerators and freezers. Fresh and salt water lines are available in the lower deck, in the wet laboratory and astern. A 1,5 m^3 afterpeak is available to hold oceanographic instrumentation under the 13 sqm wide stern (Figure 4). The boat is equipped with sampling and measuring instruments for biological, coastal oceanography and monitoring researches. Scientific instruments: SBE 32C rosette with 12 - 8 liters

Figure 2: The steering commands: in the cockpit (a), on the upper deck (b), astern near the crane (c), and particular crane/winches (d).

GO-flow bottles and multiparametric probe SBE 911/plus provided with an independent data processing and restitution system for vertical profiles of pH, temperature, conductivity/salinity, oxygen, pressure, density, redox, altimeter, and SCUFA fluorometer-turbidimeter. Its instrumentation includes an acoustic Doppler current profiler (ADCP), flow-through seawater sampling system, CTD system with conducting wire winch, and meteorological station. Large transducer wells are available for project use, and the transducers can be changed out from inside the boat while in the water. System for continuous monitoring on surface waters (Figure 5), comprising a SBE 19 plus CTDO probe (Temperature, conductivity/salinity, pH, oxygen, density, redox), SCUFA integrated fluorometer-turbidimeter (Scufa II) from chlorophyll a (Chla), Systea nutrient analyzer Micromac fast MP3 (nitrate-nitrite, ammonium and orthophosphate) determinations based on Loop Flow Analysis able to detect low nutrient concentrations every 150 sec. [8]. The on-board implemented measuring system is constituted by two connected instruments both automatically collecting parameters quickly (in time and in space). The output provides a real-time measurements stream and consequent data transmission to a PC by a multiplexed serial port. Integrated meteorological box supplied with: barometer, thermometer, anemometer, psycrometer (all system is connected to a microcomputer, true motion data). The scientific instruments are interfaced together with the positioning system to the main data acquisition computer, the data are available by video in the two laboratories.

Figure 3: "Wet" Laboratory (a left-side, b starboard), and "dry/computer" laboratory (c).

Figure 4: Afterpeak locker of stern with the rosette housing.

3 Ship Activities

The first investigations: that have been achieved were the Milazzo Gulf monitoring. The study was performed over 11 months (from February to December 2003) in the framework of Cluster 10 SAM Programme (Advanced Monitoring Systems) funded by the Italian National Ministry for Scientific Research [11, 3]. The adopted measurement approach couples an automatic coastal platform and periodic surveys by a research vessel. Meteorological and water column parameters were hourly collected by the platform. The survey strategy implemented with the research boat included a seasonal surface tracking along the coast with the on-board automatic system to measure CT-Fl and nutrients of N and P and two oceanographic campaigns in 11 stations along three transects vertical CTD profiles, nutrients of N and P, chlorophyll a). The study area is the Gulf of Milazzo, a natural bay of about 25 km^2 laying other northern coast of Sicily and open to the Tyrrhenian Sea. The central stretch of coast hosts two seasonally-controlled stream outflows. Cruises data allowed to reconstruct the distribution of Chla integrated in the euphotic layer (0-80 m), which reflects the general hydrodynamic features of the Gulf. Surface distribution of physico-chemical and biological parameters obtained along tracking survey are presented in Figure 6. The R/V Luigi Sanzo demonstrated to be a versatile, useful floating laboratory for coastal operations, enabling scientists to obtain sinopticity of observations also in rapidly changing water masses.

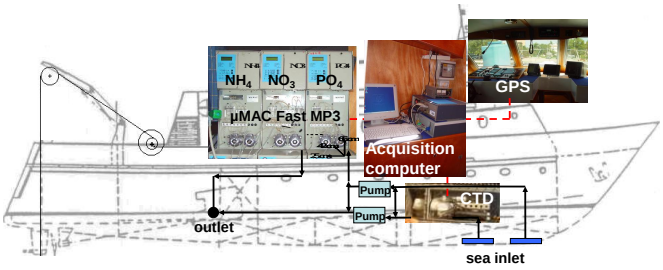

Figure 5: System for continuous monitoring on surface waters.

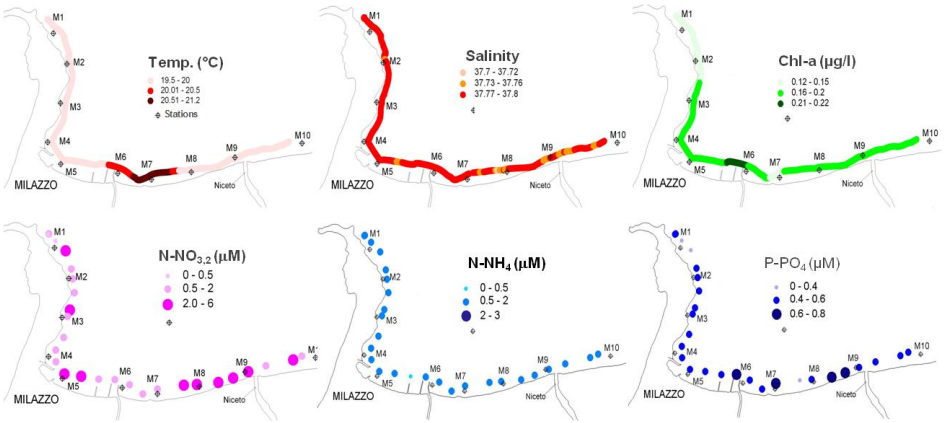

Figure 6: The representative surface distribution of physico-chemical and biological parameters (T, S, Chla and nutrients of N and P) obtained in tracking cruises.

4 Acknowledgements

The authors thank Mr. Franceso Soraci and Mr. Gianfranco Pandolfino, crew of the boat for their help during surveys.

References

[1] L. Alberotanza, F. Azzaro, F. Braga, R.M. Cavalli, S. Pignatti, S. Salviato, and F. Santini. Definizione di un modello bio-ottico per le acque dello Stretto di Messina. 1:51–56, 2004.

[2] F. Decembrini, F. Azzaro, M. Galletta, and F. Raffa. Short-term changes of hydrobiological features in the Gulf of Milazzo (Tyrrhenian Sicily). 37:511, 2004.

[3] F. Decembrini, F. Azzaro, A. Bergamasco, and F. Raffa. Real-time tracking and monitoring of sea-surface water quality: an experimental approach in a gulf of Tyrrhenian Sicily. 7:3763, 2005.

[4] A. Bergamasco, F. Decembrini, F. Azzaro, L. Guglielmo, and E. Crisafi. Caratteristiche Idrologiche nell'AMP Isole Ciclopi (Costa Ionica Sicilia) e relazione con la biodiversità del comparto planctonico. *Biol. Mar. Medit*, 12(1):52–62, 2005.

[5] G. Zappalà, G. Caruso, F. Azzaro, and E. Crisafi. Marine environment monitoring in coastal Sicilian waters. 95:337–346, 2006.

[6] G. Caruso, C. Garoppo, F. Azzaro, F. Raffa, and F. Decembrini. Comunità microbica nello stretto di Messina distribuzione e diversità funzionale. *Biol. Mar. Medit.*, 13:112–113, 2006.

[7] G. Caruso, G. Zappalà, G. Maimone, F. Azzaro, F. Raffa, and R. Caruso. Assessment of the abundance of actively respiring cells and dead cells within the total bacterioplankton of the Strait of Messina waters. 99:10, 2008.

[8] F. Azzaro and M. Galletta. Automatic colorimetric analyzer prototype for high frequency measurement of nutrients in seawater. *Marine Chemistry*, 99:191–198, 2006.

[9] F. Azzaro, F. Raffa, A. Marini, and P. Rinelli. Caratteristiche idrobiologiche del Golfo di Gioia (Tirreno Sud Orientale): estate 2005. *Biol. Mar. Medit.*, 14(2):336–337, 2007.

[10] F. Azzaro, E. Gangemi, A. Marini, and F. Raffa. Monitoraggio idrobiologico in un'area marina protetta: "Isole Ciclopi" (Sicilia orientale). 19:31–41, 2008.

[11] G. Zappalà, G. Caruso, and E. Crisafi. The SAM integrated system for coastal monitoring. pages 341–350, 2002.

Water Quality Remote Sensing of the Largest European Lagoon

C. Giardino[1], M. Bresciani[1], M. Bartoli[2]
1, Institute for Electromagnetic Sensing of the Environment, CNR, Milano, Italy
2, Department of Environmental Sciences, University of Parma, Parma, Italy
giardino.c@irea.cnr.it

Abstract

Coastal lagoons are transition zones between terrestrial and marine environments, characterized by high rates of primary and secondary productivity and elevated biodiversity. Worlwide deterioration of these aquatic bodies, resulting from excess nutrient inputs, has stimulated monitoring actions, addressed in particular to noxious blooms of microalgae.
In this study we use MERIS images to assess water quality in the highly eutrophied Curonian Lagoon, the largest European coastal bay (1584 km^2), bordering the southeastern part of the Baltic Sea. The algorithm developing was firstly addressed on atmospheric correction and secondly on water quality parameters retrieving. In particular, we focused on chlorophyll-a being an indicator of trophic level and on yellow substances because their role in protecting the aquatic biota from ultraviolet solar radiation and their influence on overall microbial activity in the water column. Two MERIS images respectively acquired in spring and summer 2009 were elaborated by using physically based approaches build using in-situ data collected synchronously to the sensor overpass. The results showed the patchy distribution of water quality in the lagoon with higher average chlorophyll-a concentrations observed in summer (50 $mg \cdot m^{-3}$) than in spring (27 $mg \cdot m^{-3}$) and a slightly opposite situation for yellow substances (1.6 m^{-1} in spring and 1.3 m^{-1} in summer).

1 Introduction - Lagoon ecosystems

Coastal lagoons are bodies of shallow salt or brackish waters separated from the deeper sea by sand bars, coral reefs, or similar features [1]. Lagoon ecosystems are complex habitats at the interface between terrestrial and marine environments, where light and nutrient availability and hydrodynamic features promote primary and secondary productivity and elevated biodiversity.
Highly productive in their ideal state, lagoons accumulate most anthropogenic and synthetic pollutants and are liable to become eutrophic. The coastal lagoons are habitats of conservation importance and as in other parts of the world [2] support communities which are unique in structure and diversity. They make up about 13% of global coastal environments [3] and have a number of physiographic attributes which increase habitat heterogeneity not only spatially by the presence of a multitude of ecotones providing refugia for diverse marine fauna and flora [4], but also temporally with the seasonal hydrological cy-

cle [5, 6]. These environments have also a high economic value, as locations for extensive aquaculture, and scientific value as natural laboratories to investigate short-medium term effects of anthropogenic impacts, as well as restoration plans.
Unfortunately, in many countries deterioration of lagoon's habitats has occurred (e.g., [7, 8, 9]) and to prevent further loss and ensure the safeguard of existing ecosystems, it is essential to monitor their contiguous uplands, and their water components. Similarly to any aquatic natural environment, the continuous monitoring of key biological and environmental parameters might present some major concerns since the phenomena to be observed in the lagoon might be characterized by a high rate of change, both in time and space. In particular, the collection of in-situ data with traditional techniques may not be sufficient for understanding the characteristic of such targets where the water quality conditions may change rapidly as a consequence of tides or meteorological constraints.
When deterioration of water quality is caused by optically active substances, the effect of these changes can be observed with optical remote sensing instruments. Remote sensing may therefore present a significant integrating technique for monitoring water quality in coastal lagoons. Besides to improve the spatial and temporal frequency of observation, satellite sensors also provide useful data to monitor lagoons located in remote regions.

2 Backgrounds - Water quality remote sensing

Remote sensing techniques have been extensively adopted for assessing water quality in oceans, coastal zones, lakes and transitional ecosystems as lagoons and deltas (e.g., [10, 11]). For their investigations, these aquatic environments have been traditionally split into two main categories, depending by the complexity of their inherent optical properties [12, 13]: case-1 waters are those waters whose optical properties are determined primarily by phytoplankton and related yellow substances and degradation products (e.g., oceans and seas). Case-2 waters are everything else, namely waters whose optical properties are significantly influenced by other constituents such as mineral particles, yellow substances originated either from degradation of phytoplankton or land runoff and tributaries inputs, whose concentrations do not covary with the phytoplankton concentration (e.g., coastal zones, estuaries, lagoon and inland waters). In the late 1970s and early 1980s the idealized concept of case-1 and case-2 water provided useful guidance for the development of the first generation of bio-optical models while nowadays it might be considered too much restrictive [14].
In recent years, the developments in water quality algorithms have mainly been driven by the advent of the SeaWiFS (Sea-viewing Wide Field of View Sensor), MODIS (Moderate Resolution Imaging Spectroradiometer) and MERIS (Medium Resolution Imaging Spectrometer) satellites and their specific capacities to sense the low radiances of aquatic ecosystems. The specifications of these sensors, their frequent data acquisition, high signal-to-noise ratio, and number and position of spectral bands, make them better suited than higher resolution sensors with broad bands, such as Landsat, for regular/real-time monitoring applications observing change occurring over short time scales. However, the

spatial resolution of ocean colour satellites is usually only about 1 km, which means that the satellite does not show variability at a small-local scale and is not adequate for the monitoring of small to medium-sized targets. Only MERIS, with its spatial resolution of about 300 m at Full Resolution (FR) mode, offers possibilities for improved coastal remote sensing. Furthermore, it also has a better spectral resolution than SeaWiFS and MODIS. The MERIS band 9, centered at 708 nm, has been shown to be vital for the detection of chlorophyll in turbid waters [15]. The MERIS band 6 around 620 nm was shown to be of high interest in the detection of cyanobacterial blooms since this band coincides partially with the absorption peak of the main cyanobacterial pigment phycocyanin [16].

In general, the parameters that have been identified in the literature as detectable in aquatic environments by modern satellites are: (1) the diffused attenuation as measure for the water transparency in the euphotic zone (e.g., [17]). The euphotic zone depth (Ezd) reflects the depth where photosynthetic available radiation is 1% of its surface value. The value of Ezd is an important parameter regarding ecosystems since in the Ezd most of the aquatic life occurs. (2) Green algae pigments mainly as chlorophyll-a (chl-a) used as a proxy of phytoplankton biomass and primary production (e.g., [18]). (3) Total suspended matter (TSM) which is placed in suspension by wind-wave stirring of shallow waters and is a tracer for inflowing pollutants (e.g., [19]). (4) Yellow substance (YS, also known as CDOM or coloured dissolved organic matter), which protect the aquatic biota from ultraviolet solar radiation and influence on overall microbial activity in the water column [20]. (5) The cyanobacterial pigment phycocyanin, potentially associated to harmful algal blooms [21].

Various methods were developed to estimate the water constituents from remote sensing images. Empirically based approaches using experimental data sets and statistical regression techniques generate empirical algorithms relating the water-leaving reflectances or radiances at the sensor in specific spectral bands or band ratios/combinations to in-situ water quality parameter measurements (e.g., [22]). The simplicity of the empirical approach means that it is easy to implement (especially in instances where in-situ data is regularly collected) and that the algorithms are generally robust [23]. However, the algorithms are limited to the specific constraints of the data set from which they are derived (and are thus not applicable across seasons or areas), perform accurately only inside their range of derivation, and have a limited ability to separate signals from different water constituents, especially in instances where there is covariance.

More complex semi-analytical approaches use a variety of inversion techniques, either as in-water or coupled water atmosphere algorithms, and are potentially more powerful in their ability to separate the signal of different in-water constituents (e.g., [24]) but their use of many, if not all of the spectral bands available, makes them more sensitive to errors in the atmospheric correction [25]. This approach have the advantage of being independent of concurrent in-situ measurements which makes them well suited to operational water quality monitoring systems, however it requires that the bio-optical specific inherent optical properties of the water body are known beforehand.

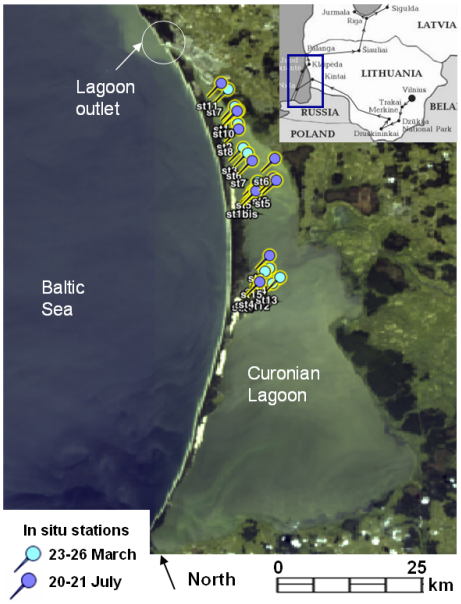

Figure 1: MERIS data acquired on 22 July 2009 with location of in-situ stations sampled in March and July 2009. The pseudo true colour MERIS image clearly shows the different optical behaviour of the Curonian Lagoon and the Baltic Sea waters.

3 Case study - The Curonian Lagoon

The Curonian Lagoon (Figure 1), belonging to Lithuania and to Russian Federation, is located in the south-eastern part of the Baltic Sea, from which it is separated by a narrow sand spit. With a total area of 1584 km^2, it is the largest lagoon in Europe. This water body receives nutrient-rich freshwater inputs from different tributaries, mainly from the Nemunas River, and occasionally wind-driven low-salinity water from the Baltic sea. Complex water circulation, variable depth, different sediment features and nutrient availability affect primary production and influence the concentration and distribution of nutrients and bio-chemical elements, thus leading to complex ecosystem.

Formed about 9,000 years ago, the Curonian Lagoon might be more properly considered as a freshwater body since the salt water intrusion is limited to the northern area only, where salinity varies from 0 to 8 PSU (Practical Salinity Unit) [26]. It is a shallow (average depth 3.7 m) transitory basin which is highly biodiverse, although troubled by water pollution. In particular, cyanobacterial blooms, which were observed recently [27] represent a major concern for water quality issues and potential risk for human health. The need and imminence for water quality monitoring in the Curonian Lagoon have been therefore recognized by the increasing of eutrophication that overall remains the main ecolog-

ical problem in the Baltic coastal lagoons and estuaries [26].
The Curonian Lagoon is also a good site for testing and developing techniques for remote sensing in optically complex waters, dominated by cyanobacteria and, similarly to both Boreal lakes and Baltic Sea, rich of yellow substances. The lagoon's wide size, the spatial heterogeneity of water quality patterns, and covariant water constituents present a challenging case for remote sensing both in terms of algorithm development and atmospheric correction.

4 Material and methods

4.1 Field campaigns

Field campaigns represent an important task to both develop robust image processing algorithms and to validate remote sensing-inferred products. In this study they were in particular performed for: (i) validating the performances of the atmospheric correction models, (ii) building a semi-empirical band-ratio based model for chl-a and (iii) assessing the accuracy of MERIS-derived products. Two field campaigns were conducted in March 2009 and July 2009 in coincidence to MERIS acquisitions. Remote sensing reflectance (Rrs) values were derived from submerged measurements of upwelling radiance and downwelling irradiance subsequently corrected for the emersion factor.
Water samples were collected at the surface and filtered for laboratory analysis of water quality parameters. Chl-a concentrations were determined according to the analytical method ISO 10260-E [28]. For YS, the absorbance of the filtered water was measured in a 5-cm cuvette, by using another cuvette filled with distilled water as a blank. A baseline correction in the range around 685 nm was applied and absorbance was converted into absorption coefficient of YS at 440 nm as showed in Strömbeck and Pierson [29]. In the same station a multi-wavelength probe was used in-situ to derive the algal composition of phytoplankton.

4.2 Image processing

MERIS is a medium resolution imaging instrument carried aboard the ESA's Envisat-1 satellite and operating since 2002 within a mission covering open oceans, coastal zone and land surfaces. The instrument's 68.5° field of view around nadir covers a swath width of 1150 km. MERIS is designed to acquire 15 spectral bands in the visible near-infrared wavelengths. Table 1 shows the position of MERIS spectral bands determined following a detailed spectral characterization of the instrument. The spectral range is restricted to the visible near-infrared part of the spectrum and the spectral bandwidth is variable depending on the width of a spectral feature to be observed and the amount of energy needed in a band to perform an adequate observation. Driven by the need to resolve spectral features of the oxygen absorption band occurring at 760 nm a minimum spectral bandwidth of 2.5 nm was designed. In order to derive water quality parameters from MERIS data it is firstly necessary to correct image data for the atmospheric effects. Compared to other natural surfaces, such as soils and vegetation, the fraction of light reflected from water is very small [30]. Water-leaving radiances are commonly less than 10% of the total radiance measured at the sensor while the 90% is represented by the signal reflected towards the sensor by the atmo-

Band number	Band centre (nm)	Bandwidth (nm)	Potential Applications
1	412.5	10	Yellow substance, turbidity
2	442.5	10	Chlorophyll absorption maximum
3	490	10	Chlorophyll, other pigments
4	510	10	Turbidity, suspended sediment, red tides
5	560	10	Chlorophyll reference, suspended sediment
6	620	10	Suspended sediment
7	665	10	Chlorophyll absorption
8	681.25	7.5	Chlorophyll fluorescence
9	705	10	Atmospheric correction, red edge
10	753.75	7.5	Oxygen absorption reference
11	760	2.5	Oxygen absorption R-branch
12	775	15	Aerosols, vegetation
13	865	20	Aerosols corrections over ocean
14	890	10	Water vapour absorption reference
15	900	10	Water vapour absorption, vegetation

Table 1: Position of MERIS spectral bands (band centre and bandwidth) and potential field of application.

sphere [30, 31]. Atmospheric correction models are numerous but they are almost all based on the radiative transfer equations that might be resolved in more simple or rigorous way depending by initial assumptions. It is also quite common to distinguish the atmospheric correction models into two categories: image-based techniques and radiative transfer codes [32]. In any case, both the low signals that need to be retrieved and the optical complexity of coastal, transitional and inland waters make quite challenging the atmospheric correction of satellite images for water quality applications. In fact, incorrect values in obtaining water-leaving radiances consequently produce large errors in retrieving concentrations of water quality parameters [33].

In this study two MERIS FR level-1 images, acquired on 26 March and 22 July 2009 were corrected for the atmospheric effects with two radiative transfer codes chosen verifying they performances by using in-situ measured Rrs data. One algorithm [34] is implemented in the Basic ERS & Envisat (A)ATSR and MERIS (BEAM) toolbox and it was chosen because appropriately designed both for performing the atmospheric correction and for assessing the water quality parameters in inland waters. In particular the plug-in Case 2-Regional (C2R) was used. The other model is 6S (Second Simulation of the Satellite Signal in the Solar Spectrum) [35, 36] that was run using appropriate atmospheric and aerosol models. The comparison of atmospheric correction outputs with in-situ data revealed an overall better agreement when the BEAM C2R code was used but focusing on red and near infrared wavelengths, which are commonly used to assess chl-a in eutrophic waters (e.g., [18, 23], cf. Table 1), the 6S code performed better [37].

4.3 Water quality algorithms

As seen in the previous paragraph, the C2R algorithm appropriately designed to correct MERIS data for the atmospheric effects and simultaneously providing concentrations of water quality in case-2 waters has been recently developed [34]. In this study it was used to generate the map of YS, since the algorithms used for assessing YS mainly uses the shorter wavelengths [24]

where the BEAM C2R processor provided accurate values of Rrs. For mapping chl-a concentrations image data atmospherically corrected with 6S code were preferred since more reliable to capture the relative peak of Rrs around 700 nm. The 6S-derived Rrs values in bands 9 and 7 were combined in a band-ratio algorithm developed by using in-situ data [37]. The algorithm, which is similar to those developed in eutrophic lakes (e.g., [18, 23], was enough robust (R2=0.94) to be applied to the atmospherically corrected MERIS images.

For detecting cyanobacterial blooms research activities are rather new but in case of abundant concentrations preliminary results are promising [21]. In this study, Rrs values in MERIS bands 6 and 7 were investigated for detecting phycocyanin absorption feature near 630 nm and a small peak in reflectance spectra near 650 nm, characteristic of cyanobacteria only.

5 Results and discussion

Widely variable water components conditions were measured in the study area: in-situ derived chl-a concentrations varied between 12 and 32 $\mathrm{mg{\cdot}m^{-3}}$ in March and between 44 and 73 $\mathrm{mg{\cdot}m^{-3}}$ in July. The variation range of YS was lower and limited from 0.7 to 2 $\mathrm{m^{-1}}$ with slightly higher values in March than in July (Figure 2). As shown in Figure 2, chl-a and YS were not related (R^2 <0.15), suggesting that the Curonian Lagoon waters belong to case-2. The phytoplankton composition revealed (Figure 2) that in March diatoms and dinoflagellates species (58%) prevailed, while in July the most predominant were cyanobacteria species (63%), with concentrations ranging from 17 to 50 $\mathrm{mg{\cdot}m^{-3}}$. According to Kutser [21], who suggested that MERIS can be used in detecting cyanobacteria if they are present in relatively high quantities only, the cyanobacteria map was derived for image data acquired on 22 July 2009 only.

Figure 4 presents the pseudo true colour MERIS image and related products in the seasons. The pseudo true colour MERIS images qualitatively describe the diversity of waters within the lagoon. The brownish yellow colours observed in March are due to combinations of yellow substances and phytoplankton, while in July the waters are greenish indicating the phytoplankton as the major responsible of water colour. Both images show significant colour variations within the lagoon and several patterns with eddies structure. Then, it is also very evident the differences in water colour of the lagoon with respect the nearby Baltic Sea, caused by the differences in the optical properties of their waters. The water quality maps show a quite heterogeneous pattern of YS in March while in July the distribution is more homogeneous. The chl-a concentrations are highly heterogeneous in both seasons with values definitely greater than those observed in the Baltic Sea.

The concentrations of both chl-a and YS derived from image data in correspondence of the sampling stations are in agreement with in-situ data (Table 2), confirming the capabilities of the proposed method in assessing water quality in this complex ecosystem. Figure 5 shows the map depicting the distribution of the cyanobacterial bloom observed in July 2009 the event observed one week later, on 28 July 2008. The map shows a degree of correlation with the map of chl-a concentration of the same day as revealed by in-situ data too. Nevertheless it is interesting to observe the patchy distribution of algae in

		chl-a [mgm^{-3}]		YS [m^{-1}]	
		Mean	Std-Dev.	Mean	Std-Dev.
26 March 2009	MERIS	27.00	4.08	1.59	0.46
	In-situ	22.96	7.76	1.60	0.14
22 July 2009	MERIS	50.52	3.13	1.33	0.07
	In-situ	56.49	11.12	1.29	0.38

Table 2: Comparison of MERIS-derived products and in-situ data. The statistics, both for in-situ and image data, are computed for the 15 and 10 stations measured in March and July, respectively.

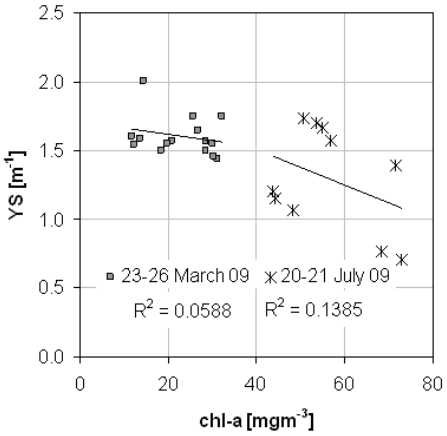

Figure 2: Chl-a concentrations plotted versus and YS concentrations. The poor correlation (R^2 <0.15 in both seasons) is typical of case-2 waters.

the lagoon: with higher values in the northern part nearby the city of Klaipeda, in the central area in correspondence of the main tributary and in the southern part close to coastlines of the Russian Federation.

6 Conclusions - Limitations and challenges

This study showed how remote sensing might offer an important source of information for monitoring water quality in complex ecosystems, as the Curonian Lagoon. The results indicate the feasibility of using MERIS for monitoring water quality in transitional water bodies. The maps produced enabled the temporal and spatial variability and range of water constituent concentrations to be observed in a synoptic manner unequalled by conventional monitoring techniques. The MERIS-derived products provided insights which might be combined with water circulations maps, meteorological parameters (wind speed and direction), inventory of punctual nutrient inputs and map of sediment features for a better understanding of

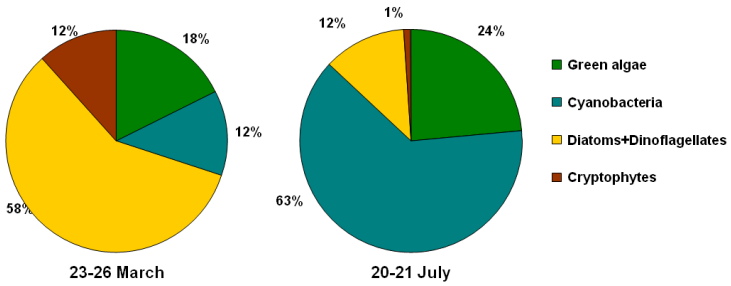

Figure 3: Phytoplankton composition measured in-situ (mean value of the stations) in March and July 2009.

the Curonian Lagoon ecology.
Nevertheless, the algorithm developing in optically complex waters, both in terms of atmospheric correction and water quality retrieval still needs further improvements to fulfil a real-time monitoring. In particular, efforts are needed to establish robust relationships between remote sensing-inferred data (e.g., Rrs or inherent optical proprieties) and concentrations of water quality parameters since in optically complex waters the relations between those parameters might have a local-regional behaviour and vary over time. The demonstrated capabilities of MERIS in detecting cyanobacterial algal blooms, at least in case of massive blooms, might also receive increasing attention in the wider scientific community and water managers since there is evidence to suggest that eutrophic conditions lead to increasing dominance of cyanobacterial species. We believe that further studies on MERIS time-series will allow accurate, reliable and frequent screening of water quality, in particular phytoplankton blooms, in this vast area permitting to explore the complex dynamics and the short-term evolution of blooms in the Curonian Lagoon. Finally, the findings present substantial opportunities for improving monitoring in other transitional and coastal waters with similar water quality problems.

7 Acknowledgements

MERIS data were made available through the ESA AO-553 MELINOS project. This study was co-funded by the University of Klaipeda-Coastal Research and Planning Institute. We are grateful to all the people involved in the fieldwork activities and laboratory analyses performed in this study, special thanks are due to Renata Pilkaitytė and Artūras Razinkovas (University of Klaipeda).

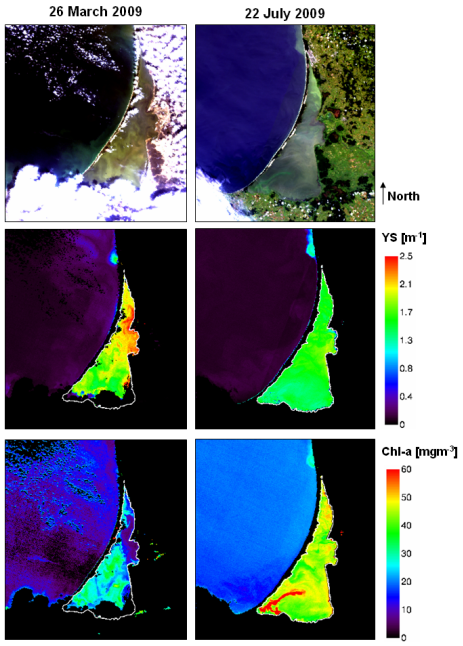

Figure 4: The pseudo true colour image and the two water quality products obtained from MERIS data acquired on 26 March (column on left) and on 22 July 2009 (column on right).

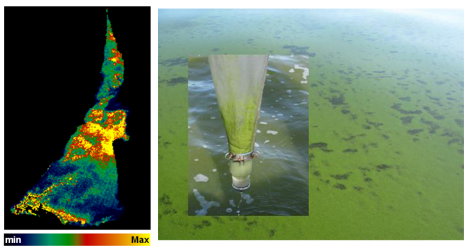

Figure 5: Cyanobacterial bloom in the Curonian Lagoon: on left the map of phycocyanin pigments derived from MERIS data acquired on 22 July 2009, on right the photos of the bloom and of its sampling taken some days later.

References

[1] G.K. Reid. Ecology of Inland Waters and Estuaries. 1961.

[2] R.N. Bamber, S.D. Batten, N.D. Bridgwater, and M. Sheader. On the ecology of brackish water lagoons in Great Britain. *Aquatic Conservation: Marine and Freshwater Ecosystems*, 2:65–94, 1992.

[3] R.S.K. Barnes. The coastal lagoons of Britain. An overview and conservation appraisal. *Biological Conservation*, 49:295–313, 1989.

[4] L.J. Chapman, C.A. Chapman, and M. Chandler. Wetland ecotones as refugia for endangered fishes. *Biological Conservation*, 78:263–270, 1996.

[5] C. Gordon. Hypersaline lagoons as conservation habitats: macro-invertebrates at Muni Lagoon, Ghana. *Biodiversity and Conservation*, 9:465–478, 2000.

[6] G. Izzo, G. Massini, G. Migliore, and C. Varrone. Indicatori funzionali della stabilità ecologica degli ambienti lagunari. 2004.

[7] J.W. Day, F. Scarton, A. Rismondo, and D. Are. Rapid deterioration of a Salt Marsh in Venice Lagoon, Italy. *Journal of Coastal Research*, 14:583–590, 1998.

[8] A. Newton and S.M. Mudge. Lagoon-sea exchanges, nutrient dynamics and water quality management of the Ria Formosa (Portugal). *Estuarine, Coastal and Shelf Science*, 62:405–414, 2005.

[9] W. Gong, J. Shen, and J. Jia. The impact of human activities on the flushing properties of a semi-enclosed lagoon: Xiaohai, Hainan, China. *Marine Environmental Research*, 65:62–76, 2008.

[10] T. Lindell, D.C. Pierson, G. Premazzi, and E. Zilioli. Manual for monitoring European lakes using remote sensing techniques. page 164 pp, 1999.

[11] V.E. Brando and A.G. Dekker. Satellite hyperspectral remote sensing for estimating estuarine and coastal water quality. *IEEE Transaction on Geoscience and Remote Sensing*, 41:1378–1387, 2003.

[12] A. Morel and L. Prieur. Analysis of variations in ocean color. *Limnology Oceanography*, 22:709–722, 1977.

[13] A. Morel. Optical modeling of the upper ocean in relation to its biogeneous matter content (Case 1 waters). *Journal of Geophysical Research*, 93:10749–1076, 1988.

[14] C.D. Mobley, D. Stramski, W.P. Bissett, and E. Boss. Optical Modeling of Ocean Waters: Is the Case 1 - Case 2 Classification Still Useful? *Oceanography*, 17:61–67, 2004.

[15] R.J. Vos, J.H.M. Hakvoort, R.W.J. Jordans, and B.W. Ibelings. Multiplatform optical monitoring of eutrophication in temporally and spatially variable lakes. *The Science of the Total Environment*, 312:221–243, 2003.

[16] S.G.H. Simis, S.W.M. Peters, and H.J. Gons. Remote sensing of the cyanobacterial pigment phycocyanin in turbid inland water. *Limnology Oceanography*, 50:237–245, 2005.

[17] Z. Lee, B. Casey, R. Arnone, A. Weidemann, R. Parsons, M.J. Montes, B.C. Gao, W. Goode, C.O. Davis, and J. Dye. Water and bottom properties of a coastal environment derived from Hyperion data measured from the EO-1 spacecraft platform. *Journal of Applied Remote. Sensing*, 1, 2007.

[18] A.A. Gitelson, J.F. Schalles, and C.M. Hladik. Remote chlorophyll-a retrieval in turbid, productive estuaries: Chesapeake Bay case study. *Remote Sensing of Environment*, 109:464–472, 2007.

[19] A.G. Dekker, R.J. Vos, and S.W.M. Peters. Comparison of remote sensing data, model results and in-situ data for total suspended matter (TSM) in the southern Frisian lakes. 268:197–214, 2001.

[20] T. Kutser, D.C.Pierson, K. Kallio, A. Reinart, and S. Sobek. Mapping lake CDOM by satellite remote sensing. *Remote Sensing of Environment*, 94:535–540, 2005.

[21] T. Kutser, L. Metsamaa, N. Strömbeck, and E. Vahtmäe. Monitoring cyanobacterial blooms by satellite remote sensing. *Estuarine, Coastal and Shelf Science*, 67:303–312, 2006.

[22] C. Giardino, M. Pepe, P. A. Brivio, P. Ghezzi, and E. Zilioli. Detecting chlorophyll, Secchi disk depth and surface temperature in a Subalpine lake using Landsat imagery. *The Science of the Total Environment*, 268:19–29, 2001.

[23] M. Bresciani, C. Giardino, D. Longhi, M. Pinardi, M. Bartoli, and M. Vascellari. Imaging spectrometry of productive inland waters. Application to the lakes of Mantua. *Italian Journal of Remote Sensing*, 41:147–156, 2009.

[24] C. Giardino, V. E. Brando, A. G. Dekker, N. Strömbeck, and G. Candiani. Assessment of water quality in Lake Garda (Italy) using Hyperion. *Remote Sensing of Environment*, 109:183–195, 2007.

[25] L. Guanter, A. Ruiz-Verdù, D. Odermatt, C. Giardino, S. Simis, V. Estellès, T. Heege, J. A. Domìnguez-Gòmez, and J. Moreno. Atmospheric correction of ENVISAT/MERIS data over inland waters: Validation for European lakes. *Remote Sensing of Environment (in press)*, 2010.

[26] A. Krevs, J. Koreiviene, R. Paskauskas, and R. Sulijiene. Phytoplankton production and community respiration in different zones of the Curonian lagoon during the midsummer vegetation period. *Transitional Waters Bulletin*, 1:17–26, 2007.

[27] A. Paldavičiene, H. Mazur-Marzec, and H. Razinkovas. Toxic cyanobacteria blooms in the Lithuanian part of the Curonian Lagoon. *Oceanologia*, 51:203–216, 2009.

[28] ISO 10260-E. Water quality Measurement of biochemical parameters Spectrophotometric determination of Chlorophyll-a concentration. 1992.

[29] N. Strömbeck and D.C. Pierson. The effects of variability in the inherent optical properties on estimations of chlorophyll a by remote sensing in Swedish freshwater. *The Science of the Total Environment*, 268:123–137, 2001.

[30] G.A. Maul. Introduction to satellite oceanography. *Martinus Nijhoff Publisher, Dordrecht*, 1985.

[31] P. A. Brivio, C. Giardino, and E. Zilioli. Calibration and validation of satellite data for quality assurance in lakes monitoring applications. *The Science of the Total Environment*, 268:3–18, 2001.

[32] Y.J. Kaufman. The atmospheric effect on remote sensing and its correction. In: Theory and applications of optical remote sensing. pages 336–428, 1989.

[33] P.A. Keller. Comparison of two inversion techniques of a semi-analytical model for the determination of lake water constituents using imaging spectrometry data. *The Science of the Total Environment*, 268:189–196, 2001.

[34] Doerffer R. and Schiller H. MERIS regional, coastal and lake case 2 water project - Atmospheric Correction ATBD. Version 1.0. 2008.

[35] E.F. Vermote, D. Tanre, J.L. Deuze, M. Herman, and J.J. Morcette. Second Simulation of the Satellite Signal in the Solar Spectrum, 6S: an overview. *IEEE Transaction on Geoscience and Remote Sensing*, 35:675–686, 1997.

[36] S.Y. Kotchenova, E.F. Vermote, R. Matarrese, and F.J. Klemm Jr. Validation of a vector version of the 6S radiative transfer code for atmospheric correction of satellite data. Part I: Path radiance. *Applied Optics*, 45:6762–6774, 2006.

[37] C. Giardino, M. Bresciani, R. Pilkaitytė, M. Bartoli, and A. Razinkovas. In situ measurements and satellite remote sensing of case2 waters: preliminary results from the Curonian Lagoon. *Oceanologia*, 52:197–201, 2010.

The Erythropoietin and Regenerative Medicine: a Lesson from Fish

G. Maricchiolo[1], A. Lacquaniti[2], D. Bolignano[2], A. Favaloro[2], A. Buemi[2], G. Grasso[3], V. Donato[2], G. Giorgianni[2], L. Genovese[1], G. Coppolino[2], A. Sfacteria[2], M. Buemi[2]

1, Institute for Coastal Marine Environment, CNR, Messina, Italy

2, University of Messina, Messina, Italy

3, Faculty of Mathematical, Physical and Natural Sciences, University of Palermo, Palermo, Italia

giulia.maricchiolo@iamc.cnr.it

Abstract

Erythropoietin (EPO), the main haematopoietic growth factor for the proliferation and differentiation of erythroid progenitor cells, is also known for its angiogenic and regenerative properties.

In our research we demonstrated the regenerative effects of EPO administration in an experimental model of sea bass (*Dicentrarchus labrax*) subjected to amputation of the caudal fin.

EPO-treated fish (3000 UI of human recombinant EPO-alpha) show an increased growth rate of their fins compared to those untreated. By analyzing fin length at established times (15 and 30 days after cut), EPO-treated fish always show an increased length compared to untreated ones. Moreover, exogenous EPO administration induces an enormous increase in EPO-blood levels at each observation time whereas these levels remained quite unmodified in untreated fishes. Immunochemical analyses performed by confocal laser scanning microscopic observations show an increased expression of EPO-receptors and PECAM-1 (an endothelial surface marker of vessels sprout) in the regenerating tissue, whereas no signs of inflammation or fibrosis are recognizable. All these findings confirm EPO as a new factor involved in regenerative processes, also suggesting a potential, future utility for new therapeutical applications in the field of human regenerative medicine.

1 The research context

The regeneration has always been deeply fascinating and of considerable scientific interest.

The ability to funtional recovery after loss or reduced function of an organ varies significantly in mammals, amphibians and fish.

Among vertebrates, only teleosts fish and urodel amphibians naturally keep their ability to regenerate injured or amputate parts for life.

Regenerative Medicine, a new medical domain, tries to develop therapeutic pathways through the stimulation of natural regenerative processes also in humans. The mechanisms for functional recovery are under the observational lens of researchers, whose purpose is to know the natural net-

work that regulates the regeneration process and the intricate connections that lead to the production of hormones and mediators fundamental to the regeneration of different tissues [1].

In the field of Regenerative Medicine, Erythropoietin (EPO) represents a particularly significant subject of research [2]. Erythropoietin (EPO) is a glicoproteic hormone mainly products in the kidney and to a lesser extent in the liver. It is the principal haematopoietic growth factor for the proliferation and differentiation of erythroid progenitors cells.

EPO acts by binding with EPOr, a tyrosine kinase receptor. Binding EPO-EPOr triggers the enzymatic function of JAK2, the receptors-associated tyrosine kinase, and allows phosphorylation and nuclear traslocation of STAT5, leading to progenitor cell proliferation and differentiation [3].

The induced-production of EPO has been demonstrated, not only in the kidney and partly in the liver, but also in other tissues. This aspect underlines that besides the ability of stimulating red blood cell production, this hormone has many pleiotropic effects; that is to say that it can act on several types of cells through different mechanisms, carrying out functions additional to the role which is classically attributed to it.

Recents studies suggest that function of EPO and EPO-receptor (EPOr) are not limited to erythroid linage. EPOr expression has, in fact, been detected in placental endothelial cell lines and EPO is capable of stimulating endothelial cell proliferation in vitro [4]. Moreover, EPO is known to induce a pro-angiogenic phenotype in cultered endothelial cells, stimulated neovascularization in the chick chorioallantoic membrane [5], and the hormone seems to play an important role in cardiac morphogenesis and in myoblast proliferation [6, 7]. The relationships between EPO and cardiovascular system are demonstrated by the presence of high levels of EPO and EPO-r expression in the vasculature and the heart. "Preconditioning" with EPO activates cell survival pathways in myocardial tissue in vivo and adult rabbit cardiac fibroblasts in vitro. These pathways, activated by erythropoietin in both whole hearts and cardiac fibroblasts, are also activated acutely by ischemia/reperfusion injury [8].

Moreover, in vivo studies indicate that EPO treatment either prior to or during ischemia significantly enhances cardiac function and recovery, including left ventricular contractility, following myocardial ischemia/reperfusion.

This amazing link between EPO and hearth is further defined in the Japanese pufferfish, *Fugu rupripes* and zebrafish, *Danio rerio*, where physiological hormone production occurs in the hearth.

This tissue-protective effect of EPO involves various natural mechanisms of action including the angiogenesis, a set of functional processes appointed to the formation of new blood vessels starting from the pre-existent ones [9]. Angiogenesis is one of the few natural regenerative activities of humans. The regeneration is a process by which damaged or lost structures are perfectly or almost perfectly replaced.

It is known that mammals contain several organ systems capable of regeneration, such as blood and liver, but the majority of organs heal by scarring, while non mammalian vertebrates like urodele amphibians and teleost fish restore complex tissues much more effectively than mammals, creating tantalizing examples of successful organ regeneration [10].

Danio rerio is taking an increasingly dominant role in the study of the possible mech-

anisms that underlie the processes of tissue regeneration. This is a small freshwater fish that reaches 4-6 cm in length in adulthood. In recent years, it has been increasingly used as a model for studying the development of vertebrates and for many human diseases; in fact small size, big proliferative capacity, short interval between one generation and the next, embryo transparency make this fish an experimental model increasingly used in Regenerative Medicine.

The final site of hematopoiesis, as for all fish, is the kidney since seventh day from fertilization. Chu et al., [11] have recently cloned the gene coding for erythropoietin in zebrafish, highlighting in the codified protein a sequence homology equal to 90%, 55% and 32% respectively with the carp, humans and pufferfish EPO. It was also shown that the main sites of expression of the gene for EPO are represented by heart and liver.

Other authors, on the other hand, believe that in some fish the kidney is not only the main erythropoietic organ but also the largest source of erythropoietin. Wickramasinghe [12] has in fact shown that supernatants prepared by kidney homogenates of rainbow trout (*Salmo gairdneri*) contain more immunoreactive erythropoietin compared with autologous plasma, serum and supernatants obtained by homogenates of liver or spleen.

The mechanisms that underlie the production of erythropoietin are similar in humans and in fish and are recognized as the main factor hypoxia. In fact, in fish, there is a relationship between the increase of renal erythropoietin levels, reduced levels of splenic erythropoietin and spleen somatic index. Under conditions of hypoxia, spleen contraction and the subsequent release of erythrocytes justifies the initial increase of oxygen in the blood, while the erythropoietin action is probably responsible for increasing levels of haemoglobin which occur at a later stage [13].

Even the paper of Rojas et al. [14] highlighted the existence of an important sequence homology between Hypoxia-Inducible Growth Factors (HIF) 1α and 2α between zebrafish and vertebrates on confirmation of a pathophysiological identity.

However, one of the foundations that differentiate zebrafish, vertebrates and humans is the natural regenerative capacity involving fins, skin, heart and brain in the larval stage of these primordial living beings. Regeneration seems to be an archaic tract of the animal world: it was kept in some metazoaria organisms and secondly lost in others for unknown reasons. However, the study of regenerative capacity of zebrafish is an experimental basis to study and understand why human beings have lost this extraordinary ability and what routes should be given to "recall the past."

The caudal fin of the zebrafish has become a popular model for studying the molecular mechanisms regulating regeneration due to its accessibility to amputation and its fairly simple structure, consisting of segmented bony fin rays [15].

Recently, our research group has shown that, even the sea bass, *Dicentrarchus labrax*, as well as the zebrafish, represents another interesting and simple experimental model.

In particular has been shown the regenerative effects of EPO administration in *D. labrax* subjected to amputation of the caudal fin, by analyzing the expression of specific EPO-receptors and the angiogenic properties [2].

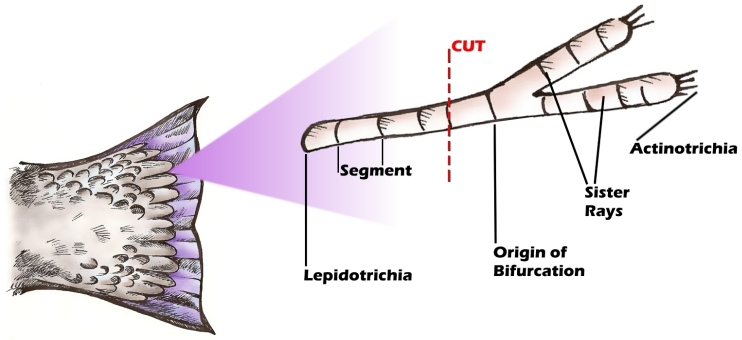

Figure 1: Schematic representation of the skeleton of a ray in sea-bass fin. Dermal bone forms two segmented, concave and opposing hemirays. The image illustrates the position of amputation, which was performed below the origin of bifurcation. From Buemi et al.[2]. European Journal of Clinical Investigation. Figure 1. Copyright Wiley-Blackwell. With permission.

2 The research method

The research was conducted at aquaculture experimental plant of Institute for the Coastal Marine Environment (Territorial Unit of Messina, Sicily, Italy) of the National Research Council (IAMC-CNR).
D. labrax were acclimatized for at least 3 weeks in 2 m^3 indoors tanks (T= 18 $\pm$ 0.2 °C) provided with a flow-through supply of aerated seawater and maintained under natural photoperiod.
Fish were fed to satiation daily, but were fasted for 24 h before the start of the experiments to avoid problems during anaesthesia.

2.1 Experiment procedure and erythropoietin administration

Fish were randomly assigned to the experimental group. Before amputation, fish were anaesthetised with tricaine methanesulphonate, MS-222 (0.1g·L^{-1}). In particular fish were placed in the anaesthetic bath and monitored until they reach the plane of surgery anaesthesia (Stage 3, plane II according Stoskopf [5]) characterized by a total loss of reflex and by slowing of hearth and respiratory rate. Fish anaesthetized were placed in an operating sling where the gills were irrigated with anaesthetic.
The caudal fin was amputated, with a razor blade, one segment proximal to the level of the first ray bifurcation. (Figure 1).
Following application of the anaesthesia, fish were immediately removed from the anaesthetic bath and placed in a recovery tank containing sea water without anaesthetic and were monitored until complete recovery of normal swimming.
At two established times (immediately after cutting and after 15 days) a dose of 3000 UI of Recombinant Human Erythropoietin alfa (Eprex® Janssen Cilag), was administered to 5 fish (experimental group) through a subcutaneous injection at dor-

sal level, while a similar quantity of solvent was administered to the others animals (control group).
The fish length was measured from the tip of the mouth to the caudal peduncle using a ruler. For fin length and segment measurements, the skin and muscle surrounding the most proximal ends of the fin rays were dissected away before mounting in 100% glycerol under a coverslip. Measurements were facilitated with a 10 3 10 reticule in the eye-piece of the dissecting microscope (stemiscope 2000, Zeiss, Thornwood, NY) at low magnification.
Fish were evaluated at established times (baseline, after cutting (T-0), after 15 days (T-15), after 30 days (T-30) by measuring the length of maximum outgrowth, represented by the distance from the centre of the amputation plane to the tip of the regenerating fin.
Simultaneously, a dosage of EPO levels was performed in blood samples obtained from the caudal vein and assayed by commercial ELISA kit (Predicta EPO Genzyme Diagnostics USA).

2.2 Histological Analysis: Immunohistochemistry (IHC) and Immunofluorescence (IF)

In order to evaluate the different angiogenic response between the two groups of fish (EPO-treated and untreated), histological analysis was made using immunofluorescence and immunohistochemistry.
At the end of the study the amputated fish were euthanized and fixed in 4% paraformaldehyde at 1 day after amputation. The fixed fins were postfixed in 1% osmium tetroxide and embedded in Embed 812-Araldite 502 resin. Semithin serial sections were cut, stained with toluidine blue, and analyzed by light microscopy.
For IHC and IF, the samples were fixed in 10% formalin and embedded in paraffin. Section of 5µm were deparaffinized and steamed in 0.01 $mol \cdot L^{-1}$ sodium citrate buffer, pH 6, in a microwave oven for 15 min. Only for IHC, endogenous peroxidase activity was quenched by 0,3% hydrogen peroxide in methanol. Aspecific proteic reactions were blocked by incubation with 5% BSA for 30 min. Slides were then incubated over night at 4°C with anti-EPOr (rabbit polyclonal clone C-20 Santa Cruz) and PECAM-1 (goat polyclonal clone M-20 Santa Cruz), a 130 Kd transmembrane glycoprotein belonging to the immunoglobulin superfamily of cell adhesion molecules, mainly found at the cell-cell borders of neighboring endothelial cells primary antibodies followed by an incubation at room temperature with a horse anti-goat (Vector Laboratories) and goat anti-rabbit biotynilated IgGs (BioSpa). For IHC, the reaction was developed by an avidin peroxidase complex (Biospa), revealed with Vector Nova Red (Vector Laboratories) and counterstained with hematoxylin.
For IF, the reaction was revealed by an avidin conjugated with Alexa Fluor 488 (Molecular Probes). For each sample, negative controls were also performed by omission of primary Ab, substitution of primary Ab with normal IgGs and substitution of primary Ab with indifferent rabbit and goat primary Abs. Immunochemical stain was interpreted by assessing the intensity of staining. Cytoplasmic and/or membrane immunoreactivity was considered positive.
Samples were then observed and photographed using a Zeiss LSM 5 DUO laser scanning microscope. All images were dig-

italized at a resolution of 8 bits into an array of 2048 x 2048 pixels. Optical sections of fluorescence specimens were obtained using HeNe laser (543 nm) and Argon laser (458 nm) at a 1-min 2-sec scanning speed with up to eight averages 1.50-μm-thick sections were obtained using a pinhole of 250. Contrast and brightness were established by examining the most brightly labeled pixels and choosing settings that allowed clear visualization of structural details while keeping the highest pixel intensities close to 200. The same settings were used for all the images obtained from the other samples that had been processed in parallel.
Digital images were cropped and figure montages prepared using Adobe Photoshop 7.0.

2.3 Statistical Analysis

A statistical analysis of data was made using the GraphPad Prism (version 4.0) package. Analysis of variance among groups of fishes was established by ANOVA followed by Bonferroni's test. Furthermore, an unpaired t-test was employed to assess statistical differences in fin length between EPO-traited fish and controls at established times (immediately after cutting: T-0, 15 days after cutting: T-15 and 30 days after cutting: T-30). All results were considered significant when $p \leq 0.05$.

3 The main results

3.1 Fin growth in EPO-treated and untreated fish

During the whole observational period, a statistically significant trend in fin growth was noticed in both groups (ANOVA variance for EPO-treated: p = 0.01; for EPO-untreated p = 0.04). Furthermore, EPO-treated fishes showed an increased growth rate compared to those untreated (ANOVA variance: p = 0.01; F = 1.8 vs p = 0.04; F = 1.0). By analyzing fin length at established times, EPO-treated fishes always showed an increased length compared to untreated (T-15: p = 0.03, F = 1.0; T-30: p = 0.01, F = 1.4).
Finally, exogenous EPO administration induced an enormous increase in EPO-blood levels at each time of observation (T-15: $p < 0.001$, F = 12.41; T-30: $p<0.001$, F = 9.42); on the contrary, predictably, these levels remained quite unmodified in untreated fishes. A resume of these findings is reported in Figure 2 and Table 1.

3.2 Histochemical analyses

Analyses were performed by confocal laser scanning microscopic observations.
Hematoxylin and eosin examination of the stump of both EPO-treated and untreated groups showed a structure composed by a completely restored epidermal structure with a distinct apical cap. Underneath the cap a well vascularized mesodermic tissue, composed of fusiphorm cells with the appearance of fibroblasts-like and endothelial-like cells was detectable. No signs of inflammation or fibrosis were recognizable (Figure 3a and 3b).
At immunofluorescence, EPOr was widely distributed in the epithelium, above all in the basal layer of the epidermis. Moreover, inside the blastema, some blood vessels were positive.
Immunodetection of PECAM-1 allowed the visualization of blood vessels and endothelial cells in the mesodermic blastema. In particular a higher number of PECAM-1 positive structures and fusiphorm cells,

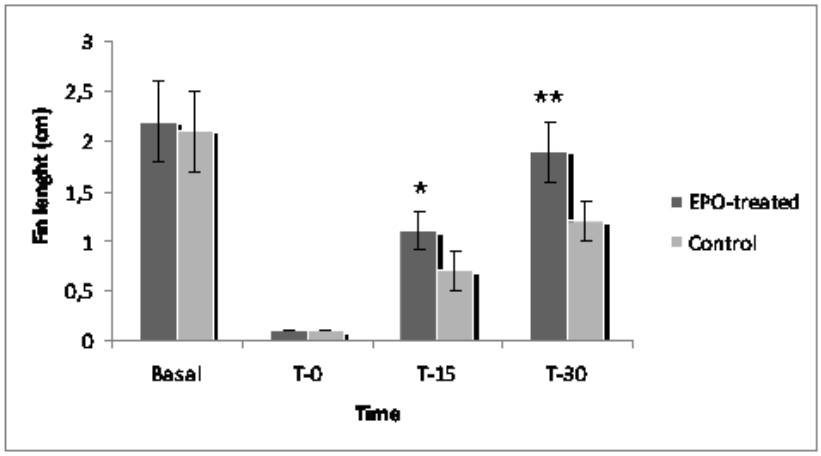

Figure 2: Differences in fin length (cm) between EPO-treated fish and controls at established times. * P: 0.03; ** P: 0.01. Modified from Buemi et al. [2].

	FIN lenght	EPO levels	FIN lenght	EPO levels	FIN lenght	EPO levels	FIN lenght	EPO levels
Treated (*n* 5)	2.2 ± 0.4	16.7 ± 1.8	0.1 ± 0.0	16.8 ± 1.6	1.1 ± 0.2[a]	2240 ± 210[c]	1.9 ± 0.3[b,d]	2340 ± 190[c]
Controls (*n* 5)	2.1 ± 0.4	17.0 ± 1.7	0.1 ± 0.0	16.9 ± 1.8	0.7 ± 0.2	16.7 ± 1.8	1.2 ± 0.2	17.1 ± 1.9
Time	**Basal**		**T=0**		**T=15**		**T=30**	

[a]*P*: 0.03 *vs* untreated; [b]*P*:0.01 *vs* untreated; [c]*P* < 0.01 *vs* untreated; [d]*P* for trend (ANOVA): 0.01; [e]*P* for trend (ANOVA): 0.04.
Basal, starting values; T=0, immediately after cut; T=15, 15 days after cut; T=30, 30 days after cut.

Table 1: Differences in length (cm) and EPO-blood levels ($mU \cdot mL^{-1}$) between EPO-treated fish and controls at established times. (Modified from Buemi et al. [2]).

most likely endothelial cells, were detectable, by visual inspection, in treated fish compared to untreated ones. Microvessels were distributed along the mesodermic blastema showing an increasing density near the apical epidermal cap (Figure 3c and 3d).

4 Conclusions and future perspective

Results from this study suggest that EPO may exert important regenerative effects, even in an experimental fish model. This can be evidenced by the fact that EPO treated fish subjected to amputation of the caudal fin showed an increased growth rate compared with those untreated, thus allowing us to hypothesize that this hormone may be directly involved in stimulating the regenerative and angiogenic processes. The presumed direct action of EPO on fin growth is also supported by hystochemical analyses, which demonstrated an increased expression of EPO-receptors and PECAM-1 (a marker of vessel sprout) in the regenerating tissue, whereas on the contrary, no

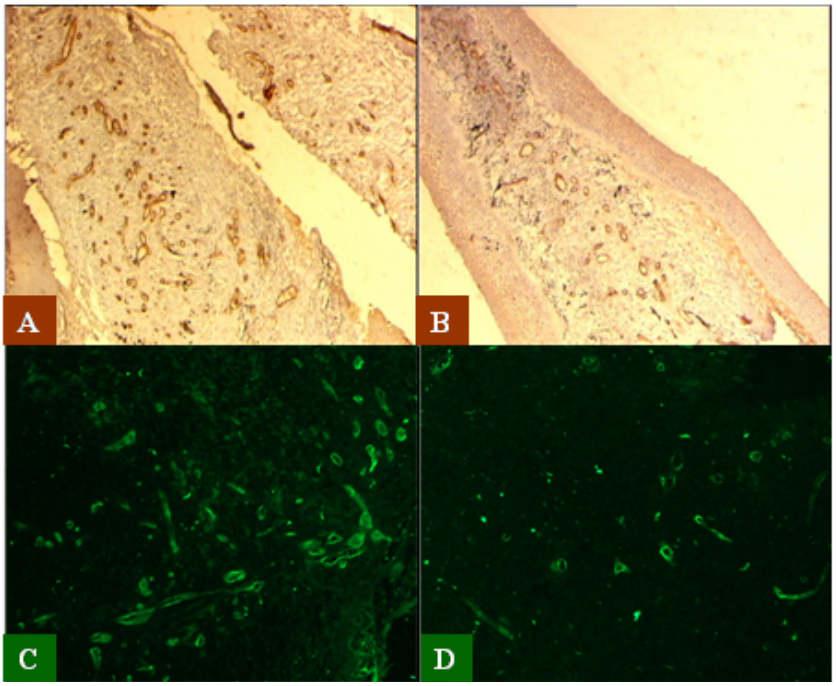

Figure 3: A-B. Confocal laser scanning microscopic observations of EPO-treated fish (A) and controls (B). A well vascularized mesodermic tissue composed of fusiphorm cells with the appearance of fibroblast-like and endothelial-like cell is detectable. No signs of inflammation or fibrosis were present. (C-D). Immunofluorescence of PECAM-1. A high number of PECAM-1 positive structures are detectable in EPO-treated fish (C) compared with the controls (D). Modified from Buemi et al. [2].

signs of inflammation or fibrosis were detectable.

The regeneration of organs and appendages after injury occurs in diverse animal groups and the goal of regenerative medicine is to restore cells, tissue and structures that are lost or damaged after disease, injury or ageing.

The use of fish has been born out by previous by previous studies aimed to evaluating anomalies in angiogenic mechanisms and disorders genetically determined by the cardiovascular system.

Among teleost fish, zebrafish, is taking an increasingly dominant role in the study of the possible mechanism that underlines the processes of tissue regeneration. In fact in previous studies, it has shown the remarkable capability to regenerate their fins, optic nerve, scales heart and spinal cord [16, 17, 15, 18, 19].

In our study, we have convalidated an other experimental model using specimens of *D. labrax*, which being bigger than zebrafish, are probably more suitable for morphological analysis.

Moreover, fish appear to be a particularly appropriate model for evaluated the erythropoietic and extra-erythropoietic effects of EPO. It is in fact well known that the solubility of oxygen in water is just 1/30 of that in the air, and the rate of oxygen diffusion in water is only 1/10000 than in air. Therefore, fish would be expected to possess a sensitive and rapid mechanism to regulate the level of erythrocytes. Fish have indeed been shown to maximize oxygen uptake and economize oxygen expenditure, under hypoxic condition, by a variety of measures such us increased ventilation, bradycardia, cardiorespiratory synchrony, constriction of peripheral blood vessels and increased release of catecolamines. Blood erythrocyte levels are increased, initially, due to release from the spleen and then, subsequently, due to erythropoiesis in response to the hormone EPO, produced by kidney [20, 21], organ in which the same erythropoiesis occurs.

Our data confirm the capacity of EPO to directly stimulate angiogenic capacity of tissue, promoting an adequate regenerative activity after amputation.

However, it is likely that the efficacy of EPO observed in our and other model systems depends on EPO's key role in multiple protective pathways, including an inhibition of apoptosis, restoration of vascular autoregolation, attenuation of inflammatory responses and augmentation of restorative functions, including the direct recruitment of stem cells [22], as shown by the fact that regenerative tissue in animal treated with EPO do not reveal signs of fibrosis or phlogosis.

To conclude, there are some questions posed by Regenerative Medicine on the table of experimentation. One of these is: "What are molecular differences that permit tissue regeneration in fish and make mammalian tissue recalcitrant to regeneration?".

One aspect of adult wound healing in mammals that has been discussed in relation to the curtailment of regeneration is the occurrence of fibrosis, and also of immune and inflammatory responses.

Fish recover the lost caudal fin tissue after amputation through a process of epimorphic regeneration, and this occurs in a stepwise manner with the formation of an epithelial wound cap, followed by blastema formation and finally the regenerative outgrowth. This complex regenerative process is orchestrated by sequential interactions between biomolecules and cells in a spatiotemporal manner.

In animals treated with erythropoietin, tissue regeneration occurs through a premature formation of angiogenic sprouts and without an important fibrotic or phlogistic component.

Although erythropoietin has a significant angiogenic effect similar to the effect of the other angiogenic factor bFGF, this is probably only one of the mechanisms through which the hormone exercises its protective action on tissues.

Further studies of regenerative mechanisms induced by erythropoietin could perhaps new perspectives on the possibility of regenerative medicine in more evolved animals.

References

[1] N. DeWitt. Regenerative medicine. *Nature*, 453:301, 2008.

[2] M. Buemi, A. Lacquaniti, G. Maricchiolo, D. Bolignano, S. Campo, V. Cernaro, A. Sturiale, G. Grasso, A. Buemi, A. Allegra, V. Donato, and L. Genovese. Regenerative medicine: does Erythropoietin have a role? *Current Pharmaceutical Design*, 15(17):2026–36, 2009.

[3] S.S. Watowich, H. Wu, M. Socolovsky, U. Klingmuller, S.N. Constantinescu, and H.F. Lodish. Cytokine receptor signal transduction and the control of hematopoietic cell development. *Annual Review of Cell and Developmental Biology*, 12:91–128, 1996.

[4] A. Anagnostou, Z. Liu, M. Steiner, K. Chin, E.S. Lee, N. Kessimian, and C.T. Noguchi. Erythropoietin receptor mRNA expression in human endothelial cells. *Proceeding of the National Academy of Science of the United States of America*, 91:3974–3978, 1994.

[5] M. Stoskopf. Anaesthesia. Aquaculture for veterinarians. Fish husbandry and medicine, Ed. Brown L. *Pergamon Press, New York, USA*, pages 161–167, 1993.

[6] H. Wu, S.H. Lee, J. Gao, X. Liu, and M.L. Iruela-Arispe. Inactivation of erythropoietin leads to defects in cardiac morphogenesis. *Development*, 126:3597–3605, 1999.

[7] M. Ogilvie, X. Yu, V. Nicolas-Metral, S.M. Pulido, C. Liu, U.T. Ruegg, and C.T. Noguchi. Erythropoietin stimulates proliferation and interferes with differentiation of myoblasts. *The Journal of Biological Chemistry*, 275:39754–761, 2000.

[8] C.J. Parsa, J. Kim, R.U. Riel, R.U. L.S. Pascal, R.B. Thompson, J.A. Petrofski, A. Matsumoto, J.S. Stamler, and K.J. Koch. Cardioprotective effects of erythropoietin in the reperfused ischemic heart: a potential role for cardiac fibroblasts. *The Journal of Biological Chemistry*, 279(20):20655–662, 2004.

[9] P. Carmeliet. Angiogenesis in health and disease. *Nature Medicine*, 9(6):653–660, 2003.

[10] C.L. Stoick-Cooper, R.T. Moon, and G. Weidinger. Advances in signaling in vertebrate regeneration as a prelude to regenerative medicine. *Genes & Development*, 21(11):1292–315, 2007.

[11] C.Y. Chu, C.H. Cheng, G.D. Chen, Y.C. Chen, C.C. Hung, K.Y. Huang, and C.J. Huang. The zebrafish erythropoietin: functional identification and biochemical characterization. *FEBS Letters*, 581:4265–4271, 2007.

[12] S.N. Wickramasinghe. Erythropoietin and the human kidney: evidence for an evolutionary link from studies of Salmo gairdneri. *Comparative Biochemistry and Physiology*, 104(1):63–65, 1993.

[13] J.C.C. Lai, I. Kakuta, H.O.L. Mok, J.L. Rummer, and D. Randall. Effects of moderate and substantial hypoxia on erythropoietin levels in rainbow trout kidney and spleen. *Journal of Experimental Biology*, 209:2734–2738, 2006.

[14] D.A. Rojas, D.A. Perez-Munizaga, L. Centanin, M. Antonelli, P. Wappner, M.L. Allende, and A.E. Reyes. Cloning of hif-1alpha and hif-2alpha and mRNA expression pattern during development in zebrafish. *Gene Expression Patterns*, 7(3):339–45, 2007.

[15] K.D. Poss, M.T. Keating, and A. Nechiporuk. Tales of Regeneration in zebrafish. *Developmental Dynamics*, 226:202–210, 2003.

[16] R.R. Bernhardt, E. Tongiorgi, P. Anzini, and M. Schachner. Increased expression of specific recognition molecules by retinal ganglion cells and by optic pathway glia accompanies the successful regeneration of retinal axons in adult zebrafish. *Journal of Comparative Neurology*, 376:253–264, 1996.

[17] T. Becker, M.F. Wullimann, C. G. Becker, R.R. Bernhardt, and M. Schachner. Axonal regrowth after spinal cord transection in adult zebrafish. *Journal of Comparative Neurology*, 377:577–595, 1997.

[18] A.L. McDowell, L.J. Dixon, J.D. Houchins, and J. Bilotta. Visual processing of the zebrafish optic tectum before and after optic nerve damage. *Vision Neuroscience*, 21:97–106, 2004.

[19] R.J. Major and K.D. Poss. Zebrafish heart regeneration as a model for cardiac tissue repair. Drug Discovery Today: Disease Models. *Disease Models*, 4:219–225, 2007.

[20] G.H. Satchell. Physiology and form of fish circulation. pages 8–22, 1991.

[21] D.J. Randall and S.F. Perry. Catecholamines in fish physiology. Vol. XII B: the cardiovascular system (Ed. Hoar and Andrandall). *Academic Press, New York, USA*, pages 5–33, 1992.

[22] G. Grasso, A. Sfacteria, A. Cerami, and M. Brines. Erythropoietin as a tissue-protective cytokine in brain injury: what do we know and where do we go? *Neuroscientist*, 10:93–98, 2004.

A Powerful Versatile Data Acquisition and Transmission System for Environmental Monitoring

G. Zappalà
Institute for Coastal Marine Environment, CNR, Messina, Italy
giuseppe.zappala@iamc.cnr.it

Abstract

In recent years particular attention has been given to marine offshore and coastal environments. Offshore measurements can be used to detect and understand large scale phenomena, while coastal monitoring is useful to preserve and protect those coastal areas where multiple interests converge (related to tourism, recreational or productive activities) and which could be heavily damaged from local anthropic activities or remote events (e.g. an oil spill from a ship accident or tank washing).
All modern instruments are designed to be interfaced to a computer system, running a data acquisition program often provided by the instrument manufacturer, but usually neither flexible nor remotely manageable.
Connecting together instruments from different manufacturers might be complex.
To overcome these limitations an integrated hardware-software system was developed, that can be customized in various versions to fit the different needs of data acquisition and transmission both on buoy-based and on ship-based instrumentation.
The system uses modular IEEE 696 boards implementing a PC-like architecture; according to the measurement needs a variable number of serial ports, digital I/O and power outputs, analog input and outputs can be connected; GPS receivers, satellite and/or cellular phone modems can be interfaced.
The embedded macro-commands allow to easily write mission programming sequences, that can be also remotely modified without interfering with normal activity.

1 Introduction

The need for advanced systems to survey water quality and meteorological parameters, both at medium and long term scales, stimulated in recent years the development of different kinds of coastal and offshore buoys, platforms and networks [1, 2, 3, 4, 5, 6, 7, 8, 9]. Anthropic pressure on the environment, together with the risk of pollution deriving from accidents (oil spills, failure in waste water treatment plants...) stressed the importance of (near) real time data to assess water quality and to activate proper measures in emergency situations to protect both the environment and the related activities (aquaculture plants, fishing, recreational uses...).
To obtain a good synopticity of observations both in spatial and temporal domains, it is necessary to complement traditional ship observations with measurements from fixed stations (buoys moored in sites chosen to be representative of wider areas, or to constitute a sentinel against the arrival of pollutants), satellite observations, use of ships of opportunity and of newly developed instruments.

An ideal monitoring system should be rugged, cost effective and simple to manage in various and changing operating conditions.
This paper focuses on the development of an universal data acquisition and transmission system, developed at CNR-IAMC in Messina, able to satisfy environment monitoring needs from buoys, ships or fixed stations [10].

2 Integrating software and hardware: design rules

The system design must face several different (and somehow contrasting) needs:

- The CPU must offer high elaboration speed and low power consumption: really, power consumption vs speed is a compromise, sometimes managed using sleep (halt) states;
- The software must be portable among different hardware platforms: this means it should be written in a high-level language, but high-level languages are not as efficient as low-level ones, so requiring higher elaboration speed (and more memory, which increases power consumption);
- The software must be very efficient: this means it must be strictly tailored on the hardware, but this assumption contrasts with former one;
- Mission programming (i.e. setting of kind and frequency of measurements) must be performed "on the fly", without recoding the managing software; this can be obtained using sequence files of macro-commands;
- New instruments must be added to the system easily and quickly.

3 The firmware

The software architecture was designed to be as modular as possible; it is based on three main modules, the "event machine", the "sequence manager" and the "parser", a number of "device" and "instrument" modules to fit the installed instruments and the data communication hardware, some auxiliary functions modules, written in various high and low level languages to run in ROMDOS. During inactivity periods, the system enters if required a low-power "sleep" mode from which it is wakened up synchronously each hour by the sequence manager or asynchronously by the reception of a communication interrupt. A watch-dog timer automatically resets the system in case of hanging.

3.1 The Event Machine

The event machine runs in an endless loop, waiting for one of the following events:

- arrival of a character from the communication device or from the keyboard
- occurrence of a timed or "position" event

3.2 The Modem Input Manager

The arrival of a character activates a routine scanning the input string looking for the "Z" character, that is recognised as the start of the remote command sequence; following characters up to the "LF" are then considered the command and sent to the parser to be interpreted.

3.3 The Keyboard Input Manager

The Keyboard Input Manager allows to locally interact with the data acquisition system during setup and test phases, issuing

local commands, running a DOS shell, executing a macro-command sequence, accessing the communication menu, running a terminal program.

3.4 The Sequence Manager

The Sequence manager is activated when an event occurs; according to the type of event, it opens the proper sequence file containing the macro-commands for that event, reads it line by line, sending each line to the "parser" to be interpreted and executed.

3.5 The Parser

The "Parser" receives in input a string supposed to contain a valid macro-command, that, if found and recognised, is executed. The macro-commands (that can be combined into sequences using a simple text editor) enable to fully control the system, the connected instruments, and the data transmission. Conditional branch commands are also available; this feature can be very useful in case of partial operativity of the system due, for instance, to low battery level or failure of some instruments.

3.6 The "Device" modules

These modules are written in assembly language to fit the peculiarities of the computer hardware and are installed as Interrupt Service Routines.

3.7 The "Instrument" modules

These modules are written to interface the computer with various measuring instruments, taking into account their peculiarities. To obtain the maximum flexibility, parameters can be passed to the modules to specify the instrument address and the command to be performed.

3.8 The data transmission routines

The system can receive remote commands; it is possible to choose among different data transmission systems, using either terrestrial or satellite modems. The first method uses a service offered by some telecom providers enabling to send e-mails encoded in a SMS; this solution is usually quite expensive and it should be used only where it is impossible to obtain an Internet connection. The second method simply connects the measuring station to Internet using a tcp-ip protocol, so allowing to directly send e-mails. The data path was designed to be fault tolerant:

- A copy of collected data is locally stored in the measuring station;
- A copy of the sent e-mail is also locally stored in the measuring station;
- In case of failure of the receiving mail server, the sending server (managed by the telecom company) will retry the delivery for some time, so allowing to repair the defective server without loss of messages;
- All the mail messages are numbered, so enabling to detect undelivered ones and ask the remote station for retransmission;
- As soon as they are received, the mail messages are immediately assimilated into the data bank, and a copy remains for some time in the mail server;
- Periodic back-up operations are performed on the data base.

The command-data flow is described in Figure 1.

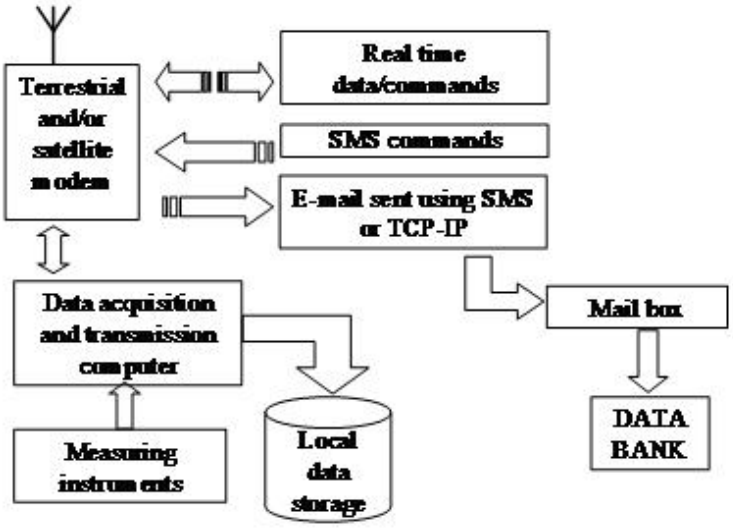

Figure 1: The command-data flow

4 The hardware

The data acquisition and transmission system is conceived to implement a PC-like architecture running a ROMDOS (a ROM based operating system similar to MS-DOS) environment; this choice was due to the availability of both industry-grade boards and of native software development tools in high and low level languages. The boards comply with IEEE 696 (PC104) standard. The system meets with some variations and exceeds the capabilities of the ARES architecture [11]. Usually, the board set could comprise:

- A CPU board including RAM and ROM (usually rewritable) memory, Disk-on-chip or Disk-on-module memory hosting, keyboard and video interface, disk interface, serial port interface (up to 4), parallel port interface, other interfaces (USB, audio, mouse...) not used in this application
- Serial ports expansion board (usually 8 ports/board)
- Analog to digital converter (up to 16 single-ended input channels) with 12 bit (for system diagnostic) or 16 bit (for measurement purposes) resolution.
- Remote communication device board (GSM-GPRS-UMTS modem) often integrated with a GPS module; sometimes this board is substituted with devices connected to serial ports obtaining better performances (higher data transmission speed, satellite communication, tcp-ip integrated stack...)
- Digital I/O board
- Relay board to switch on and off the connected instruments, or semiconductor power interfaces driven by the digital I/O board or by the parallel printer interface usually included in the CPU board.

According to the measuring needs and to power supply availability, the hardware can be fully or only partly implemented.

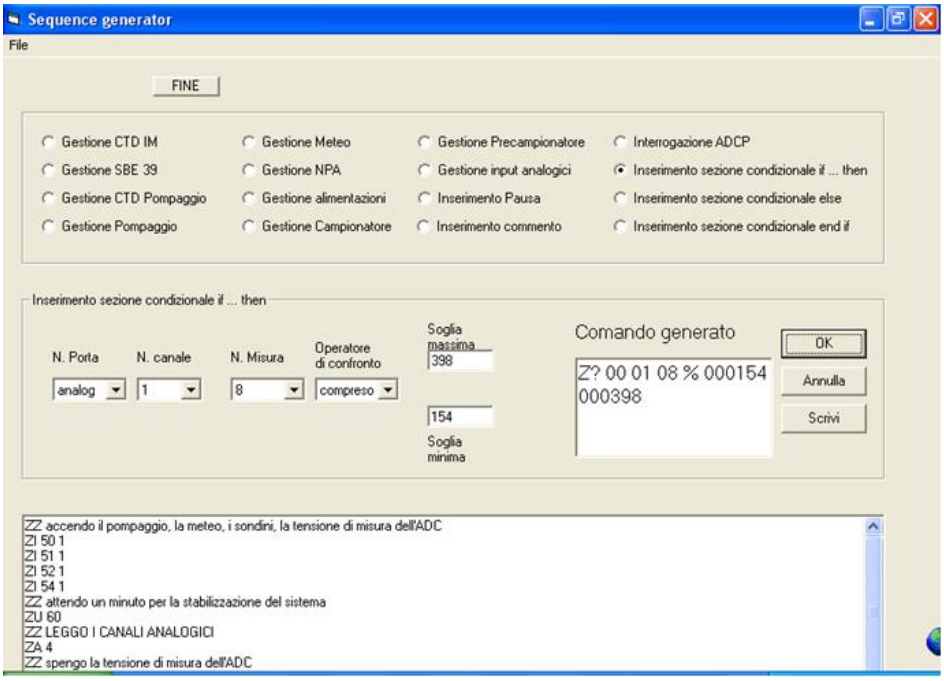

Figure 2: The sequence generator screen

5 Utility software

Softwares were developed in Visual Basic to run in Windows environment to help manage the systems.

5.1 The Control Terminal

This program integrates a Terminal program with some utilities: an “application sequence generator”, a ”launch scheduling module”, an “HEX file generator”, a “file upload manager” and a ”remote file manager module”. From the main terminal window it is possible to customize and use the terminal program or to activate the specific utilities.

5.2 The Application Sequence Generator

The ”application sequence generator” is a menu-driven utility that generates the ”sequence” files containing the macro commands for mission programming. A screenshoot is displayed in Figure 2; the top frame is used to choose the kind of operation to be performed (instrumental measurements, device management, program management).

5.3 The Launch scheduling module

This module was developed to enable setting probe release parameters in operation from ships of opportunity.

Figure 3: A buoy near Messina. The wind generator is evident on the top, under it the radar reflector, the solar panels, the pumping system on the deck, on the left, the meteo station

5.4 The HEX file generator

It is possible to transfer files to the data acquisition and transmission system coding them in a specifically designed format, somehow similar to an ascii coded hexadecimal dump, with checksum and transmission order informations.

5.5 The File Upload Manager

This utility was designed to perform automatic uploads of ”HEX” files to the data acquisition and transmission systems in the buoys; it can work in a “manual”, “automatic”, or “blind” mode.

5.6 The Remote File Manager Module

This module gives remote control of the measuring station file system offering DIR, COPY, DELETE and RENAME facilities.

6 Some applications

Various versions of the data acquisition and transmission system were built: the

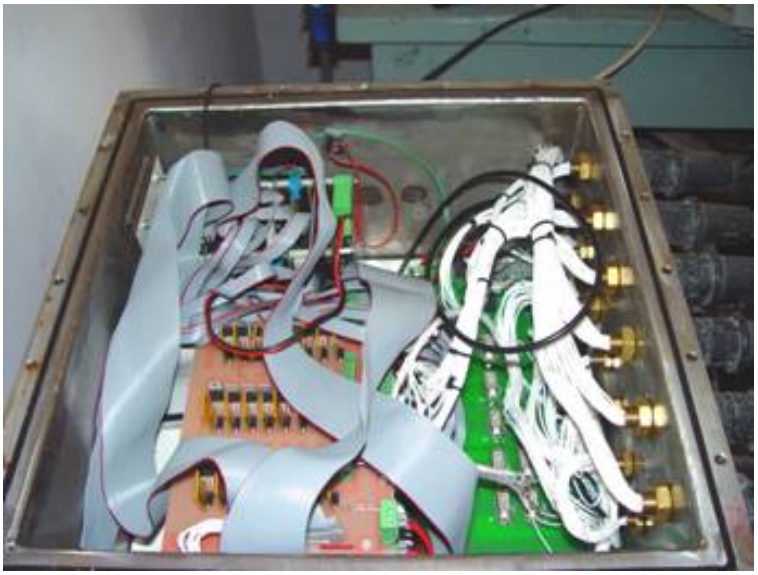

Figure 4: The buoy control electronics; on the left the power control board, on the right the watertight connectors

first one was used in a network of coastal monitoring buoys; a second one equips an automatic multiple launcher for expendable probes; a microcontroller-based version was also designed to equip small instruments. Some examples of data acquired with the system here described are shown in this same volume in the papers by Zappalà [12] and Zappalà et al. [13]

6.1 The "buoy" version

This release was used at the beginning of the century to equip a network of coastal monitoring buoys in the South of Italy ([14]), one of which is shown in Figure 3; the control electronics is shown in Figure 4.

6.2 The "Launcher" version

A main goal of a Ship Of Opportunity Programme (SOOP) is the provision of sea temperature profiles in (near) real time. The use of commercial ships and expandable probes allows the reduction of costs, in comparison with research ship cruises. An autonomous multiple launcher was developed in the framework of the Mediterranean Forecasting System - Toward Environmental Prediction Project (MFSTEP), able to automatically collect eight temperature profiles, using a software-programmable sampling strategy [15, 16, 17]. The device is shown in Figure 5 and its control electronics in Figure 6. In the "launcher" version, more than waiting for an hourly event, the program monitors the position of the hosting ship, comparing GPS data against the programmable set of launch points-times.

Figure 5: The launcher on the deck of Magnaghi Ship; the eight launch tubes are evident on the right, together with the boxes containing the electronics and the electropneumatic valves

7 Discussion

The availability of data to satisfy the policy, stakeholders, environment managers and scientists relies on continuous advancements in technological equipments in order to obtain cost-effective and reliable systems to assess and monitor environmental status. In this framework the systems here described constitute an improvement and application of the know-how acquired in the last decade of past century [18, 19, 20, 21], and were funded by the Italian ("SAM" Sistemi Avanzati di Monitoraggio - Advanced Monitoring Systems and "PI-CNR" Potenziamento Infrastrutture - Infrastructure Increase, both part of the Cluster 10 of the Italian Ministry for University and Research) and European ("MFSTEP" Mediterranean Forecasting System Towards Environmental Predition) programmes. The first application has been the network of coastal monitoring buoys of the SAM program [14, 22]. Further developments were obtained in the framework of the EU-funded MFSTEP program in which the computer system was refitted with a new, more powerful CPU, a Wavecom modem managing an embedded TCP-IP stack and a new set of programs to control an automatic launcher for expendable probes. The observing systems can perform meteorological observations and measurements of physical, chemical and physico-chemical parameters characterizing sea water state and quality, current speed and direction; the measuring devices range from "static" sensors to colorimetric analyzers for nutrients, a water sampler, taking samples for further labora-

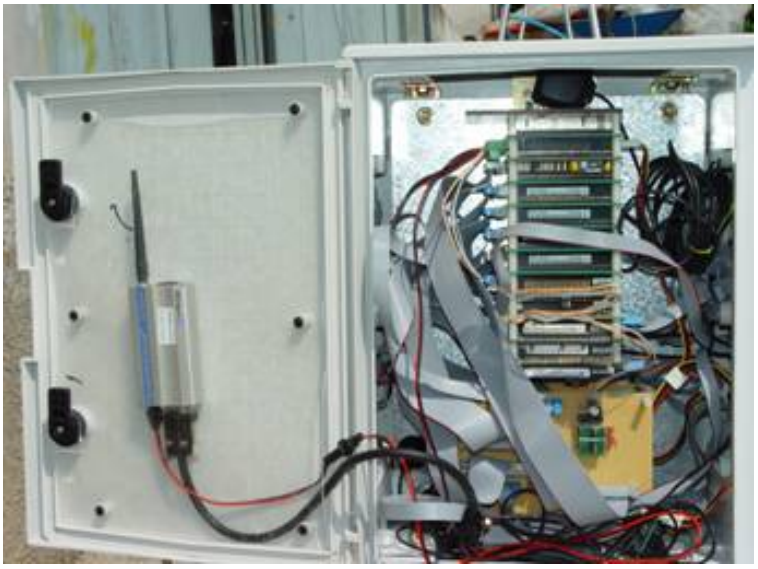

Figure 6: The launcher control electronics; the GSM-GPRS modem is fixed on the back of the watertight box door (left), the electronics with the signal conditioning board is on the right.

tory determinations, may also be included in the systems to complete the series of measurable parameters. Water measurements can be carried out in situ at fixed depths, on samples pumped from various depths into a measurement chamber, using expendable profiling probes, or profiling instruments, like the SAVE [23, 24], that adopted a microcontroller reduced version of the "launcher" electronics, with a software subset. New releases of the software and of the sequences are uploadable to the system without suspending its normal activity and without opening the watertight computer box. The macro-commands enable to manage the data acquisition and transmission, the mission programming, the system hardware and the measuring instruments. Thanks to the hardware-software architecture, it is easy to upgrade the system to more powerful processors without the need to completely rewrite the software, which can be easily coded using standard development packages. The use of e-mail enables to allocate the data centre in the most convenient place, without any need of proximity to the measuring station. The flexibility in mission programming, given by the execution of simple "sequence" files, allows to fit the measurements to the different and varying requirements of scientific research and environment monitoring (e.g. early warning or follow-up of pollution phenomena). The standard interval between measurements is one hour (buoy system) or the occurrence of a launch event (launcher system), but it is possible to program the sequence files (one for each hour plus the launch ones) to obtain higher or lower frequency, the

only limit deriving from the time needed by the measuring instruments and from power consumption. The systems have proven to be flexible, reliable and cost effective.

References

[1] A.H. Carof, D. Sauzade, and Y. Henocque. Arcbleu, an integrated surveillance system for chronic and accidental pollution. *Proc. of OES-IEEE OCEANS '94 Conference*, III:298–302, 1994.

[2] K. Grisard. Eight years experience with the Elbe Estuary environmental survey net. *Proc. of OES-IEEE OCEANS '94 Conference*, I:38–43, 1994.

[3] C.C. Eriksen. Instrumentation for physical oceanography: the last two decades and beyond. *NSF APROPOS Workshop, Ailomar, CA, December 15-17*, 1997.

[4] G. Griffiths, R. Davis, C. Eriksen, D. Frye, P. Marchand, and T. Dickey. Towards new platform technology for sustained observations. *Proc. of OceanObs 99. Online www.bom.gov.au/OceanObs99/Papers/Griffiths.pdf*, 1999.

[5] W. Paul. Buoy Technology. *Marine Technology Society Journal*, 35(2):54–57, 2001.

[6] H. Seim, F. Werner, J. Nelson, R. Jahnke, et al. SEA-COOS: SouthEast Atlantic Coastal Ocean Observing System. *Proc. of MTS-IEEE OCEANS 2002 Conference*, I:547–555, 2002.

[7] K. Nittis, C. Tiavos, I. Thanos, P. Drakopoulos, V. Cardin, et al. The Mediterranean Moored Multi-sensor array (M3a): system development and initial results. *Ann. Geophys.*, 21:75–87, 2003.

[8] N. Pinardi, I. Allen, E. Demirov, P. De Mey, G. Korres, et al. The Mediterranean Ocean Forecasting System: first phase of implementation (1998-2001). *Annales Geophysicae*, 21:3–20, 2003.

[9] H.W. Jannasch, L.J. Coletti, K.S. Johnson, S.E. Fitzwater, et al. The Land/Ocean Biogeochemical Observatory: A robust networked mooring system for continuously monitoring complex biogeochemical cycles in estuaries. *Limnol. Oceanogr.: Methods*, 6:263–276, 2008.

[10] G. Zappalà. A versatile software-hardware system for environmental data acquisition and transmission. *Computational Methods and Experimental Measurements XIV*, pages 283–294, 2009.

[11] P. Lessing and D. Henderson. Architecture and development of an environmental acquisition and reporting system. *Proc. of MTS-IEEE OCEANS '99 Conference*, II:785–788, 1999.

[12] G. Zappalà. Development and test of an automatic multiple releaser for expandable probes. *Marine Research at CNR*, 2011.

[13] G. Zappalà, F. Azzaro, and G. Caruso. Coastal water monitoring from automatic oceanographic platforms. *Marine Research at CNR*, 2011.

[14] G. Zappalà, G. Caruso, and E. Crisafi. The SAM integrated system for coastal monitoring. *Coastal Environment IV*, pages 341–350, 2002.

[15] G. Zappalà and G. Manzella. An automatic multiple launcher for expendable probes. *Operational Oceanography: Present and Future*, pages 188–191, 2006.

[16] G. Zappalà, F. Reseghetti, and G. Manzella. Development of an automatic multiple launcher for expendable probes. *Ocean Sciences*, 3:173–178, 2007.

[17] G. Zappalà. Development of advanced instrumentation for operational oceanography. *Computational Methods and Experimental Measurements XIII*, 46:841–850, 2007.

[18] E. Crisafi, F. Azzaro, G. Zappalà, and G. Magazzù. Integrated automatic systems for oceanographic research: some applications. *Proc. of OES-IEEE OCEANS '94 Conference*, I:455–460, 1994.

[19] G. Zappalà, L. Alberotanza, and E. Crisafi. Assessment of environmental conditions using automatic monitoring systems. *Proc. of MTS-IEEE OCEANS '99 Conference*, II:796–800, 1999.

[20] G. Zappalà. Advanced technologies: equipments for environmental monitoring in coastal areas. *Science-technology synergy for research in marine environment - Developments in Marine Technology*, pages 261–268, 2002.

[21] G. Zappalà, G. Caruso, and E. Crisafi. Design and use of advanced technology devices for sea water monitoring. *Operational Oceanography. Implementation at the european and regional Scales*, pages 273–280, 2002.

[22] G. Zappalà. A software set for environment monitoring networks. *Envirosoft 2004*, pages 3–12, 2004.

[23] M. Marcelli, A. Di Maio, V. Piermattei, G. Zappalà, and G. Manzella. Development of new technologies for the high variability phenomena data acquisition in the MFSTEP-VOS project. *Operational Oceanography: Present and Future*, pages 184–187, 2006.

[24] G. Zappalà, M. Marcelli, and V. Piermattei. Development of a sliding device for extended measurements in coastal waters. *WIT Transactions on Ecology and the Environment,*, 111:187–196, 2008.

Development and Test of an Automatic Multiple Releaser for Expendable Probes

G. Zappalà
Institute for Coastal Marine Environment, CNR, Messina, Italy
giuseppe.zappala@iamc.cnr.it

Abstract

In operational oceanography great amounts of data are required to validate and feed numerical models predicting environmental trends. To avoid the high cost of traditional oceanographic cruises, for some applications, Ships of Opportunity (commercial ships periodically returning on the same route) have been used to collect and transmit in (near) real time water profiles measured by expendable probes (XBTs for temperature, XCTDs for temperature and conductivity, T-FLAPs for temperature and fluorescence). Costs can be further reduced using automatic devices requiring minimum personnel effort (one person only, possibly a member of the ship's crew).
Funded by the "Mediterranean Forecasting System-Toward Environmental Prediction" Project (MFSTEP FP5), a device allowing to release eight expendable probes, collecting and transmitting the measured profiles was designed. The system includes the mechanical hardware (the tubes in which the expendable probes are fitted), electro-pneumatic actuators to release the probes, an electronic circuit to interface the expendable probes, the control computer and communication devices. The measurement and data transmission strategy is easily programmable. The data acquisition system can be remotely controlled in every functionality, and data can be transmitted by GSM-GPRS or satellite telephone systems.
Some examples of measurements are reported. The device was granted the Italian patent and is under examination at the European Patent Office.

1 Introduction

The assessment of environmental conditions requires a series of measurements, with a good spatial and temporal resolution. The high cost and limits of traditional oceanographic surveys stimulate the use of new techniques to obtain a proper coverage. So, traditional moorings and oceanographic cruises are complemented with autonomous devices (e.g. drifters and gliders) and with the use of ships of opportunity.
As a part of the "Mediterranean ocean Forecasting System Pilot Project" (MFSPP), a Voluntary Observing Ship (VOS) program started in 1999 to collect temperature XBT profiles along seven Mediterranean transects, designed to study, in each of the sub-basins (the Algero-Provencal, the Tyrrhenian, the south Adriatic, the lonian and the Levantine), the variability of the main circulation features [1, 2, 3, 4, 5, 6, 7, 8].
In the framework of the EU funded "Mediterranean ocean Forecasting System Toward Environmental Prediction" (MFSTEP), several experiences were performed both in the use and in the develop-

Figure 1: A close-up view of a launch cylinder with the pneumatic actuators during the assembly. The small pneumatic cylinder at the bottom locks the launch door, the vertical bigger one operates it.

ment of advanced instrumentation, including the design and test of the automatic device this paper is about, also called "automatic multiple launcher" [9, 10, 11].
Although less expensive than dedicated oceanographic cruises, the use of commercial ships to launch XBT probes requires however the presence of one or more technicians on board the ship, with the related costs. In order to obtain cheaper operations, an automatic system was designed, to release unattended up to eight probes, easy enough to be recharged by a member of the crew.

2 Materials and methods

An XBT probe has the shape of a small missile, contained in a plastic canister with an overall length of 36 centimetres and external diameter of 7 centimetres; its weight is about 1200 grams.
The temperature sensor is a precision thermistor enclosed in the lead nose; the electrical wire to connect it to the measuring system is contained in two spools, one in the plastic body of the probe and the other one in the canister, that also hosts on its back the electrical connections towards the data acquisition system.

Figure 2: The inboard version of the multiple launcher in laboratory.

Traditional use of XBT (expendable bathythermograph) probes implies the presence of at least one technician on board the ship to manually perform the "launch" (or, better "release") of the probe using an handheld "gun" where the plastic canister is inserted; pressing the trigger the probe is released; while the probe falls into water, the wire inside it starts unreeling. The wire unreels also from the spool in the canister, compensating the movement of the ship and allowing the probe to freefall from the sea surface down to several hundred meters depth.
A data acquisition board connected to a computer controls the measurement when the wire breaks, the profile is completed and the system can be prepared for another launch. The nominal accuracy of the probe is 0,1 °C. The depth is estimated as a function of time, using a formula of the kind: $Z(t) = At - Bt^2$.

3 The new device

The new system is an integrated set of mechanical and electronic hardware and software programs offering the maximum of flexibility.

3.1 The mechanical hardware

Heart of the mechanical hardware is the launch tube, built in AISI 316 steel, in which the probe is fitted with its envelope. An upper cap, holding the electrical connections of the probe, closes the launch tube; opening the lower door the probe is released and falls into seawater.
Two pneumatic cylinders control the door: a small one keeps it closed acting as a safety lock also in case of pressure loss, a bigger one moves it. In the actual MFS-VOS design, the system assembles on a frame eight launch tubes with their pneumatic actuators (Figure 1). A small compressor supplies compressed air to the system, keeping a reserve of 5 litres at 6 bar,

Figure 3: The watertight box containing the electro-pneumatic valves feeding the pneumatic actuators.

a filtered pressure regulator is mounted to prevent damages to the pneumatic system.
Two versions of the launcher were built: the first to work hanged outboard the ship, the second to stay inboard, on a deck. Figure 2 shows "inboard" version, mounting a funnel with a pipe to drive probes outboard. Two watertight boxes host respectively the electro-pneumatic valves feeding the cylinders (Figure 3) and the computerized control system (Figure 4).

3.2 The control computer hardware and software

The control computer hardware and software are enhanced versions of those formerly designed to be used in environmental monitoring network [12, 13].

3.2.1 The electronic hardware

All operations are coordinated by an industrial grade Pentium computer, based on IEEE 696 compliant boards, interfaced with GPS, data acquisition and communication devices (Figure 5). Both analog and digital interfaces are available, to collect data coming from the most various devices (passive and active expendable probes, meteo sensors. . .).
Remote communications are performed using a GPRS modem with an embedded TCP-IP stack; a serial port is available to connect other communication devices (e.g. satellite modems) but also other communications systems could be used.
A balanced source circuit (Figure 6) was designed to interface standard passive temperature probes with 12 or 16 bit Analog to Digital Converters (ADC). Two equal cur-

Figure 4: The watertight box containing the control computer; the vertical bottom board hosts the XBT probe interface.

rents are injected in both the wires coming from the probe and the potentials V_A and V_B are measured: the circuit is closed by the sea water to which the circuit is "grounded" through the ship's hull; the switch Sw1 (a relay contact) allows to test the continuity of the probe circuit before the launch.
The use of sea water as a third wire is necessary because of the high variability in the wire resistance also in probes belonging to the same production lot. Applying Ohm's law, we obtain the voltage across the wires, the thermistor and the fictitious resistor constituted by the sea water multiplying their resistance by the flowing current. Assuming I_1=I_2=I and R_{wire1}=R_{wire2}=R_{wire}, we can write:

- V_{sea} = R_{sea} x 2 I
- V_{w1}= R_{wire} x I
- V_{w2}= R_{wire} x I
- V_{w1} = V_{w2} = V_w
- V_{th}= R_{th} x I
- V_A = V_{sea} + V_w
- V_B= V_{sea} + V_{th} + V_w
- V_B= V_A + V_{th}

So, V_A is the sum of the voltage across R_{wire1} and R_{sea} (the resistance of sea water), V_B is the sum of the voltage across R_{wire2}, $R_{thermistor}$ and R_{sea}. The voltage across the thermistor is obtained subtracting V_A from V_B.
To avoid any perturbation to the measurement, a multiple stage amplifier was used to adapt the signal coming from the probe to the need of the ADC; the circuit was built using high quality precision instrumentation amplifier ICs. The first stage

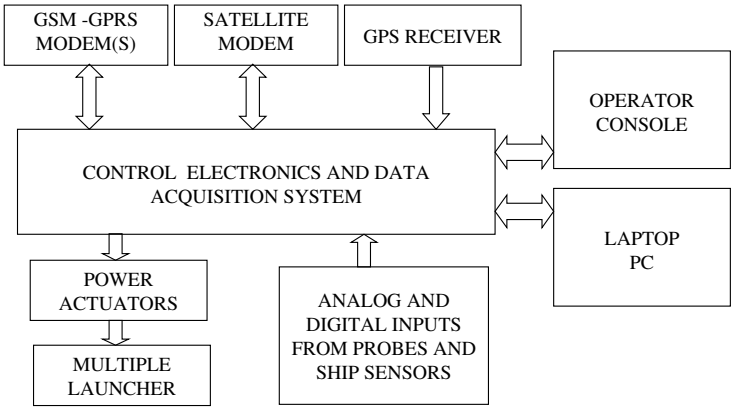

Figure 5: The system block schematics.

uses unity gain configuration, having high input and low output impedance; the second stage is a differential amplifier with gain = 2; the third stage is a low output impedance low-pass filter. Ten times a second, 16 measurements are performed and their mean is calculated; the resistance of the thermistor is obtained using Ohm's law, or, better, using the regression coefficients or the conversion table obtained after calibration of the circuit against a set of standard high precision resistors (Figure 7). The measured temperature is finally obtained using the standard formula [14]:

$$T = -273.15+1/[A+(B\times \ln R)+C\times (\ln R)^3],$$

where: A = 1.29502 x 10^{-3}, B= 2.34546 x 10^{-4} and C = 9.9434 x 10^{-8}. The constants were determined from laboratory tests of XBT thermistors [15].

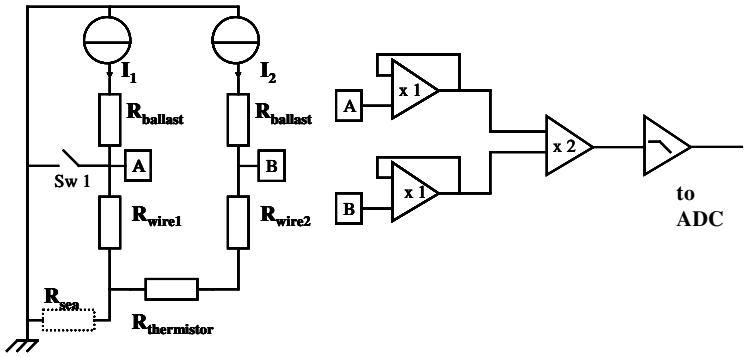

Figure 6: The XBT probe interface board schematics.

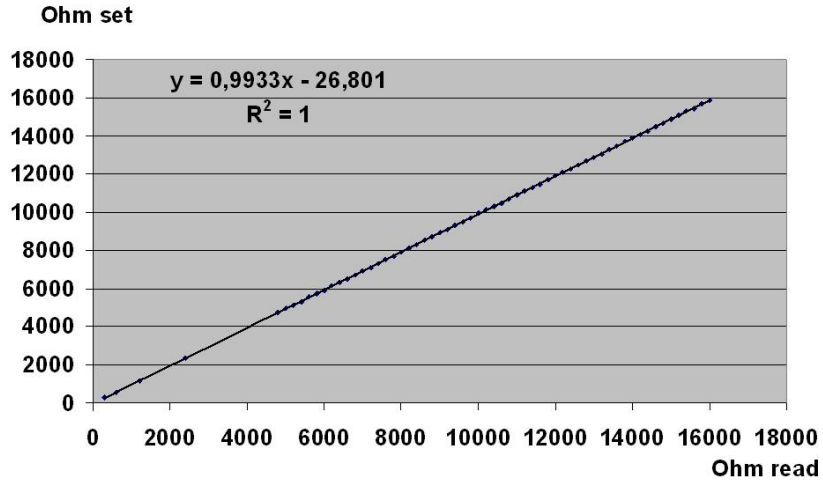

Figure 7: Calibration of the conversion circuit against a set of high precision resistors.

3.2.2 The software

A local and a remote control programs were developed, able to manage 96 launch events. Launch options are:

- northern than a defined latitude
- southern than a defined latitude
- eastern than a defined longitude
- western than a defined longitude
- far from a previous launch
- at GPS time
- at PC time.

Collected data are locally stored and can be transmitted as e-mails. The local control program was written in Microsoft Compiled Basic v. 7.1 and runs in Datalight DOS environment. Assembly language routines are used to manage the Analog to Digital Converter. This program is able to fully control the instrument functions, i.e. real time and position acquisition, comparison against set points-times, probe release, data acquisition and transmission, ancillary functions.

Every hour and at every launch event, a "sequence manager" starts a macro-command sequence, that can be different for each time and is remotely reprogrammable; new releases of the software and of the sequences are uploadable to the station without suspending its normal activity. The macro-commands enable to manage the data acquisition and transmission, the mission programming, the station hardware and the measuring instruments.

The system can be connected to a computer (local laptop or remote desktop), using a remote control program (Figure 8), written in Microsoft Visual Basic, running in Windows environment. This program enables to set up all the launcher functionalities, prepare launch event sequences, transfer files to and from the launcher, and, if needed, to take control of all the launcher operations, including the time-position acquisition and comparison.

4 Tests

The system was tested in laboratory and during two short cruises. The in situ tests were performed in March 2006 using the Italian Hydrographic Institute vessel Magnaghi (Figure 9) and in June 2006 with the ENEA boat S. Teresa, in the Ligurian Sea — Northwestern Mediterranean. During these tests, data was recorded with the automatic system to verify the efficiency of its hardware and software, and, for comparison, XBT probes were launched with a standard Sippican System (hand launcher LM 3A, MK21 read-out card).

Figure 10 shows a profile obtained by the multiple launcher (A) together with a profile measured simultaneously by the Sippican system (B); comparison of values demonstrates the high quality of the automatic system.

5 Discussion and conclusion

The multiple launcher development aimed at improving the cost-effectiveness of an operational observation system. The possibility to have a light, simple and robust system allows easy use by ship personnel. This instrument requires a simple power connection and very limited space (about 1×0.5 m). As usual, the best solution is to have a place on a ship side, possibly leeward. The profiles recorded by the multiple launcher system show temperature values congruent with other measurements. Compared to the existing hand launcher system,

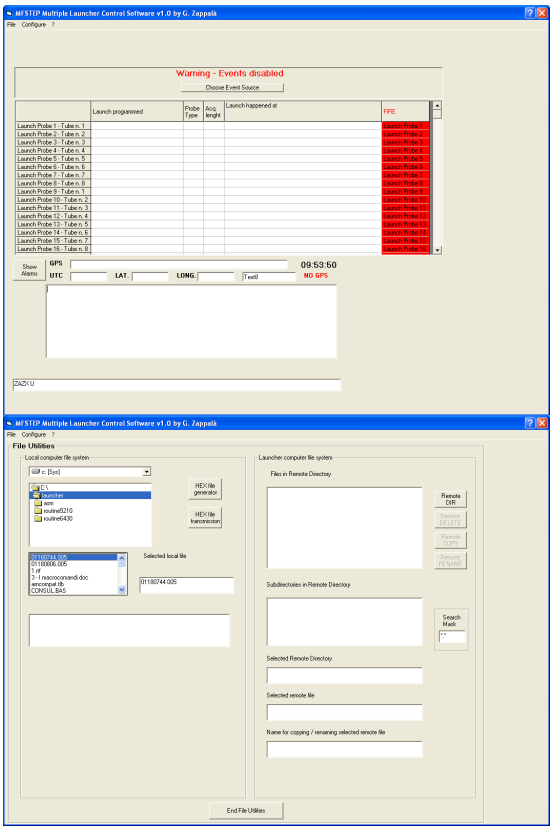

Figure 8: Two screenshots of the remote control software.

the improvement is evident. The multiple launcher allows automatic launches of a certain number of probes (eight XBTs, in the actual arrangement) without human intervention. With respect to the commercial TSKA AL-12 multiple launcher, the newly developed device has a minor amount of electric or mechanic parts, increasing the reliability of the entire system. Significant improvement is achieved by the lighter weight (about 30 kg instead of about 120 kg), also due to the absence of electric motors with related protections from sea water. A further advantage is the possibility to manage the system remotely. The multiple launcher (just like the Sippican manual one) requires the manual removal of the security pin from each xbt canister, whereas in the TSKA AL-12 the pin is removed by a motor, but this functionality causes weight and cost.

Another advantage of the multiple launcher is that it is an "all-in-one" system. The transmission system, GPS, data logger and computer are all housed inside the apparatus, therefore there is no need for the external PC required by Sippican and TSKA and the acquisition time can be easily set

Figure 9: The multiple launcher installed on the deck of the Magnaghi ship.

by the operator.
The small number of electric and mechanic components reduces the risks of malfunctions; the remote control capability enhances the flexibility of the instrument and allows real time operations.
The system proved its reliability and is open to further developments and improvements to be used with other expendable probes (XCTDs, T-FLAPs...) simply adding new interface boards.
A final remark is devoted to cost reduction that can be achieved by using a multiple launcher.
Working in the Mediterranean Sea with commercial ships (cruise speed greater than 20 knots), it is necessary to launch a probe every 20-30 minutes to obtain a good spatial resolution of the mesoscale phenomena on sections several hundreds of miles long, lasting up to 24-36 hours. So, using the manual launcher, at least two technicians are needed, with a cost up to 2000 USD for each travel; using the automatic launcher, it is possible to avoid this cost, or at least halve it, engaging one person only.
The cost of a multiple launcher is about 15000 USD, that can be recovered in 10-20 travels by engaging only one person. The device was granted the Italian patent 0001359525 and is intended to be granted the European Patent EP 1886197.

6 Acknowledgements

The activity was funded in the frame of the MFSTEP project, 5th EU FP. The Author acknowledges the support provided by N. Pinardi and G. Coppini. The work of technicians during these years has provided the necessary information for the design. The Author thanks G. Manzella and F. Reseghetti for the useful suggestions and A. Baldi and F. Conte from ENEA, for their technical support.

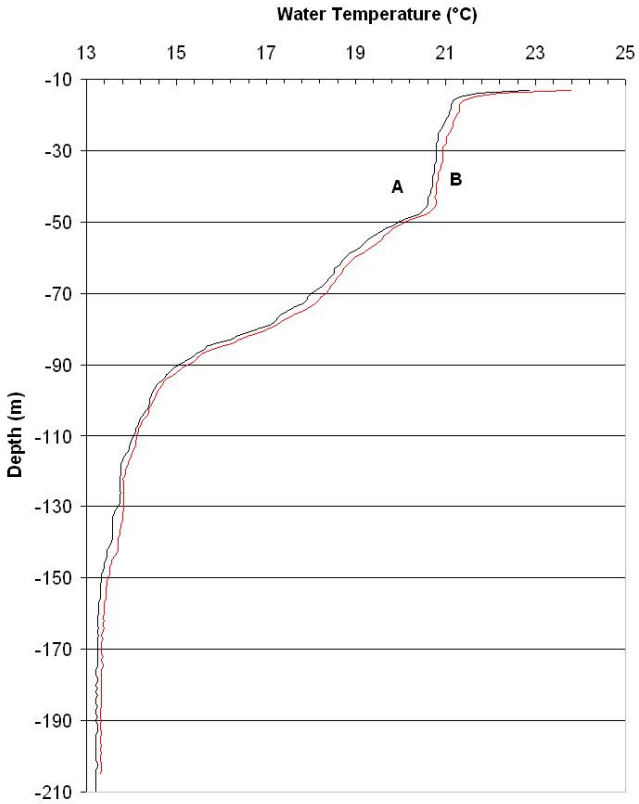

Figure 10: Temperature profiles measured using the multiple launcher (A) and the Sippican system (B).

References

[1] A. Hecht and I. Gertman. Physical features of the eastern Mediterranean resulting from the integration of POEM data with Russian Mediterranean cruises. *Deep-Sea Research*, (48):1847–1876, 2001.

[2] G. Fusco, G. M. R. Manzella, A. Cruzado, M. Gacic, et al. Variability of mesoscale features in the Mediterranean Sea from XBT data analysis. *Ann. Geophys.*, 21:21–32, 2003.

[3] E. Özsoy, A. Hecht, Ù. Ùnlüata, S. Brenner, et al. A review of the Levantine Basin circulation and its variability during 1985-88. *Dyn. Atmos. Oceans*, 15:421–456, 1991.

[4] E. Özsoy, A. Hecht, Ù. Ùnlüata, S. Brenner, et al. A synthesis of the Levantine

Basin circulation and hydrography, 1985-1990. *Deep-Sea Res.*, 40:1075–1119, 1993.

[5] N. Pinardi, I. Allen, E. Demirov, P. DeMey, et al. The Mediterranean ocean Forecasting System: first phase of implementation (1998 -2001). *Ann. Geophys.*, 21:3–20, 2003.

[6] POEM Group. General circulation of the Eastern Mediterranean Sea. *Earth Sci Rev.*, 32:285–309, 1992.

[7] C. Millot and I. Taupier-Letage. Additional evidence of LIW entrainment across the Algerian Basin by mesoscale eddies and not by permanent westward-flowing vein. *Progress in Oceanography*, 66:231–250, 2005.

[8] G. Zodiatis, P. Drakopoulos, S. Brenner, and S. Groom. Variability of the Cyprus warm core Eddy during the CYCLOPS project. *Deep Sea Res.*, 52:2897–2910, 2005.

[9] G. Zappalà and G. Manzella. An automatic multiple launcher for expendable probes. *Operational Oceanography: Present and Future*, pages 188–191, 2006.

[10] G. Zappalà, F. Reseghetti, and G.M.R. Manzella. Development of an automatic multiple launcher for expendable probes. *Ocean Sci.*, 3:173–178, 2007.

[11] G. Zappalà. Development of advanced instrumentation for operational oceanography. *Computational Methods and Experimental Measurements XIII*, pages 841–850, 2007.

[12] G. Zappalà. A software set for environment monitoring networks. *Envirosoft 2004*, pages 3–12, 2004.

[13] G. Zappalà. A versatile software-hardware system for environmental data acquisition and transmission. *Computational Methods and Experimental Measurements XIV*, pages 283–294, 2009.

[14] J.S. Steinhart and S.R. Hart. Calibration curves for thermistors. *Deep-Sea Res.*, 15:497–503, 1968.

[15] D.T. Georgi, J.P. Dean, and J.A. Chase. Temperature calibration of expendable bathy-thermographs. *Ocean Engineering*, 7:491–499, 1980.

Atomic Force Microscopy as a Tool to Investigate the Cytotoxicity in Marine Organisms: Detection of Emerging Nanostructured and Metal-Based Pollutant

M. Girasole[1], G. Longo[1], G. Pompeo[1], A. Cricenti[1], P.F. Moretti[2]
1, Institute of Structure of Matter, CNR Research Area of Tor Vergata, Roma, Italy
2, Department of Earth and Environment, CNR, Roma, Italy
girasole@ism.cnr.it

Abstract

The Atomic Force Microscopy (AFM) is a well established technique to study the surface of samples. After its invention the technique has diffused in different scientific communities and has been largely applied in several research fields including surface and material sciences, solid state physics and biology. Such a spreading reflects the advantages of AFM compared to more traditional microscopes: AFM provides quantitative 3-dimensional morphological images and, simultaneously, other non-morphological data on the material properties. These latter can be the surface friction (related to the sample's chemistry), hardness, elasticity, hydrophobicity etc. and can all be probed on the nanoscale and mapped in non-topography images. Moreover the imaging is totally non-destructive, requires minimal or no sample preparations and the AFM can be operated in various environments (including physiological buffers).

In this paper we present a novel AFM-based approach capable to detect metal-based and/or nanostructured pollutants in marine organisms. This environment- and toxicology-relevant research subject has many intriguing aspects that can also be preliminary studied in vitro. Our approach consists in an operative method combining different microscopies (including AFM and SEM) to detect the consequences of the occurrence of nanostructured pollutants at different level of the hierarchic organization of the body of marine natural bioaccumulators (*Mytilus edulis*).

1 Introduction

Scanning Probe Microscopies (SPM) [1] are a class of versatile techniques, the most popular being Scanning Tunneling Microscopy (STM) [2] Atomic Force Microscopy (AFM) [3, 4, 5] and Scanning Near-field Optical Microscopy (SNOM) [6, 7], whose invention has remarkably changed and modernized the concept of microscopy. Historically, the SPM techniques have been introduced in the eighties, when the development of the STM deserved a Nobel price to the inventors Binnig and Roher [8]. In the following years, the concepts underlying the development of STM have been generalized and novel techniques, such as the AFM and, later, the SNOM, were introduced.

The main idea behind these techniques is

the use of a sharp probe, driven in subnanometric steps over a sample by a piezoelectric actuator, while maintained at very small distance from the surface, to locally investigate topography and additional properties. Indeed the SPMs, initially developed as pure imaging techniques, allow to record magnified images of the sample with a resolution well below the limit of the conventional optical microscopy and, at the same time, can produce maps of physical quantities not always linked to the bare sample's morphology. The detection of these properties and their correlation with the sample morphology are a precious method to solve many scientific problems that could not be addressed by a pure morphological analysis [9, 10, 11]. The additional physical quantities that can be collected through SPMs can differ, strictly depending on the nature of the probe employed (i.e. on the specific SPM employed). For instance, the AFM probe is an extremely sharp, pyramidal (or conical), silicon (or silicon nitride) tip mounted at the apex of a very flexible cantilever to detect, through the deflection of the cantilever, the magnitude of the forces between the tip and the sample's. In the magnetic force microscopy (MFM), the choice of a magnetic probe enables the map of magnetic domains at a high spatial resolution. Similarly, in the STM, the probe is a conductive tip brought very close to a conductive sample in such a way that the quantum tunneling current between the two can be collected and monitored, obtaining information on the local electronic state of the sample. In the SNOM, finally, the probe is a tapered optical fiber used to illuminate and/or to collect light from the sample in the near-field regime enabling the investigation of the local optical properties well-below the diffraction limit.

Obviously, the choice of a specific probe allows the investigation of definite properties of the sample and determines the intrinsic sensitivity of the related microscopy as well as the spatial resolution that can be achieved in an experiment. Namely, the dependence of the force vs. distance typical of the AFM (following, according to the theoretical models, a d6 behavior, where d is the probe-sample distance), as well as the d4 of the SNOM, makes such techniques particularly appropriate for molecular scale studies, while the exponential dependence from the distance of the tunneling current makes STM the most sensitive SPM technique, enabling studies down to the atomic scale. In technical terms, the probe size and shape are the most important factors affecting the spatial and non-topographic resolution that can be achieved in an SPM experiment. To improve this resolution, novel setups, such as the tapping mode operation for SNOM and AFM, have been developed in the laboratory of ISM-CNR [12].

The present work is focused on applications of the AFM. Indeed, its ability to detect the normal and lateral forces between tip and sample can be exploited to collect high-resolution, quantitative, three-dimensional topographies while probing the local chemical properties (maps of surface friction) of the sample. These capabilities are unique tools in many research fields, ranging from the tribology (the study and application of friction, lubrication and wear) that, with AFM, can be studied on the nanoscale [13] to the cellular or molecular biology. In particular, the biological applications of AFM are remarkably interesting because the technique allows non destructive imaging that can be performed in different environments including physiological buffers [14] enabling

high-resolution studies of the time evolution of biomolecules or entire living systems [15].
Thus, the AFM peculiarities makes such a technique, not only a valuable tool to characterize the morphology of the samples on the nanoscale in a quantitative and non destructive way, but also a powerful instrument to study the material properties and a valid support to the development of applications in a variety of different research field.
In this paper we describe the potential of innovative investigation techniques based on the use of AFM in the study of aquatic organisms and in the analysis of emerging topics of environmental and toxicological interest. In particular, we will give examples of the capability of AFM to detect the direct presence and the biological consequences of the exposure of biosystems to metal-based and nanostructured pollutants. Nanostructured pollutants [16] can be of natural origin or anthropogenic. These latter, mainly produced by the industry of nanotechnology and increasingly released into the environment, owe most of their properties to the small size and to chemical functionalization. Such treatments can change the surface properties of the nanoparticles enhancing their specific reactivity. Once released into the environment, their fate will be a probable dissolution in rainwater and groundwater that could lead them in the freshwater and, finally, into the sea. While several studies have focused on the interaction of nanosized pollutants with terrestrial organisms, there are still very few experimental data on their interactions with the marine flora and fauna. This is partially due to the extra degree of difficulty imposed by the aquatic environment, in which nanostructured pollutants may interact with pre-existing surfactants, changing their surface chemistry and enhancing the properties and the bioavailability of individual pollutants. Cytotoxicity due to different types of nanoparticles has been observed in various freshwater and marine organisms (including algae, bacteria, small fish and crustaceans). Naturally, different types of nanoparticles or different organisms show a different degree of toxicity. In the mussels, we cite the induction of oxidative stress by gold nanoparticles [17], reduction of phagocytosis after administration of cadmium-containing nanoparticles and the detection of apoptosis and damage to the membranes after exposure to various contaminants [18, 19, 20]. Overall, unfortunately, the research conducted on mussels or other shellfish, are rather scarce, and, thus, the effects of new pollutants on the marine organisms are still largely unknown.
The rationale of the present work consists in the description of the abilities of AFM (and, in particular, of the instruments developed at CNR) in the detection of cytotoxic effects due to different heavy metals administered to cells in culture, first in the form of salts and then as nanoparticles. This approach, based on a morphological analysis conducted in a highly controlled way, allows to adequately highlight the potential of the methodology and to point out the information that can be obtained. Subsequently, an approach to the analysis of marine organisms is shown. The method combines data from conventional optical microscopy, AFM and SEM and allows to detect the presence and the effects of nanostructured pollutants at different levels of the hierarchical organization of the organism.

2 Materials and Methods

2.1 AFM: Instrument and data collection

The microscopy group at ISM-CNR has a long term experience in the development of new AFM, STM and SNOM microscopes for a variety of applications. The design includes mechanical and electronic components and the development of dedicated software for image collection and data analysis. As consequence of such activities, several patents and a continuous improvement in the performances and in the range of application of the microscopes have resulted over the years.
The home-built AFM instrument employed in this study was described in detail elsewhere [21] and has already been used in the study of different kind of biological samples [22, 23, 24].
Briefly, the instrument consists of a $\sim$20 cm long stainless-steel unit made of two separable hollow cylindrical supports equipped with a vibration isolating system. The lower unit contains the sample holder, that is mounted at the top of a piezoelectric scanner that allows a maximum scan size of 40 um x 40 um x 8 um. Additionally, an X-Y-Z motor controlled translator is used for larger motion and allows to select suitable areas of the sample. The upper unit contains the cantilever holder, the mirror deflection system and a four sector position sensitive photodiode used as deflection detector. An electronic feedback loop is used to integrate the optical signal allowing to maintain a constant cantilever deflection during the data acquisition. The nominal capabilities of the microscope include a typical lateral resolution $\leq$10 nm and 0.1 nm in the Z direction (for a sample placed on a flat surface).
The friction images arise from the recording of the lateral torsion of the cantilever. These are the consequence of forces exerted at the base of the tip (i.e. the contact point) during the scan and can be related to differences in the friction coefficient of different zones of the sample under investigation. In other terms, the lateral force images can be related to the chemical composition of the specimen and are particularly sensitive to contrasts between soft (biological) and hard (metallic) matter.
Regarding the AFM images presented in this work, cconstant force and lateral friction images were acquired simultaneously in air, (at room temperature and controlled 30% relative humidity) with a typical scan rate of 3-4 sec/row and with the microscope working in the weakest possible regime of repulsive forces (less than 1 nN from zero cantilever deflection). Gold coated Si_3N_4 cantilevers with a spring constant of 0.03 $\mathrm{N{\cdot}m^{-1}}$ and a statistical apical radius of about 10 nm were used. The raw data were treated only by a background subtraction and, when required, a plane alignment. The reproducibility of the data (including the absence of sample damage due to the measurement procedure) was carefully and successfully tested.

2.2 Sample preparation

2.2.1 In vitro experiments: Heavy metal doping and metal nanoparticles doping

The protocol for handling and doping the cultured cells can be summarized as follows: at confluence, the pancreatic cells INS-1, cultured at 37°C and 5%CO_2, were seeded on poly-lysine treated glass cover slides. After 24h the medium was removed and the cells were incubated for 3

h, at 37°C, with complete RPMI medium (Gibco laboratories; Paisley, Scotland UK) in the presence of 100 uM of metal compounds ($CdCl_2$; $ZnCl_2$ or $PbCl_2$). A control sample not exposed to the metal was prepared as well. Then, the cells were fixed in para-formaldehyde (2.5 % for 20 min), washed twice with PBS (not containing Ca^{+2} or Mg^{+2} ions) and twice with distilled water to eliminate metal sediments from the cell surface. Finally, the samples were air dried, to allow a detailed AFM analysis spanning over several days. All reagents (from Carlo Erba or Fluka, Milan, Italy) are of analytical grade.

A mixture of Hematite (Fe_2O_3) and Magnetite (Fe_2O_3) nanoparticles (Nanostructured & Amorphous Materials Inc., Los Alamos, New Mexico, USA) were used. The nominal mean size of the chosen particles was 60 nm ($\pm$ 30 nm, rms) for hematite and 35 nm ($\pm$ 15 nm, rms) for magnetite. Before use, all particles were de-pyrogenated at 210°C in glass tubes for about 2 hours. The particles were, then, stored in a mother solution of sterile Dulbecco's Phosphate Buffered Saline (Invitrogen Corporation, CA USA) at the concentration of 1mg/ml at 4°C temperature. For each test, a different concentration of particles was used in order to detect the threshold toxic concentration.

NHI 3T3 mouse fibroblast cells were cultured in Dulbecco's Mem (GIBCO tm ,U.K.), supplemented with 100 IU/100 $ug \cdot ml^{-1}$ Penicillin/Streptomycin, 2 mM L-glutammin, 1 mM Sodium piruvate, 10% foetal bovine serum and incubated at 37°C in presence of humidified atmosphere (95%) and CO_2 (5%). After this preliminary incubation, the 3T3 cells were seeded in 96-well microplates (NUNC Micro well plates, USA), at a concentration of $7x10^4$ cells per 100 ul/well. After a 24 hours incubation, the different nanoparticles were introduced in the wells and the cells were incubated for 24 hours. The chosen nanoparticle concentration was varied in each well and for each material: 15 mg, 3 mg, 0.6 mg, 1.2 x 10^{-1} mg, 2.4 x 10^{-2} mg, 4.8 x 10^{-3} mg (concentration values calculated x 10^6 cells). A well containing the pristine cells acted as control.

2.2.2 Marine organisms

The experiments on sea-life creatures were performed on mussels, that are natural bioaccumulators and, thus, particularly appropriate for studies of environmental pollution. We collected different mussel tissues, mostly digestive glands and gonads, that have been investigated after histological sample preparation. Mussels (*Mytilus edulis*) were collected in the central Tyrrhenian inshore. The organs of interest were excised and immediately fixed. Specifically, two fixation protocols were chosen: for the preparation of the AFM and SEM samples, a Bouin's solution (picric acid: formalin: acetic acid=15:5:1 v/v) was used, while for the sections to be investigated by conventional microscopy, a Methacarn-based fixative was preferred (methanol:chloroform:acetic acid=5:3:1 v/v). The sample preparation requires dehydration, embedding in paraffin blocks and, when necessary, staining of the sections.

Dehydration was performed according to the following: immersion in 70% ethanol (several steps of 2 hours), 80% ethanol (2 hours) 90% ethanol (1,5 hours), 95% ethanol (1 hour) 100% ethanol (2 x 15 minutes each). For the samples fixed with Methacarn, the dehydration was much simpler, consisting only in two baths in 100% ethanol.

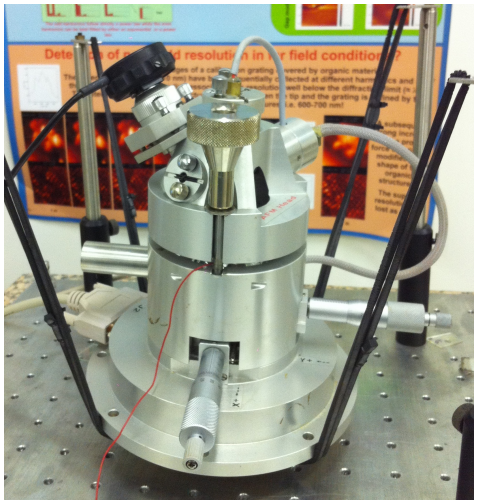

Figure 1: The Atomic force microscope employed in the present study, designed and built at ISM-CNR.

After dehydration, the tissues were treated with a solvent (toluene or xylene) that prepares the sample to the paraffin embedding protocol: immersion in 100% Histoclear (2 x 15 minutes); 50% paraffin and 50% Histoclear (1 hour at 60 °C); 100% liquid paraffin (2 x 1,5 hours at 60 °C); inclusion in a new paraffin block. Subsequently, the samples were cut with a rotary microtome (Leitz 1512) and the sections were deposited on a substrate coated with bovine albumin or poly-lysine to promote adhesion and, finally, dried overnight at 37 °C.
The staining gives no benefits for SEM or AFM analysis, yet its use allows a useful preliminary screening of the sections through conventional optical microscopy. The protocol used requires a preliminary immersion in Histoclear, followed by the inverse path of the dehydration. This procedure is required in order to get rid of the paraffin and to prepare the samples for the true Ematossilina/Eosina based staining, performed as follows: immersion in Hemalum for 4-6 minutes; rinsing in distilled water; immersion in eosin for 1 minute; rinsing in 95% ethanol; 100% ethanol 2 x 5 minutes; Histoclear, 2 x 5 minutes. Finally the sections were treated with a protective agent (Eo-Kit), covered with a glass slide and dried.

3 Results and Discussion

At first, we will describe the potential of AFM to investigate the effects of the in vitro exposure of cultured cells to heavy metals [11] administered as either chlorine salts or nanoparticles.
Heavy metals are key components of proteins and enzymes, nevertheless, the effect on biological systems of the exposure to heavy metals is an important issue due to possible implications on human health caused by the increasing environmental pollution [25]. The uptake of heavy met-

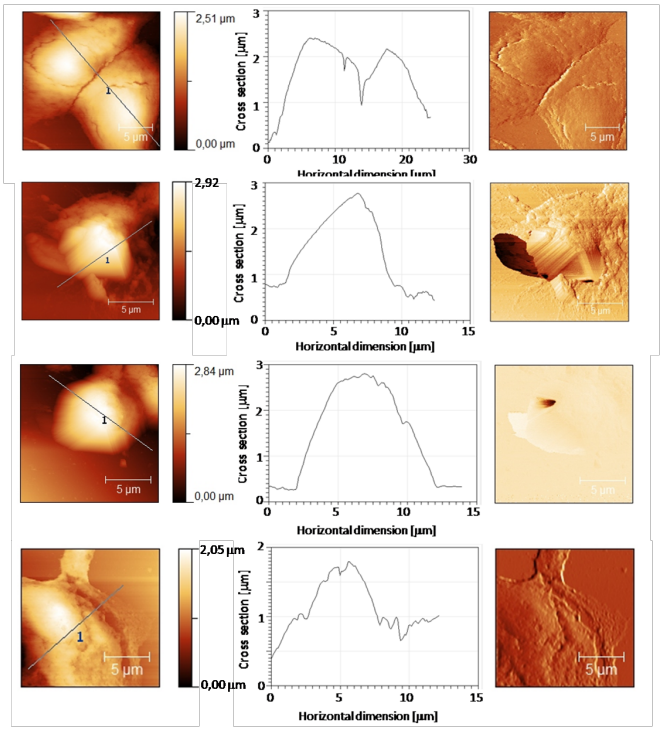

Figure 2: AFM topography, cross sections and lateral force images of, from top to bottom, control cells, cadmium, zinc and lead-doped cells. Pristine cells have a typical dome shape, with higher quotas in the nuclear region, that can change upon exposure to exogenous metals. The most evident effect is the appearance of strong contrasts in the lateral force images after doping the cells with cadmium or zinc.

als in many biosystems, indeed, results in different effects depending on the characteristics of the metal and of the cell line. The most important aspects of the interaction between a generic cell and an heavy metal are governed by the bioavailability (related to concentration, exposure time, temperature) and the nature of the metal (intrinsic toxicity and cell uptake). As consequence of these interaction parameters, the intrinsic toxicity of the considered metals follows the order Cd $>$ Pb $\geq$ Zn. To describe the cell response to heavy metals, in vitro cultured cells were exposed to 100 uM chlorine salts of Cd^{+2}, Zn^{+2} or Pb^{+2} and the effect of such administration were characterized by AFM.

The data reveal that two major classes of effects appear on the cultured cells: overall shape variation and occurrence of friction contrasts. In particular all the metal treatments induce a change of the cell shape that become more spherical. Besides that, Cd and Zn produce an increase in the cell height while Pb behaves oppositely. These morphological patterns distinguish Cd and

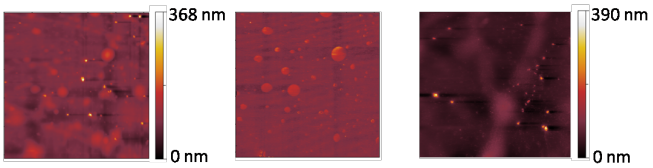

Figure 3: AFM topography (left) and lateral friction (center) images of iron nanoparticles in a cell culture. Right panel shows human 3T3 cell in the presence of iron nanoparticles that can be detected above and around the cell surface. A detailed analysis of the images allows to understand if the nanoparticles have been uptaken by the cell.

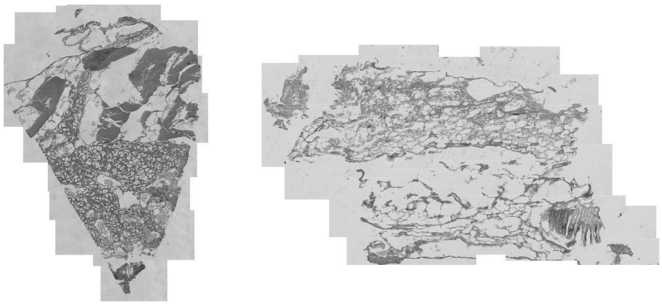

Figure 4: Maps of gonads slices from the mussel *Mytilus edulis* show the arrangement of different tissues in the organ. For instance, in the left image, filamentous matrixes in the upper and fibrous tissue in the lower part can be recognized. Some secretive glands can also be seen in the image. The right panel shows a different organs whose texture is dominated by secretive cavities.

Zn behaviour from Pb, that seems quite effective in killing the cells by inducing necrosis.

More impressive differences are revealed by the analysis of the lateral force images. Indeed, in both the Zn and Cd-doped samples strong friction contrasts were observed at the edge of the cells, as well as on their plasma membrane. The contrasts observed at the edge of the cells are likely to be associated to the direct detection of metal aggregates: the AFM tip feels dramatically different lateral interactions when in contact with a cell surface or with a metal agglomerate. On the other hand, the friction contrasts on the plasma membrane are more deeply related to the cell metabolism. Indeed, these latter contrasts reveal that there are hot spots on the plasma membrane whose chemical characters changes after the metal incorporation. A deeper analysis of the observed friction contrasts reveal minor differences between what can be observed in the cases of Cd and Zn. For instance, differences in the localization of the friction effects on the membrane or other qualitative differences between the two cases are likely to reflect different biochemical signals occurring in a common degradation pathway. In the same context

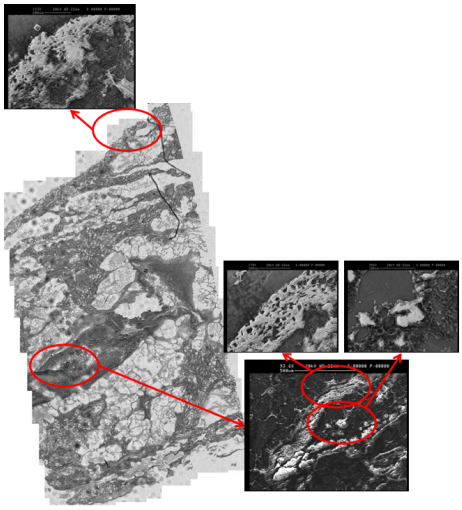

Figure 5: Normal digestive gland: optical microscopy reconstruction and SEM imaging.

the absence of friction contrasts observed for lead doped cells corresponds, in biological terms, to a qualitatively different situation.

As a whole, these data demonstrate that AFM can detect the direct accumulation of metal clusters in the extracellular matrix. This is a non-trivial result because the heavy metals, in the presence of biosystems, are expected to be chemically neutralized by the cells in such a way that their detectability may be altered. Moreover, our study shows that a quantitative AFM analysis of morphological variations, coupled with the detection of chemical inhomogeneity on cells membrane, allows to discriminate the different pathways of cell damage induced by Cd, Zn and Pb on cultured cells. In the case of Pb the observed morphological pattern unequivocally suggest that this metal, basically, kills the cells by necrosis. The consequence of Cd or Zn administration are more subtle: they disturb the cell morphology and the homogeneity of the plasma membrane suggesting that a more complex biochemical patterns, for some points resembling the early apoptotic response, takes place. Next, we want to exploit the high-resolution of the AFM to study the interaction of nanostructured materials of metallic nature with biosystems. Indeed, nano-sized pollutants interact in different ways with living organisms: their effects originate both from their chemical composition and from their size and shape. This makes them a new kind of pollutants that must be closely studied.

In our in-vitro experiments, cultured cells were exposed to iron-based nanoparticles and the consequence of the exposure was evaluated by AFM. Typical images collected on these samples are reported in Figure 3, where the potential of the technique to detect the nanoparticles, both alone and in the presence of cells, is evident. The peculiarities of AFM, in this case, can be used to understand the basic interactions between the nanostructures and a biosys-

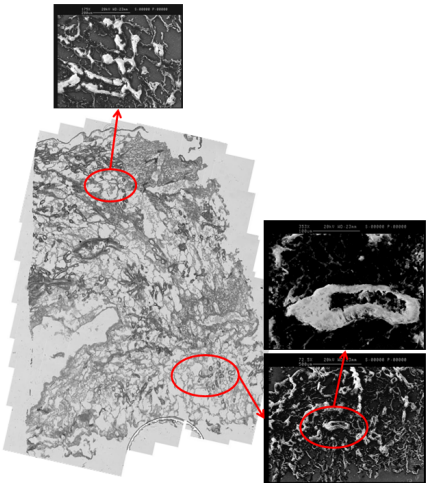

Figure 6: A partially destructured digestive gland: optical microscopy reconstruction and SEM imaging.

tem, as well as to understand the long-term consequences of these interactions. Indeed, for instance, a careful observation of the AFM and of lateral force images allows to understand whether or not the particles are interacting with the outer leaflet of the cell membrane or have been incorporated, presumably by endocytosys or pinocitosys, into the cell, leaving just a weak morphological fingerprint on the plasma membrane. Moreover, a series of experiments performed at different times after the administration of the nanomaterials can couple the uptake of exogenous materials with the evolution of the cell morphology and the development of cellular disorders.

The above reported in vitro experiments have introduced the reader to the capability of the AFM to study the interaction between metal-based nanostructured materials and biosystems.

With this essential knowledge we can approach another topic of this work: the application of AFM to the study of real-life marine organisms to detect the fingerprints of nanostructured pollutants. A due premise is that in vitro experiments involving cell culture from mytilus or other marine organisms would be highly envisaged in this scientific context too.

The experiments on marine organisms were carried out on mussels of the species *Mytilus edulis* collected in the inshore of the middle Tyrrhenian sea. Indeed, the bioaccumulation ability of these animals makes them ideal candidates for this research. Two organs of the mussels, thought to be among the most sensitive to environmental agents, were considered: the digestive gland and the gonads. The first screening were performed through a reconstruction of the slices through conventional optical microscopy at relatively low magnification (typically 200x). An example is given in Figure 4 where the reconstruction

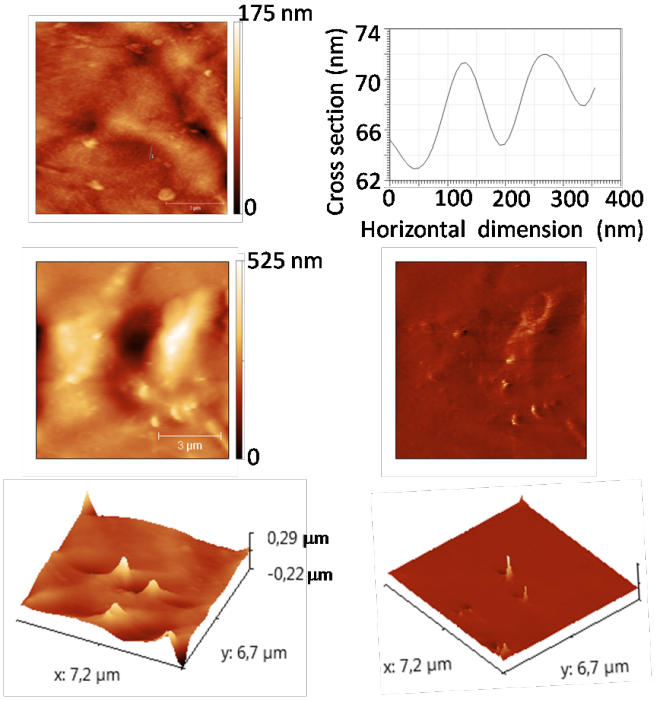

Figure 7: AFM topographies (left images), cross section and lateral force images (right side images) collected on digestive glands of M. edulis. The contrasts in the lateral force images clearly evidence presence and exogenous nature of the nanomaterials.

of a gonad's slice from an healthy subject is shown. These optical maps identify the most interesting samples for further analysis, are useful to provide information on the tissue's texture and on the occurrence of extensive or localized alteration at the sub-tissue level.

The most interesting sections were subsequently investigated by Scanning Electron Microscopy (SEM) at a much larger magnification (up to 5000x). These measurements allow to describe in greater detail the fine texture of selected areas of the organs (for instance specialized domains) and to analyze the differences in the microscopic structure of normal or altered tissues occurring in a given organ. The SEM and the conventional microscopy data, have been coupled providing a joined morphological characterization of the sample. Interesting examples are shown in Figures 5 and 6.

Among the analyzed samples, there are few cases where anomalies in the tissue's texture were identified. Such destructured features have been recognized mostly in the digestive glands that, hence, will be taken as illustrative examples for a more detailed discussion. Indeed, comparing the optical images of the two reported digestive glands (Figures 5 and 6), the most prominent structure in both the slices are the ducts and the secretive glands for the nutri-

ents' assimilation (the segmented irregular-shaped clusterized light area). Despite that, a comparison of the two slices clearly evidences a much higher degree of tissue organization and of functional domain segregation in the case of the normal section (Figure 5), while a large number of small, hollow grain-like structures are detectable in the case of the tissue of Figure 6. More data on the tissues and on the observable structures is provided by the corresponding SEM images.

A deeper morphological characterization has been provided by AFM. Indeed, in this work, AFM has mostly been used to refine the information on sections of particular interest This is mostly because, despite AFM characterization can produce extremely high spatial resolution quantitative images, such analysis is limited to quite small areas of the samples (maximum scan size is 40 um x 40 um) and is, therefore, not the best technique to provide an overview of the slices. Hence, the AFM measurements have been performed only on selected samples and revealed quite interesting data. Indeed, while the morphology of the normal-shaped digestive glands is basically featureless, several clusters of nanostructured exogenous material has been observed, through AFM topography and lateral force imaging (see Figure 7), in the partially destructured digestive gland of Figure 6.

The topographies collected on the partially destructured digestive gland clearly show the presence of nanomaterials as clusters or as single sparse spots, with sizes in the tens of nanometer (FWHM) scale. Such spots seems to be mostly embedded in the tissue texture or, sometimes, protruding from the cell surface rather than incorporated into the cell body. Their presence is even more clear in the lateral-force images (see Figure 7), where friction contrasts, similar to those observed in the case of the in vitro heavy metal doping of cells, are shown. The chemical composition of the nanostructures cannot be determined with accuracy, although the images acquired in the friction mode indicate that the nanoparticles' chemistry is different than their surroundings. No evidence of the presence of nanostructured materials incorporated in the tissues has been reported after extensive AFM analysis of normal-shaped glands. A preliminary interpretation of topography and lateral force data suggests that the characteristic of the friction contrasts are compatible with a metallic nature for the nanoparticles that apparently has not been transformed by the organism.

This relevant finding fully demonstrates the potential of our approach to detect and correlate tissue anomalies to nanostructured materials in the organs of marine species.

The advantages of the presented method compared to the standard investigations based on biochemical methods can be easily pointed out. Indeed, the standard methods of investigations are, mostly, based on the evaluation of biomarkers that are specific molecules, mobilized in the presence of one, or several, external stimuli. Thus, by analyzing such molecules, one can demonstrate that animals have been subjected to environmental stresses, but it is quite difficult to directly trace down the specific cause of the stress or to identify the chemical mechanisms that caused the stress [19, 25, 26]. In this context, our study proposes an integrated approach based on convergence of various morphological techniques that can address the problem at different level of the hierarchic organization of the marine organisms. In particular, it can add information on the localization, preliminary identifica-

tion and transformation or neutralization of the nanomaterials and on their correlation with the occurrence of morphological alterations of tissues.

4 Conclusions

Atomic force microscopy is an high resolution, non destructive, technique that produces intrinsically three-dimensional and quantitative topography images while, simultaneously, probing the local chemical properties (maps of surface friction) of the sample.
The ability of AFM to evaluate the effects of an external stimulus on a biosystem has been highlighted by an in vitro study of cultured cells treated with heavy metals administered as either chlorine salts or as nanoparticles. This approach provides a method to help understanding the basic mechanisms of interaction in reproducible and controlled conditions. The AFM investigation succeeded both in the direct localization of the pollutants and in the identification of different paths of cell degradation determined by the uptake of the various metals.
Moreover, a more sophisticated morphological approach devoted to the detection of nanostructured pollutant in the tissues of a marine organisms has been described. The method integrates conventional optical microscopy, SEM and AFM to address the problem of the presence of exogenous nanomaterials at different levels of the hierarchic organization of the organism.
The reported data showed that the coupling of optical images and SEM approach is very promising as it contains the potential to describe tiny features at high resolution and to complement their occurrence with the morphological status of the entire tissue. The implementation of the AFM, give to this approach the capability to detect the presence of exogenous material on the nanoscale, thus providing the basic information for a comprehensive understanding of the pollutant-to-biosystem interaction.
In conclusion, the proposed approach, based on the implementation of AFM with more conventional microscopies, has been proved an interesting and novel investigation method in the study of the impact of novel and emerging nanostructured pollutant on marine species.

References

[1] E. Meyer, H.U. Hug, and R. Bennewitz. Scanning Probe Microscopy: The Lab on a Tip. 2003.

[2] G. Binnig and H. Rohrer. In touch with atoms. *Review of Modern Physics*, 71:S324–S330, 1999.

[3] H.G. Hansma and L. Pietrasanta. Atomic force microscopy and other scanning probe microscopies. *Current Opinion in Chemical Biology*, 2:579–584, 1998.

[4] F.J. Giessibl. Advances in atomic force microscopy. *Reviews of Modern Physics*, 75:949–981, 2003.

[5] K.D. Jandt. Atomic force microscopy of biomaterials surfaces and interfaces. *Surface Science*, 491:303–332, 2001.

[6] C. Dunn. Near-Field Scanning Optical Microscopy. *Chemical Reviews*, 99:2891–2927, 1999.

[7] S.F. Wu. Review of near-field optical microscopy. *Frontiers of Physics in China*, 3:263–274, 2006.

[8] G. Binnig, H. Rohrer, C. Gerber, and E. Weibel. Surface Studies by Scanning Tunneling Microscopy. *Physical Review Letters*, 49:57–61, 1982.

[9] G.J. Simpson, D.L. Sedin, and K.L. Rowlen. Surface roughness by contact versus tapping mode AFM. *Langmuir*, 15:1429–1434, 1999.

[10] S.N. Magonov, V. Elings, and M-H. Whangbo. Phase imaging and stiffness in tapping-mode atomic force microscopy. *Surface Science*, 375:L385–L391, 1997.

[11] M. Girasole, A. Cricenti, R. Generosi, G. Longo, G. Pompeo, S. Cotesta, and A. Congiu-Castellano. Different Membrane Modifications Revealed by Atomic Force/Lateral Force Microscopy After Doping of Human Pancreatic Cells With Cd, Zn, or Pb. *Microscopy Research and techniques*, 70:912–917, 2007.

[12] M. Girasole, G. Longo, and A. Cricenti. An Alternative Tapping Scanning Near-Field Optical Microscope Setup Enabling the Study of Biological Systems in Liquid Environment. *Japanese Journal of Applied Physics*, 45:2333–2336, 2006.

[13] E. Tocha, H. Schönherr, and G.J. Vancso. Quantitative Nanotribology by AFM: A Novel Universal Calibration Platform. *Langmuir*, 22:2340 –2350, 2006.

[14] C. Bustamante, C. Rivetti, and D.J. Keller. Scanning force microscopy under aqueous solutions. *Current Opinion in Structural Biology*, 7:709–716, 1997.

[15] Y.F. Dufrene and G.U. Lee. Advances in the characterization of supported lipid films with the atomic force microscope. *Biophysica Biochimica Acta*, 1509:14–41, 2000.

[16] A. Vaseashta, M. Vaclavikova, S. Vaseashta, G. Gallios, P. Roy, and O. Pummakarnchana. Nanostructures in environmental pollution detection, monitoring and remediation. *Science and Technology of Advanced Materials*, 8:47–59, 2007.

[17] S. Tedesco, H. Doyle, G. Redmand, and D. Sheehan. Gold nanoparticles and oxidative stress in *Mytilus edulis*. *Marine Environmental Research*, 66:131–133, 2008.

[18] M. Fafandel, N. Bihari, L. Peric, and A. Cenov. Effect of marine pollutants on the acid DNAse activity in the hemocytes and digestive gland of the mussel *Mytilus galloprovincialis*. *Acquatic Toxicology*, 86:508–513, 2008.

[19] D.M. Lowe, V.U. Fossato, and M.H. Depledge. Contaminant-induced lysosomal membrane damage in blood cells of mussels *Mytilus galloprovincialis* from the Venice Lagoon: an in vitro study. *Marine Ecology Progress Series*, 129:189–196, 1995.

[20] M.N. Moore. Do nanoparticles present ecotoxicological risks for the health of the aquatic environment. *Environment International*, 32:967–976, 2006.

[21] A. Cricenti, R. Generosi, and M. Barchesi. A multipurpose scanning near-field optical microscope: Reflectivity and photocurrent on semiconductor and biological samples. *Review of Scientific Instruments*, 69:3240–3244, 1998.

[22] M. Girasole, A. Cricenti, R. Generosi, A. Congiu-Castellano, G. Boumis, and G. Amiconi. Artificially Induced Unusual Shape of Erythrocytes: An Atomic Force Microscopy Study. *Journal of Microscopy*, 204:46–52, 2001.

[23] G. Pompeo, M. Girasole, A. Cricenti, F. Cattaruzza, A. Flamini, T. Prosperi, J. Generosi, and A. Congiu-Castellano. AFM characterization of solid-supported lipid multilayers prepared by Spin-coating. *Biochimica Biophysica Acta*, 1712:29–36, 2005.

[24] G. Longo, M. Girasole, G. Pompeo, A. Cricenti, G. Andreano, F. Cattaruzza, L. Cellai, A. Flamini, C. Guarino, and T. Prosperi. An AFM investigation of oligonucleotides anchored on unoxidized crystalline Silicon surfaces. *Biomolecular Engineering*, 24:53–58, 2007.

[25] P.A. Olsvik, P. Gundersen, R.A. Andersen, and K.E. Zachariassen. Metal accumulation and metallothionein in brown trout, Salmo-trutta, from two Norwegian rivers differently contaminated with Cd, Cu and Zn. *Comparative Biochemistry and Physiology*, 128:189–201, 2001.

[26] D.R. Livingstone. Contaminant-stimulated Reactive Oxygen Species Production and Oxidative Damage in Aquatic Organisms. *Marine Pollution Bullettin*, 42:656–666, 2001.

A new Versatile Reconfigurable Acquisition Board: an Application to Marine Acoustic Signals Monitoring

M. Zora[1,2], G. Sottile[2], G. Nunzio Gallì[2], S. Aronica[1], A. Bonanno[1,2], G. Buscaino[1,2]

1, Institute for Coastal Marine Environment, CNR, Capo Granitola (TP), Italy

2, Daimar s.r.l. Innovation for Science (IAMC-CNR Spin-off), Mazara del Vallo (TP), Italy

marco.zora@iamc.cnr.it

Abstract

Make a multi-channel data acquisition system is often complex, expensive and cumbersome in marine applications. A new compact system for acoustic data acquisition and elaboration has been made by the Hardware Development Team of Capo Granitola IAMC-CNR.

The system, is based on a custom board with an FPGA (Field Programmable Gate Array), four parallel acquisition chains with charge amplifier, variable gain, selectable high-pass filter and Analog to Digital converter up to 1.33 MS$\cdot$s^{-1} with a 16 bit sample resolution. All in a PCB measuring just 10cm x 7.5cm. All electronic signals and control lines, flow in a single FPGA chip that manages the low level I/O operations of the whole board, so system operation can be modified changing only the firmware of the FPGA. Today, high performance, small size and low cost FPGAs, allow researchers to build reconfigurable instruments for various scientific applications.

Preliminary tests results are presented.

1 Introduction

In the last decade, marine scientific instruments have been in high demand, particularly autonomous instruments that are capable of staying under water for a long time while performing continuous data acquisition and storage. This paper introduces an instrument, under development, based on a concept of *reconfigurable measurement instrument*. The "reconfiguration" term is referred as hardware reconfiguration, performed via software.

Development of such equipment is a joint effort between different disciplines, such as physics, electronics, marine biology etc.

Long Term monitoring of marine ecosystems is today a challenge, logistically difficult and expensive.

Many instruments are capable of measuring a wide range of environmental parameters but only a few of these can record biological activity such as acoustic data. Acoustic monitoring can improve the knowledge of marine environment, because sounds can be an indicator of background noise and health status of biological habitat [1].

Some marine species use underwater sounds to help them navigate, locate food

and communicate with other animals.
For example, dolphins make many types of sounds: whistles, clicks and burst pulses. Some Whistles are used like a signature to serve as identification of individual dolphins. The approximate frequency range of bottlenose dolphin whistles is 200 Hz to 24 kHz [2]. Clicks are used exclusively for echolocation and are produced in rapid sequence. The frequency range for echolocation clicks is 200 Hz to 150 kHz [2]. Dolphins use lower repetition rate of clicks when echo-locating an object at a great distance, and higher when they move closer to an object, increasing spatial resolution of echolocation.
Man-made noise such as sonar, explosives and ships traffic, can have an adverse affect on marine mammals and ecosystems. Several scientific studies are needed to investigate this issue to preserve the safety and protection of marine mammals and their environment.
Scientific instruments used to record marine acoustic data, are often build by researchers assembling many different devices in order to obtain each time the best experimental results. These assembly some times are cumbersome, high power consuming and expensive. To meet underwater requirements, marine researchers need small size instruments and low power consumptions user friendly devices.
A new compact, low power, high performance reconfigurable electronic system has been developed by IAMC-CNR hardware development team in Capo Granitola (TP, Italy).
The Digital Acquisition System named DAQsys, is a four channel reconfigurable hardware for real-time marine acoustic data acquisition and elaboration. This prototype is a FPGA-based board that manages up to four high frequency signals simultaneously. The acquisition system was tested in the laboratory under controlled conditions.

Abbreviations

Refer to appendix for further acronyms and abbreviations.

2 System Description

An overview of the DAQsys board is shown in Figure 1. This board contains everything an engineer needs to create and implement a complete, small size, instrument for acoustic measurements.
The board is made up of three main sections: analog to digital front-end, data-management and data-storage.
Analog to digital front end includes four programmable gain amplifiers, four programmable high-pass filters and four ADC devices (Analod Devices AD7983).
Data management is absolved by a central FPGA device that is reprogrammable, flexible, low cost and low power. Thanks to its reprogrammability, the non recurring engineering costs are removed from prototyping and testing stages and, in addition, the platform can be reconfigured for future applications.
Data-storage section includes a Memory Card interface and an expansion bus, which can be connected to a PC through an USB adapter.

3 Hardware

Field Programmable Gate Arrays are semiconductors devices containing programmable logic components, memory elements and programmable interconnects.

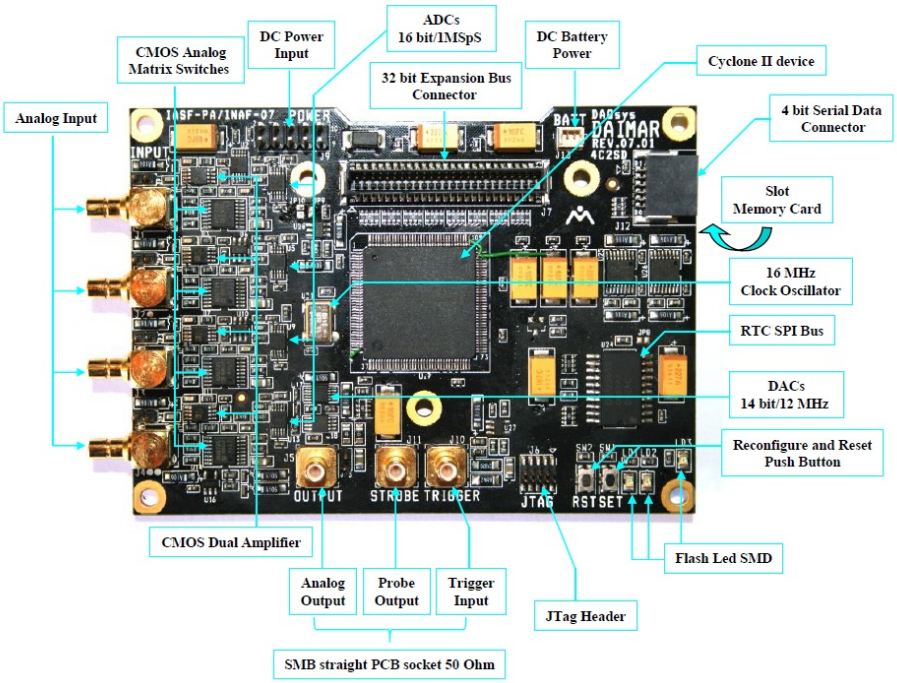

Figure 1: DAQsys board overview. All components are mounted on a small card (100mm x 75mm x 13mm).

Programming the interconnections and the logic components, is possible to implement simple logic gates such as AND, OR, XOR, NOT or more complex combinatorial functions and sophisticated micro-controllers. Current FPGAs contain up to tens of thousands of basic building blocks, with this number increasing rapidly. The main difference between FPGA and CPU is the ability to perform parallel computations. CPU performs operations in a strictly sequential mode and needs several steps to complete a task whereas in the FPGA the same task can be often solved in only one step building hardware components that work in parallel. This last solution in some cases can significantly reduce the execution time compared to a pure software implementation.

All input and output devices are connected directly to the FPGA in a star topology [3] and in order to take full advantage of this architecture, the features are implemented in the form of "system-on-a-chip" within this single electronic component. This allows you to control all activities in parallel with response times of a few nanoseconds.

FPGA

The FPGA chip employed is the Altera Cyclone II EP2C5T144C6N [4]. In order to implement the needed logic functions, the FPGA must be programmed with

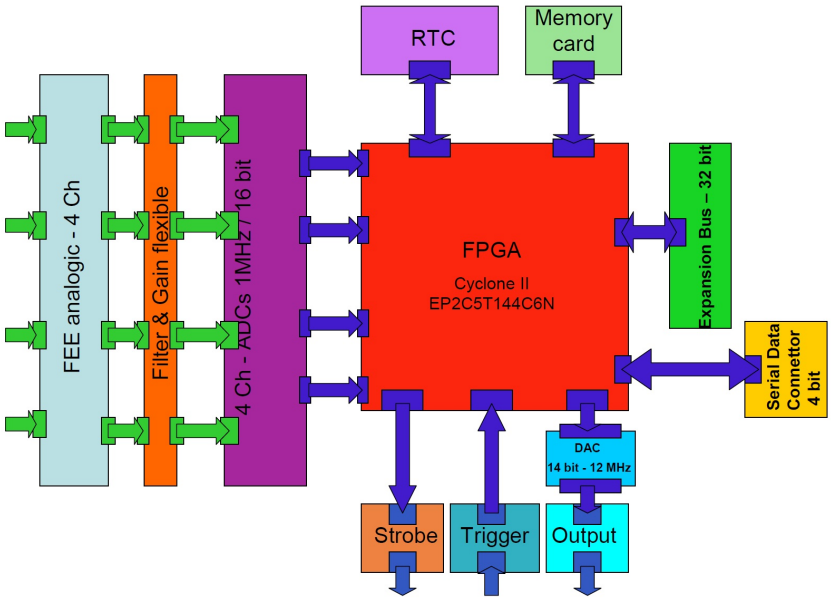

Figure 2: DAQsys architecture overview.

a Hardware Description Language such as. VHDL, Verilog, etc. .. or with a schematic design. The firmware can be developed and tested with software such as Altera Quartus II and Mentor Graphics ModelSim.
Many complex logic functions are provided for free by FPGA vendors or are available on the market in the form of intellectual property (IP core), then the development of an application can be fast and flexible.
Among them all, an interesting IP core is the so-called soft-processor. It is a microprocessor with reconfigurable architecture that can be programmed through the high-level language C / C + +. By implementing this component inside the FPGA, users can build complex solutions using appropriate combinations of hardware and software with a simpler approach.
Altera's Embedded portfolio offers the broadest selection of soft processor cores in the industry. From Nios® II, the FPGA industry's 1^o soft processor, to popular architectures from ARM and Freescale.
During the testing and debugging, the FPGA is programmed via the standard JTAG interface (boundary-scan test devices [5]). When the firmware is complete and ready for use, it is stored in an EEPROM and every time you restart the system, the FPGA loads its configuration from the memory and executes it.

Analog to Digital Front End

DAQsys card can handle up to four data acquisition chains, each consisting

of a charge amplifier with high input impedance (100 M Ω) and programmable gain (6dB, 20dB, 32dB, 40dB and 50dB), a first-order High-Pass filter (cutoff frequency: 16 kHz, 5 kHz, 1.6kHz, 160Hz, 16Hz) and a low power 1.33MS·s^{-1} - 16 bit ADC converter. The input impedance of the charge amplifier can be set also to 50 Ω via a jumper.
The gain factor and the cutoff frequency of the filter are selected via serial interface from the FPGA.
The high impedance, high gain and low noise front-end makes the system suitable for interfacing with piezoelectric sensors such as hydrophones.
The ADC voltage reference is 2.5V and it matches the full scale voltage (FS).
The voltage gain Av_{dB} in dB is:

$$Av_{\mathrm{dB}} = 20 \log \frac{V_{out}}{V_{in}},$$

where V_{out} and V_{in} are respectively the output and the input voltage of the charge amplifier.

$$V_{out} = 10^{Av_{\mathrm{dB}}/20} \cdot V_{in};$$

substituting the values and assuming a gain of 50dB:

$$V_{out} \simeq 316 \cdot V_{in}$$

The maximum theoretical sensitivity of the system, is given by:

$$S_x = \frac{FS}{2^N \cdot Av},$$

where N is the ADC resolution and Av is the voltage gain. For a 16 bit resolution we obtain:

$$S_x = \frac{2.5}{2^{16} \cdot 316} = 120\mathrm{nV}.$$

As we will see in the section of Preliminary Results, we must take into account the Effective Number of Bits of a system, because this is what gives the true resolution.
A useful feature of DAQsys board is the ability to synchronize the four ADC with a single clock or to target a single input to all the ADC and then use four sampling clock signals with a mutual phase shift of T / 4, where T is the sampling period.
In this way, the analog signal can be oversampled at up to 5.3 MS·s^{-1} to significantly improve signal to noise ratio.

Real Time Clock (RTC)

DAQsys comes with a Dallas Semiconductor RTC [6] mounted on board. This device is a low cost, extremely accurate SPI bus real time clock with an integrated temperature compensated crystal oscillator (TCXO). The accuracy is ±2 ppm from 0^{o}C to 40^{o}C and device maintains seconds, minutes, hours, day, date, month and year with leap year compensation valid up to 2099.
It allows to join precise time information with collected data or other interesting events. DAQsys card is equipped with a secondary connector to power the RTC with a back-up battery even when the main power of the card is turned off, so as to keep in memory the time data. This integrated circuit gives information about temperature as a 10-bit code with a resolution of 0.25^{o}C and temperature accuracy within the range of ±3^{o}C, allowing temperature monitoring of the system.

I/O peripherals and connectors

The DAQsys board has many pins used for I / O, expansion and programming interface and all are linked directly to the FPGA

- One 14bit-12MHz DAC digital to analog converter with SPI interface [7] and a couple of strobe (out) and trigger (input) available on 50Ω SMB connectors which are useful to generate analog signals or to synchronize DAQsys with other electronic boards.
- One standard JTAG (Join Test Action Group) interface is used for: Production Test, Prototype Debug and In-circuit Programming.
- One 9 pin multimedia connector allows data storage into a multimedia card (or SD card) or loading FPGA firmware from it.
- One 50 pin - 32bit and a 12 pin - 4bit expansion connectors are used to interfacing with 3.3V TTL compatible external devices. Currently, USB interface is available to connect the DAQsys board to a standard PC through the 50 pin connector.

4 Data Format

DAQsys saves data in RAW format, even though a simple compression algorithm can be implemented in the FPGA's firmware.
RAW data are sequences of 16 bit unsigned words coming from the ADC converters in the little-endian format.
To take full advantage of the connected PC, we perform a real time compression of the acoustic data using the free FLAC codecs available on the web. This application convert RAW data into FLAC files or into standard WAV format. Researchers can therefore use the preferred tools for analysis and elaboration of acoustic data.

FLAC conversion

FLAC means Free Lossless Audio Codec. In short, it is a way of reducing a very large acoustic file size into something more manageable. It is similar to making a ZIP file. An acoustic file can be reduced in size by 50% to 60%. As the conversion is lossless, the audio quality is preserved.
FLAC stands out as the fastest and most widely supported lossless audio codec, and the only one that at once is non-proprietary, is unencumbered by patents, has an open-source reference implementation, has a well documented format and API, and has several other independent implementations.
FLAC supports tagging, cover art, and fast seeking. FLAC is freely available and supported on most operating; systems, including Windows, "unix" (Linux, *BSD, Solaris, OS X, IRIX), BeOS, OS/2, and Amiga.
There are many programs and devices that support FLAC, but the core FLAC project here maintains the format and provides programs and libraries for working with FLAC files. Notable features of FLAC:

- Lossless: The encoding of audio (PCM) data incurs no loss of information, and the decoded audio is bit-for-bit identical to what went into the encoder.
- Fast: FLAC is asymmetric in favor of decode speed. Decoding requires only integer arithmetic, and is much less compute-intensive than for most perceptual codecs. Real-time decode performance is easily achievable on even modest hardware.
- Hardware support: FLAC is supported by dozens of consumer electronic devices, from portable players, to home stereo equipment, to car stereo.
- Seekable: FLAC supports fast sample-

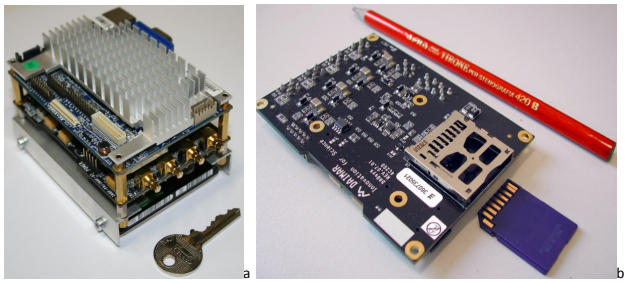

Figure 3: a) DAQsys board, VIA PICO-ITX and hard-disk assembled. b) Bottom view of DAQsys board with memory card

Condition	DAQsys+USB current @5V	PC current @12V	Total Power
wait-state	330mA	751mA	10.7W
execution	604mA	800mA	12.6W

Table 1: Total power consumption during wait-state and execution. During execution only one ADC is active and works at a rate of 750 KS·s^{-1}.

accurate seeking. Not only is this useful for playback, it makes FLAC files suitable for use in editing applications.

- Error resistant: Because of FLAC's framing, stream errors limit the damage to the frame in which the error occurred, typically a small fraction of a second worth of data. Contrast this with some other lossless codecs, in which a single error destroys the remainder of the stream.

A Custom C++ software has been written to take advantage of FLAC compression algorithm before saving data on hard disk. FLAC allows an optimization of the storage space without loss of information,so increasing the maximum acquisition time.

5 Preliminary Results

Some tests have been performed and a complete data acquisition system has been assembled.
The first experimental set-up consists of DAQsys connected to a PC via USB card interface.
We built a simple application in C++ running on the PC, which collects data from the DAQsys board and save it on hard disk.
The second experimental set-up consists in the DAQsys alone that saves data directly to memory card installed on board.
In the following measurements, the sample rate was set to 750 kS·s^{-1}. To facilitate the analysis of acoustic data, the application reads a continuous stream of data and creates a file of about 4 MB each time.

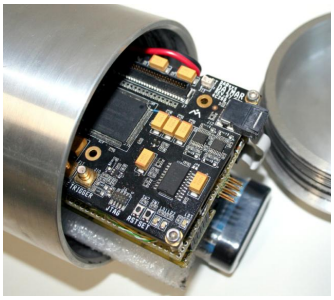

a

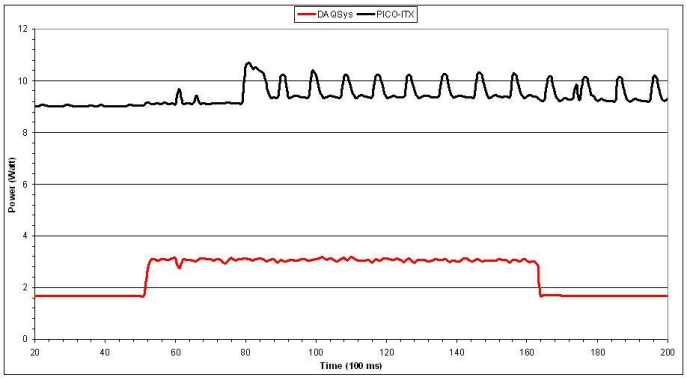

b

Figure 4: a) The complete embedded acquisition system. b) Power consumption during execution. Lower power is referred to DAQsys + USB interface whereas the Higher power is refereed to the PICO-ITX PC.

Power Consumption

Power consumption is been measured in wait state and during execution with the Agilent DC Power Analyzer [8]. In wait state, the DAQsys and the PC are powered but no acquisition is made. In execution, data is acquired continuously and saved on hard-disk.Table 1 shows averaged total power in the wait-state and with a single channel acquisition.

Power considerations are important if we want to make a complete battery powered, reduced size system for underwater measurements. We are currently testing such a system with several different lithium-ion batteries.

Figure 4 shown the complete system layout and the power consumption.

As we can see, the most part of power consumption is due to the PC, the USB interface and the hard-disk. In order to reduce power consumption, the DAQsys board must save data directly on the memory card (MMC). In these preliminary tests

Condition	DAQsys current @5V	MMC max current @3.3V	Total Power
wait-state	153mA	150μA	0.76W
execution	160mA	80mA	1.06W

Table 2: Power consumption of the DAQsys alone. "MMC max current" is the maximum current absorbed by the MMC during read/write cycles.

we have measured power consumption of DAQsys in two conditions: the first with all the ADC off, the second with a single channel running at 750kS$\cdot$s^{-1}. Table 2 summarizes the results.
A typical battery pack of small size, has an energy capacity of $14.5V \cdot 5Ah = 72.5Wh$ in only 700g weight.
Using first set-up, the embedded PC can work uninterruptedly for about 5.7 hours, with the second set-up DAQsys can run uninterrupted for 68 hours.
We are investigating other solutions, to further reduce the power required by the system, overcoming the typical memory limitations of the MMC. One of these possible solutions is the "mixed mode operation".
In this mode, just DAQsys board must be always powered on, and data is saved on the MMC only during significant acoustic events. DAQsys will turn on the pc as soon as the MMC memory will be almost full then the PC will copy the entire contents of memory on the hard disk, and turns off again.

Signal to Noise Ratio Measurements

In handling real-world signals, analog circuitry sometimes becomes the limiting factor on overall accuracy, for this reason, a dynamic test is needed to show exactly what you can expect from your data acquisition system.
There are several methods used to take information about accuracy of a system. We want estimate the Effective Number of Bit (ENOB) of the ADC and the signal-to-noise-ratio.
Shorting to ground a channel of the DAQsys, the value sampled should be theoretically 0V. What we get instead is a set of points distribuited around a costant value. The total noise can be estimated as the mean of the squared deviation of these points from the mean value.
The variance is defined as:

$$\sigma_x^2 = \frac{1}{N} \sum_{i=0}^{N-1} (x_i - \mu)^2,$$

where N is the number of measurements and x_i is the i-th measurement. We have setted the amplifier's gain of the acquisition channel to +6db and the high-pass frequency to 5kHz. A LabView application, has been built to find the value of σ_x^2. Preliminary result on a dataset of about 500 points give:

$$\sigma_x^2 = 6.3.$$

The on-board ADC converters have a 16 bit resolution (N) and a Full-Scale (FS) of 2.5V, so the minimal theoretically voltage step δV that can be detected, due to the quantization of the analog signal, is:

$$\delta V = \frac{FS}{2^N} = \frac{2.5V}{2^{16}} = 38\mu V.$$

Gain$_{dB}$	σ_x^2	**ENOB**	**SNR**$_{dB}$
6	6.3	14.7	90
50	110	12.6	77.6

Table 3: ENOB (Equivalent Number Of Bit) and SNR (Signal to Noise Ratio) when gain is 6dB, 50dB and input is shorted.

This is also the conversion factor between digital samples and voltage. Now we calculate the standard deviation as the square root of σ_x^2 and multiply it by the conversion factor to obtain the minimum effective voltage step ΔV detectable by our system *under these experimental conditions*:

$$\Delta V = \sigma_x \cdot \delta V$$

substituting the values:

$$\Delta V = 95\mu V.$$

Being ΔV the minimum effective voltage step, it is related to the effective number of bit ENOB by:

$$\Delta V = \frac{FS}{2^{ENOB}}$$

and by simple manipulations:

$$ENOB = \log_2\left(\frac{FS}{\Delta V}\right) \qquad (1)$$

$$ENOB = 14.7\text{bit}$$

The signal-to-noise-ratio can be computed by the following expression:

$$SNR_{dB} = ENOB \cdot 6.02 + 1.76 \qquad (2)$$

substituting the values:

$$SNR_{dB} = 90\text{dB}.$$

The previous calculation was repeated with 50dB gain setted on amplifier. The results are summarized in Table 3. As verification of these results, the short to ground was removed from the input. A sinusoidal signal with frequency of 20kHz and amplitude of 500mVpp, generated by Agilent 81150A function generator, has been sent to the DAQsys input channel and acquired to compute the Mean Squared Error of the measured data. The input impedance of the charge amplifier is matched to the impedance of the function generator (50Ω). The resolution of the function generator is 14bit and this value definitely will affect the measurement of the ENOB. The gain and the cut-off frequency of the high-pass filter have been setted respectively to +6dB and 5kHz.
The Mean Square Error (MSE) for two set of samples x_i and y_i is defined as:

$$MSE = \frac{1}{N}\sum_{i=0}^{N-1}(x_i - y_i)^2.$$

We can use the MSE to compare a set of software generated samples x_i with the acquired ones y_i. The measurements will be affected by random noise, but we know that the acquired signal is a sinusoid with known frequency and amplitude, then we can find a sinusoidal function that best fit with our experimental data and take the MSE as a noise estimation. If we change amplitude, offset or phase of the software generated sinusoid, the value of MSE will

increase or decrease according to these values. For noise estimation we must consider the minimal value of MSE.
Preliminary result on a dataset of about 500 points give:

$$MSE = 44.18.$$

In analogous way, we calculate the square root of MSE (RMSE), to obtain the effective minimal voltage step ΔV in this condition:

$$\Delta V = RMSE \cdot \delta V = \sqrt{MSE} \cdot \delta V.$$

and substituting the values for RMSE and previous calculated δV, we obtain:

$$\Delta V = 0.25\mathrm{mV}.$$

The ENOB of DAQsys ADC is computed as before and then from (1) we have:

$$ENOB = 13.27\mathrm{bit}.$$

With function generator that feeds the input, the ENOB is smaller than that evaluated with input channel shorted to ground. This value reflects in some way, the resolution of the function generator which is just 14 bit, so we can't expect more.
Again, using the equation (2) of SNR and ENOB we have:

$$SNR_{dB} = 81.6\,\mathrm{dB}.$$

This calculation was obtained manually changing parameters of the generated sinusoidal function to obtain the minimal MSE, so it is only a coarse value for the SNR and it is underestimated.

Time Delay Accuracy

To evaluate accuracy in time delay measurement we have arranged the system as follow:
Two analog signals having the same amplitude and frequency with a precise time delay between them ("true delay") are generated by the function generator and feed two inputs of DAQsys board. These inputs are setup with the same gain and same cut-off frequency respectively of 6dB and 5kHz. The two signals are sampled synchronously and, to avoid ADCs saturation, their amplitude was kept below 600 mV.
Two comparators was used to compare the sampled signals to a threshold and generate two trigger events, one to start and another to stop a counter, whose count will be proportional to the delay between the two signals. The clock used to increment the counter is faster than sampling clock, and it is exactly 16 MHz (f_{count}). Under these conditions the number of counts multiplied by the clock period (1/16MHz = 62.5 ns) gives the time delay between the two input signals ("measured delay").
The Firmware on the FPGA has been modified to include these comparators and the fast counter.
The indetermination on a sample time is related to the sampling period of the AD converters. Therefore given a sampling rate f_s of $750\mathrm{kS}\cdot\mathrm{s}^{-1}$, the indetermination Δt can't be lower than:

$$\Delta t = \frac{1}{f_s} = \frac{1}{750\mathrm{kS}\cdot\mathrm{s}^{-1}} = 1.33\mu\mathrm{s};$$

if no other parameters affect the measurement, Δt would also be the measurement indetermination. In real situation several factors must be taken into account.
Measured values and expected ones are shown in Table 4.
For each true delay, we found two different counter values: a minimum count and a maximum count.The measured delay is obtained by:

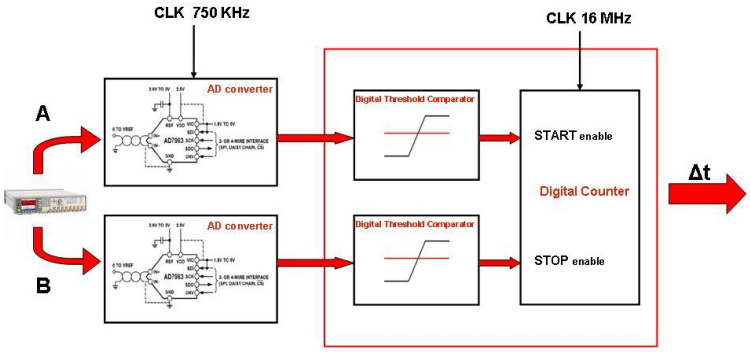

Figure 5: Schematic block diagram illustrating the architecture used to measure time delay.

measured delay =

$$= \frac{max.count + min.count}{2} \cdot \delta_t,$$

where δ_t is:

$$\delta_t = \frac{1}{f_{count}} = \frac{1}{16MHz} = 0.065\mu\text{s}$$

We can define $delta\ error$ as:

$$\delta\ error = (max.count - min.count) \cdot \delta_t$$

Thus it is evident that the time sampling of ADC is the main indetermination on the measure. Other noise effects have no relevant influence.

6 Application Examples

Many different applications can be performed with the DAQsys board changing only the firmware on the FPGA and, if needed, the software running on the connected PC.
There are two main examples that emphasise the DAQsys flexibility. One regard the acquisition and storage of marine acoustic data and the other concerns passive detection of underwater acoustic sources.

Data Acquisition

Record the sound environment of marine habitats for extended periods of time, requires large amounts of resources for data storage. For example at a sampling rate of 500 kS·s^{-1}, data flow is 1MB per second, will therefore be used 3.6GB of storage space per channel for each hour of recording. Today are commercially available MMC with memory capacity up to 32 GB, so we can record up to 10 hours of continuous acoustic data using an MMC.
To increase the recording time there are at least three solutions: the first is to save only the interesting parts of a signal and discard the others, the second is to compress data with some appropriate algorithm and the third is to expand the amount of storage space.
The first solution has been investigated by implementing a discrimination circuit with adjustable threshold into the FPGA. This

true delay μs	**max. count**	**min. count**	**measured delay** μs	**delta error** μs
2	42	21	1.97	1.31
2.5	42	21	1.97	1.31
5	85	64	4.66	1.31
10	171	149	10	1.38
50	811	789	50	1.38
60	960	959	59.97	0.06
100	1600	1599	99.97	0.06
300	4800	4799	299.97	0.06
500	8000	7999	499.97	0.06
1000	16000	15999	999.97	0.06

Table 4: The true delay is setted on the function generator. When the true delay is much greater than the sampling period, the uncertainty on the measured delay is negligible.

circuit is essentially a real-time 16 bit comparator, which enables data memorization only when the ADC output is greater than a selected threshold. Further improvements can be achieved by adding a band-pass digital filter in the acquisition chain, so as to record only the signals of interest. Reduce the number of memory accesses, also helps to reduce energy consumption.
The second solution requires more FPGA resources and an increased development time to be satisfactorily achieved.
We also investigated the third solution exploiting an external PC. It was connected to the DAQsys board through an USB adapter card. The PC used in our tests was an embedded VIA PICO-ITX based on Windows XP operating system. A custom software was written to acquire data and save on hard disk.
To meet the requirements of a real-time system for data acquisition and storage it was necessary to design an interface module inside the FPGA between the serial ADC converters and the USB bus, both operating at different clock frequencies. We compared two architectures, with different clock for read and write operations: one based on a FIFO (First In First Out) and the other based on a double-buffered RAM. Both architectures have allowed to mantain a sustained data streaming on the hard-disk at the maximum sampling rate of $5.3\mathrm{MS}\cdot\mathrm{s}^{-1}$.

Passive Detection

Multilateration, also known as hyperbolic positioning, is the process of locating an object by accurately computing the time difference of arrival (TDOA) of a signal emitted from that object to four or more receivers.
If a sound pulse is emitted from a source, it will arrive at slightly different times at two spatially separated receivers, TDOA is due to the different distances of each receiver from the source. Given two receivers positions and a known TDOA, the locus of possible emitter positions in a 3D space is a two-sheeted hyperboloid. To obtain a

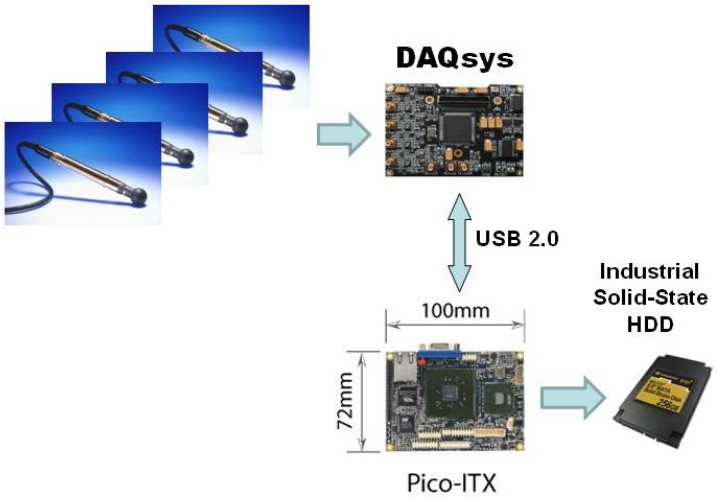

Figure 6: Four hydrophones can be connected directly to the DAQsys. Data can be saved on hard disk exploiting an embedded PC.

unique position of the source in a 3D space, we need at least four receivers and calculate the hyperboloids intersection.
Four hydrophones can be connected directly to the four high impedance channels of the DAQsys board and synchronous sampling the four signals, we can measure TDOA with high precision.
We have performed some investigations about the ability to get a measure of time difference between two signals and we have evaluated the maximun error. These tests are reported in the Preliminary Results section.

7 Conclusion

The results show that the new DAQsys board provide an effective combination of hardware and software for acquisition and elaboration of acoustic signals.
Thanks to its small size and low power consumption, DAQsys is very useful in marine underwater applications where high performance are required.
Preliminary tests have revealed that the DAQsys board is very helpful to developing a long-term recorder of biological sounds.
The high speed of data acquisition up to 1.33 $MS{\cdot}s^{-1}$ per channel, suggests the use of DAQsys to study the sounds made by dolphins.
High system accuracy is proven by an equivalent number of bits between 12.6 and 14.7, that is a remarkable results in marine electronics.
We have achieved also an excellent accuracy in time delay measurements, valuable parameter to develop instruments for passive acoustic localization.
The main characteristic of this new hardware is the use of reconfigurable FPGA to manage all functions of the board instead

of conventional CPU. The system can be customized by researchers for new future applications and experiments, giving life to concept of *Lab On Module*, similarly to the concept of *Computer On Module* widely used in the electronics field.

Future Works

We are working on various projects and many applications are under development to make use of DAQsys easier in the next future.
An advanced firmware for TDOA passive localization will be developed to allow Dolphins localization.
Power consumption will be reduced following differents strategies to give power supply only to essential circuitry, disabling the unused peripherals.
For example, when PC is needed to exploit data-storage space on HDD, its power supply will be switched on from DAQsys only during storage operations.
We must study data compression algorithms in hardware to improve efficiency in data storage and test the system under real conditions to evaluate the results.

Abbreviations

DAQsys = Digital Acquisition System, with reconfigurable hardware.
FPGA = Field Programmable Gate Array.
HDL = Hardware Description Language.
JTAG = Join Test Action Group. In the 1980s, the Joint Test Action Group developed a specification for boundary-scan testing that was later standardized as the IEEE Std.1149.1 specification.
ADC = Analog to Digital Converter.
DAC = Digital to Analog Converter.
RTC = Real Time Clock.
MMC = Multimedia Memory Card.
FIFO = First In Fist Out. A memory array working like a shift register.
TDOA = Time Difference of Arrival.
RAW = Data coming from the Analog to Digital Converter without any elaborations.
FLAC = Free Lossless Audio Codec. Similar to ZIP file but optimized for acoustic data.
WAV = Standard audio format.
PCM = Pulse Code Modulation.
API = Application Programming Interface.

References

[1] M. Lammers and R. et al. Brainard. An ecological acoustic recorder (EAR) for long-term monitoring of biological and anthropogenic sounds on coral reefs and other marine habitats. *Acoustical Society of America*, 2008.

[2] J.E. Reynolds and S.A. Rommel. Biology of Marine Mammals edited by J.E. Reynolds and S.A. Rommel. *Smithsonian Institution Press, Washington*, page 578 pp., 1999.

[3] Imaging & Microscopy. Scanning Probe Microscope Control. New Electronic Concept for Utmost SPM Demands. *G.I.T. Imaging & Microscopy, GIT VERLAG GmbH & Co. KG, Darmstadt, Germany*, 1:52–55, 2007.

[4] Altera. Cyclone II Device Handbook, Volume 1. *Altera Corporation (http://www.altera.com)*, 1, February 2007.

[5] Altera. IEEE 1149.1 (JTAG) Boundary-Scan Testing in Altera Devices. *Altera Corporation, ver. 6.0 Application Note 39*, June 2005.

[6] Dallas Semiconductor. Extremely Accurate SPI Bus RTC with Integrated Crystal and SRAM: DS3234. *Dallas Semiconductor - MAXIM integrated Products. Rev. 2*, 10, 2008.

[7] Analog Devices. 12-/14-Bit High Bandwidth Multiplying DAC with Serial Interface: AD5444/AD5446. *Analog Devices, Inc. Rev. A*, 2006.

[8] Agilent Technologies. Agilent DC Power Analyzer Models: N6705A, N6715A, N6731B-36B,N6741B-46B, N6751-54A,N6761A-62A, N6773A-76A. *Agilent Technologies, Inc.*, January 30, 2008.

Phytosterols from Marine Microalgae *Dunaliella tertiolecta* and *D. salina*: a Potentially Novel Industrial Application

M. Francavilla[1], P. Trotta[1], R. Luque[2]
1, Institute of Marine Sciences, CNR, Lesina, Italy
2, Department of Organic Chemistry, University of Córdoba, Córdoba, Spain
matteo.francavilla@fg.ismar.cnr.it

Abstract

Sterols have been extracted and analysed from Dunaliella tertiolecta and Dunaliella salina, in order to evaluate a potentially novel industrial exploitation of these microalgae as source of phytosterols. The effect of salt concentration on sterols yields has been studied varying the quantities of NaCl into culture medium. Twelve sterols were identified by Gas chromatographic MS/MS analysis for both algal strains. The most abundant phytosterols were (22E,24R)-methylcholesta-5,7,22-trien-3β-ol (ergosterol) and (22E,24R)-ethylcholesta-5,7,22-trien-3β-ol (7-dehydroporiferasterol). The whole sterol fraction consisted mainly of phytosterols (C28 and C29 sterols). Good yields of total sterols were achieved at lower salt concentration (1.3% and 0.89% of dry weight in *D. tertiolecta* and *D. salina*, respectively, at 0.6M NaCl), while an increase in salt concentration resulted in a significant decrease in total sterols yield.
The exploitation of *D. tertiolecta* and *D. salina* (at 0.6M NaCl) as source of phytosterols might be an achievable target taking into account that microalgae biotechnology has reached high levels of development; biomass productivity for microalgae is much higher than that of land-based crops; the production of phytosterols could be considered as an added value for Dunaliella biomass applying the conceptual model of biorefinery; and that phytosterols have grown in popularity and market.

1 Introduction

Algal biotechnology has made major advances in the past three decades, and several microalgae like Botryococcus, Chlorella, Dunaliella, Haematococcus and Spirulina are cultivated for the production of proteins, astaxanthin, β-carotene, glycerol, liquid fuels, pharmaceutical formulations and also for fine chemicals [1]. Among these algae, those of the genus Dunaliella, especially *D. salina* and *D. tertiolecta*, are microalgae most studied for mass culture [2].
Dunaliella is a unicellular, bi-flagellate, naked, green alga (Chlorophyta, Chlorophyceae) which is widely distributed and may be found in fresh water (e.g. *D. flagellate, D. chordate, D lateralis, D. paupera*), in mixed and euryhaline waters (e.g. *D. tertiolecta, D. bioculata, D. primolecta*) and in hypersaline waters (e.g. *D. salina, D. minuta, D. parva, D. virdis*) [2]. Dunaliella spp. are grown as a food source in aquacul-

ture and *D. salina* is the richest algal source of β-carotene and glycerol [3, 1]. *D. salina* can produce β-carotene up to 14% of its dry weight under conditions of high salinity, light and temperature, as well as nutrient limitation. Dunaliella β-carotene has an increasing demand and a wide variety of market applications: colouring agent in food industries; component in pharmaceutics, cosmetics and health foods; dietetic industries; diagnostics and biomedical research.

Among chemical constituents of microalgae, sterols are of increasing interest since: a) the presence of these natural products in microalgae determines their food values; b) these compounds are useful biomarkers for identifying sources of organic matter in sediments [4]; c) and they are not only essential components of biomembranes, but function in cell proliferation and signal transduction of microalgae, and other eukaryotic organisms, modulating the activity of membrane-bound enzymes [5].

In contrast with higher plants, algae (including microalgae) contain a larger diversity of different sterols [6]. Although some sterols are widespread in many taxa of algae, sterol profiles can be sometimes characteristic of a particular class, family, genus, or even species of microalgae, and so are often used for chemotaxonomic and phylogenetic comparisons [7, 8].

Wright [9, 10] identified in *D. tertiolecta* by GC-MS and 13C NMR a mixture of 24-methyl (C28) and 24-ethyl (C29) Δ7, Δ7,22, Δ8,14, Δ5,7,22 sterols. He found that two major sterols were (22E,24R)-methylcholesta-5,7,22-trien-3β-ol (trivial name ergosterol, C28) and a closely related C29 trienol, (22E,24R)-ethylcholesta-5,7,22-trien-3β-ol (trivial name 7-dehydroporiferasterol), but he did not quantify them. Patterson et al. [8] identified in the same microalga two rare tetraene sterols, (22E,24R)-methylcholesta-5,7,9(11),22-tetraen-3β-ol and (22E,24R)-ethylcholesta-5,7,9(11),22-tetraen-3β-ol but even in that study, sterols were not quantified. In two other scientific works [11, 12], authors made reference to sterol composition of *D. salina*, but they reported the most abundant sterols only (ergosterol and 7-dehydroporiferasterol) and did not analyse the sterols percentage in relation to dry weight.

Nowadays the phytosterols, C28 and C29 sterols, are playing a key role in nutraceutic and pharmaceutical industry because they are precursors of some bioactive molecules (eg.: ergosterol is a precursor of Vitamin D2 and it is also used for the production of cortisone and hormone flavone and have some therapeutic applications to treat hypercholesterolemia. In particular, phytosterols have been shown to lower total and LDL cholesterol levels in humans by inhibiting cholesterol absorption from the intestine. High serum concentrations of total or low-density-lipoprotein (LDL)-cholesterol are major risk factors for coronary heart disease, a major cause for morbidity and mortality in developed countries [13]. It is understandable that efforts are made to minimize such risks, and reduction of serum cholesterol is a feasible approach, since a risk reduction of coronary heart disease of about 3% can be achieved through a 1% decrease in total cholesterol [14]. In addition to their cholesterol lowering properties, phytosterols possess anti-inflammatory and anti-atherogenicity activity and may possess anti-cancer and anti-oxidative activities [15].

Today, consumers are actively seeking products containing health-promoting ingredients to improve their health and well-being. In keeping with this trend, nutraceu-

ticals such as phytosterols, that have a beneficial impact on heart health, have grown in popularity.
Currently, higher plants are the main industrial sources of phytosterols. Phytosterols isolation in large scale is based in two major raw materials, vegetable oils and tall oil [13].
In this study we analyzed and quantified sterols in two species of Dunaliella, *D. tertiolecta* and *D. salina* (already studied but not for quantitative sterol analysis). We evaluated the effect of salt concentration of medium culture on quali-quantitative composition of sterols in order to find optimal conditions for major yields of phytosterols. The aim of this work is to evaluate the feasibility of using the two strains of Dunaliella as a new commercial source of phytosterols.
The findings of this study could lead to a new industrial exploitation of Dunaliella biomass for phytosterols production in the light of a forecast increase of European Phytosterols market (from $103.9 million in 2005 to $196.7 million in 2012) [16].

2 Materials and methods

2.1 Biomass preparation

Monoxenic strains of *D. tertiolecta* and *D. salina* collected from local algal strains bank (Fitoteca of ISMAR-CNR Lesina) were grown in 1 L flasks containing Walne's medium (modified from [17]). Cultures were grown at constant temperature (20 $\pm$ 0.5°C), under artificial light with an intensity of 150 $\mu\,\mathrm{E}{\cdot}\mathrm{m}^{-2}\cdot\mathrm{s}^{-1}$ and a light periodicity of 12/12 light/darkness. Cultures were under air bubbling agitation (1 L min 1) with a CO_2 concentration of 1% v/v. *D. tertiolecta* and *D. salina* were grown at three different salt concentrations (0.6, 1.4 and 2.1 M NaCl), obtained varying the amount of NaCl dissolved in the Walne's culture medium.
After cultures reached the end of logarithmic growth phase (approximately 7-10 days), *D. tertiolecta* and *D. salina* were collected in a pyrex glass container and then centrifuged at 4500 rpm for 10 minutes. The harvested biomass was washed with 0.5 M NaCl and distilled water to remove non-biological material such as mineral salt precipitates and finally it was freeze-dried and stored at -30°C until lipid analysis.

2.2 Lipid extraction

Lipids from the cell containing pellets were extracted according to Bligh and Dyer [18]. The mixture was centrifuged and the solid residue resuspended in a chloroform/methanol mixtur. The combined supernatants were cleaned using a saturated NaCl water solution and the chloroform phase was recovered using a separatory funnel. The chloroform phase was combined and dried with sodium sulfate overnight. Purified lipids were weighed after the solvent was removed on a rotary evaporator.

2.3 Saponification of lipids and sterols isolation

Lipids (50 mg under N2) were saponified by refluxing in 20 mL of a 5% (w/v) KOH methanol/water (4:1, v/v) solution for 2 h. Unsaponified was extracted with n-hexane and then combined, dried with sodium sulfate overnight, filtered and evaporated.
Total sterols from unsaponified material were isolated by preparative thin layer chromatography (TLC 20 $\times$ 20 cm, silica

gel 60 Å, layer thickness 500 μm) developed in one dimension in n-hexane /ethyl acetate 8:2 (v/v). Sterols bands, which were large and single bands, were identified on TLC plate according to the Rf values of standards and visualized with iodine vapour. Such bands were scrapped off and the silica was eluted with a mixture of chloroform/methanol (1:1, v/v). The mixture solvent/silica was filtered off and the organic phase was evaporated under vacuum and then the purified sterols fraction was weighed and quantified (mg sterol per g of dry weight-d.w.-algae).

2.4 Analyses by gas chromatography-mass (tandem) spectrometry (GC-MS/MS)

Purified sterols fraction of *D. tertiolecta* and *D. salina* were analyzed by gas chromatography-mass spectrometry. A Varian Saturn 2200 GC/MS/MS ion trap (Varian Analytical Instruments, Walnut Creek, CA) was used. The GC-MS was operated in the electron ionization (EI) and chemical ionization (CI) mode over a mass range of 50-650 m/z. The chemical ionization mode was used to confirm the molecular weight (M+1) of sterols. The analysis of sterols was also performed using the tandem mass spectrometry (MS/MS), where a target compound ion is isolated from matrix and then fragmented to generate very unique spectra.

Identification of sterols was based on the comparison of their retention times relative to authentic standards, mass spectra of authentic standards, and available spectra in NIST05 and Wiley 07 mass spectral libraries. Sterol standards used for identification include cholesterol (C27 Δ5) and ergosterol (C28 Δ5,7,22). The identification of fungisterol (C28 Δ7) and 7-dehydroporiferasterol (C29 Δ5,7,22) was established based on mass spectra described in literature [19, 8, 20].

3 Results

Figure 1 shows values of yields in respect to dry weight of total sterols extracted from *D. tertiolecta* and *D. salina* and purified by means of preparative TLC.

Yield of total sterols in *D. tertiolecta* grown in a medium at salt concentration of 0.6M NaCl was 1.13% of dry weight, whereas the yield in *D. salina* was slightly lower (0.89% d.w.). In the algae grown at 1.4M and 2.1M NaCl we found a decrease in total sterols yield. In particular, the sterols yield in *D. tertiolecta* decrease to 0.49% d.w. at 1.4M NaCl, and to 0.58% d.w. at 2.1M. Total sterols amount in *D. salina* was 0.41% d.w. at 1.4M NaCl and 0.28% d.w. at 2.1M NalCl.

Trend of sterols yield (Figure 1) in *D. salina* was almost linear with increasing salinity, whereas the trend in *D. tertiolecta* was almost hyperbolic and showed a drastic decrease in sterol yield between salt concentration of 0.6M and 1.4M, and any significant variation between 1.4M and 2.1M NaCl. Therefore, at 2.1M NalCl, *D. tertiolecta* had a higher concentration of total sterols compared to that one in *D. salina*, whereas at 0.6M and 1.4M NaCl concentrations of total sterols in two algae strains were statistically comparable, although the sterol concentration tended to be higher in *D. tertiolecta* than in *D. salina*.

Gas chromatography method used in the present study separated twelve sterols from *D. tertiolecta* and *D. salina*. Sterols that we identified were the

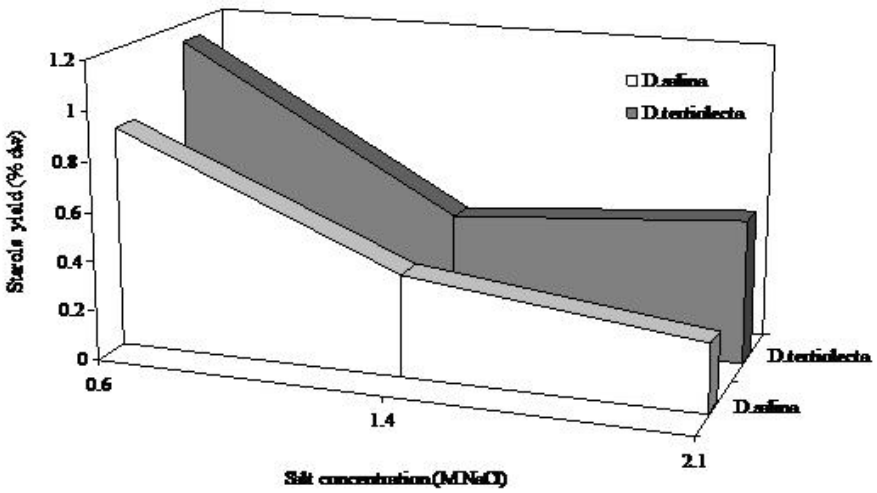

Figure 1: Trend of sterols yield in *Dunaliella tertiolecta* and *D.salina*.

same ones in the two algae strains: cholesta-5-en-3β-ol (St1), (22E,24R)-methylcholesta-5,7,9(11),22-tetraen-3β-ol (St2), (22E,24R)-methylcholesta-5,7,22-trien-3β-ol (St3), (22E,24R)-methyl-5α-cholesta-7,22-dien-3β-ol (St4), (24ξ)-methyl-5α-cholesta-8(14)-en-3β-ol (St5), (22E,24R)-ethylcholesta-5,7,9(11),22-tetraen-3β-ol (St6), (24S)-methyl-5α-cholesta-7-en-3β-ol (St7), (22E,24R)-Ethylcholesta-5,7,22-trien-3β-ol (St8), (22E,24R)-ethyl-5α-cholesta-7,22-dien-3β-ol (St9), (24ξ)-ethyl-5α-cholesta-8(14)-en-3β-ol (St10), (24ξ)-ethylcholesta-5,7-dien-3β-ol (St11), (24S)-ethyl-5α-cholesta-7-en-3β-ol (St12). We did not identify stereoisomery of C-24, and, when possible, we assigned C-24 orientation by means comparison with published data.

Figure 2 shows the yield (mg·g^{-1} d.w.) of twelve detected sterols in *D. tertiolecta* (Figure 2a) and *D. salina* (Figure 2b) at three salt concentrations (0.6, 1.4 and 2.1M NaCl). St8 and St3 were the most abundant sterols in both algae strains, followed by St7, St9 and St12. These sterols were the most abundant in each of salt concentration of medium we assayed.

Concentration of St3,7,8,12 in *D. tertiolecta* grown at 0.6M NaCl was higher than that one we found in same alga grown at 1.4 M NaCl. In particular, the concentration of St8 at 0.6M NaCl was 5.18 mg·g^{-1} d.w. and decreased to 1.98 mg·g^{-1} d.w. at 1.4M NaCl. Concentration of St3 decreased from 2.94 mg·g^{-1} d.w. to 1.27 mg·g^{-1} d.w., whereas concentrations of St7 an St12 decreased from 1.49 and 0.78 mg·g^{-1} d.w. to 0.68 and 0.33 mg·g^{-1} d.w

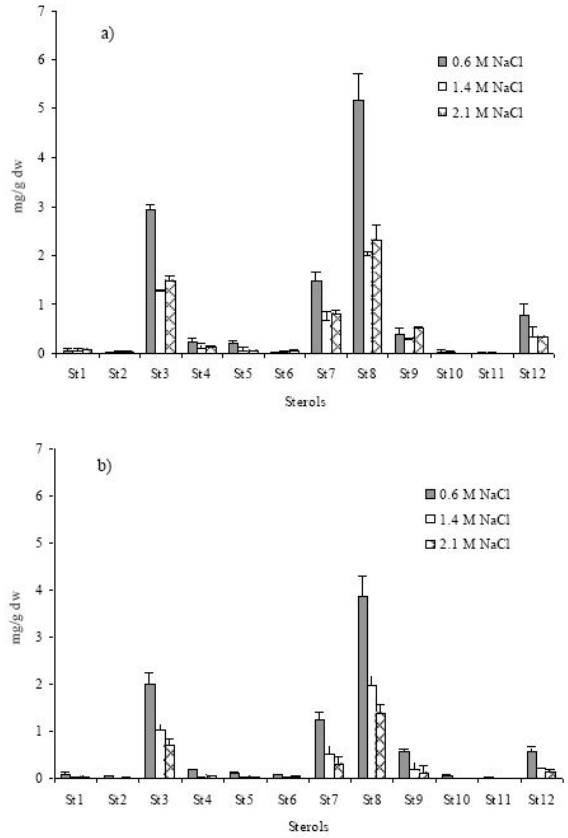

Figure 2: Yield of the most abundant phytosterols detected in a) *Dunaliella tertiolecta* and b) *D.salina* at three salt concentrations.

respectively. There seemed to be no significant variations in concentration of other minor sterols with varying salinity.

At 2.1M NaCl, concentration of St3,7,8,9 in *D. tertiolecta* slightly increased in respect to concentration in same alga strain at 1.4 M NaCl. In fact the concentration of St8 increased from 1.98 to 2.32 mg·g^{-1} d.w., and St3 increased from 1.27 to 1.47 mg·g^{-1} d.w., whereas concentrations of St7 and St9 increased from 0.54 and 0.27 mg·g^{-1} d.w. to 0.86 and 0.48 mg·g^{-1} d.w. respectively. We did not find changes in quantities of minor sterols.

St3,7,8,9,12 were also the main sterols in *D. salina* in each salinity condition we assayed. Increase in salt concentration of medium from 0.6M to 1.4M NaCl caused in *D. salina* as well as in *D. tertiolecta* a decrease in concentration of main sterols. St8 decreased from 3.86 to 1.99 mg·g^{-1} d.w., St3 decreased from 2.01 to 1.02 mg·g^{-1} d.w. and St7 from 1.26 to 0.52 mg·g^{-1} d.w., whereas concentrations of St9 and

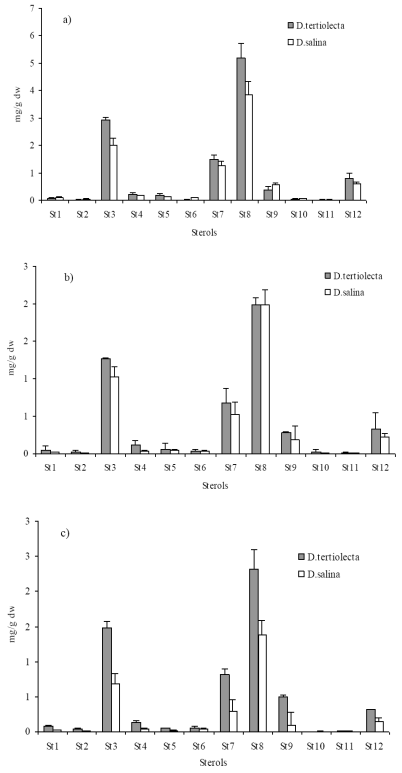

Figure 3: Comparison of the most abundant phytosterols in *Dunaliella tertiolecta* and *D. salina* at three salt concentrations: a) 0.6 M NaCl, b) 1.4 M NaCl, c) 2.1 NaCl.

St12 decreased from 0.58 and 0.59 mg·g^{-1} d.w. to 0.19 and 0.22 mg.g d.w respectively. Even in this case, we did not found quantitative variation in minor sterols.

Increase in salt concentration from 1.4M to 2.1M NaCl caused a further decrease of sterols amount in *D. salina*. In particular, at 2.1M NaCl concentrations of two most abundant sterols (St8 and St3) decreased to 1.38 and 0.69 mg·g^{-1} respectively. Concentrations of St7,9,12 also decreased to 0.29, 0.10 and 0.15 mg·g^{-1} d.w respectively, whereas there were not significant variations in minor sterol amount.

In order to evaluate the salt effect on yield of each sterol, we compared sterol composition of two algae strains at three salt concentrations (Figure 3). At 0.6M NaCl (Figure 3a), concentrations of St8 and St3 were significantly higher in D.teriolecta than in *D. salina*. In fact, the concentration of St8 was 5.15 mg·g^{-1} d.w. in *D. tertiolecta* and 3.86 mg·g^{-1} d.w. in *D. salina*, whereas the concentration of St3 was 2.94 and 2.00 mg·g^{-1} d.w. in *D. tertiolecta* and *D. salina* respectively. Concentrations of other sterols in two strains were statistically not different. At 1.4 M NaCl (Figure

3b), concentrations of all twelve sterols detected in *D. tertiolecta* and in *D. salina* were comparable, whereas at 2.1 M NaCl (Figure 3b) concentrations of St3,7,8,9,12 were higher in *D. tertiolecta* than in *D. salina*.

Some characteristic mass fragments for the detected sterols are summarized in Table 1. The most abundant sterol found in all sample (St8) showed a molecular ion (M+) of m/z 410 in the mass spectrum, while in the mass spectrum of ergosterol (St3, the second in abundance), the molecular ion (M+) occurred at 396 m/z. Principal peaks of the mass spectrum of St3 can be explained by the same fragmentation pattern of St8. The identity of the mass peaks for the two sterols after removal of the side chain (m/z 271, 253, 211, 145, 143) confirm that the two sterols differs only in their side chains. The mass spectrum of St9 was similar to that of homologous, St4, with two characteristic peaks for $\Delta 7$ sterols at m/z 255 and 229. St7 showed a molecular ion at m/z 400 which was also the base peak and the homologous C29, St12, showed a similar mass spectrum with fragments which were different in 14 m/z units.

4 Discussion

Dunaliella is a unicellular green alga that can adapt to an extremely wide range of salinities, from 0.1 to 5.5M NaCl. Variation in the salinity of medium can induce changes in metabolic pathways that lead to a quali-quantitative variation of metabolites in algal cells.

Synthesis and accumulation of glycerol in Dunaliella spp. are certainly the most know effects induced by increasing salinity. The role that glycerol plays in the salt adaptation of Dunaliella was firmly established by the studies of Ben-Amotz and Avron (1973). Liska at al. [21], in a proteomic study found that salinity stress up-regulated: key enzymes in the Calvin cycle, starch mobilization, and redox energy production; regulatory factors in protein biosynthesis and degradation and a homolog of a bacterial Na+-redox transporters.

Effect of salt concentration on the accumulation of lipids and triacylglyceride in Dunaliella was investigated by Takagy et al. [22] in order to get high liquefaction yield from marine algae cell mass to fuel oil. They obtained that the increase of NaCl concentration from 0.5 to 1.0M resulted in higher lipid and triacylglyceride content (from 60% and 41% to 67% and 57% respectively).

Salt concentration can affect also the carotenoids content in Dunaliella. Gomez et al. [23] working on Dunaliella bardawil found the highest carotenoids contents per cell at extreme salinity and reported an increase of 9-cis/ all-trans β-carotene ratio with increase in salt concentration. Fazeli et al. [24] found that although high salinity favoured total carotenoid production by *D. tertiolecta* on a cellular basis, it negatively affected on a per volume basis because cell growth was repressed at elevated salt concentrations.

Among secondary metabolites, sterols are undoubtedly very important components. They are essential components of the membranes of all eukaryotic organisms. In particular, the amount of sterols in the structure of membrane cell and the sterol / phospholipid molar ratio rule the flexibility and permeability of membrane itself [25]. Sterols can function also in cell proliferation and signal transduction of microalgae, and other eukariotic organisms, modulating the activity of membrane-bound en-

Sterol	Structure	RRT	Molecular weight	MS-data
St1	$C_{27}\,\Delta^{5}$	1.00	386	386(57), 371(32), 368(86), 353(83), 301(100), 275(60), 255(50), 213(60), 145(41)
St2	$C_{28}\,\Delta^{5,7,9,22}$	1.50	394	394(vis CI), 376(41), 361(12), 251(100), 209(10), 69(14), 55(13)
St3	$C_{28}\,\Delta^{5,7,22}$	2.03	396	396(43), 378(18), 363(100), 337(5), 271(9), 253(27), 211 (9), 145(7), 143(6)
St4	$C_{28}\,\Delta^{7,22}$	2.19	398	398(7), 380(3), 365(8), 300(16), 271(100), 255(40), 253(22), 229(15) 213(16), 147(20)
St5	$C_{28}\,\Delta^{8}$	2.51	400	400(100), 385(71), 367(31), 273(36), 255(26), 213(31), 147(24)
St6	$C_{29}\,\Delta^{5,7,9(11),22}$	2.57	408	408 (vis CI), 390(44), 375(9), 347(3), 251(100), 83(10), 69(6), 55(13)
St7	$C_{28}\,\Delta^{7}$	3.03	400	400(100), 385(61), 367(20), 273(36), 255(93), 213(37), 147(18).
St8	$C_{29}\,\Delta^{5,7,22}$	3.25	410	410(57), 392(24), 351(5), 377(100), 271(9), 253(29), 211(9), 145(7), 143(6)
St9	$C_{29}\Delta^{7,22}$	3.42	412	412(8), 397(7), 379(4), 369(10), 351(7), 300(12), 273(16), 271(100), 255(32), 253(19), 213(11), 147(15)
St10	$C_{29}\Delta^{8}$	3.67	414	414(100), 399(65), 381(26), 287(12), 273(31), 255(30), 213(38), 147(24).
St11	$C_{29}\,\Delta^{5,7}$	3.94	412	412(40), 397(23), 379(100), 353(32), 271(61), 253(21), 213(14), 145(21)
St12	$C_{29}\,\Delta^{7}$	4.21	414	414(100), 399(58), 381(21), 287(9), 273(35), 255(96), 229(22), 213(35), 147(21).

Table 1: Relative retention time (RRT) and some characteristic mass fragments of detected sterols.

zymes [5].

In our experiments, we purified from *D. tertiolecta* and *D. salina* a sterol fraction (total sterols) which consisted of twelve sterols (Figure 2). The sterol profiles of two algal strains was the same, according to Volkman [7] and Patterson [8] who asserted that sterol profiles can be sometimes characteristic of a particular class, family, genus, or even species of microalgae, and so could be used for chemotaxonomic and phylogenetic comparisons.

Comparing our results with those reported by other authors [9, 10, 8], we found some differences, however, only in minor sterols (Table 2). In particular, we did non find (22E,24ξ)-methyl-5α -cholesta-7,9(11),22-tetraen-3β-ol, 24(ξ)-methyl-5α-cholesta-8,14-dien-3β-ol, 24(ξ)-ethyl-5α-cholesta-8,14-dien-3β-ol and 24(ξ)-ethyliden-5α-cholest-7-en-3β-ol detected by Wright, whereas we confirmed the presence of two tetraenols (22E,24R)-methylcholesta-5,7,9(11),22-tetraen-3β-ol and (22E,24R)-ethylcholesta-5,7,9(11),22-tetraen-3β-ol detected by Patterson et al. [8]. Furthermore, in this study we found in *D. tertiolecta* and *D. salina* traces of cholesterol and (24ξ)-ethylcholesta-5,7-dien-3β-ol that were not reported in previous studies. The analytical techniques we used allow us to do not have great un-

Sterol	Stucture	Our study	Wright (1979, 1981)	Patterson et al. (1992)
Cholesta-5-en-3β-ol	C27 Δ^{5}	D (**St1**)	N.D.	N.D.
(22*E*,24*R*)-Methylcholesta-5,7,9(11),22-tetraen-3β-ol	C28 $\Delta^{5,7,9,22}$	D (**St2**)	N.D.	D
(22*E*,24*R*)-Methylcholesta-5,7,22-trien-3β-ol	C28 $\Delta^{5,7,22}$	D (**St3**)	D	D
(22*E*,24*R*)-Methyl-5α-cholesta-7,22-dien-3β-ol	C28 $\Delta^{7,22}$	D (**St4**)	D	D
(24ξ)-Methyl-5α-cholesta-8(14)-en-3β-ol	C28 Δ^{8}	D (**St5**)	D	N.D.
(22*E*,24*R*)-Ethylcholesta-5,7,9(11),22-tetraen-3β-ol	C29 $\Delta^{5,7,9(11),22}$	D (**St6**)	N.D.	D
(24*S*)-Methyl-5α-cholesta-7-en-3β-ol	C28 Δ^{7}	D (**St7**)	D	D
(22*E*,24*R*)-Ethylcholesta-5,7,22-trien-3β-ol	C29 $\Delta^{5,7,22}$	D (**St8**)	D	D
(22*E*,24*R*)-Ethyl-5α-cholesta-7,22-dien-3β-ol	C29 $\Delta^{7,22}$	D (**St9**)	D	D
(24ξ)-Ethyl-5α-cholesta-8(14)-en-3β-ol	C29 Δ^{8}	D (**St10**)	D	N.D.
(24ξ)-Ethylcholesta-5,7-dien-3β-ol	C29 $\Delta^{5,7}$	D (**St11**)	N.D.	N.D.
(24*S*)-Ethyl-5α-cholesta-7-en-3β-ol	C29 Δ7	D (**St12**)	D	D
(22*E*,24ξ)-Methyl-5α-cholesta-7,9(11),22-tetraen-3β-ol	C28 $\Delta^{7,9,22}$	N.D.	D	N.D.
24(ξ)-Methyl-5α-cholesta-8,14-dien-3β-ol	C28 $\Delta^{8,14}$	N.D.	D	N.D.
24(ξ)-Ethyl-5α-cholesta-8,14-dien-3β-ol	C29 $\Delta^{8,14}$	N.D.	D	N.D.
24(ξ)-Ethyliden-5α-cholest-7-en-3β-ol	C29 $\Delta^{7,28}$	N.D.	D	N.D.

D: detected; N.D.: Not detected.

Table 2: Comparison of sterol composition of Dunaliella tertiolecta achieved in this study with those reported by[9, 10] and [8].

certainty in data achieved. These small differences between our data and those reported in previous studies, but between published data also (e.g., Wright's results are partly different from those of Patterson et al. [8]), can probably be due to differences in culture conditions [5], but also to differences in extraction and purification methods and in sensitivity of analytical techniques which have been used.

We observed a significant decrease in total sterol amount in *D. tertiolecta* and *D. salina* with the increase of salt concentration from 0.6M to 1.4M NaCl (Figure 1). At 0.6M NaCl concentration, *D. tertiolecta* and *D. salina* showed a similar concentration of total sterols (not statistically different). At 1.4M, the concentration of total sterols in both strains decreased significantly of about 55% in respect to total sterols concentration at 0.6M NaCl. At 2.1M NaCl concentration, the amount of total sterols in *D. tertiolecta* remained (statistically) unchanged in respect to sterols amount obtained at 1.4M NaCl, whereas total sterol amount in *D. salina* further decreased of 69% and 32% in respect to sterol concentration at 0.6M and 1.4M NaCl.

There are previous studies reporting the effect of salt concentration on sterol composition of Dunaliella salina using different approaches. Firstly, Peeler et al. [11] studied the lipid composition of plasma membranes of *D. salina* grown under varying salinities. They reported that sterols were the major components of membrane fractions (accounting for 55% of the total lipid content), comprising of ergosterol

(St3) and 7 dehydroporiferasterol (St8). The sterol/phospholipid molar ratio was approximately constant (1.7) at three salt concentrations (0.85, 1.7 and 3.4 M NaCl). The relative amount of individual sterols in the plasma membrane fraction changed only slightly with a change in NaCl concentration. However, they did not report the quali quantitative variation of total sterols with respect to dry weight.

Comparatively, Zelazny et al. [12] reported that sterols were essential for volume recovery, and therefore for glycerol synthesis, following hyperosmotic shock. In particular, they observed that the enzymatic inhibition of sterol biosynthesis suppressed the volume recovery of cells of *D. salina*, whereas the volume recovery was found to be fully restored upon addition of exogenous sterol. Consequently, they claimed that a hyperosmotic shock caused an increase of sterol content in plasma membranes.

This data seem to be in disagreement with that obtained by Peeler et al. [11] who did not observe any significant variations of sterol/phospholipid molar ratio and/or content of individual sterols in the plasma membrane at varying salinities. However, Peeler et al. [11] studied cells in osmotic equilibrium conditions (at long times after osmotic shocks). They also reported a decrease in phospholipid content (from 75.7% to 64.5% of polar lipids) at increasing salt concentrations (from 0.85M to 3.4M). A reduction of phospholipid content implies an intrinsic reduction of sterol content in the plasma membrane as the sterol/phospholipid molar ratio was constant at the different investigated salt concentrations.

Combining all experimental findings reported above, we hypothesize that the significant decrease in total sterol amount in *D. tertiolecta* and *D. salina* with increasing salt concentrations can be explained by a two-stage process in which the sterol concentrations are differently affected:

1. In a first stage (at time of hyperosmotic shock), sterols (already present in the plasma membrane and in cytoplasmic lipid vesicles) function as a fast system to increase the low lipid membrane order, also inducing glycerol synthesis (in agreement with [26] and [12]). The increased quantities of sterols at low salt concentration (0.6 M) is consistent with this function as the cells have to accumulate and make available greater quantities of sterols (to quickly develop a high ordered lipid membrane) to face a possible hyperosmotic shock.
2. In a second stage (with increasing intracellular glycerol concentration and upon reaching a new state of osmotic equilibrium), the sterol content decreases (in agreement with results reported by [11]) and the new status of membrane lipid order (higher than that prior to hyperosmotic shock, [26]), is maintained by major concentrations of diacylglyceryltrimethylhomoserine (DGTS) and sulfoquinovosyldiacylglycerol (SL) and by a decreased unsaturation degree of fatty acids (in agreement with reported results by [11]. Indeed, at higher salt concentration (1.4 M and above), the cells do need to provide only small quantities of sterols to further increase the lipid membrane order.

St3, St7, St8, St9 and St12 were the main sterols that changed significantly in concentration at varying salinities. St7, St9 and St12 might be either biosynthetic intermediates of St3 and St8 or rapidly turning-over sterols [12]. The different responses observed for *D. tertiolecta* and *D. salina* at

2.1 M salt concentration (in terms of total sterols amount) may be related to different adaptation capacities to increasing salinity (*D. tertiolecta* is an euryhaline species, while *D. salina* is a hypersaline species).

Actually, phytosterols isolation in large scale is based in two major raw materials: vegetable oils and tall oil [13]. The total contents of phytosterols in vegetable oils are very variable and range from nearly $8\mathrm{g} \cdot \mathrm{kg}^{-1}$ in corn oil to $0.5\ \mathrm{g} \cdot \mathrm{kg}^{-1}$ in palm oil, with intermediate levels being found in commonly used oils. Another major source of phytosterols is tall oil, the fat-soluble fraction of the hydrolysate obtained from trees during the pulping process. The most notable characteristic of tall oil is its high stanol concentration (approximately 20%), and fibre oils such as maize.

The exploitation of sterols from microorganisms for biotechnological or nutritional purposes is in its infancy apart from the ergosterol production by fermentation of Saccharomyces cerevisiae [27] and the use of sterol-containing microalgae as natural feedstocks in aquaculture [5] for crustaceans and some molluscs that lack de novo sterol-synthesizing ability. Volkman [5] suggested that a limitation in the use of microalgae in phytosterols production was the low content of sterols. In diatoms, sterols represent 0.06-0.57% of cell dry weight, whereas in dinoflagellates total sterols are usually more abundant (e.g. 1.5 and 3.1% dry wt). These data are in agreement with our experimental data (about 1% dry wt for Dt and Ds at 0.6M NaCl).

However, we believe that, even if sterol yields do not seem to be particularly high, it needs to do some remarks: a) the biotechnology of microalgae has reached high levels of development due to new production technologies which allow to obtain high biomass productivities [28] and major yields of extracted organic compounds [29]; b) the biomass productivity (in terms of dry metric tons$\cdot\mathrm{ha}^{-1} \cdot \mathrm{yr}^{-1}$) for microalgae is much higher than productivity for land-based crops [3]; c) the production of phytosterols could be considered as an added value for Dunaliella biomass which could be cultivated to produce also β-carotene and biofuels as well as to reduce atmospheric CO_2 (CO_2 biomitigation) applying the conceptual model of biorefinery; d) today, consumers are actively seeking products containing health-promoting ingredients to improve their health and well-being. In keeping with this trend, nutraceuticals such as phytosterols, that have a beneficial impact on heart health, have grown in popularity.

In the light of these remarks, we believe that exploitation of Dunaliella tertiolecta and *D. salina* (grown at 0.6 M NaCl) as commercial source of phytosterols may be an achievable hypothesis. The whole sterols fraction extracted from two strains of Dunaliella could be used in nutraceutic and pharmaceutical industry because it consist mainly of phytosterols which have therapeutic applications to treat hypercholesterolemia.

In view of these premises, we believe that the exploitation of *D. tertiolecta* and *D. salina* (grown at 0.6 M NaCl) as commercial source of phytosterols may be an achievable target. The whole sterol fraction extracted from two strains of Dunaliella, comprising of phytosterols involved in therapeutic applications to treat hypercholesterolemia, could be used in the nutraceutical and pharmaceutical industries.

Moreover, *D. tertiolecta* and *D. salina* could be potentially utilised as commercial sources of ergosterol (St3) and 7-dehydroporiferasterol (St8) as these sterols reached a relatively high concentration

(0.29% and 0.52% d.w., respectively) in *D. tertiolecta* grown at salt concentrations of 0.6M (Figure 2).
Finally, to the best of our knowledge, there are no reported studies on bioactivity of 7 dehydroporiferasterol (St8), the most abundant sterol of *D. tertiolecta* and *D. salina*. However, the structural similarity with ergosterol (with only an extra methyl group present in the molecule) could suggest a bioactivity similar to this phytosterol. Investigations are currently ongoing in our laboratories to test the anti-inflammatory bioactivity of 7-dehydroporiferasterol (St8) and we have managed to achieve interesting preliminary results. If successful, these studies may also pave the way to the utilisation and exploitation of Dunaliella species as sources of bioactive compounds.

5 Conclusions

We have reported the isolation and identification of a range of phytosterols from two microalgae species: *D. tertiolecta* and *D. salina*. Total phytosterol content in these algae was close to 1% dry weight and was found to decrease, in general, with increasing salinities (from 0.6 to 2.1 M). This phenomenon was related to the cell functions of these components that are initially produced by the algae at high concentrations to build-up a consistent lipid membrane (at low salt concentrations) to face hyperosmotic shocks and then produced in low quantities to support the maintenance of the membrane structure. In the light of these remarks, we can conclude that exploitation of *Dunaliella tertiolecta* and *D. salina* (grown at 0.6 M NaCl) as commercial source of phytosterols may be an achievable hypothesis.

References

[1] R. Raja, S. Hemaiswarya, and R. Rengasamy. Exploitation of Dunaliella for β carotene production. *Appl. Microbiol. Biotechnol.*, 74:517–523, 2007.

[2] M.A. Borowitzka and L.J. Borowitzka. Microalgal biotechnology. 1998.

[3] G.C. Dismukes, D. Carrieri, N. Bennette, G.M. Ananyev, and M.C Posewitz. Aquatic phototrophs: efficient alternatives to land-based crops for biofuels. *Curr. Opin. Biotech.*, 19:235–240, 2008.

[4] J.K. Volkman, S.M. Barrett, S.I. Blackburn, M.P. Mansour, E.L. Sikes, and F. Gellin. Microalgal biomarkers: a review of recent research developments. *Org. Geochem.*, 29:1163–1179, 1998.

[5] J.K. Volkman. Sterols in microorganisms. *Appl. Microbiol. Biotechnol.*, 60:495–506, 2003.

[6] L.P. Ponomarenko, I.V. Stonik, N.A. Aizdaicher, T.Y. Orlova, G.I. Popovskaya, G.V. Pomazkina, and V.A. Stonik. Sterols of marine microalgae Pyramimonas cf. Cordata (Prasinophyta), Attheya ussurensis sp. nov. (Bacillariophyta) and a spring

diatom bloom from Lake Baikal. *Comp. Biochem. Physiol.*, 138(Part B):65–70, 2004.

[7] J.K. Volkman. A review of sterol markers for marine and terrigenous organic matter. *Org. Geochem.*, 9:83–99, 1986.

[8] G.W. Patterson. Sterols of algae. page 118–157, 1991.

[9] J.L.C. Wright. The occurrence of ergosterol and (22E,24R)-24-ethylcholesta-5,7,22-trien-3β-ol in the unicellular chlorophye *Dunaliella tertiolecta*. *Can. J. Chem.*, 57:2569–2571, 1979.

[10] J.L.C. Wright. Minor and trace sterols of *Dunaliella tertiolecta*. *Phytochemistry*, 20:2403–2405, 1981.

[11] T.C. Peeler, M.B. Stephenson, K.J. Einspahr, and G.A.Jr. Thompson. Lipid Characterization of an Enriched Plasma Membrane Fraction of *Dunaliella salina* Grown in Media of Varying Salinity. *Plant Physiol.*, 89:970–976, 1989.

[12] A.M. Zelazny, A. Shaish, and U. Pick. Plasma-membrane sterols are essential for sensing osmotic changes in the halotolerant alga Dunaliella. *Plant Physiol.*, 109:1395 1403, 1995.

[13] P. Fernandes and J.M.S. Cabral. Phytosterols: Applications and recovery. *Bioresource Technol.*, 98:2335–2350, 2007.

[14] S.M. Mel'nikov, J.W.M.S. ten Hoorn, and B. Bertrand. Can cholesterol absorption be reduced by phytosterols and phytostanols via a cocrystallization mechanism? *Phys. Lipids*, 127:15–33, 2004.

[15] D. Platt, D. Pelled, and A. Shulman. Oils enriched with diacylglycerols and phytosterolesters for use in the reduction of cholesterol and tryclycerides. 2004.

[16] Frost and Sullivan. Strategic Analysis of the U.S. Phytosterols Market June 6, 2006, MC1397684. 2006.

[17] I. Laing. Cultivation of marine unicellular algae. MAFF Laboratory. Leaflet No. 67. 1991.

[18] E.G. Bligh and W.J. Dyer. A rapid method of total lipid extraction and purification. *Can. J. Biochem. Phys.*, 37:911–917, 1959.

[19] M.A. Gealt, J.H. Adler, and W.R. Nes. The sterols and fatty acids from purified Xagella of Chlamydomonas reinhardi. *Lipids*, 16:133–136, 1981.

[20] F.L.E. Chu, E.D. Lund, P.R. Littreal, K.E. Ruck, E. Harvey, J.R. Le Coz, Y. Marty, J. Moal, and P. Soudant. Sterol production and phytosterols bioconversion in two species of heterotrophic protists, Oxyrrhis marina and Gyrodinium dominans. *Mar. Biol.*, 156:155–169, 2008.

[21] A.J. Liska, A. Shevhenko, U. Pick, and A. Katz. Enhanced photosynthesis and redox energy production contribute to salinity tolerance in Dunaliella as revealed by homology-based proteomics. *Plant Physiol.*, 136:2806–2817, 2004.

[22] M. Takagi, K. Yoshida, and T. Yoshida. Effect of salt concentration on intracellular accumulation of lipids and triacylglyceride in marine microalgae Dunaliella cells. *J. Biosci. Bioeng.*, 101:223–226, 2006.

[23] P.I. Gomez, A. Barriga, A.S. Cifuentes, and M.A. Gonzalez. Effect of salinity on the quantity and quality of carotenoids accumulated by *Dunaliella salina* (strain CONC-007) and *Dunaliella bardawil* (strain ATCC 30861) Chlorophyta. *Biol. Res.*, 36(2):185–192, 2003.

[24] M.R. Fazeli, H. Tofighi, N. Samadi, and H. Jamalifar. Effects of salinity on β carotene production by *Dunaliella tertiolecta* DCCBC26 isolated from the Urmia salt lake, north of Iran. *Bioresource Technology*, 97:2453–2456, 2006.

[25] D. Chapman. Recent studies of lipid, lipid cholesterol and membrane system. *Biological Membranes*, 2:91–122., 1973.

[26] C.C. Curtain, D. Looney, D.L. Reran, and N.M. Ivancic. Changes in the ordering of lipids in response to osmotic pressure changes. *Biochem. J.*, 213:131–138, 1983.

[27] X. He, X. Guo, N. Liu, and B. Zhang. Ergosterol production from molasses by genetically modified Saccharomyces cerevisiae. *Appl. Microbiol. Biotechnol.*, 75:55 60, 2007.

[28] Y. Chisti. Biodiesel from microalgae. *Biotechnol. Adv.*, 25:294–306, 2007.

[29] E. Molina Grima, E.H. Belarbi, F.G. Acién Fernández, A. Robles Medina, and Y. Chisti. Recovery of microalgal biomass and metabolites: process options and economics. *Biotechnol. Adv.*, 20:491–515, 2003.

Unmanned Surface Vehicles for Coastal and Harbour Monitoring: the CNR Experience

M. Caccia, M. Bibuli, G. Bruzzone
Institute of Intelligent Systems for Automation, CNR, Genova, Italy
max@ge.issia.cnr.it

Abstract

In the last decade Unmanned Surface Vehicles (USVs) emerged as a potentially game-changing technology for naval operations as well as coastal and harbour monitoring and surveillance. In particular, the position of the USVs at the air-sea interface allows them to play a key role both in relaying radio frequency transmissions in air and acoustic transmissions undersea, and in monitoring ocean and atmosphere dynamics as well as surface and underwater intrusions. As a consequence of their networking capabilities, USVs are naturally seen as a part of flotillas of heterogeneous vehicles executing large scale surveys and supporting rapid environmental assessment: the result is that an increasing number of prototype vehicles has been developed for science, bathymetric mapping, defence and generic robotics research. This paper presents an overview of USV development and applications, discussing the main technological and legal issues related to their use in everyday operations. In this context, attention focuses on the CNR experience in developing vehicles for coastal and harbor applications. The design, development and exploitation of the Charlie and ALANIS USVs is discussed. In particular, general aspects either infrastructural, e.g. software and hardware embedded real-time architecture and communication systems, or methodological, e.g. navigation, guidance, control and mission supervision systems, are clearly distinguished by vehicle-related mechanical design and applications.

1 Introduction

In the last decade Unmanned Surface Vehicles emerged as a potentially game-changing technology for naval operations [1] as well as for coastal and harbour monitoring and surveillance. After the pioneer development of prototype autonomous surface craft basically used for automated collection of bathymetries at the MIT Sea Grant College Program [2] around the mid of the Nineties, at the beginning of the new Millennium the development of USV technology was dramatically boosted by the successful operation of the shallow water influence mine sweeping system (SWIMS) to support the British Royal Navy mine countermeasures operations in Iraq in 2003 [1]. In particular, the position of the USVs at the air-sea interface allows them to play a key role both in relaying radio frequency transmissions in air and acoustic transmissions undersea, and in monitoring ocean and atmosphere dynamics as well as surface and underwater intrusions. As a consequence of their networking capabilities, USVs are naturally seen as a part of flotillas of heterogeneous vehicles executing large

scale surveys and supporting rapid environmental assessment (REA): the result is that an increasing number of prototype vehicles was developed for science, bathymetric mapping, defence and general robotics research.
In the following an overview of USV development and applications is presented discussing the main technological and legal issues related to their use in everyday operations. In this context, the CNR experience in developing vehicles for coastal and harbour applications is discussed focusing attention on the design, development and exploitation of Charlie and ALANIS USVs. In particular, general infrastructures, e.g. software and hardware embedded real-time architecture and communication systems, and methodologies, e.g. navigation, guidance, control and mission supervision systems, will be clearly distinguished by vehicle-related mechanical design and applications. Moreover, the most significant exploitations of USV technology will be discussed.

2 Background

2.1 Prototype USVs and applications

As mentioned before, from the Nineties of the last century the MIT Sea Grant College Program developed a family of autonomous vessels for education and civil applications, consisting of the fishing trawler-like vehicle ARTEMIS, the catamarans ACES (Autonomous Coastal Exploration System) and AutoCat [3, 2] , and the kayak SCOUT (Surface Craft for Oceanographic and Undersea Testing) [4]. These USVs demonstrated the feasibility of automatic heading control and DGPS-based way-point navigation, as well as the possibility of operating autonomously collecting hydrographic data. After the integration with the MIT Odyssey class AUVs, from the point of view of human operator interface, mission planning and computer architecture [5], the SCOUT kayaks are supporting the development and test of distributed acoustic navigation algorithms for undersea vehicles.
As far as the European research community is concerned, the concept of USV was introduced by the University of Rostock (Germany) with the design and development of the Measuring Dolphin, devoted to high accuracy positioning and track guidance and carrying of measuring devices (e.g. depth and current) in shallow water [6]. The idea of a USV acting as communication relay with a companion AUV was exploited in the European Union funded project ASIMOV (Advanced System Integration for Managing the coordinated operation of robotic Ocean Vehicles) with the development of the autonomous catamaran Delfim by the DSOR lab of Lisbon IST-ISR [7].
In the wake of these pioneer prototypes, two autonomous catamarans, ROAZ and ROAZ II, were developed by the Autonomous Systems Laboratory at ISEP, Institute of Engineering of Porto, for environmental monitoring, bathymetry, science data gathering, search and rescue support and security missions [8]. In the meantime, the autonomous catamaran Springer has been developed by the University of Plymouth (UK) for tracing pollutants [9].
The development of the autonomous catamaran Charlie, originally exploited for the collection of sea surface microlayer [10], and then upgraded for robotic research on autonomous vessels, and of the aluminum Rigid Inflatable Boat-like USV

ALANIS for coastal monitoring by CNR-ISSIA Genova (Italy) will be deeply discussed in the following sections.
On the other hand, after the success of SWIMS, which basically consisted in the development of a conversion kit to transform existing Combat Support Boats, already operated by the British Royal Navy, in remote controlled vessels, numerous USVs were developed for military purposes. Examples are given by the SSC San Diego, based on the Bombardier SeaDoo Challenger 2000 [11], the Israeli Stingray with a top speed up to 40 knots, and Protector, equipped with electro-optic sensors, radar, GPS, inertial navigation system and a stabilised 12.7 mm machine gun, and the French Inspector basically developed for coastal and port security and mine countermeasures.

2.2 Legal issues

The main limitations to an extended use of USV technology for civil applications, i.e. in areas not restricted to maritime traffic, rely in the lack of rules for the operations of autonomous vehicles at sea and of a reliable methodology for anti-collision. As far as legal issues are concerned the reader can refer, for instance, to the document of the Society for Underwater Technology "Issues Concerning the Rules for the Operation for Autonomous Marine Vehicles (AMV) - A consultation paper (7 August 2006)", while the first basic steps in the direction of implementing collision avoidance strategies according to the rules of the road were presented in [12]. Preliminary work on automatic obstacle detection is being carried out in the military field, e.g. integrating a radar and artificial vision devices on the SSC San Diego [11]. Laser-gated intensified CCD (LGICCD) could represent a dramatic improvement in obstacle detection at sea, at least during night operations, thanks to the property of the auxiliary laser light source of being completely absorbed by the water. In addition, recently ASTM International has established the subcommittee F41.90.01 Unmanned Surface Vehicles for addressing standardisation issues related to this technology.

3 USV Projects @ CNR

Since 2003 a couple of prototype USVs have been designed and developed by CNR-ISSIA for operations in coastal and harbour areas: Charlie [13], a fibreglass catamaran with electrical propulsion, and ALANIS (ALuminum Autonomous Navigator for Intelligent Sampling) [14], an aluminum rubber dinghy like craft with a fuel powered outboard motor, funded by the Parco Scientifico e Tecnologico della Liguria scpa. The generic system consists of a robotic vessel, with on-board computing resources for navigation, guidance and control, and a portable human operator station for remote control and supervision. Both Charlie and ALANIS are autonomous from the point of view of power supply.
The remarkable differences between the vessels, presented in the following, from the naval-mechanical, steering, propulsion, and degree of autonomy points of view allowed the acquisition of a wide spectrum experience in the development and exploitation of this class of vehicles.

3.1 Charlie USV

The Charlie USV, as shown in Figure 1, has a catamaran-like shape, chosen for stability with respect to roll, redundancy

Figure 1: View of the Charlie USV during trials in the Genova Prà harbour (April 2009)

in hull buoyancy, and capability of payload transport with respect to the hydrodynamic drag. The vehicle length of 2.40 m and width of 1.80 m were determined by transportation constraints on support vessels and lab trucks. The hull height of about 0.60 m, for a weight of about 300 Kg in air, gives the possibility of carrying a payload of about 120 Kg.

The vehicle is equipped with two propellers, each actuated by a DC motor (330 W at 48 V) with corresponding tachometer and rotary joint. A set of servo-amplifiers perform proportional-integral-differential (PID) control of the thruster velocity on the basis of the error between the signal of the motor tachometer and the reference speed. After the 2003-04 Antarctic campaign, the steering system, originally based on differential propeller revolution rate for working basically at very low speed, was integrated by two rigidly connected rudders mounted behind the propellers. The rudders are actuated by a brushless motor driven by a standard motion controller able to handle out-of-range signals. Magnetic and mechanical switches generate suitable signals in order to keep the rudder angle module lower than 45 degrees and to automatically locate the zero position when the system is turned on.

Power is supplied by a serial package of four lead batteries (42 Ah at 12 V each one), integrated with a set of four flexible solar panels (32 W at 12V).

3.2 ALANIS USV

The ALANIS USV, see Figure 2, based on a commercial boat Mancini Multiprofessional 450, has a stern hole with a diameter of 0.20 m for deploying and recovering of scientific instrumentation by mean of a winch. The aluminum hull, 4.50 m long,

Figure 2: View of the ALANIS USV during preliminary trials in the Genova Prà harbour (May 2008)

2.20 m wide and weighting 600 Kg for a load capacity of 800 Kg, has a number of separate watertight compartments. A couple of traverse rods are welded on the floor to mount the pilot console, the battery box, the winch and any generic device for future needs. The stern hole can be closed with a plug which, when inserted, smoothly continues the hull profile.

The propulsion is guaranteed by a 40 HP outboard motor, which allows human operators lacking in nautical license to pilot the vessel. Steering is performed by rotating the motor with respect to its vertical axis.

In order to allow a dual, i.e. manned and unmanned, use of the vessel, a manually (dis)connectible electro-mechanical system for servo-actuating steering and throttle has been designed and developed. A couple of reduction gears connected to the axis of the steer and throttle respectively are controlled by two servo brushless motors. The throttle and steering automation mechanisms can be fast electrically (dis)engaged through a main switch, and, mechanically, acting on a couple of knobs, which (dis)engage the automation gearboxes (un)screwing the respective threaded bar. The problem of signalling the reaching of safety limits, as well as of fixing an absolute known position during initialization, was solved by introducing a couple of micro switches at two ways for each subsystem.

The automatic deployment and recovery system for scientific instrumentation is based on a winch actuated by a servo brushless motor piloted by the vehicle control system. The cable, which is 200 m long, contains 5 wires for power, 2 twisted couples for data, and 1 twisted couple for video transmission in order to

be able to support different payloads. A micro switch is used to signal the complete recovery of the scientific device. The amount of displaced cable is computed on the base of signals generated by two magnetic switches positioned on a pulley.
The fuel tank for the outboard motor has a capacity of 65 l, for a vehicle autonomy of about 12 hours. It is in aluminium too and embedded in the hull below the floor.
A set of 4 lead batteries (42 Ah at 12 V each one) supplies the control system electronics and sensors.

4 Embedded real-time platform

The basic requirement in designing and implementing the robotic vessel software architecture was the definition of a common infrastructure for managing an embedded system supporting real-time thread scheduling and communications, and the levels of an intelligent control architecture, including asynchronous modules implementing potentially unbounded search algorithms.
Advances in computing power of commercial-off-the-shelf boards and in performance of free software allowed the development of a platform based on Single Board Computers, PC-104 modules and GNU/Linux. In particular, research focused on developing an embedded real-time infrastructure for industrial automation and robotics, constituted by a real-time custom scheduler, which guarantees an effective scheduling of the control application threads according to the required priorities and policies, integrated with a set of utilities for thread creation and data access synchronization and communication.
A detailed description of the developed methodology can be found in (Bruzzone, 2008). Here it is sufficient to remind that, from the kernel release 2.5.4-pre6, a native fair Unix-like system such as GNU/Linux can be used for real-time applications with strict time requirements thanks to the so-called pre- emption and low-latency patches. They guarantee maximum latency and jitter of the order of a few tens of milliseconds also when particularly demanding activities, which are usually avoided by typical real-time embedded system programming techniques, are performed (e.g. video output, dynamic allocation of large amount of memory, process fork, etc.). Thus it was possible to implement a real-time custom scheduler to manage real-time threads, both synchronous and asynchronous, while non real-time ones continue to be scheduled under the default universal time sharing Linux scheduler policy. As a result the proposed solution allows the scheduling of all the threads in user space without requiring any complex development of kernel modules.

5 Navigation package

The basic navigation package of CNR-ISSIA USVs is constituted by compass and GPS for the measure of the vessel orientation and position. Pitch and roll measurements are provided by clinometers, while wind conditions are detected by an ultrasound anemometer.
In addition to the basic Charlie system constituted by a GPS Ashtech GG24C providing geographic coordinates at 1 Hz, integrated with a KVH Azimuth Gyrotrac, able to compute the True North at 2 Hz on the basis of the measured Magnetic North and

the GPS-supplied data, devices of different classes were tested and evaluated. Results demonstrated that standard commercial GPS are sufficient for basic line-of-sight guidance through way-points, simply heading the vessel bow towards the current target. In the case an accurate localisation of the vehicle is required, for instance for coordinated motion control or bathymetric surveys, high positioning GPS systems experimentally demonstrated satisfactorily performance without requiring any structuring of the operating environment. On the other hand, due to the relatively fast dynamics of the yaw motion of the considered vessels, high sampling rate heading signals, and thus relatively high quality compasses, are required for automatic control of the vehicle orientation.

6 Navigation, guidance and control architecture

6.1 Control architecture

A classical hierarchical intelligent control architecture upgraded with a Petri net based execution control level, as an interface between the synchronous execution of motion estimation and control modules and the asynchronous discrete event systems handling mission control and supervision, was designed and implemented (see Figure 3).

Drivers, located at the lowest layer, are software modules in charge of handling Input/Output operations on actuation (e.g. thrusters and rudder) and sensing devices (e.g. GPS and compass).

The Execution Level is in charge of the synchronous execution of a set of elementary navigation, guidance and control tasks communicating among them through shared variables. It communicates with the Drivers, sending reference values to actuation devices and receiving instrumental measurements by sensors.

The Execution Controller handles the activation/deactivation of navigation, guidance and control tasks, solving conflicts and dependencies on task resources, typically variables, and thus guaranteeing the system consistency. As discussed in [13], this capability is based on the definition and on-line reconfiguration of a controlled Petri net describing the I/O relationships of execution level tasks. Differently from the Execution Level, which acts at synchronous continuous-time layer, the asynchronous evolution of the Execution Controller is event-driven, i.e. it changes its state when receiving a command from another architecture component or from the human operator.

On the other hand, the NGC Monitor in responsible of the generation of events related to the semantics of the tasks execution, signaling particular interactions of the robot with the operating environment and the state of motion estimation and control tasks. On this basis, the mission control level (or human pilot) dynamically schedules the motion control and estimation tasks in order to accomplish the desired mission.

In addition, the Path Planner is in charge of online computing and handling a collision free path to a desired location with additional constraints on way-points, local path direction and so on. On this basis it supplies the guidance modules with the coordinates, orientation, curvature of the actual point of the path that has to be tracked. Currently, only functions computing basic paths such as straight lines, splines for a sequence of way-points and circumference arcs have been implemented. The imple-

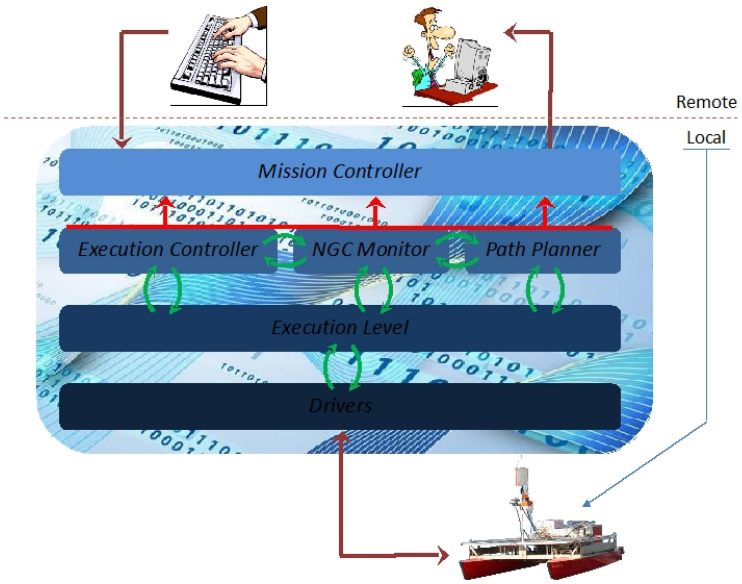

Figure 3: Intelligent control architecture scheme.

mentation of an on-line path generation, on the basis of position data received from a moving master vehicle, is a fundamental tool for the execution of coordinated and cooperative control of multiple vehicles as, for instance, in the case of vehicle-following.

The overall control system architecture is managed and supervised by the Mission Controller, that has not to be considered like a raw mission plan executor, but more like a coordinator between predefined automatic operations and unpredictable user interventions which can take place whenever during mission execution. For this reason, user presence is considered "in the loop" as an intelligent sub-system that interacts with the mission evolution, usually interrupting automatic routines to switch to manual operations and giving control back to the automatic system. The Mission Controller collects all the asynchronous discrete-time event that are generated from the other modules of the architecture, on the basis of such events reception the state of the mission is updated.

6.2 Motion estimation

As far as motion estimation is concerned, conventional Kalman filter techniques were applied, providing good results in terms of precision and smoothness of linear and angular position and speed estimates. In particular, experimental results with the Charlie USV demonstrated that the virtual acceleration measurements provided by an accurate model of the vehicle dynamics allow a smooth estimate, and not particularly delayed, of the vehicle speeds, which can be used by motion controllers with relatively high gains.

Anyway, it is worth noting some anomalies verified in the GPS measurements

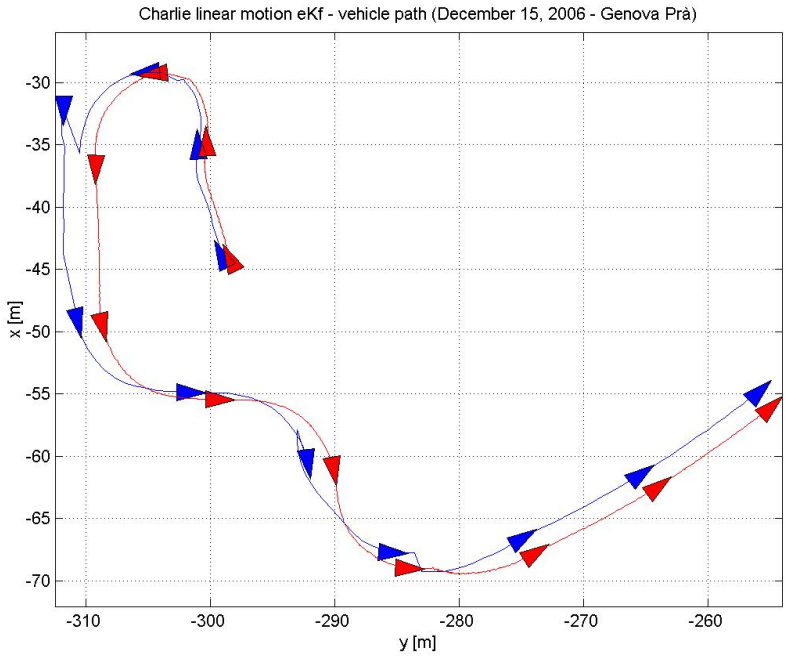

Figure 4: Charlie USV GPS raw and filtered data, Genova Prà harbour (December 2006)

as well as the adopted countermeasures. The Ashtech GG24C provides piecewise continuous latitude and longitude signals, presenting random-like steps of the type shown in Figure 4, where the blue and red lines represent the raw and filtered GPS x and y measurements respectively. Excepting the discontinuity points, the position signal is quite smooth with a standard deviation of the noise of about 0.17 m. These results seem to confirm the fact that although the artificial degradation of the signal through the process of selective availability was removed in 2000, the accuracy of GPS, when used in instantaneous standalone mode, remains of the order of 10-20 m. Thus, the Kalman filter for linear motion estimation was upgraded with an online detector of signal discontinuities. Results are shown by the red path of Figure 4.

6.3 Guidance and control

The operating experience with the Charlie and ALANIS USVs demonstrated that many practical applications do not require the design and implementation of advanced nonlinear controllers. For instance, basic line-of-sight guidance and PD heading control were sufficient for controlling the Charlie motion when collecting water samples from the sea surface micro-layer and immediate sub-surface during the XIX Italian Expedition to Antarctica in 2004 (see section 8.1).

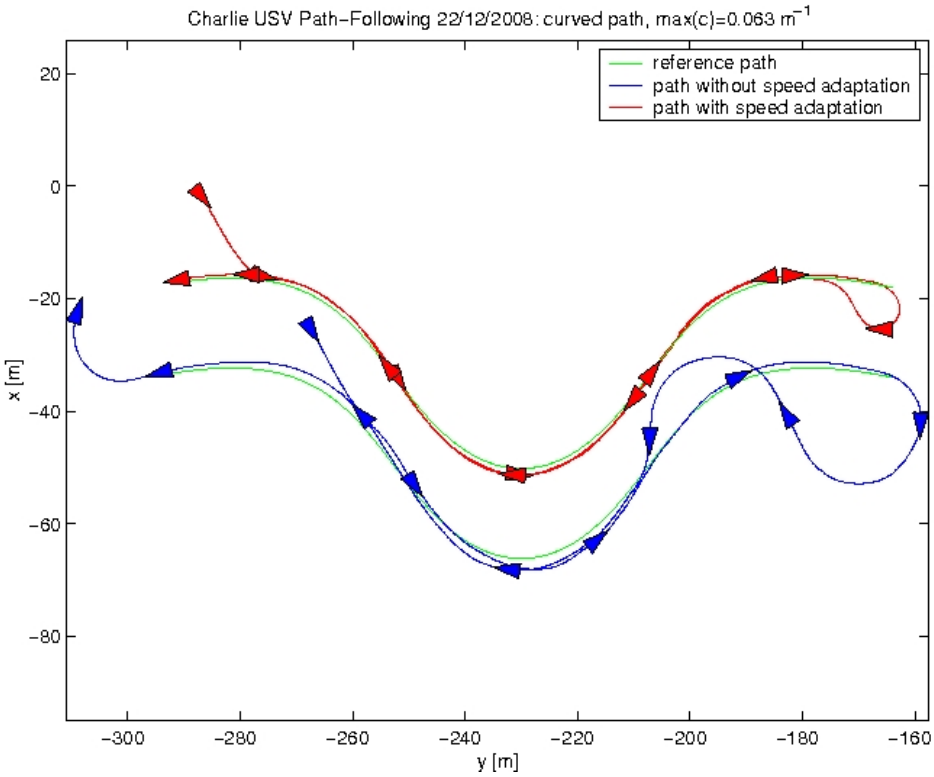

Figure 5: Charlie USV path-following performance with and without speed adaptation (red and blue line respectively), Genova Prà harbour (December 2008). The target path is represented with a green line.

Guidance and control research focused on the design and implementation of high precision autopilots (heading and speed controllers) and path-following controllers. In this context, a dual nested loop architecture decoupling the management of dynamics and kinematics, i.e. speed and position control respectively, proved its effectiveness in the case of the Charlie USV, even using only linear and angular position sensors, i.e. GPS and compass. This structure facilitates the design of guidance task functions at the kinematic level, i.e. position controllers generating reference speed signals, implementing different vehicle manoeuvres from basic auto-heading to straight line and path following. Thanks to the physical properties of the system, simple position controllers can be defined for executing more complex tasks too. This is, for instance, the case of straight line following, where sea current and wind disturbances are naturally compensated by the presence of a physical integrator between the vehicle yaw rate and the angle of attack between the desired line orientation and the vehicle heading.

As far as generic path-following is con-

Figure 6: View of the Charlie USV on the deck of the support vessel Malippo, Terra Nova Bay, Ross Sea, Antarctica (February 2004).

cerned, the effectiveness of virtual target based techniques, developed in cooperation with CNRS-LIRMM in the framework of an international bilateral research agreement, was experimentally proven. The basic idea consists in moving a virtual target on the desired path in such a way as to guarantee the convergence of the vehicle, steering according to a suitable algorithm, to the target itself [15]. An example of the accuracy of the proposed algorithm in tracking a generic path with the Charlie USV is given in Figure 5, where results obtained both at fixed speed and controlling the vehicle velocity according to the path shape are presented.

On the other hand, automated autotuning procedures, based on induced self-oscillations of the system to be controlled, were transferred from the field of automation industry to basic USV guidance and control, being easy to use and not requiring expert knowledge from the USV operator. These procedures, developed and tested with the Charlie USV in cooperation with the Laboratory for Underwater Systems and Technologies of the University of Zagreb, Croatia, demonstrated their feasibility in designing, implementing and tuning not only auto-heading controllers, but also a straight line-following guidance module able to generate suitable heading reference for a generic autopilot [16].

7 Communications and pilot interface

Communications with the remote control and supervision station are guaranteed by a radio wireless LAN at 1.9 Mbps, supporting robot telemetry, operator commands,

Figure 7: View of the Charlie USV sampling sea surface micro-layer, Terra Nova Bay, Ross Sea, Antarctica (February 2004).

and video image transmission. Anyway, due to the poor performances, mainly in terms of reliability, offered by commercial, relatively low cost, wireless line-of-sight links, the communication system was upgraded with a radio modem working at 169 MHz, guaranteeing a safe transfer of commands and basic telemetry. In the case of cooperative control of the two USVs, communications between the vessels are supported by a low bandwidth radio modem, working at 436 MHz.
The human operator station is constituted by a laptop computer, running a Human Computer Interface, implemented originally in C++ and then in Java, and the power supply system, which integrates a couple of solar panels (32 W at 12V) and one lead battery (100 Ah at 12 V) thus guaranteeing its full autonomy and portability.

8 Exploitation

Among the large spectrum of possible applications of USV technology, the activities of research and exploitation of the Charlie and ALANIS prototype vehicles focused on the study of the sea-air interface, harbour protection and REA.
The possibility of integrating USVs in coastal and harbour underwater anti-intrusion systems was investigated in a project funded by PRAI-FESR Regione Liguria in the period 2005-2007, where basic NGC techniques presented in sections 6.2 and 6.3 were developed, and will be exploited in the Industria 2015 project ”SLIMPORT - Integrated management system for logistics and safety of port intermodality”. In the following the exploitation of the Charlie USV for the study of the sea-air interface and current research

Figure 8: View of the Charlie USV following ALANIS in the Genova Prà harbour (July 2009)

in developing basic tools for the support of REA operations are presented.

8.1 Study of the sea-air interface

The first version of the Charlie USV was basically designed to satisfy the operational requirement of sampling the sea surface micro-layer and immediate subsurface water for the study of sea-air interactions in the Ross Sea, Antarctica, in cooperation with the CNR Institute for the Dynamics of Environmental Systems, Venice. In the framework of the SEa Surface Autonomous Modular unit (SESAMO) project, funded by the Italian National Program of Research in Antarctica, the vessel was equipped with a scientific payload consisting of a rotating glass drum for micro-layer collection, a seawater intake for immediate sub-surface water sampling, and a number of teflon membrane pumps and three-way valves in order to distribute the sampled water in suitable stocking buckets for organic and inorganic samples (see Figure 6). The system could stock up to 20 l of organic samples and 10 l of inorganic ones both for micro-layer and immediate sub-surface, for an overall load of about 60 Kg. In order to maintain about constant the vessel weight during sampling, a couple of ballast water tanks were positioned in the hulls to be emptied in the course of the mission. The rotating glass drum was 0.33 m in diameter and 0.50 m in length and, actioned by an electrical brushless thruster, could rotate between 4 and 10 rpm. The hull was painted with a special epoxidic resin in order to minimise the risk of polluting the collected inorganic samples.

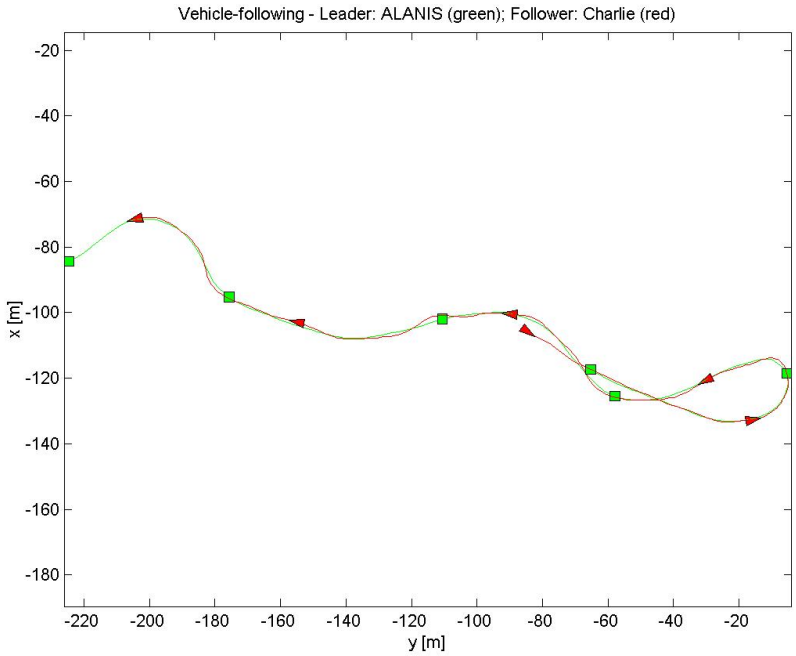

Figure 9: Path of the Charlie USV following ALANIS in the Genova Prà harbour (July 2009)

In January-February 2004, during the XIX Italian Expedition to Antarctica, the vehicle worked in the proximity of the M. Zucchelli station of Terra Nova Bay, Ross Sea. The Charlie USV was deployed and recovered by the Malippo, a 16 m support vessel hosting the human operator station. Compatibly with weather and sea conditions, the robotics catamaran executed six missions (two for communications, navigation, guidance and control tests and four for water sampling) working for more than 20 hours and collecting about 95 l both of micro-layer and immediate sub-surface water samples. A view of the Charlie USV collecting samples among the Antarctic ices is given in Figure 7. A detailed discussion of system requirements for the study of sea-air interface, guidance and control system, and Antarctic exploitation can be found in [10].

8.2 Towards Rapid Environmental Assessment

The 21st century's scenarios of marine operations, regarding environmental monitoring, border surveillance, warfare and defence applications, foresee the cooperation of networked heterogeneous manned/unmanned air, ground and marine platforms. Examples are given by the Autonomous Ocean Sampling Network, integrating robotic vehicles and ocean mod-

els to increase the capacity of observing and predicting the ocean behaviour, and the Barents 2020 vision, optimising marine resources thanks to historical and real-time information collected by a large network of cooperating vehicles.
In this context, as a consequence of their networking capabilities, USVs are naturally seen as a part of flotillas of heterogeneous vehicles executing large scale surveys and supporting REA: in addition to operate as communication relays for acoustic communications with companions unmanned underwater vehicles, they can act as force multipliers both extending the use of the same device to a formation of vehicles and allowing the displacement of different sensors in the same place about at the same time. Research carried out with CNR-ISSIA USVs focused on the theoretical and experimental study of the problem of a slave vehicle following a master vessel at a predefined range, constituting, for instance, a force multiplier in executing bathymetric surveys. Preliminary experiments, carried out in cooperation with the Hydrographic Institute of the Italian Navy in the Genova Prà harbour in July 2009, with logistical support of the personnel of A.S.D.P.S. Prà Sapello, demonstrated the effectiveness of an approach relying on virtual target based path-following techniques combined with on-line path generation, on the basis of position data received from a moving master vehicle. As shown in Figure 8, during preliminary trials the Charlie USV autonomously followed the ALANIS vessel piloted by a human operator. The accuracy of the proposed algorithms, supported by high positioning GPS systems aboard the two vessels, was very good shown in Figure 9.

References

[1] S.J. Cornfield and J.M. Young. Unmanned surface vehicles - game changing technology for naval operations (in Advances in unmanned marine vehicles). pages 311–328, 2006.

[2] J.E. Manley, A. Marsh, W. Cornforth, and C. Wiseman. Evolution of the autonomous surface craft AutoCat. *Proc. of Oceans'00*, 1:403–408, 2000.

[3] J.E. Manley. Development of the autonomous surface craft "ACES". *Proc. of Oceans'97*, 2:827–832, 1997.

[4] J. Curcio, J. Leonard, J. Vaganay, A. Patrikalakis, A. Bahr, D. Battle, H. Schmidt, and M. Grund. Experiments in moving baseline navigation using autonomous surface craft. *Proc. of Oceans'05*, 2005.

[5] J.E. Manley, J. Curran, B. Lockyer, J. Morash, and C. Chryssostomidis. Applying AUV lessons and technologies to autonomous surface craft development. *Proc. of Oceans'01*, 1:545–549, 2001.

[6] J. Majohr and T. Buch. Modelling, simulation and control of an autonomous surface marine vehicle for surveying applications Measuring Dolphin MESSIN (in Advances in unmanned marine vehicles). pages 329–352, 2006.

[7] A. Pascoal and et al. Robotic ocean vehicles for marine science applications: the European ASIMOV Project. *Proc. of Oceans 2000*, 2000.

[8] A. Martins, J.M. Almeida, E.P. Silva, and F.L. Pereira. Vision-based autonomous surface vehicle docking manoeuvre. *Proc. of 7th IFAC Conference on Manoeuvring and Control of Marine Craft*, 2006.

[9] T. Xu, J. Chudley, and R. Sutton. Soft computing design of a multi-sensor data fusion system for an unmanned surface vehicle navigation. *Proc. of 7th IFAC Conference on Manoeuvring and Control of Marine Craft*, 2006.

[10] M. Caccia, R. Bono, Ga. Bruzzone, Gi. Bruzzone, E. Spirandelli, G. Veruggio, A.M. Stortini, and G. Capodaglio. Sampling sea surface with SESAMO. *IEEE Robotics and Automation Magazine*, 12(3):95–105, 2005.

[11] J. Ebken, M. Bruch, and J. Lum. Applying UGV Technologies to Unmanned Surface Vessels. *SPIE Proc. 5804, Unmanned Ground Vehicle Technology VII*, 2005.

[12] M.R. Benjamin and J. Curcio. COLREGS-Based Navigation in Unmanned Marine Vehicles. *IEEE Proceedings of AUV-2004*, 2004.

[13] M. Caccia and G. Bruzzone. Execution control of ROV navigation, guidance and control tasks. *International Journal of Control*, 80(7):1109–1124, 2007.

[14] M. Caccia, M. Bibuli, and G. Bruzzone. ALuminim Autonomous Navigator for Intelligent Sampling: the ALANIS Project. *Sea Technology*, 50(2):63–66, 2009.

[15] M. Bibuli, G. Bruzzone, andM. Caccia, and L. Lapierre. Path-Following Algorithms and Experiments for an Unmanned Surface Vehicle. *Journal of Field Robotics*, 26(8):669–688, 2009.

[16] N. Miskovic, Z. Vukic, M. Bibuli, M. Caccia, and G. Bruzzone. Marine vehicles' line following controller tuning through self-oscillation experiments. *Proc. of the 17th Mediterranean Conference on Control and Automation*, 2009.

Design, Development and Exploitation of the Romeo ROV

M. Caccia[1], R. Bono[1], G. Bruzzone[1], G. Veruggio[2]
1, Institute of Intelligent Systems for Automation, CNR, Genova, Italy
2, Institute of Electronics, Computer and Telecommunication Engineering, CNR, Genova, Italy
max@ge.issia.cnr.it

Abstract

The design, development and exploitation of Romeo, a networked ROV capable of supporting heterogeneous payloads for both robotics research on intelligent vehicles and scientific missions in very harsh environment, are presented.
The over-actuated open-frame vehicle, designed for high precision maneuvering for benthic applications minimising the interactions with the operating environment, is characterised by: an interchangeable toolsled with common electrical and mechanical interfaces for the integration of heterogeneous scientific and technological devices a hierarchical control architecture and the definition of logical interfaces between its levels for the integration with advanced mission control systems the connectivity to Internet and satellite communication channels for remote teleoperation the capability of deploying and recovering scientific instrumentation on the seabed.
This allowed the exploitation of the vehicle in a number of scientific missions in Mediterranean and polar environment, both Arctic and Antarctica, demonstrating its capabilities in supporting benthic sample and data acquisition as well as robotics research.
This paper presents the vehicle design, development and exploitation focusing on the development of payloads interoperable by other ROVs such as IFREMER Victor, Internet based tele-operation of the vehicle in Antarctica and Svaalbard islands from Europe, and the deployment and recovery of a benthic chamber under the Antarctic ice-pack.

1 Introduction

In the last years Remotely Operated Vehicles (ROVs) emerged as a consolidated technology for underwater intervention for both industrial, mainly in the offshore area, and scientific applications. Indeed, although the tether connection with the support vessel constrains the vehicle operating area, amplifies the disturbance induced by the sea currents and increments logistic requirements, on the other hand it dramatically increases the vehicle autonomy, making possible the supply of electrical power from the surface and allowing strict interactions with the operating environment thanks to the possibility of transmitting high quality live video streams to the operator station, in particular with the use of fibre optics. The result is the current production of more than 450 types of ROVs in the world covering a wide spectrum of applications, user requirements and physical characteristics ranging from the heavy working ROVs to the light micro-ROVs.
Here, the main technical facts that, in the

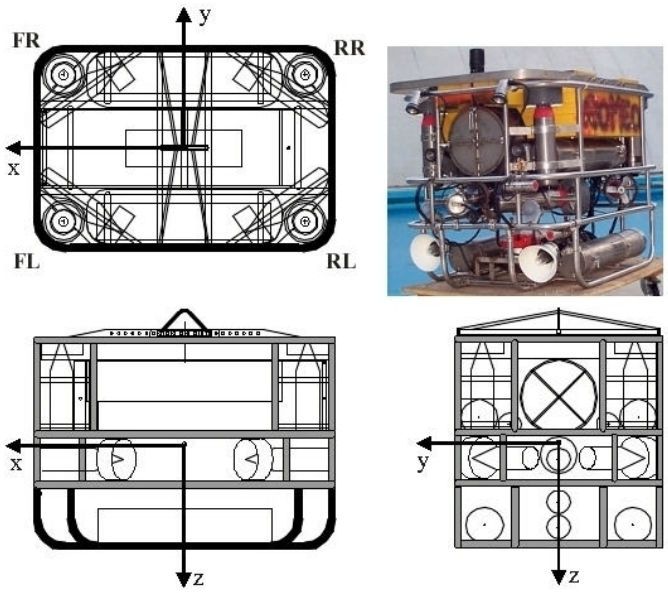

Figure 1: Romeo ROV mechanical design.

authors' opinion, have characterised the evolution of research ROVs in the last fifteen years are discussed.

In the mid Nineties of the last century, the marine robotics research community examined the possibility of sharing hardware and software resources in order to foster cooperation between different research groups and to reduce development costs. An example of this discussion is given by the Proceedings of the IARP Workshop on mobile robots for subsea environment, held in Monterey, USA, in 1994. The result was the adoption of hierarchical control architectures, the rigorous definition of the logical interfaces between their continuous and discrete time levels, and of common electrical and mechanical interfaces in order to facilitate the integration of heterogeneous scientific and technological payloads on different vehicles. Thus, the concept of interchangeable toolsled, able to handle the data acquisition and control of the aboard instruments, and connected with the ROV only through standard power supply and communication interfaces, was developed. In this way, the integration of additional instrumentation did not require any more to modify the control and system management software of the vehicle. Victor 6000 by IFREMER, France, [1] and Tiburon by the Monterey Bay Aquarium Research Institute, USA [2] are a couple of typical examples of this class of vehicles. Moreover, these vehicles are fully networked, i.e. able to broadcast the acquired data.

The fast development of embedded systems computing power, as well as the increasing diffusion of free software and the enhancement of its real-time capabilities, at the beginning of the Millennium led to the use of free operating systems, in

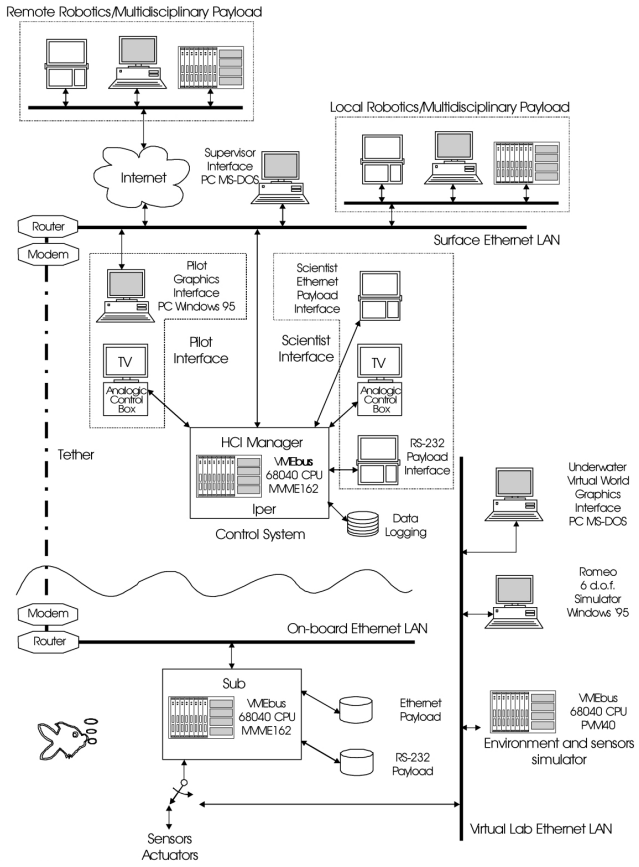

Figure 2: Romeo ROV networked architecture.

particular GNU/Linux, as embedded real-time platforms for the implementation of research ROV control systems. This is, for instance, the case of Jason II [3], the new version of the historical Jason ROV by Whoods Hole Oceanographic Institution (WHOI) [4]. Moreover, the high communication bandwidth guaranteed by fibre optics tethers motivated, with respect to intelligent ROVs, such as Victor 6000 and Tiburon, characterised by a high aboard computer power, a return to the past of ROV control system located inside the surface station in order to facilitate its upgrade and maintenance.

More recently, dramatic developments in marine fibre optics made possible the implementation of the concept of hybrid ROV, i.e. a vehicle that can work both connected to the mother ship by a very thin fibre optic tether (diameter of about 0.8 mm) when the transmission of large bandwidth data is required for strict interactions with the operating environment and, releasing the tether, as an Autonomous Underwater Vehicle able to explore and mapping the

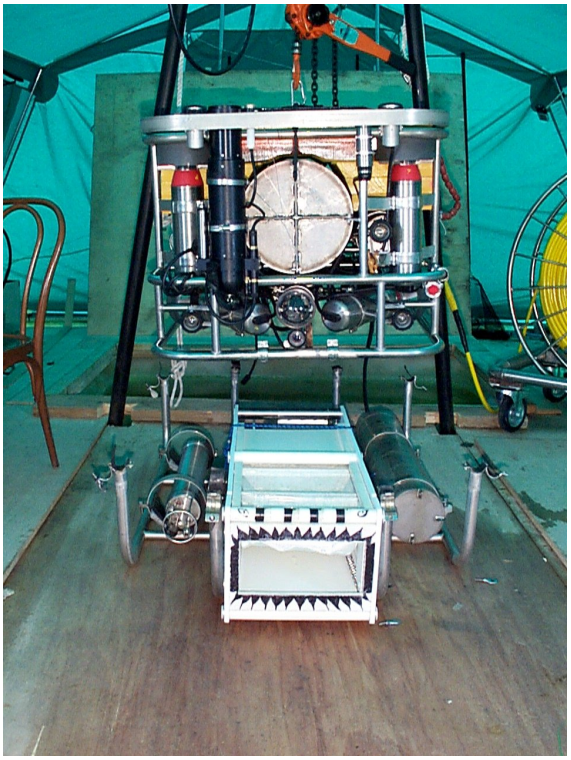

Figure 3: Plancton sampling configuration of the Romeo ROV, Terra Nova Bay, Ross Sea, Antarctica (November 1997).

seafloor with optical and acoustic devices. This is the case of Nereus [5], developed by WHOI in cooperation with John Hopkins University and U.S. Navy Space and Naval Warfare Systems Center of San Diego, that in 2009 reached the deep of about 11000 m in the Marianne Trench more than ten years after the Japanese ROV Kaiko [6].

In this context, in the Mid of the Nineties, the robotics group of the Institute for Ship Automation (Institute of Studies for Intelligent Systems for Automation from 2002) of the Italian National Research Council developed a mid class networked ROV, named Romeo, for robotics research and scientific applications, according to the structure of Victor 6000 and Tiburon. In the following, after a short discussion of the vehicle architecture, Romeo's scientific exploitation is presented focusing on its main features such as its capability of carrying heterogeneous payloads and of working as a benthic shuttle, and its full connectivity to Internet from harsh and remote environments.

2 Romeo ROV architecture

2.1 Mechanical design

Romeo's mechanical design should satisfy basic scientific needs in terms of manoeuvring and payload capabilities, and operational requirements in terms of logistics and maintainability. During typical missions the vehicle had to operate in different payload configurations, also in harsh environment and from vessels of opportunity, as in the case of polar under-ice and open sea applications, in order to execute pelagic and benthic surveys and data sampling.
The need of an easily portable system operable by a team with few people induced the design of a shallow water ROV (up to 500 m), weighting about 450 kg in air and about 1 m in height, 0.9 m in width and 1.3 m in length. This allowed the vehicle to be operated from relatively small vessels (at least 16 m) or from remote camps by a dedicated crew of four people.
The main scientific requirement, that is being able to operate different sets of devices during the same campaign, was satisfied by the possibility of mounting an interchangeable toolsled below the vehicle's basic frame. As shown in Figure 1, Romeo, which is intrinsically stable in pitch and roll, is divided into three sections. The bottom section of the vehicle carries an interchangeable toolsled for scientific devices, which in the standard version is equipped with two cylindrical canisters for batteries and payload electronics. The middle section, the core vehicle, is made up of a basic frame carrying one 100x32 cm (ld) cylindrical canister for the control system, plant management and communication electronics, two 80x15 cm (ld) cylinders for batteries and battery chargers, one 60x15 cm (ld) cylinder for compass, gyro, and inclinometers, four thrusters for propulsion in the horizontal plane, four for the vertical propulsion, and the basic sensor package (CTD, pilot and scientist TV cameras, etc.). The top section, carried by the basic frame, is made up of foam for buoyancy. The thrusters, canisters, and instruments are allocated so that the overall structure of the vehicle is symmetric with respect to both the x-z and y-z planes. The thrusters are arranged two by two in the corners, with the horizontal ones parallel to the diagonals of the x-y section. This thruster configuration enables full control of the vehicle's motion even in cases of faults in one horizontal or vertical actuator, making space available for vision devices in front of the vehicle and for electronics equipment in the middle. In addition, the allocation of the vertical propellers on the top of the vehicle reduces their pull-up efficiency because of propeller-hull interactions, but minimizes the interactions between the boosted water and the sediments during benthic operations, satisfying a basic scientific requirement. The result was a vehicle whose dynamics was modelled and identified as discussed in [7].

2.2 Computing and communication architecture

An architecture for unmanned underwater vehicles basically consisting of three Ethernet LANs (surface, on-board and lab LAN), which can be connected to the world-wide web for remote control and data access, was designed and implemented in order to allow fast system development through hardware-in-the-loop simulations and to enhance the ROV ca-

pabilities by integrating it with a multidisciplinary payload, i.e. a robotic and scientific system which can supervise the mission and pilot the ROV, coordinating its manoeuvres with the acquisition of scientific data and samples.

As shown in Figure 2, the surface Ethernet LAN connects a connection manager computer (IPER) and a multi-machine distributed Human Computer Interface (HCI), which allows a number of different operators to interact with the robot at various levels of the control system. The conventional HCI for scientific applications consists of three interfaces: one for the pilot, who tele-operates the vehicle, one for the supervisor, who supervises plant behaviour and resources allocation, and one for the marine scientist, who examines real-time images and sensors data to detect areas of interest. The IPER machine acquires all the vehicle's surface sensors as, for instance, acoustic positioning system, ship GPS and gyro-compass, and manages communications from the human interfaces and the robot control system aboard the vehicle, dispatching telemetry data and collecting, while solving conflicts, the user commands. The surface LAN can also support the connection of local and remote robotics and multidisciplinary payloads, which can automatically supervise and manage the vehicle missions.

The on-board Ethernet LAN connects a control system computer (SUB), which executes the basic navigation, guidance and control (NGC) tasks and manages the vehicle plant and on-board scientific/multidisciplinary payloads. Due to the limited computing power of the SUB machine, consisting of a VMEbus with a Motorola 32 MHz 68040 CPU MVME162 board, providing an Ethernet interface, carrying four IP piggy-back modules for digital and serial I/O, and an additional board for analog I/O, an additional MVME162 board was added for managing the automatic coordination of navigation, guidance and control tasks. On these boards runs the Romeo's control system, a real-time application developed using the VxWorks operating system.

The surface and on-board Ethernet LANs were originally connected by two twisted pairs in the 600 m long tether. In order to overcome the problem lying in the fact that Ethernet cannot operate with twisted cables longer than 100 m, a modem and a router were added on each side of the cable for the modulation/demodulation on the tether and the dispatching of Ethernet packets. The main drawback of this solution was in limiting to approximately 2 Mbps the maximum speed of Ethernet obtainable through the tether. However, in 1999 the system modularity allowed an easy upgrade to a fibre optic link supporting Ethernet at 10 Mbps, 5 RS-232 serial channels at 115 Kbps, and 5 RS-422 serial channels at 250 Kbps and 4 video channels.

At last, the lab Ethernet LAN supports the Underwater Virtual World facilities allowing hardware-in-the-loop simulation of the vehicle 6 d.o.f. dynamics, environment and sensors [8].

As far as the vehicle navigation, guidance and control system, performing auto-heading, auto-depth, auto-altitude and vision-based motion control, as well as execution control of basic tasks, the reader can refer to [9, 10, 11], and [12].

3 Integrability with heterogeneous payloads

The Romeo ROV capability of carrying toolsleds with heterogeneous devices was exploited already during its first Antarctic campaign, performed during the austral summer 1997-98 at the Italian station of Terra Nova Bay (TNB), Ross Sea, in the framework of the project PRISMA, funded by the National Program of Research in Antarctica (PNRA). As a consequence of the success of that experience, Romeo was employed for collecting samples and data in the proximity of the Antarctic coast in a number of further expeditions, when other important vehicle characteristics, in terms of benthic and networked operation capabilities, were exploited too. Anyway, it is worth remembering the integration in the vehicle toolsled of: i) a LIDAR (XXI expedition, 2001-02), developed by ENEA, for the detection of the chemical composition of the substances dissolved in the sea in order to detect different algae chromophore groups, water impurities and to analyse the plankton photosynthesis; ii) a fish eggs collection pump for the study of Antarctic silverfish reproduction conditions and habitat.

Anyway, the integrability of the data acquisition and control system of the Romeo ROV payload was fully demonstrated in the EC MAS3 "Advanced ROV package for Automatic Mobile Inspections of Sediments (ARAMIS)" project, where a scientific and technological toolsled were integrated with both the Romeo ROV and a larger toolsled mounted below Victor 6000.

3.1 PRISMA project

During the Italian XIII Expedition to Antarctica, which took place from October 1997 to February 1998 at Terra Nova Bay Station (Lat. 74.41'.42" S, Lon. 164.07'23" E), Romeo supported marine biology and oceanographic research in the framework of the PNRA - Integrated Robotics Project for the Study of Antarctic Sea (PNRA-PRISMA). Romeo's activity was organized in three legs. In the first two legs, from the end of October to mid January), the vehicle was operated from a hole in the ice-pack to collect data about under-ice biological processes and to evaluate the under-ice performances of a set of acoustic devices (echosounders, high-frequency pencil beam profiling sonar, Doppler speed-meter) preparatory to the study of SARA, the Italian Antarctic AUV. In the third leg (from mid January to end of February) Romeo was operated from a small boat to monitor the benthic environment in the Marine Antarctic Specially Protected Area established nearby the Italian TNB Station. The implementation of a serial tunnelling mechanism between the surface and on-board Ethernet LANs enabled scientific end-users to transparently control instruments mounted on the ROV directly from the surface.

During the first leg Romeo was operated to support the Project 2.b.3 Ecology and Bio-geo-chemistry of the Southern Ocean about the paths of the material substances and flow of energy in the cryosystems. The scientific payload was constituted by a multi-parametric gauge (conductivity, temperature, depth, oxygen, fluorimeter), and a "microness" (zooplancton sampler), mounted on the toolsled. In addition, as shown in Figure 3, a spectral irradiance meter was mounted vertically in front

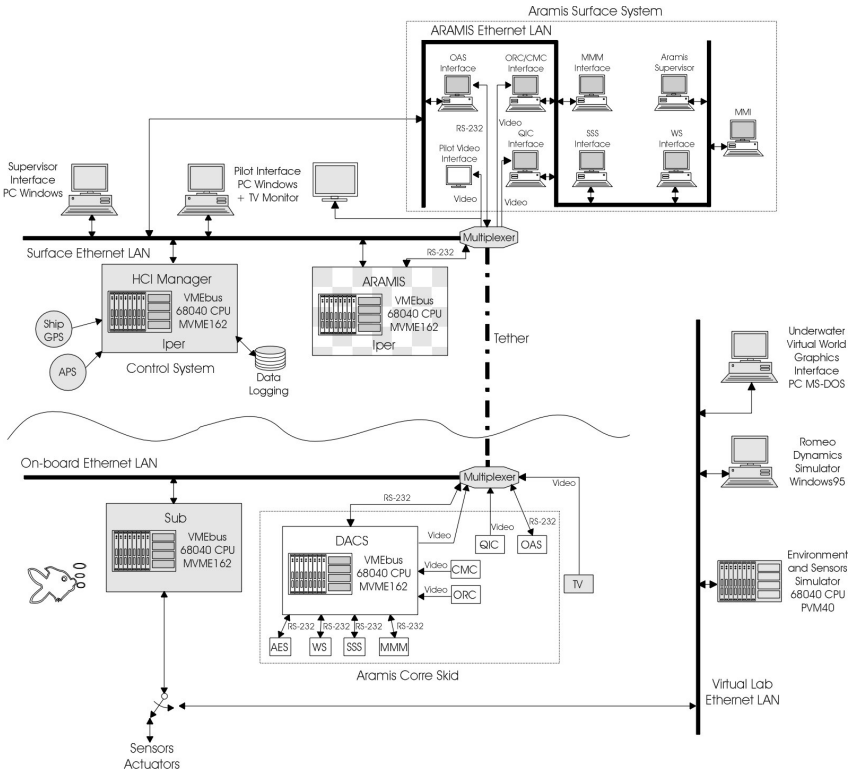

Figure 4: ARAMIS adaptation of the Romeo ROV networked architecture.

of the vehicle. Romeo's principal missions consisted in zoo-plankton sampling with the microness in an area of 200 meters from the hole, by means of horizontal traverses at different depths between 3.5 m and 20 m at the constant speed of 25 cm/s, and horizontal and vertical traverses to collect data with the spectral irradiance meter.

During the second leg of the expedition Romeo supported the Project 4.a Robotics and Telescience in Extreme Environment. In order to test under-ice behaviour of acoustic devices, Romeo was equipped with two Tritech ST-200 echo-sounders at 200 kHz, a high frequency pencil beam profiling sonar at 1.25 MHz, and a RDI Workhorse Navigator Doppler velocimeter at 300 kHz. The capability of the echo-sounder and profiling sonar in tracking the ice-canopy at different angles of incidence was tested, and interference trials were performed with the two echo-sounders mounted in upward/downward looking configuration. The feasibility of the upward/downward looking sonar configuration to execute the task of automatically following the ice-canopy and mapping the seabed were also demonstrated. A number of radial traverses from the deploying ice-pack hole were executed, allowing the mapping of the bathimetry and ice-canopy profile of the area.

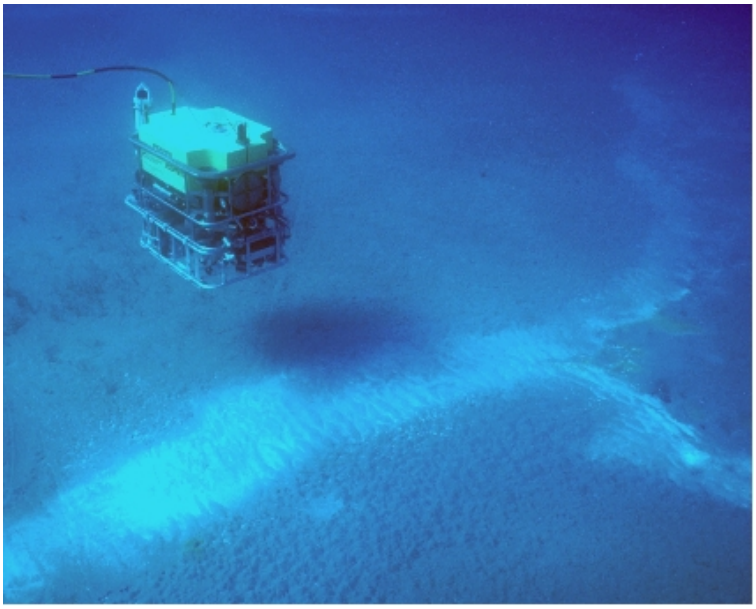

Figure 5: View of the Romeo ROV over the thermal vents of the Milos island (September 2000).

During the third leg Romeo collected benthic data (water samples, TV images and photos) in the Marine Antarctic Specially Protected Area established nearby the Italian TNB Station. A high number of traverses at constant range from the seabed were performed in order to collect high quality and stable video images useful for the counting and sizing of the organisms living in the explored area. The vehicle was equipped with the complete suite of acoustic instruments plus a set of scientific devices consisting of two Niskin bottles for water sampling, still camera and strobe lights, and calibrated laser pointer matrix for the sizing of the observed features of interest. Moreover, the keel of the Campbell Ice Tongue, reaching the depth of 160 m, was explored collecting water samples below it at a depth of 216 meters.

3.2 ARAMIS project

In the period 1997-2000, ROMEO and Victor 6000 were used as carrier ROVs in the EC funded ARAMIS project. This project aimed at developing a scientific and technological system to be integrated with typical mid class existing ROVs to form a highly automated and robotised scientific tool for carrying out benthic investigations both in shallow and deep waters. The ARAMIS system consisted of a skid equipped with technological instruments, e.g. altitude echo-sounder, obstacle avoidance sonar, and quantitative image cameras, and scientific devices, e.g. water sensors, small sediment sampler, mini multipurpose multi-sampler, object recognition camera, and coring monitoring camera. The system was completed by a data acqui-

Figure 6: View of the Romeo ROV pilot interface during coring operations over the thermal vents of the Milos island (September 2000).

sition and control system of the ARAMIS instruments, located on-board the toolsled, and a surface controller, constituted by a network of computers devoted to the management of scientific devices and pilot interfaces and to acoustic and video image processing tasks. In particular, the ROV, making available a conventional auto-pilot, was guided by the ARAMIS supervisor. The integration of the ARAMIS modules in the Romeo networked architecture, in that case including a fibre optic link between the surface and the vehicle, is shown in Figure 4.

The operability of the ARAMIS system integrated with the Romeo ROV with respect to scientific specifications was demonstrated in a test campaign carried out in September 2000 in the Aegean Sea in the hydrothermal vent areas near the island of Milos. Seven dives were performed over a hydrothermal vent area, where the sea bottom was constituted by loose sand with ripples, some sea grass patches and bacterial/colloidal silica mats (the white stripe clearly visible on the seabed in Figure 5). It is worth noting that Romeo was able to support direct interactions of devices mounted in the toolsled with the seabed during sediment probing (with four sensors: temperature, pH, sulphide, oxygen) and coring. In particular, the ROV agility in manoeuvring allowed, together with the detailed view of the scene provided by the coring monitoring camera, the ARAMIS human operator to position the sediment probes right over a thermal vent. A view of the ROV pilot station during coring operations is shown in Figure 6, where the images taken by the Coring Monitoring camera are clearly visible.

4 Benthic shuttle

In the wake of the demonstration of manoeuvring accuracy shown in the ARAMIS

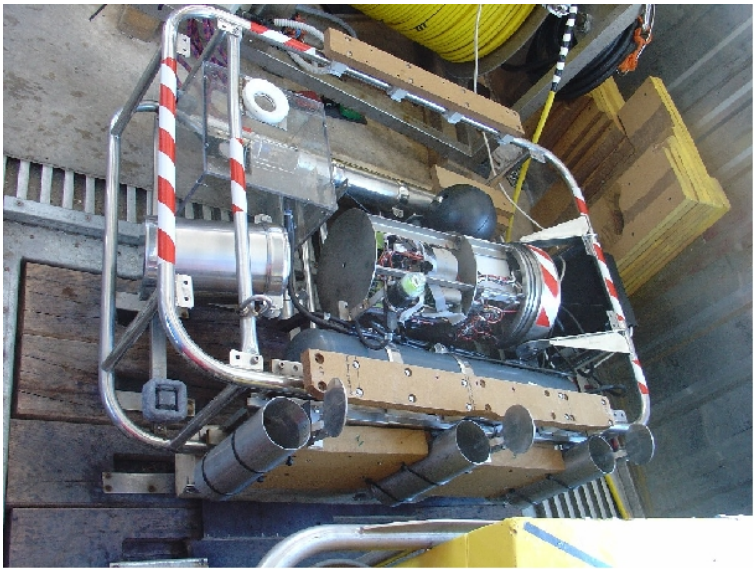

Figure 7: View of the ABS benthic chamber during mission preparation, Terra Nova Bay, Ross Sea, Antarctica (January 2004).

project and of the experience of SIRENE, the IFREMER AUV for the deployment of benthic stations at sea [13], Romeo was exploited as benthic shuttle for the deployment and recovery of a benthic chamber over the sea floor below the ice-canopy during the XIX Italian expedition to Antarctica in 2003-04. Thanks to the video cameras mounted aboard the ROV, the scientific end-user could choose with high accuracy the place where releasing the instrumentation and recovering it after 24 hours with the vehicle equipped with a teleoperated automated hooking system. Benthic module localisation was simply performed by tracking the ROV and benthic chamber positions with a SSBL acoustic positioning system, whose transducer was mounted in a fixed location, i.e. a hole in the ice canopy, in the ice field.

The project Antarctic Benthic Shuttle (ABS) was carried out in cooperation with DIPTERIS-UNIGE (Department for the Study of the Territory and its Resources - University of Genoa) to study the structure and long-term variations of the benthos in the Protected Marine Area of Baia Terra Nova, from Road Cove to Adelie Cove, as required by the ASPA and the SCAR CS - EASIZ (Coastal Shelf - Ecology of the Antarctic Sea Ice Zone) programs. The standard benthic module consisted of a benthic chamber for the in-situ analysis of sediment-water interactions in different conditions of ice cover, and of a time-lapse image and data acquisition system. Benthic chambers, isolating a known volume of seawater and a known surface of sediments, allow the estimation of oxygen consumption by different benthic compartments, e.g. macrofauna, meiofauna and bacteria, assessing their relative contribu-

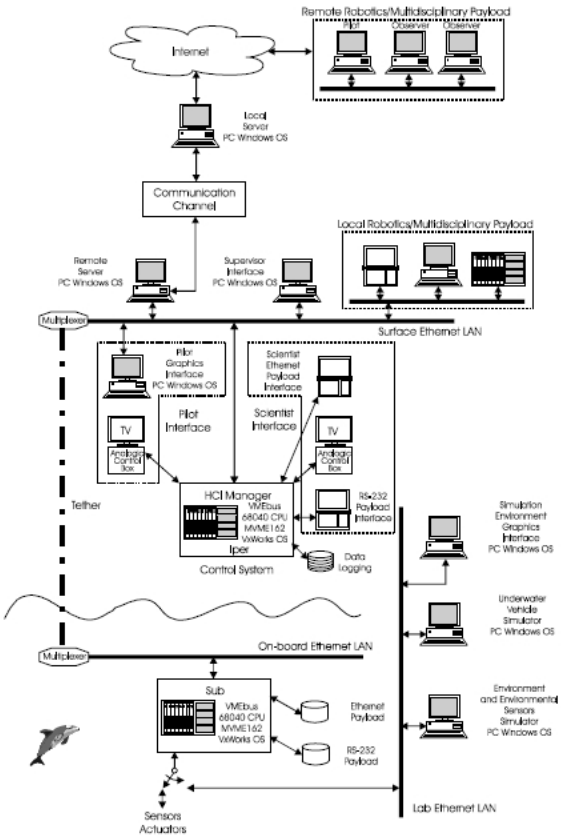

Figure 8: Adaptation of the Romeo ROV networked architecture for Internet-based teleoperation.

tion in different environmental conditions. In particular, the project attention focused on bacteria, which exert a major role in the turn-over of organic matter and in remineralization processes (microbial loop). In addition, benthic chambers allow direct measurements of benthic fluxes, taking into account bio-turbation and sediment mixing. Particular interest relayed on diagenetic reactions in surface sediments, with changes in concentrations of organic matter, nutrients, dissolved oxygen at water-sediment interface. Photographic systems (video-tape and time-lapse photographs) allowed the visual analysis of the evolution of some proliferative and bioturbative processes, as well as behavioural observations. A dedicated toolsled, see Figure 7, was designed and built for the ABS project, basically consisting of a benthic chamber, i.e. a glass box of 30x30x20 cm (lwh), equipped with a CTD with oxygen sensor, two camcorders, which monitored the space inside and the sea floor nearby the chamber, and

Figure 9: Romeo ROV ice camp for Internet satellite tele-operation, Terra Nova Bay, Ross Sea, Antarctica (December 2001).

three bottles for suspended particle sampling. The data acquisition system was controlled by means of a single board computer mounting an Intel 486 CPU and running a software application written using the RTKernel operating system.
A total of eight missions were performed both through a hole in the ice-pack (seven trials) and from a support vessel (one trial), with successful recovery of the instrumentation.

5 Networked ROV

After preliminary experiments of Internet based mission control carried out in cooperation with the Instituto Superior Técnico of Lisboa in 1999, the accessibility of the Romeo ROV through Internet was mainly demonstrated remotely tele-operating the vehicle in polar regions in the projects E-robot 1 and E-robot 2 in the period 2001-02.
As shown in Figure 8, the Romeo networked architecture can support the vehicle Internet-based tele-operation with the integration of a couple of modules, the so-called Remote and Local servers. The Remote Server is a computer located in the vehicle operating site handling communications between the ROV and a generic communication channel, which can be also a point-to-point connection with the Local Server guaranteed by a radio or satellite link. In addition to transmit/receive vehicle telemetry and commands, the Remote Server acquires, by means of a frame grabber, the video images provided by the ROV cameras coming from Romeo's video camera and send them after compression through the communication channel. On the other hand, the Local Server, a com-

puter usually located in the Genova marine robotics lab, handles Internet communications between the Remote Server and Romeo's remote users connected to the World Wide Web, by means of suitable software applications.

5.1 Internet-based mission control

In Fall 1999 a preliminary demonstration of Internet-based mission control of unmanned underwater vehicles was performed in cooperation with the Instituto Superior Técnico of Lisboa [14]. During the experiment, the CORAL robotics mission planner running remotely in Lisbon coordinated the activity of the Romeo ROV in a test pool in Genoa, in order to execute a user-defined mission. Although the problem of mission control of autonomous vehicles through the Internet network was mainly addressed, the success of the experiment showed that a ROV tele-operation by means of Internet was possible and that it was worth addressing research in that direction.

5.2 E-robot 1 project

On December 2001, during the XVII Italian Expedition to Antarctica, in the framework of the E-robot 1 project, in cooperation with CNR-SRT, several experiments of Internet-based satellite tele-operation with Romeo were carried out [15]. To allow the connection to Antarctica, Romeo's control system was integrated with a satellite communication system. Several users connected to the World Wide Web and, in particular, on December 18, 2001, from the CNR headquarters in Rome, had the possibility of remotely operating Romeo immerse in the sea in the Marine Antarctic Specially Protected Area nearby the Italian Terra Nova Bay Station. As shown in Figure 9, where the surface field is shown, the Romeo ROV was operated from a surface station located on the ice-pack. These experiments were, to authors' knowledge, the first example of satellite tele-operation of a ROV directly usable by users surfing on the web. The main purpose of these tests was to evaluate the possibility of executing reliable Internet tele-operation of remote robotic systems in actual operating conditions. Given the preliminary phase of that research, the experiments focused on verifying the possibility of piloting the remote ROV from a generic Internet interface by non-specialised end-users rather than on the execution of an Internet-controlled scientific mission.

5.3 E-robot 2 project

In September 2002, in the framework of the E-Robot2 project in cooperation with CNR-SRT, Romeo was remotely operated through Internet while operating in the Arctic sea, more precisely in the Kongsfjord in Norway, nearby the Italian Station "Dirigibile Italia" situated in Ny-Ålesund, Svalbard islands [16]. The ROV was operated by means of a support working boat, on which was installed the Remote Server and connected to the Italian ground station of Ny-Ålesund with a wireless link at 11 Mbps (IEEE 802.11b standard). The connection between the Italian Station and the Local Server located in the Genova lab consisted of 4 ISDN lines at 64 Kbps . Of the 256 Kbps available communication band, one half was used to set up a standard H323 video-conference system that allowed the marine scientist to communicate with Romeo team operating in Kongsfjord during experiment operations

and the other half was reserved for ROV commands, data telemetry and video images. Operating in this way it was possible to be world-wide connected with the underwater vehicle to follow the experiments and even to pilot it by means of high level commands. This allowed, for the first time, the execution of a number of missions under the control of a few teams of marine scientists from different European countries (the Scottish Association for Marine Science, the Norwegian College of Fishery Science of University of Tromsø, the Institute of Protein Biochemistry and the Enzymology and Institute of Biomolecular Chemistry of Naples) who, without moving from their laboratories, had the opportunity to conduct real-time experiments in the underwater environment in the Kongsfjord. The campaign in the Arctic Region reached its two main goals: i) to carry out a set of preliminary dives in various sites in the Kongsfjord giving the marine scientists a preliminary set of data to plan a more systematic investigation in the future years; ii) to test and demonstrate the effectiveness of the remote control of robots used in extreme environment for tele-science applications, along with the methodology already used in the E-robot 1 project.

References

[1] J.L. Michel et al. Victor 6000: design, utilization and first improvements. *Proc. of the 13th International Offshore and Polar Engineering Conference*, 2003.

[2] J.B. Newman and D. Stokes. Tiburon: development of an ROV for ocean science research. *Proc. of Oceans '94*, 2:483–488, 1994.

[3] L.L. Whitcomb, J.C. Howland, and D.A. Smallwood. A new control system for the next generation of US and UK deep submergence oceanographic ROVs. *Proc. of the 1st IFAC Workshop Guidance and Control of Underwater Vehicles*, pages 137–142, 2003.

[4] D.R. Yoerger, J.B. Newman, and J.E. Slotine. Supervisory control system for the Jason ROV. *IEEE Journal of Oceanic Engineering*, 11(3):392–400, 1986.

[5] Fletcher et al. Proof of concept demonstration of the Hybrid Remotely Operated Vehicle (HROV) light fiber tether system. *Proc. of Oceans'08*, 2008.

[6] S. Takagawa. Advanced technology used in Shinkai 6500 and full ocean depth ROV Kaiko. *J. of Mar. Techn. Soc.*, 29(3):15–25, 1995.

[7] M. Caccia, G. Indiveri, and G.Veruggio. Modelling and identification of open-frame variable configuration unmanned underwater vehicles. *IEEE Journal of Oceanic Engineering*, 25(2):227–240, 2000.

[8] G. Bruzzone, R. Bono, M. Caccia, and G. Veruggio. A Simulation Environment for Unmanned Underwater Vehicles Development. *Proc. of MTS/IEEE Oceans 2001*, 2001.

[9] M. Caccia and G. Veruggio. Guidance and control of a reconfigurable unmanned underwater vehicle. *Control Engineering Practice*, 8(1):21–37, 2000.

[10] M. Caccia, G. Bruzzone, and G. Veruggio. Bottom-following for remotely operated vehicles: algorithms and experiments. *Autonomous Robots*, 14:17–32, 2003.

[11] M. Caccia and G. Bruzzone. Execution control of ROV navigation, guidance and control tasks. *International Journal of Control*, 80(7):1109–1124, 2007.

[12] M. Caccia. Vision-based ROV horizontal motion control: near-seafloor experimental results. *Control Engineering Practice*, 15(6):703–714, 2007.

[13] J. Opderbecke, V. Rigaud, and D. Semac. Autonomous navigation of the free-swimming vehicle SIRENE. *Proc. of Oceans'98*, 3:1650–1654, 1998.

[14] G. Bruzzone and et al. Internet mission control of the Romeo unmanned underwater vehicle using the CORAL mission controller. *Proc. of MTS/IEEE Oceans'99*, 3:1081–1087, 1999.

[15] G. Bruzzone and et al. Internet-based satellite teleoperation of the Romeo ROV in Antarctica. *Proc. of 10th IEEE Mediterranean Conference on Control and Automation*, 2002.

[16] G. Bruzzone, R. Bono, M. Caccia, P. Coletta, and G. Veruggio. Internet-based tele-operation of the Romeo ROV in the Arctic region. *6th IFAC Conference on Manoeuvring and Control of Marine Craft*, 2003.

Proteolytic Marine Enzymes and their Applications

M. Salamone[1], A. Cuttitta[1], G. Seidita[2], L. Tutino[1], T. Masullo[1], S. Rigogliuso[3], F. Bertuzzi[4], G. Ghersi[3]
1, Institute for Coastal Marine Environment, CNR, Capo Granitola (TP), Italy
2, Department of Biopathology and Biomedical Methodology, University of Palermo, Palermo, Italy
3, Department of Cell and Developmental Biology, University of Palermo, Palermo, Italy
4, Hospital System "Niguarda Ca' Granda", Milano, Italy

monica.salamone@irma.pa.cnr.it

Abstract

The use of proteinases from marine organisms has several advantages over commercial proteinases since their optimal temperatures and other enzymatic characteristics differ from homologous proteinases obtained from warm-blooded animals. High activity of these enzymes at low temperatures is interesting for many industrial applications.
Enzymes used in tissue digestion to isolate the islets of Langherans for transplantation are extracted from *Clostridium histolyticum* bacteria; they have strong collagenolytic activity compared to vertebrate collagenases. However, several impediments persist in human islet success probably due to the variability in composition and concentration of collagenases used during the digestion phase and to the toxicity effect of the enzyme blend. Also the temperature used during tissue dissociation is a critical step since all the endogenous human proteases are active at 37°C.
We analyse different batches of commercial enzymes, used in Langherans islets purification, both in proteins composition by SDS-PAGE electrophoresis and in enzymatic activities by zimography analyses. We propose an innovative evaluation essay to select enzymes useful in islet pancreas isolation procedure. Using this approach, we characterized and tested marine enzyme from hepatopancreas of different marine invertebrates. We show that marine enzymes have a stronger proteolytic activity, also at low temperature on several interesting substrates, compared to the commercial ones.

1 Introduction

Enzymes are molecules involved in several processes; they have the capability to accelerate a reaction, activate or inhibit functions, and are involved in life processes. They are an essential target for the adaptation of an organism to a cold environment. In recent times, several studies have been carried out in order to understand the rules governing their molecular adaptation to low temperatures. These fundamental aspects are strongly connected with a strong biotechnological interest in the exclusive properties of these molecules [1]. They

present important advantages regarding their specific activity, lower stability and unusual specificity. Enzymes with these characteristics are well represented in sea organisms.

Innumerable tons of fish are harvested each year, about 70% of which, including viscera, head, skin, bone and some muscle tissue, are considered as waste during fishery products processing. These are actually discarded and few attempts to recovery them are done; recently, more severe ecological policies have pushed several seafood producers to find alternative ways in using secondary raw materials [2, 3]. Fish viscera, about 5% of the total, are rich potential sources of many enzymes that may have some exclusive interesting properties for both basic research and industrial applications.

Main digestive proteinases detected in fish hepatopancreas are trypsin and chymotrypsin. Trypsin has been extracted, purified and characterized in several fish species including the sardine (*Sardinops melanostictus*) and the arabesque greenling (*Pleuroprammus azonus*) [4] from the pyloric ceca of jacopever (*Sebastes schlegelii*), yellowfin tuna (*Thunnus albacores*) [5], skipjack tuna (*Katsuwonus pelamis*) [6] and Monterey sardine (*Sardinops sagaxcaerulea*) [7].

Moreover, with the new molecular biology technology it is possible to clone single genes and to produce marine organism enzymes by *in vitro* synthesis systems. For example, enzyme with collagenolitic activity are synthesized from *Paralithodes camtschaticus* and cystein proteases cathepsin has been produced from *Metapenaeus ensis* [8].

One of the first applications of cold-adapted enzymes, such as described proteases, lipases, alfa-amylases and cellulases, were their use as additives in detergents. They were used also in bioremediation; in fact, the high catalytic efficiency, together with the unique specificity at low and moderate temperatures, should render them suitable for bioremediation purposes [9].

Furthermore, the use of cold-adapted enzymes in the food industry are several. For example, in the milk industry, beta-galactosidase is used at low temperature to reduce the amount of lactose responsible for severe induced allergies; infant formula is an artificial substitute for human breast milk, destined to infant consumption. Generally, these enzymes are obtained as hydrolysates from bovine milk proteins in order to match with infant nutritional requirements. However, whey protein and caseins may induce the formation of specific immunoglobulin E antibodies in children that develop an allergy to cow's milk. alfa-lactoglobulin is considered to be one of the main allergens in bovine whey.

Generation of bioactive peptides is another important application of marine enzyme. For example, bioactive peptides with antioxidant properties derived from various proteins by enzymatic hydrolysis have become a topic of great interest for pharmaceutical, health food and processing/preservation industries. Antioxidant activity has been reported for protein hydrolysates obtained from different sources such as whole capelin, squid skin Pacific whiting [10]. Furthermore, controlled enzymatic hydrolysis of proteins may produce a series of small polypeptides which can modify and even improve the functional properties of proteins.

Gelatin is produced by heat denaturation of collagen; fewer studies have been done on the potential uses of gelatin derived from aquatic animal skin compared to mam-

malian. Kim et al. [11] showed that fish skin gelatin can be modified into biologically active peptides by protease treatments; in particular some purified peptides exhibited the potential to act as inhibitors of angiotensin I converting enzyme and antioxidants against peroxidation of linoleic acid. Moreover, biologically active peptides by protease treatments jumbo squid (*Dosidicus gigas*) [12] showed also antioxidative activity via radical scavenging and by retarding lipid peroxidation. Regarding fish gelatin-derived peptides, there are only a few reports dealing with their antioxidant properties [11] and no information can be found about functional properties of these peptides.

In the past, decapods enzymes obtained from hepatopancreas were used in would healing cure; in fact, their capability to remodelling the fibrin clot during wound healing process have been reported, such as to induce tissue repair in burnings, ulcerations and other [13].

Several families of proteases are involved in proteins digestion/remodeling and they were well described in mammalian systems. They can be distinguishable on the basis of their proteolytic behavior, biologic roles and structural organization. Many proteolytic enzymes were characterized; there are:

- the matrix metalloproteinases (MMPs), including members associated to plasma membrane (MT-MMPs);
- the ADAM (a family of disintegrin and metalloprotease);
- the meprins;
- the secretases (also termed sheddases or convertases);
- the collagenases;
- the serine-peptidases.

They exert their role prevalently on extracellular proteins; differently by cysteine- and aspartic- proteases that, in eukaryotic cells, generally play their functions inside the cell (cytoplasm compartment), as regulators of cell cycle and apoptotic processes. In our work, we principally focused on three different classes of proteolytic enzymes: collagenases, MMPs and serine proteases, and their role in cell extraction from tissues/organs for cell therapy and biomedical applications.

2 Proteolytic enzymes

A generic subdivision of proteolytic enzymes in mammalians puts them in four main classes: Aspartic-, Cysteine- Matrix Metallo- and Serine- proteases. Those belonging to the first two groups are commonly involved in apoptosis and cell proliferation processes, even if there are some exceptions. The other two are basically involve in cell migration/invasion processes, such as in ECM remodeling, proteins activation, digestion processes, and are commonly used in cell extraction from tissues/organs.

Some members of proteolytic enzymes belonging to MMPs and Serine-proteases families, directly or indirectly involved in proteins digestion, are listed in Table 1.

Generally, soluble forms of MMPs and Serine-proteases are all secreted in inactive forms and extracellulary enzymatically activated. A similar activation mechanism is observed for the plasma membrane associated forms of MMPs, the MT-MMPs, which are also activated by the action of specific enzymes. While, an activation dissimilar way is adopted by the integral plasma membrane serine peptidases; several of them are synthesized in monomeric inactive forms beginning in active forms when associated to form a dimer to the site

of proteolysis [14].
Differently, collagenases produced from procaryotic organisms are secreted just in active forms [15].
Plasma membrane associate proteolytic enzymes exert their function both on ECM component digestion, such as in proteolysis cascade activation, and in chemokines and factors activation.

3 Collagenases

Due to its three-dimensional organization, only a restricted number of proteases can digest collagen. Because of the variety in the collagen structure, it is not easy to discriminate true collagenases from other collagenolytic proteases and gelatinases, which just digest gelatin (denatured collagen). Moreover, the thermodynamically favored conformation of collagen at body temperature is a random coil rather than an α-helix [16]. This specifies that a variety of denatured forms of collagen are normally present in the body. It is feasible that a good number of collagenases can digest both collagen and gelatin. Moreover, as is frequently the case with collagenolytic proteases, collagenases are considerably active in hydrolyzing other protein substrates.
Mammalian matrix metalloproteinases (MMPs) have been explored better than collagenolytic proteases from bacteria. Only the collagenases ColH and ColG from *Clostridium histolyticum*, have been well studied [17, 18, 19]. As reported in Figure 1, the collagenases of bacteria are a simple organization compared to mammalians and collagen-binding regions have been identified in the structures of collagenases ColG and ColH from *C. histolyticum* and collagenase ColA from *Clostridium perfringens* [17] but not in others. However, sequences comparison between mammalian and bacterial collagen-binding sites seem to be different [20]. *C. histolyticum* ColG collagenase possesses tandem collagen-binding domains that interact with all types of collagen fibrils in spite of their diameter; thus, collagenase are said to show broad substrate specificity [21]. This is in striking contrast to the strict specificity of mammalian MMPs toward various types of collagens [22].

4 Matrix Metalloproteases

MMPs belong to a family of about thirty members zinc-containing endopeptidase activities and have the capability to digest many ECM constituents [19]. All members of the family are generated as inactive forms, pro-enzymes; they must be enzimatically modified to be active. The family members have been divided in different groups on the basis of their structure and/or digestive substrates (Table 1). The MMPs are structured in different domains, that are present in diverse number and composition inside to the family (Figure 2). The MMP3, MMP10 and MMP11 are stromelysins, they are very similar to the collagenases, but they have a broad spectrum substrate specificity and degrade components as proteoglycans, fibronectin, and laminin.

5 Serine proteases

Almost 40 members belong to serine-protease family having different functions. The members of the family are highly conserved within the human genome and

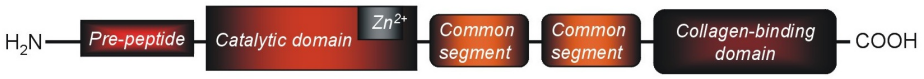

Figure 1: Structural organization of procariotic collagenases. Typical collagenolytic proteases from bacteria are organized with a pre domain followed by catalytic domain, common sequence and collagen-binding domains.

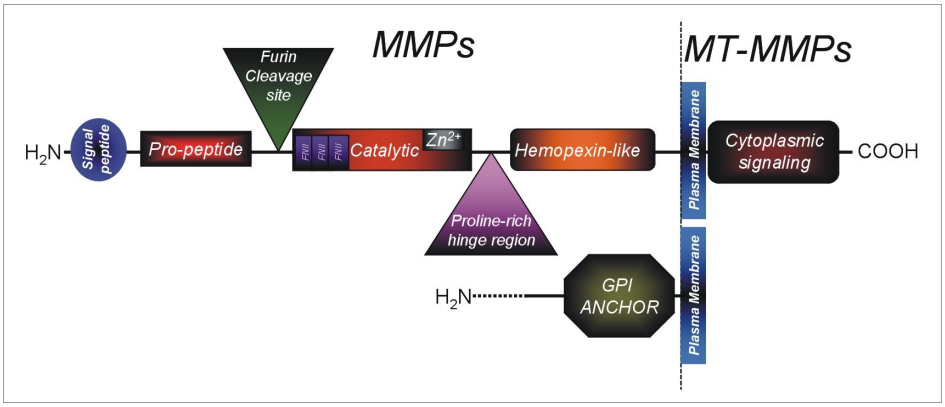

Figure 2: Structural organization of MMPs. All members of MMPs family are structurally organized in the way to have a signal peptide, the pro-peptide and the catalytic site containing the zinc-binding site. The MT-MMPs are the members of the family associated to the plasma membrane; they are connected to the plasma membrane trought a trasmembrane domain followed by a cytoplasmic tail, having signals function or via a glycosylphosphatidylinositol (GPI) membrane anchor.

amongst species. The enzymes of this family seem to have a common chemical mechanism of peptide substrate hydrolysis. The members of this family enclose enzymes involved in several functions; digestive enzymes, blood coagulation and fibrinolytic enzymes, Several of them are soluble molecules, they are secreted in inactive form to be enzymatically activated (Figure 3). Other are plasma membrane associate members and belong to the TTSP family; the prototype member could be considered dipeptidyl peptidase 4 (DPP4) (Figure 3).

The individual serine proteases show a surprisingly ample diversity in their target specificities. For example, plasmin has a very small broad specificity and it is a very efficient enzyme; its activity is analogous to trypsin, cleaving C-terminally Lys and Arg aminoacids. On the other hand, the uPA and tPA, activators of plasminogen, are tremendously precise and a very few number of substrates for these enzymes were identified.

An emerging class of serine protease belonging to TTSPs family are seprase and

Proteolytic enzymes	
Metallo-	**Serin-**
Soluble	**Soluble**
MMP1 - Collagenase 1	uPA & tPA
MMP2 - Gelatinase A	Plasminogen
MMP3 – Stromelysin 1	Trombin
MMP7 - Matrylisin	Chatepsin G
MMP8 - Collagenase 2	Elastase
MMP9 - Gelatinase B	Tripsin like
MMP10- Stromelysin 2	Serin-like FNase
MMP11- Stromelysin 3	DPPs (6, 8, 9)
MMP12- Metallo elastase of macrofages	Attractin
	DPP4-β
MMP13- Collagenase 3	QPP
MMP26 - Endometase	
MMP28- Epilysin	
Plasma Membrane Associated	**Plasma Membrane Associated**
ADAMs	Corin
MMP14 - MT1-MMP	DPPs (2, 4,)
MMP15 - MT2-MMP	Enteropeptidase
MMP16 - MT3-MMP	HAT
MMP17 - MT4-MMP	Hepsin
MMP24 - MT5-MMP	Matriptase/MT-SP1
MMP25 - MT6-MMP	Seprase
	Spinesin
	TMPRSS2-4

Table 1: Extracellular matrix metallo-proteases and serin-proteases.

DPP4; it has been demonstrated that they are directly involved in new vessel formation [23]; they are inducible, specific for proline containing peptides and macromolecules, and active on the cell surface. In particular, DPP4 has prolyl exopeptidase activity; some of its natural substrates are: neuropeptide Y [24], substance P [25] and beta chemokines such as eotaxin, SDF-1 (stromal derived factor) and RANTES (regulated on activation normal T-cell expressed and secreted) with either L-proline, L-hydroxyproline, or L-alanine at the penultimate position [26].

6 Enzymes in tissue digestion and transplantation

End-stage organ failure is a major cause of death worldwide that can occur in patients of all ages; transplantation is the current standard of care for chronic end-stage disease of many organs. Despite the success of organ transplantation, it is becoming clear that organs available through do-

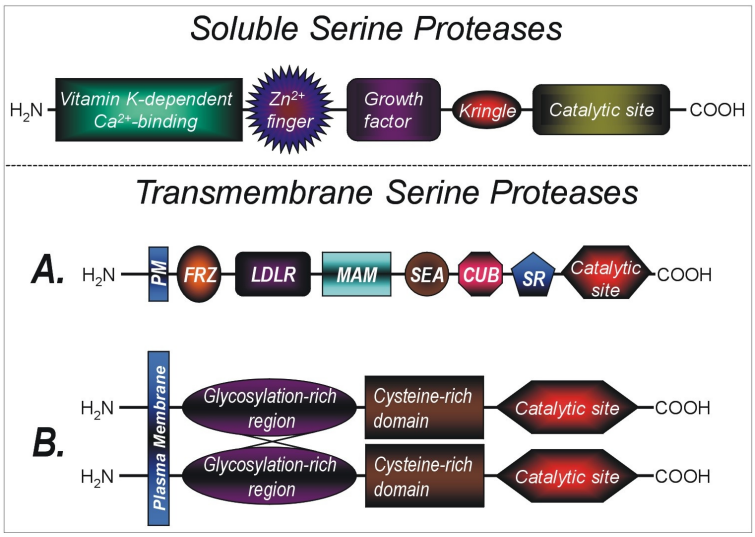

Figure 3: Structural organization of Serine proteases. The soluble forms of serine peptidases are organized with a catalytic site common to all members, some has one kringle and one growth factor domains, a Zn^{2+} finger domain, as too some vitamin K-dependent Ca^{2+} binding domains. A different organization was observed in transmembrane serine proteases. A- In all members of the family the catalytic site and the transmembrane domain are present than several different domain in number and compositions are present. The frizzled-like cysteine-rich repeats (FRZ); the LDL receptor repeats (LDLR), the meprins-like domain (MAM), the SEA repeats found in sea urchin – enteropeptidase – and agrin (SEA), the CUB repeats found in complement – urchin embryonic growth factor – and bone morphogenic protein (CUB), the scavenger receptor cysteine-rich repeat (SR). B- shows the organization of TTSPs that are functionally organized in dimmers.

nation will never be enough to meet the increasing demand. In addition, organ transplantations are basically affected by an high rate of complications, sometimes severe. The past decade's rapid advancement in cell production, stem cell biology, and tissue engineering generated an explosive outburst of reports that gave rise to cell therapy. Examples of active cell therapy include Langerhan islets, hepatocyte, condrocyte transplantation, but many other new approaches were proposed.

Hepatic progenitors were isolated from healthy liver [27].

Moreover, recent studies elucidated the ability of cardiomyocytes to regenerate in the event of myocardial injury [28]. In various tissues of the adult body, multipotent stem cells exist, they can give rise to new stem cells (self-renewal) and differentiated cells necessary for maintenance or for the restoration of damaged tissue.

Despite of these premises, one of the factors inhibiting the widespread clinical application of these new approaches is the lack of standardization of procedures for

cell production, in particular for those regarding tissue digestion and cell harvesting.
Consequently, a standardization requested for optimizing results, making them reproducible and for being fully compliant to the upcoming EU regulations on cell handling for clinical purpose.
One of the first successful example of cell therapy is represented by islet transplantation since the early '90. Clinical islet transplantation is a relatively straightforward and safe procedure. However, the procedure of human islet isolation is complex and requires a great deal of experience to yield sufficient number of productive cells to be used in transplantation approaches.
Current isolation methods involve the delivery of collagenase enzymes blend into the pancreatic duct, in order to deliver enzymes to the islet-exocrine interface followed by purification of them from exocrine tissue based on their different density. However, it is still difficult to recover the entire quantity of islets contained in a pancreas. A major obstacle in successful human islet isolation is the variability of the collagenases used in the digestion phase.
Ricordi and colleagues introduced a tissue dissociation chamber and recirculation of enzyme solution; they termed it the "automated method" [29]. They placed the collagenase-distended pancreas inside a stainless steel chamber and mechanically dissociated the pancreas by gentle agitation. The principle behind this combined enzymatic and mechanical approach is to enable minimal physical trauma to the islets by collecting the islets as they are liberated from the digestion chamber. Today, the modified "Ricordi chamber" is the universal device used in human islets isolation process.
A practical advantage was the culture of *C. histolyticum* to produce a large amounts of enzymes. Enzymes derived from *C. histolyticum* are called "crude collagenase", and its biologic and enzymatic properties were extensively studied.
In addition to the collagenases, the crude preparations also contain several other proteolytic enzymes. Due to the heterogeneity composition in lytic enzymes, the activity of crude preparations is extremely variable among different "crude collagenase" batches.
This variability was recognized as the major obstacle to successful human islet purification. The introduction of a novel collagenase blend, Liberase HI (Roche Applied Science, Indianapolis, IN), was intended to reduce the lot-to-lot variability of enzyme effectiveness. However, this enzyme blend still exhibits significant lot-to-lot and even intra lot variability. Moreover, recent studies showed that Liberase is not more efficient than "crude collagenase".
To optimize proteolyses digestion, it is important to understand the structure of the islet-exocrine interface and the nature of substrate at this interface. Collagens are the major fibrous proteins constituting islet- exocrine interface. Interactions of cells with their environment play a critical role in maintaining tissue integrity in adult life. The use of collagenases for cell tissue extraction need to be evaluated case to case, in order to optimize the method to isolate progenitive cells from different tissues. The optimization of the extractive method is crucial for cell viability and for cell therapy application.
The most important enzymes used in this application were collagenases obtained from the *Clostridium histolyticum* human pathogenic microorganism. These en-

zymes have a very strong enzymatic activity, but always present some toxic effects reducing the efficiency in cell purification.
To optimizate tissue digestion we produce recombinant col G e Col H with show a better performance compared with the commercial (Italian Patent N° RM2009A000661 15-12-2009).
Moreover we partially characterized marine enzymes extracted form hepatopancreas of *Octopus vulgaris*, *Palinurus Elephas* and *Eriphia Verrucosa*, *Maja Squinado*. Special attention was paid for analyzing the capability of extracted enzymes to digest native collagen (paper in preparation).
We compared the protein/proteolytic patterns of some commercial enzyme used in islets pancreas isolation, to the collagenolitic enzymes in different marine organisms. These comparisons were performed by SDS-PAGE and Zimography analyses. To better characterize the biophysical/functional qualities of analyzed enzymes we valued their stability/activity, using different incubation temperatures for different times.
Temperature is a very important factor for the success of cell extractive process; in fact, host endogenous proteases present in the pancreas, or in other extractive organs, can be activated during the process and contribute non-specifically in ECM disgregation/cells extraction; this effect could be toxic.
To optimize the enzyme blend and the temperature of tissue dissociation, we used a new *in vitro* method of analyses; we generated type-I collagen matrix substrates, inside which we cultured human endothelial immortalized cells. Endothelial cells were grown inside the type-I collagen three-dimensional matrix in 96-well plates to form vessel-like structure, mimic the *in vivo* tissue. After two days of culture, the time needed to reach vessel-like structures, each well was treated with diverse blend enzymes at different concentrations and diverse incubation temperatures. Endothelial cells were dissociated from vessel-like structures by enzymes' action; using a confocal microscopy approach we valued the morphology/vitality of matrix network released cells. These data allowed us to evaluate how much and how long to use different enzyme blend in cell tissue extraction. Moreover, this approach showed the presence of toxic components in the enzyme blends actually used in prancreas islets extraction (Salamone M. et al. submitted to Transplantation Proceeding); moreover, preliminary data on the marine enzymes extracted from epatopancreas of different crustacean showed very high efficiency in cell extractive process.

7 Conclusions

Future advances in enzyme technology, together with a better understanding of the characteristics of the extracellular matrix of the human pancreas, will make it possible to optimally liberate islets using "tailor-made" enzyme blends for each individual donor pancreas. Understanding the complex enzyme milieu of the dissociation process has the potential either of creating direct benefit to the islet transplant community, or to offer substantial benefits to the scientific community's understandings of tissue dissociation as a whole. Using new collagenase from marine organisms will be an evident opportunity to optimize the procedure of tissue dissociation applications. Cell therapy was successfully used to rebuild damaged cartilage in joints, repair spinal cord injuries, strengthen a weakened

immune system, treat autoimmune diseases such as AIDS, and help patients with neurological disorders such as Alzheimer's disease, Parkinson's disease, and epilepsy. Further uses showed positive results in the treatment of a wide range of chronic conditions such as arteriosclerosis and congenital defects. The optimization of islet purification from rat and porcine pancreas, such as other cell types from other tissue/organs, using new enzyme at different ratio will be applied to other organs in order to isolate progenies cells for cell therapy application. Moreover, this technique could be suitable in the emerging technology of scaffold engineering medicine.

References

[1] C. Gerday, M. Aittaleb, M. Bentahir, J.P. Chessa, P. Claverie, T. Collins, S. D'Amico, J. Dumont, G. Garsoux, D. Georlette, A. Hoyoux, T. Lonhienne, M.A. Meuwis, and G. Feller. Cold-adapted enzymes: from fundamentals to biotechnology. *Trends Biotechnol*, 18:103–107, 2000.

[2] H.G. Kristinsson and B.A Rasco. Biochemical and functional properties of Atlantic salmon (*Salmo salar*) muscle proteins hydrolyzed with various alkaline proteases. *J. Agric. Food Chem*, 48:657–666, 2000a.

[3] H.G. Kristinsson and B.A. Rasco. Fish protein hydrolysates: production, biochemical, and functional properties. *Crit Rev. Food Sci. Nutr*, 40:43–81, 2000b.

[4] Kishimura, H, Hayashi, K., Miyashita, Y., Nonami, and Y. Characteristic of trypsins from the viscera of true sardine(*Sardinopsm melanosticus*) and the pyloric ceca of arabesque greenling (*Pleuroprammus azonus*). *Food Chemistry*, 97:65–70, 2006.

[5] S. Klomklao, S. Benjakul, W. Visessanguan, H. Kishimura, B.K. Simpson, and H. Saeki. Trypsins from yellowfin tuna (*Thunnus albacores*) spleen: purification and characterization. *Comp Biochem. Physiol B Biochem. Mol. Biol.*, 144:47–56, 2006b.

[6] S. Klomklao, S. Benjakul, W. Visessanguan, H. Kishimura, and B.K. Simpson. Purification and characterization of trypsin from the spleen of tongol tuna (*Thunnus tonggol*). *J. Agric. Food Chem*, 54:5617–5622, 2006a.

[7] F.J. Castillo-Yanez, R. Pacheco-Aguilar, F.L. Garcia-Carreno, and M.L Navarrete-Del Toro. Isolation and characterization of trypsin from pyloric caeca of Monterey sardine *Sardinops sagax caerulea*. *Comp Biochem. Physiol B Biochem. Mol. Biol.*, 140:91–98, 2005.

[8] G.N. Rudenskaya, Y.A. Kislitsin, and D.V. Rebrikov. Collagenolytic serine protease PC and trypsin PC from king crab *Paralithodes camtschaticus*: cDNA cloning and primary structure of the enzymes. *BMC. Struct. Biol*, pages 4– 2, 2004.

[9] R. Margesin and F. Schinner. Biodegradation of diesel oil by cold-adapted microorganisms in presence of sodium dodecyl sulfate. *Chemosphere*, 38:3463–3472, 1999.

[10] R. Amarowicz and F. Shahidi. Antioxidant activity of peptide fractions of capelin protein hydrolysates. *Food Chemistry*, 58:355–359, 1997.

[11] S.K. Kim, Y.T. Kim, H.G. Byun, K.S. Nam, D.S. Joo, and F. Shahidi. Isolation and characterization of antioxidative peptides from gelatin hydrolysate of Alaska pollack skin. *J. Agric. Food Chem*, 49:1984–1989, 2001.

[12] E. Mendis, N. Rajapakse, H.G. Byun, and S.K. Kim. Investigation of jumbo squid (*Dosidicus gigas*) skin gelatin peptides for their *in vitro* antioxidant effects. *Life Sci*, 77:2166–2178, 2005.

[13] G.N. Rudenskaya, A.M. Shmoilov, V.A. Isaev, A.V. Ksenofontov, and S.V. Shvets. Aminopeptidase PC from the hepatopancreas of the Kamchatka crab *Paralithodes camtshatica*. *Biochemistry (Mosc.)*, 65:164–170, 2000.

[14] W.T. Chen, T. Kelly, and G. Ghersi. DPPIV, seprase, and related serine peptidases in multiple cellular functions. *Curr. Top. Dev. Biol*, 54:207–232, 2003.

[15] K. Watanabe. Collagenolytic proteases from bacteria. *Appl. Microbiol. Biotechnol*, 63:520–526, 2004.

[16] E. Leikina, M.V. Mertts, N. Kuznetsova, and S. Leikin. Type I collagen is thermally unstable at body temperature. *Proc. Natl. Acad. Sci. U. S. A*, 99,:1314,1318, 2002.

[17] O. Matsushita, K. Yoshihara, S. Katayama, J. Minami, and Okabe andA. Purification and characterization of *Clostridium perfringens* 120-kilodalton collagenase and nucleotide sequence of the corresponding gene. *J. Bacteriol.*, 176:149–156, 1994.

[18] O. Matsushita, C.M. Jung, J. Minami, S. Katayama, N. Nishi, and A. Okabe. A study of the collagen-binding domain of a 116-kDa *Clostridium histolyticum* collagenase. *J. Biol. Chem*, 273:3643–3648, 1998.

[19] O. Matsushita, C.M. Jung, S. Katayama, J. Minami, Y. Takahashi, and Okabe andA. Gene duplication and multiplicity of collagenases in *Clostridium histolyticum*. *J. Bacteriol.*, 181:923–933, 1999.

[20] K. Yoshihara, O. Matsushita, J. Minami, and Okabe andA. Cloning and nucleotide sequence analysis of the colH gene from *Clostridium histolyticum* encoding a collagenase and a gelatinase. *J. Bacteriol.*, 176:6489–6496, 1994.

[21] T. Toyoshima, O. Matsushita, J. Minami, N. Nishi, A. Okabe, and T. Itano. Collagen-binding domain of a *Clostridium histolyticum* collagenase exhibits a broad substrate spectrum both *in vitro* and *in vivo*. *Connect. Tissue Res.*, 42:281,290, 2001.

[22] L. Ravanti and V.M. Kahari. Matrix metalloproteinases in wound repair. *Int. J. Mol. Med*, 6:391–407, 2000.

[23] G. Ghersi, Q. Zhao, M. Salamone, Y. Yeh, S. Zucker, and W.T. Chen. The Protease Complex Consisting of Dipeptidyl Peptidase IV and Seprase Plays a Role in the Migration and Invasion of Human Endothelial Cells in Collagenous Matrices. *Cancer Res*, 66:4652–4661, 2006.

[24] G. Ghersi, W. Chen, E.W. Lee, and Z. Zukowska. Critical role of dipeptidyl peptidase IV in neuropeptide Y-mediated endothelial cell migration in response to wounding. *Peptides*, 22:453–458, 2001.

[25] J.S. Russell, H. Chi, L.E. Lantry, R.E. Stephens, and P.E Ward. Substance P and neurokinin A metabolism by cultured human skeletal muscle myocytes and fibroblasts. *Peptides*, 17:1397–1403, 1996.

[26] P. Proost, M. De, I, D. Schols, S. Struyf, A.M. Lambeir, A. Wuyts, G. Opdenakker, E. De Clercq, S. Scharpe, and J. Van Damme. Amino-terminal truncation of chemokines by CD26/dipeptidyl-peptidase IV. Conversion of RANTES into a potent inhibitor of monocyte chemotaxis and HIV-1-infection. *J. Biol. Chem*, 273:7222–7227, 1998.

[27] C. Fougere-Deschatrette, T. Imaizumi-Scherrer, Strick-MarchandH., S. Morosan, P. Charneau, D. Kremsdorf, D.M. Faust, and M.C. Weiss. Plasticity of hepatic cell differentiation: bipotential adult mouse liver clonal cell lines competent to differentiate *in vitro* and *in vivo*. *Stem Cells*, 24:2098,2109, 2006.

[28] A.P. Beltrami, K. Urbanek, J. Kajstura, S.M. Yan, N. Finato, R. Bussani, B. Nadal-Ginard, F. Silvestri, A. Leri, C.A. Beltrami, and P. Anversa. Evidence that human cardiac myocytes divide after myocardial infarction. *N. Engl. J. Med.*, 344:1750–1757, 2001.

[29] C. Ricordi, P.E. Lacy, E.H. Finke, B.J. Olack, and D.W. Scharp. Automated method for isolation of human pancreatic islets. *Diabetes*, 37(4):413–420, 1988.

Antifouling Coatings in Submarine Structures

V. Romairone, I. Trentin, G. Luciano
Institute of Marine Sciences, CNR, Genova, Italy
vittorio.romairone@ismar.cnr.it

Abstract

It's well known that metals are used in underwater structures (i.e. the hulls of ships or different types of boats, offshore marine platforms, the probes of tools for the detection of oceanographic data) are subject to quick deterioration due both to chemical reaction of the inorganic salts contained in sea water and to biochemical action caused by settlement of marine organisms (vegetal organism and animals).
The present paper describes the most common protection systems, developed for centuries, through the use of based copper anti-fouling paint.
This element, thanks to its toxicity, inhibits the settlement of larvae of more macroscopic organisms considered the most responsible for the functional deterioration of the structure used in the marine field.

1 Introduction

Sea water is a universe for the multitude of organisms, plants and animals that live in it and are part of the "pelagic domain" or plankton. When wood, metal or otherwise, are immersed in water and come into contact with such biological entities there is a fast deterioration. A clear example may be the hulls of boats, offshore piers, marine platforms, oceanographic probe data etc.
Many of these organisms settle and start impairing the functionality and integrity of the structures affected by their chemical-biological action.
This phenomenon is related to the life cycle and biological processes that involve the passage from larval stage to adult benthic.
The "benthic domain" is the aspect of marine biology which includes all organisms that proliferate and bind to natural and artificial hard surfaces.
Fouling involves the establishment of these organisms to artificial substrates in marine structures and in a wide range of degrees depending on the severity of several parameters of the environment under examination.
One of the most important aspects is related to seasonal changes.
Seasonal changes involve an alteration of schedule on the periods of alternating light-dark cycles, gradients of temperature, salinity and human activity impact.
It's also important to study the effect connected to climatic differences of the various areas of the world which are related to the type of organisms.
Eutrophic state of waters and the bathymetric gradient, through which one has the absorption of light rays, are more related to the quantity of the organism we can find in these environments.
The formation of fouling on structures as a whole occurs almost exclusively when they are in terms of static or slight motion of no more than 2 knots [1].

Figure 1: On the left: pelagic larvae of benthic crustaceans (*Barnacles*). On the right: establishment and growth of fouling on unprotected samples (*Barnacles, Polychaetes, Mussels, Oysters*).

Figure 2: Fouling problems highlighted in Shipbuilding.

The problems caused by fouling are varied, with significant repercussions on security and cost management systems.

A crusted hull means weight gain and changing in the frictional sliding in water, with negative influences on navigation speed and fuel consumption.
For an offshore platform, the fouling on the established pillars of support, can pose a serious threat to its stability; increases in weight and volume of the structure, affecting resistance to waves and extreme situations and can lead to its collapse of the entire structure.
Fouling inevitably causes damage to tools that rely on sensors causing alteration to data gathering. The optical parts of the sensors can, for example, be taken out of service for a quick opacification, while the formation of a thick limestone barrier fouling alters the conductivity of electrodes, or blocks the movement of moving parts.
The most common way to protect from such organisms is the use of chemicals (biocides) that inhibit larval settlement of fouling level. The scheduled mechanical cleaning of areas affected by biofouling is also a good practice to protects submersed manufacts.
Antifouling paints are an effective means, especially in the shipbuilding sector, to fight this problem. They contain fouling biocides, including copper and its derivatives (one of the former most used and popular biocides).

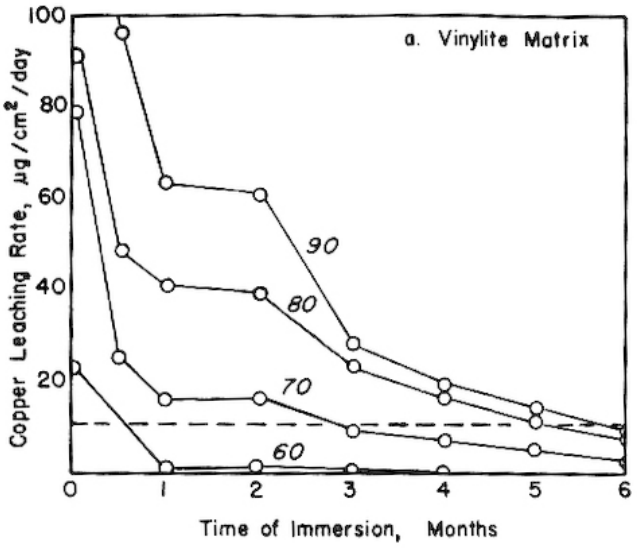

Figure 3: Leaching rates of paints containing various amounts of cuprous oxide plotted against the time of immersion in the sea. The graph refers to the cuprous oxide content as percentage dry weight of the paint film.

2 History and Methods

The formulation of antifouling paint is made by mixing a polymer matrix, solvated pigment, biocides and other minor ingredients. Biocides, after drying of the protective film, dried, are able to free themselves and gradually dissolve in the sea.
The dissolving allows the formation of a toxic barrier on the surface of the liquid-solid contact that prevents organic settlements.
How the biocides diffuse, depending on the physical and biological factors of water, hydrodynamism, temperature, pH and the composition of the biofilm (bacteria and microalgae) is an intense field of study.
The more traditional economic antifouling paints were usually prepared by dispersion of the toxic substances (mainly cuprous oxide) in a mixture of vinyl resins (insoluble) and rosin (resin plant soluble).
Cuprous oxides, in contact with sea water, are quickly converted in the bivalent form, the chlorinated and soluble one, and more toxic for marine organisms [2]:

$$\frac{1}{2}\mathrm{Cu_2O} + \mathrm{H} + 2\mathrm{Cl^-} = \mathrm{CuCl_2^-} + \frac{1}{2}\mathrm{H_2O}$$

Such paints do not show long lasting performances since the biocide exhausts rapidly due to the irregular fast film consumption.
The graph of Figure 3 reported from the book: “Marine fouling and is prevention” [3] summarized the performance of these products: in the starting and ageing test

months, a high speed rate of copper release is observed and 6 months later the products lost their antifouling efficacy; the obvious consequence was the strong impact on the environment and the short durability of the paint.
The following generation of paints was developed about 40 years ago using new resins which were reinforced by more hydrophobic polymers in order to decrease the water permeability and obtain then a thinner layer, less roughness of the external surface and a higher biocide dispersion control in the water.
In addition to traditional copper derivative biocideans, tin can be used as a biocide. It can be employed in a similar way to copper.
Tin paints releases their charge via a hydrolysis reaction with sea water (slightly alkaline). The efficacy of such products was also made to last for several years. Resins, can drive the gradual release of biocides by hydrolytic reaction.
They generally consist of acrylic polymers and are endowed with an ester bond with an organo-metallic group.
These products are particularly effective due to their relatively low cost, reduce the costs of plant maintenance and in particular those of ships berthed in dry dock.
Every new product design must also be evaluated depending on any negative consequences that may result from its use, assessing the possible risks to the environment. Organic-compounds, introduced in paints around ‘70s, used till ‘90s and now banned, caused severe damage to the ecosystem due to the lack of environmental impact in their design.
Finally, in the latest generations of antifouling paints, the dissolution speed control of copper ions takes place in synergy with the hydrolysis of the resin, generally consisting of acrylic polymers endowed with an ester bond with organo copper group.
Afterwards, the formulations based on organo-silyl-acrylate polymers showing a higher hydrophobia and a more gradual hydrolysis process were further developed.
These products should be more durable since this is proportional to the applied film thickness consumption speed rate.
Nevertheless, there are still some doubts about their efficacy in those areas which are sensitive to a dramatic fouling attack. In fact, their matrix organic radicals do not show toxicity which is comparable to the organo-tin ones of the old self-polishing paints. These antifouling paints are known as self-polishing tin-free.
Currently, to increase the effectiveness of these latest generation paints, other biocidal products have been developed which are generally organic in nature; they are called stiffeners. Before being put on the market, these products follow a strict toxicological protocol, the ultimate goal is to certify the suitability of the biocide to be effective only on the target organisms. The environmental impact is therefore limited due to the different characteristics required such as to be readily degradable.

3 Experiments

Copper and its derivatives therefore continue to be the major active ingredients used in many anti-fouling paints. However, increased sensitivity to the environment requires a particular attention to this. Copper is present in microscopic amounts in living organisms and plays functional roles in specific biological processes, but in higher concentrations, it becomes toxic and its accumulation in marine sediments,

Matrix type	**Initial 15 days immersion**		**7 months later**	
	Cu^{++} $\mu g \cdot cm^{-2} \cdot d^{-1}$	thickness loss μm	Cu^{++} $\mu g \cdot cm^{-2} \cdot d^{-1}$	thickness loss μm
1) Ablative	65.7	10.4	44.6	19.7
2) Ablative	52.2	10.3	28.1	18.5
3) Hydrolized	53.9	0.8	22.5	6.0
4) Insoluble	139.8	0.0	64.8	0.0

Table 1: Ageing test of the paints on some samples immersed in the sea, the parameters taken into account are: the biocide released and the loss of the film thickness.

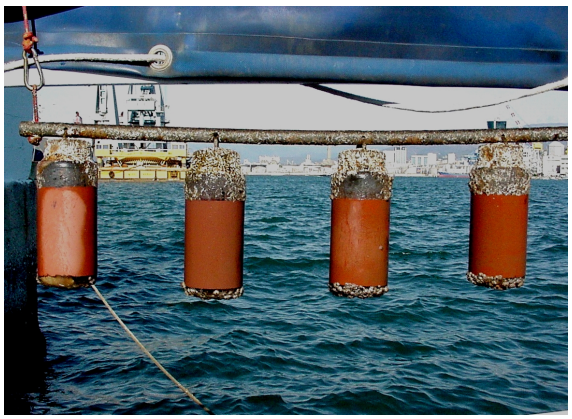

Figure 4: Testing of antifouling paints, coated specimens are immersed in the sea for the natural ageing of the products under examination.

along with other heavy metals could cause serious environmental problems [4, 5]. Its use in antifouling paints must therefore be restricted and controlled through careful monitoring.

The evaluation of the copper ions, released in the water as a function of time, is therefore, an extremely important parameter for experiments of antifouling products.

Quantitative evaluation is important both at the very beginning of the immersion of the specimens and during the various durability, but also to evaluate in quantitative terms, the potential impact which such a biocide may have on the marine environment.

Currently, after the well known IMO directive on the ban of organo-tin biocides, it is possible to increase the use of copper based paints with a high occurrence rate of this element in the marine ecosystem.

As was said above, even though the latest generations of paints should no longer release the same content rate of this element as those which were used a long time ago, the copper quantity introduced in the sea, also from other polluting sources in the urban and industrial discharges, are remarkable. Particularly as for the sea coast and harbour areas, the antifouling paints are an

important impact source. From surveys carried out at the CNR-ISMAR laboratory in Genoa, it was observed how some daily used soluble matrix paints (ablative) release in the sea every day in the first seven service months, amounts of copper ranging from 65.7 to 22.5 μg per surface square centimetre; the paints had been applied on ageing tested specimens by a static immersion in the sea. The quantities of such an element, as shown in Table 1 are rather high in comparison with the threshold values accounting for $10\mu\mathrm{g}\cdot\mathrm{cm}^{-2}\cdot\mathrm{day}^{-1}$ where, via experiments, in the past, the threshold of the settlement possibility of the fouling had been remarked.

With longer paint ageing times, generally, such values further decrease, maintaining more constant till the total exhaustion of the applied film (this happens in the case of paints soluble, self-eroding and self-polishing based matrices. In the case of the insoluble matrices till the total exhaustion, due to the escaping of the biocides inside the film through the pores of the polymer structures).

The threshold values which have been observed more recently, result in an increased accounting for about 20 $\mu\mathrm{g}\cdot\mathrm{cm}^{-2}\cdot\mathrm{day}^{-1}$. Such an increase could let one think of a higher and higher resistance or selection of copper-resistant organisms due to the higher occurrence of this element in the environment.

If this were true, the future of these products could deem a reduction of the efficacy and/or a stronger biocide impact on the environment.

In fact, it often happens that the products designed and applied to the hulls with such a thickness last more than three years, and six months later, they lose their efficacy, they have not exhausted all the copper rate in the formulation, neither has the film thickness disappeared. In this case, the causes can depend either on some formulation mistakes or on the adhesion of very resistant micro-organisms, which hamper the water chemical and physical processes in the solid-liquid interface; in both cases, the toxic barrier, needed to avoid the biologic encrustation is lacking.

When such cases happen, lengthening the dry-docking operations is always difficult, so, if the substrate is still solid enough, the new antifouling paint is usually laid over the old one, but in the end, layer by layer, the thicknesses will be more and more noticeable, with a greater external layer roughness and loss of solidity due to water hydration; sooner or later, at best, they will have to be removed at high costs due to their disposal as toxic wastes.

The evaluation of the release speed rate of one antifouling active principle is carried out during specific ageing steps of the paint applied on the specific panels. To evaluate the copper content rate released by the paint, the specimens are taken and temporary immersed in given volumes of synthetic or natural sea water; then the test goes on according to the given methods [6].

The specimens can be subjected to the natural weather test by static exposure in the sea (long times, Figure 4) or to the accelerated test (short times) in lab basins or directly in the sea using test equipment able to provide a strong hydrodynamism on the specimens themselves (rotor tests).

Defence against fouling, on the pylons of an offshore platform is generally done with regular mechanical cleaning, in order to optimize the work and lengthen the time between cleanings [7].

There are other systems such as the use of various biocides, chlorine developed electrolytically from sea water, underwater application of special anti-fouling paints or

Figure 5: Offshore platform for the extraction of methane.

other, but while enjoying an undoubted scientific interest, they are almost never implemented due to various problems such as high costs and environmental impact.
The probes or measuring instruments which operate immersed in the sea require cleaning from fouling. Organic antifouling coatings can be used but for others, even if this type of transparent barrier may interfere with the measurement.
Therefore, the most popular system is the periodic mechanical cleaning, the frequency obviously depends on the density and distribution of spores or larvae of organisms. In oligotrophic and deep sea diving the short time scale of the phenomenon may be less obvious.
Where possible the use of copper and its alloys, such as: copper-nickel, copper- tin and copper-zinc less prone to fouling is suggested [8]. The settlements are not completely inhibited but merely slowed down, also no form of galvanic protection must be activated on the system and items must be in a position to release toxic ions in water.

4 Conclusions

As was said at the beginning of this paper, antifouling paints are copper based ones; but at present, although several pollution phenomena have been highlighted, and although it is thought that among the various sources, antifouling paint is rather meaningful, a total ban forbidding the use of this biocide in antifouling paints is not feasible [9]. It might be possible, on the contrary, to aim at controlling and limiting its release rate in the environment. In fact, some countries, such as Canada, have already established the threshold accounting for 40 $\mu\mathrm{g}{\cdot}\mathrm{cm}^{-2} \cdot \mathrm{day}^{-1}$, while Sweden, as for antifouling paints for the pleasure boat sector, issued a total ban in the local seas and the threshold of 200 and 350 $\mu\mathrm{g}{\cdot}\mathrm{cm}^{2}$ respectively for the external seas during the initial 14 to 30 immersion days.
Many of the paints which were examined at ISMAR-CNR, show a good antifouling performance, but some show a copper impact which gives rise to some doubts (e.g. sample no. 4, Table 1). The specimens treated with this product prove to be the best ones but one could ask whether

it is worthwhile to face all the possible environmental problems in view of what is reported in the international literature [10, 11].
A general rule should consist of keeping the release speed rate slightly higher than the threshold values, and, of course, these can vary according to the geographic characteristics of the various regions, to the climatic conditions, to the quality and quantity of the fouling, to their food availability and to the polluting sources themselves which can select the most resistant micro organisms and fouling species.
Finally, antifouling paint performance should be evaluated keeping clearly in mind three well known properties, these being performance, durability and environmental impact, but to this latter factor it is necessary to devote the greatest attention and bear the increase in the related costs.
The feasible alternatives based on "green" systems, which avoid the release of toxic substances are tested with good results.
The most promising is the use of protective polymers with low surface free energy such as silicone resins where the antifouling effect is exercised through physical action to prevent a strong adhesion encrusting organism. The cleaning effect is further enhanced by friction with the water when the structure so protected begins to move [12]. The development of these antifouling products, however, requires further investigations.

References

[1] A. Mollica and A. Trevis. La prevenzione del fouling marino alla superficie delle condotte per adozione di opportune velocità di corrente. *L'energia elettrica*, 10:654, 1972.

[2] C.O'D. Iselin. The Physical Chemistry of Compounds of Copper and Mercury and Their Interactions with sea Water. Marine Fouling and its Prevenction. Woods Hole Oceanographic Institute, Massachusetts. United States Naval Institute Annapolis, Maryland. 15:270, 1952.

[3] C.O'D. Iselin. Mechanism of Release of Toxics from Paints. Marine Fouling and its Prevenction. Woods Hole Oceanographic Institute, Massachusetts. United States Naval Institute Annapolis, Maryland. 16:278, 1952.

[4] A. Katranitsas, J. Castritsi-Catharios, and G. Persoone. The effects of a copper-based antifouling paint on mortality and enzymatic activity of a non-target marine organism. *Marine Pollution Bulletin*, 46:1491–1494, 2003.

[5] J. Warnken, J.K. Dunn Ryan, and P.R. Teasdale. Investigation of recreational boats as a source of copper at anchorage sites using time-integrated diffusive gradients in thin film and sediment measurements. *Marine Pollution Bulletin*, 49:833–843, 2004.

[6] ASTM. Standard Test Method for determination of Copper Release Rate from Antifoulig Coating Systems in Artificial Seawater. Designation: D 6442-03. 2003.

[7] G. Relini, S. Geraci, M. Montanari, and V. Romairone. Variazioni stagionali del fouling sulle piattaforme off-shore di Ravenna e Crotone. *Bollettino di Pesca, Piscicoltura e Idrobiologia*, 31(1/2):227–256, 1976.

[8] C.O'D. Iselin. Marine Fouling and its Prevenction. Woods Hole Oceanographic Institute, Massachusetts. United States Naval Institute Annapolis, Maryland. 21:350, 1952.

[9] A. Helland and T. Bakke. Transport and sedimentation of Cu in a microtidal estuary, SE Norway. *Pollution Bulletin*, 38(6):448–462, 2002.

[10] B. Jones and T. Bolam. Copper speciation survey from UK marinas, harbours and estuaries. *Marine Pollution Bulletin*, 54:1127–1138, 2007.

[11] R.F. Brady Jr. and I.L. Singer. Mechanical factors favoring release from fouling release coatings. *Biofouling*, 15(1-3):73, 2000.

[12] L.D. Chambers, K.R. Stokes, L.C. Walsh, and R.J.K. Wood. Modern approaches to marine antifouling coatings. *Surface & Coatings Technology*, 201:3642–3652, 2006.

Corrosion Behaviour of Al Based Materials for the Naval Industry

P. Traverso, G. Luciano, P. Letardi
Institute of Marine Sciences, CNR, Genova, Italy
pierluigi.traverso@ismar.cnr.it

Abstract

This paper shows the results of the investigation on the corrosion behaviour of innovative Al- based composite materials. These classes of materials are generally used for engineering applications because of their technological properties as well as reasonable cost. Free corrosion and electrochemical tests were carried out in quiescent natural sea water for different exposure times, with the aim of evaluating corrosion attack amount and morphology, general corrosion resistance, as well as susceptibility to pitting corrosion. The corrosion layer was also characterised by different surface analysis techniques.

1 Introduction

Aluminium based materials are often used for engineering applications because of their density, hardness, corrosion resistance properties as well as thermal and power conductivity, light and heat reflectance, non toxicity and non magnetism as well as their reasonable costs.
Their use in the shipbuilding industry, which in the beginning was limited to equipment components, is now spreading to the field of structural parts and boat hulls which are expected to be very light for performance reasons (competition motorboats and hydrofoils) as well as for their special use (lifeboats). Often the hulls and very seldom the critical areas are not coated, for example, in the vicinity of the propeller, they are provided with cathodic protection by zinc sacrificial anodes. Pure aluminium shows low elongation and hardness resistance, so, even though the sea corrosion resistance is high, except for special applications, in practice it is found under the form of an alloy together with other elements which, nevertheless can influence the corrosion behaviour.
The resistance of the aluminium alloys to this failure is due essentially to a chemically inert layer formation on the exposed surface. In sea-water, because of the aggressiveness of the chlorine ions this protective film tends to break more easily in the preferential attack sites such as defects or heterogeneity spots giving rise to localized damage.
The objective of this work was:

a) To carry out a study of the corrosion behaviour of some technologically advanced aluminium based materials so as to highlight which of them shows the highest resistance to failure occurrence due to the sea environment;
b) Once a class of material has been selected, being by principle alternative to traditional ones, to point out the relevant parameters (composition, produc-

tion process, etc.) which are able to play a pivot role in corrosion resistance.

Especially, with regard to technologically advanced materials, we tested the Al-Li 8090 alloy (Al-2.5 Li-1.5 Cu) and Al 6061 T6/Al_2O_3p and Al 359/SiCp composite materials (Table 1).

Al-Li 8090 T81 is widely used in the aeronautical and aerospace fields [1, 2] as it shows very high physical-mechanical properties. The addition of lithium to aluminium, due to their highly different atomic mass (6.49 over 26.98) causes a 3% density reduction (up to max 4%) and a 6% elasticity increase [3, 4], by each percentage point added by weight, but generally it results unfavourable electrochemically because of its highly electronegative property. This alloy also contains a copper content rate accounting for about 1.5% which greatly improves the mechanical characteristics but makes it more sensitive to corrosion, especially the inter-granular type [5]. We should always bear in mind that the corrosion phenomena, with the same composition, depend on the microstructural situation of the alloy which is strictly related to the thermal treatments undergone.

The metal based composite materials consist of heterogeneous systems where a non-metal phase is dispersed in an alloy, in this specific case an aluminium based one. Such composites having a lower density than the metallic alloy matrix, generally show comparable mechanical properties [6, 7], which make them economically competitive for special uses (for example in the aeronautical and automotive fields). In these applications indeed, a decrease in density, obviously leading to lower fuel consumption, plays a special role. However, the heterogeneity of the material could compromise the service life, as it may spur its failure taking place after the corrosion [8, 9] or a mechanical stress. The corrosion resistance of composites is strictly linked to the non-metal phase type, dispersed in the matrix and to its capability by diffusion of forming intermetal compounds at the matrix-particle interface which prevent its peeling. For example, the alumina particles in those composites having a metal matrix based on aluminium alloys do not affect the localized corrosion sensitivity of the binder because the corrosion products formed on the surface are aluminium oxides. Since the latter have the same electrochemical potential as the alumina particles, they cannot give rise to microgalvanic elements between the matrix and the reinforcing material. On the contrary, the SiC particles provided with a nobler equilibrium potential than the aluminium matrix [10], make a galvanic micro circuit with the matrix itself, bringing about its dissolution. Having obtained encouraging results with the Al 6061 T6/Al_2O_3p type composite materials we changed some characteristic parameters within this class (reinforcement rate, production process) and tested the influence of this parameter on the corrosion behaviour [11].

2 Materials and experimental methods

The samples used consisted of 15 mm diameter and 1.5 mm thick discs, polished up to 800-grade emery paper and degreased with acetone before dipping them into the corrosive solution.

Some specimens used for the microstructural analysis were polished up to diamond-paste (1 micron) and subjected to metallographic attack to highlight their mi-

Specimen	Al	Si	Fe	Cu	Mg	Cr	Zn	Ti	Li	Mn	Other	% reinforcing v/v (particles)
Al-Li 8090 T81 (#)	rem	0.10	0.15	1.50	1.50	0.05	0.12	0.05	2.50	0.05	0.18	_
Al 6061 T6 /Al_2O_3	rem	0.90	1.10	0.25	1.00	0.20	----	---	---	---	---	10%Al_2O_3(*)
Al 359 /SiC	rem	9.50	0.20	0.20	0.65	----	----	---	---	---	---	20% SiC

Table 1: Nominal composition of the alloys and composite materials tested.
(#) = This alloy was tested and also subjected to thermal treatment T3.
(*) = This composite material was tested by two reinforcement content rates (10 and 20% v/v), obtained from different production processes (cast and extrusion).

crostructure (grain size and different phases of the metal binder).
In all the tests carried out (both for such test samples and the surface treated ones) we used a natural sea corrosive water solution (pH = 8.2, Mohr chlorine content rate 21.4 %, dissolved oxygen = 7.5 ppm) at T = 25°C, P= 1 atm and static flow-dynamic conditions.
The experimental trials were electrochemical tests and free corrosion ones with various corrosion times.
The electrochemical tests consisted of potentiodynamic DC polarizations (anodic and cathodic) through which the corrosion average speed rate and the localized corrosion sensitivity were evaluated.
The free corrosion tests were performed for time ranges from 120 to 1440 hours. Through this type of test, the weight loss was measured by summing the content rate of the aluminium in the solution (under the form of soluble corrosion products) with the amount of Al corrosion products adhering to the metal substrate and dissolved using a proper method which allows one to keep the metal matrix steady [12]. The quantity determination of the aluminium was carried out via spectrophotometry by atomic absorption and using a Perkin Elmer spectrophotometer (AAnalyst 100 model).
The corrosion products were characterised via X-ray photoelectron spectrometry and Auger spectrophotometry using a VG spectrophotomer (Escalab 210 model). The XPS analyses were carried out using Mg Ka radiation (E=1253.6 eV) as excitation source and the spectra were obtained at a vacuum better then 10^{-7} mbar and detection angle perpendicular to the surface. The C1s peak (Binding energy, B.E. = 284.8 eV) accounted for the internal standard which persisted as it was due to the surface contamination, which was used to evaluate and compensate the charging effects of the specimens.
Some Auger mapping was also carried out on corroded test samples to model the surface corresponding to the areas where peeling or localized corrosion had occurred.
Via free corrosion tests we obtained information concerning the corrosion morphology and intensity using a Leica metallographic microscope (DM/RME model) combined with an image analysis system; the occurrence of segregations, disbondments of the metal matrix following the localized corrosion or peeling of reinforcing particles in the composite materials was tested through X-ray micro diffractometry using a Rigaku DC-MAX microd-

iffractometer. Other data were obtained by means of an atomic force microscope (AFM; Burleigh Metris) working in contact mode with an Si_3N_4 tip on a 70x70 μm area.

3 Results and discussion

3.1 Corrosion behaviour of innovative materials based on Al

Al-Li 8090 T81 (and T3 thermal treatment) alloy

With reference to the study of corrosion behaviour in the sea environment of the Al-Li 8090 T81 alloy compared with conventional ones, we can state that the corrosion resistance proves that it cannot match the high physical-mechanical properties which characterise it [13]. The addition of an element with a much more negative equilibrium potential such as lithium (the main component of the alloy), but above all, the high copper content and the microstructural heterogeneity favoured localized aggression particularly the interstitial type (crevices).

Free corrosion tests showed that after about one month's exposure to sea water, the crevices can even become perforating on test samples about 1.5 mm thick (Figures 1 and 2). In this area red crystals were detected microscopically which turned out to be metal copper by microdiffractometric analysis. The complex form of the peaks highlights additional components corresponding to larger sizes of the crystallographic pure copper cell which may be related to a new plating after dismutation of the copper solution on the pre-existing one on the substrate [14]. The highly localized surface copper (inter-metal phases, inclusions) can give rise to galvanic microcells which can concentrate and increase the corrosion attack. The sensitivity of the localized attack is lower for the Al-Li8090 in the T3 thermal phase as no ageing thermal treatment favours the steady diffusion of the addition elements [15, 16].

The Al-Li 8090 T81 also highlighted the preferential dissolution of the lithium; the Li/Al ratio between lithium and the aluminium in oxidised solution is higher than the Li/Al ratio found in the alloy as such. Actually, a large part of lithium may solvate because of its very low standard electrochemical potential (-3.045 V; no noble element) depleting the metal binder and hampering the protection corrosion products based on aluminium; such an effect prevails for short exposure periods (up to about 100 hours).

The marine corrosion resistance of the traditional Al alloys (especially for the Al 5000 type) was higher, although all of them are sensitive to pitting or interstitial corrosion.

In order to reduce the grafting occurrence rate of the crevice it is possible to intervene in the piece moulding (avoiding indentation, slots or porous welding), and in the assembly operations (avoiding cracks which favour infiltrations), as well as in the shielding phenomenon (of the precipitated corrosion products or possible external agents).

The analytical determination, performed by several analytical techniques, enlightened hydroxy, hydroxy-oxide and aluminium oxide as prevailing compounds on the surface passivating layer.

Al 6061 T6/Al_2O_3p composite material

The analysis of electrochemical results shows by increasing the exposure time, the corrosion kinetics of the compound depends not only on the chloride concentra-

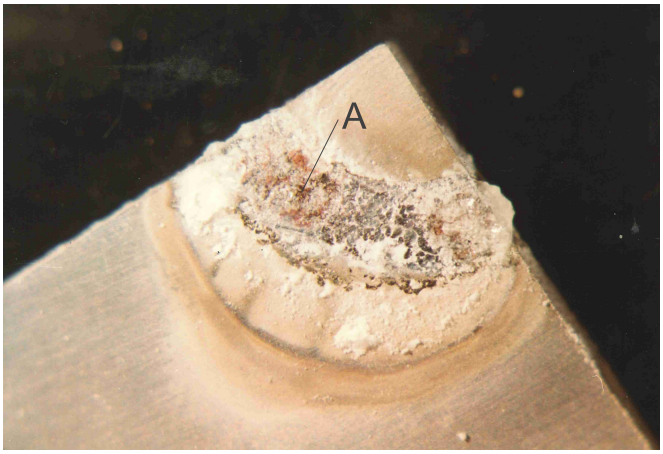

Figure 1: Macro photo of a corrosion crevice on sample of Al-Li 8090 T81 alloy after 1 month of exposure in sea water.

tion acting at the metal-solution interface, but also on other parameters such as the type of corrosion products which changes as a function of the composition of the corrosion solution.

In sea water, specimens can undergo localized corrosion. The likelihood of corrosion site formation increases with immersion time, as from the perfect passivity range value which takes more and more negative values. The longer the immersion times, the higher the passivity range of the composite material in the sea water reaching values higher than those of salty water, an environment where the passivity range keeps steady. Such a range, although not very significant, is slightly higher than the passivity range shown by the traditional Al 6061 T6 alloy free of the reinforcement material (always lower than 50 mV) [17]. This makes the use of the composite over the massive alloy competitive.

Comparing the weight loss results of the composite material in water with those which were obtained from the previous studies of the Al 6061 alloy (metal matrix of the composite) there is evidence that the weight loss of the alloy is slightly higher ($\approx$10%) than the composite's. Therefore the weight loss results confirm that Al_2O_3 reinforced composite can be considered competitive compared to the massive alloy. The optical microscopic analysis of the specimens subjected to the electrochemical tests and to free corrosion showed, for the specimen corroded in seawater, deeper and larger localized corrosion areas. To explain the origin of such sites better, analyses via Auger spectroscopy in the surrounding areas of them were performed and it was finally concluded that localized corrosion had not occurred at the metal matrix and the alumina particle interface, which did not separate from the metal matrix. On the contrary, the localized corrosion grafting sites are related to the existing microstructural heterogeneities of the metal binder, for example the Al-Cu phases (since copper is one of the minor constituents of the binder), and they are precipitated as inter-

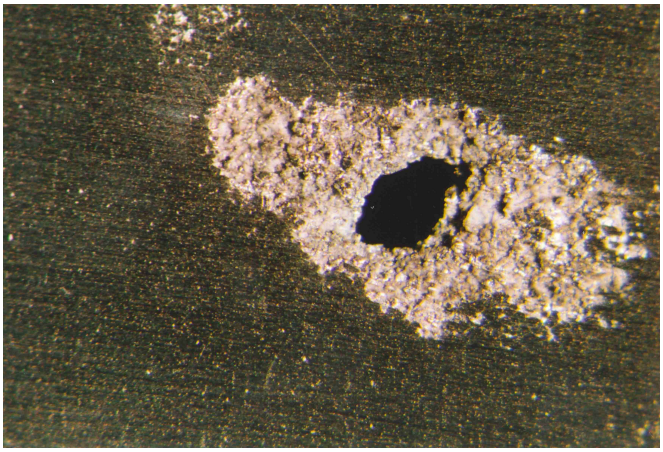

Figure 2: Detail of perforating morphology on same sample (Point A in Figure 1) after removing corrosion products.

metal compounds and they are also cathodic with respect to the Al alloy and so, they are able to bring about galvanic microcells.

Al 359/SiCp composite material

Electrochemical parameters obtained from the potentiodynamic polarization curves carried out on the specimens after different immersion periods characterize the corrosion behaviour of the composite over its general and localized corrosion resistance [18]. From the obtained data it can be concluded that:

a) Al 6061 T6/Al_2O_3 composite. The corrosion behaviour could be related to the SiC non-metal phases, as they are cathodic to the matrix;
b) the longer the exposure time, the lower the composite average corrosion rate in sea water;
c) in sea water the composite dissolution could be governed by the diffusion process of the ions through the corrosion products whose protective strength increases as much as the exposure time following the formation of hydroxides or magnesium oxycarbonates;
d) there is no passivity range for the compound studied throughout the whole exposure time. As for the Al 6061 T6/Al_2O_3p, in the case of Al359/SiCp composite the likelihood of corrosion site formation in both corrosion solutions increases with the immersion time, as from the PPd perfect passivity range value taking more and more negative values.

The weight loss tests confirm that the Al-SiC composite has an average corrosion speed rate much higher than the composite with Al_2O_3 particles. The Auger mapping carried out on non-corrosive specimens has highlighted areas rich in silica (reinforcement particles) and aluminium (metal matrix) but also a phase at the matrix/reinforcement interface, where both the aluminium and the silica are found together. The analyses executed via X-ray diffractometry gave evidence of the aluminium silicate phase occurrences (ASTM

card 6-221) at the SiC particles/matrix interface (ASTM card 22-1319). The latter consists of a phase rich in Al (ASTM card 4-787) and of another phase rich in Si (ASTM card 5-565). The aluminium silicate phase could be the matrix reinforcement binder. On the contrary, the Auger mapping, concerning the aluminium and the silicate respectively, carried out on a specimen exposed for 360 hours in sea water, points out two different areas, one rich in aluminium and the other in silica, definitely separated at the matrix-reinforcement interface. The aluminium silicate as previously observed at the interface was not detected either by the Auger analysis or by macro diffractometry.

The analysis of the corrosion products were carried out by XPS by which it was possible to obtain a quality and quantity characterization of the corrosion film components. From the qualitative analysis it resulted that the surface layer of the composite is made up of aluminium and silica compounds. The specimens exposed to sea water have a high content of magnesium coprecipitated with aluminium oxidised compounds (oxides and oxichlorides), Table 2 shows the atomic percentage values of Al, Mg and Si obtained carrying out the quantitative analysis of the surface layers of the composite before and after the corrosion attack. From the atomic ratio of the different elements the Al/Si ratio was calculated and reported in the Al/Si ratio on the surface of the specimens exposed changes with respect to the non immersed materials by changing the exposure time. Indeed, by increasing the exposure time, such a ratio increases greatly (by about 30 times) on the surfaces of the specimens dipped for 360 hours in sea water. The increased Al/Si ratio can be related to the decrease in the average silica content rate on the specimen surface. Such a decrease is due to the disappearance of the compounds with Si-O-Me bonds binding energy,(B.E. = 101.9 eV) [19, 20] and belonging to the aluminium silicate inter-metal phase at the SiC and matrix interface. Further on, the drop in the Si-C bond signal (B.E. = 98.0 eV) in the non metal phase of the silica carbon could be due to removal from the metal matrix following the dissolution of the carbon-matrix aluminium silicate phase. The appearance of the Si-O bond (B.E. = 102.9 eV) of the silica dioxide (SiO_2) on the corroded samples shows that a part of the silica belonging to the phase rich of Si (B.E. = 99.0 eV) of the matrix was oxidised following the corrosion attack in sea water. The removal of the silica carbon particles and the decrease in its surface concentration can lead to a high homogeneity of the corrosion products of the composite. Furthermore, the magnesium compounds make them more massive and protective and able to decrease the corrosion speed rate of the composite by increasing the exposure time as was observed in the weight loss tests. The decrease in the Al/Si ratio can be related to the selective dissolution of the aluminium which does not affect the SiC particles and the aluminium silicate phase at the metal matrix interphase.

Actually the XPS analysis shows that the silica is under the form of SiC carbon (B.E. = 98 eV), of a silicate (B.E. = 102.9 eV), and of metal Si (B.E. = 99.4 eV) as well as of SiO2 (B.E. = 103 eV). The latter compound could be formed through the oxidation of the metal silica following the corrosion attack.

Corrosion solution	Exposure time (hours)	% at Al	% at Mg	% at Si	Al/Si ratio
None	-----	69.00	1.36	25.64	2.69
Sea water	120	47.17	51.36	1.18	39.83
	360	48.00	49.43	0.50	95.04

Table 2: Al, Mg, Si atomic percentages and Al-Si/Si ratio on Al359/SiC detected on the composite surface before and after 120 and 360 hours of exposition in natural sea water.

3.2 Effect of the reinforcement content rate and of the production process on corrosion of the Al 6061 T6/Al_2O_3p in sea water.

With reference to the study of corrosion of the Al 6061 composite material in sea water all the experimental measurements carried out allow to know the following conclusions:

a) by increasing the particle content rate (from 10 to 20% v/v) the corrosion attack is lower (and approximately analogous to the cast and extruded material);
b) with regard only to the specimen containing 10% reinforcing agent, the extrusion process improves the material corrosion resistance;
c) the sensitivity of the composite material to the localized corrosion tends to decrease as the reinforcement increases and together with the extrusion process.

Cast specimens (in particular specimens containing 10% of reinforcement agents), observed by optical microscope, reveal a great deal of porosities, macro and microcavities and a non homogeneous distribution of the reinforcing phase (agglomerated particles were often visible).

AFM images (Figures 3 and 4) show an evident physical defect on the uncorroded specimen which can function as a nucleation site in localized corrosion phenomena.

4 Conclusion

Corrosion resistance in sea water of the Al-Li 8090 alloy showed not to be up to the high physical and mechanical properties which makes it a special material. The addition of an element provided with an equilibrium potential much more negative than the aluminium, such as lithium, (the main component of the alloy), but above all the high copper content rate as well as the microstructural heterogeneity have induced a remarkable tendency to localized attack, particularly the interstitial one. Such a situation highly improves at the T3 thermal phase as any ageing thermal treatment favours the even distribution of the addition element.
Corrosion resistance in sea water of the conventional alloys tested globally resulted better although they are all sensitive to pitting and interstitial corrosion.
They did not show dealligation occurrences; on the contrary, the Al-Li 8090

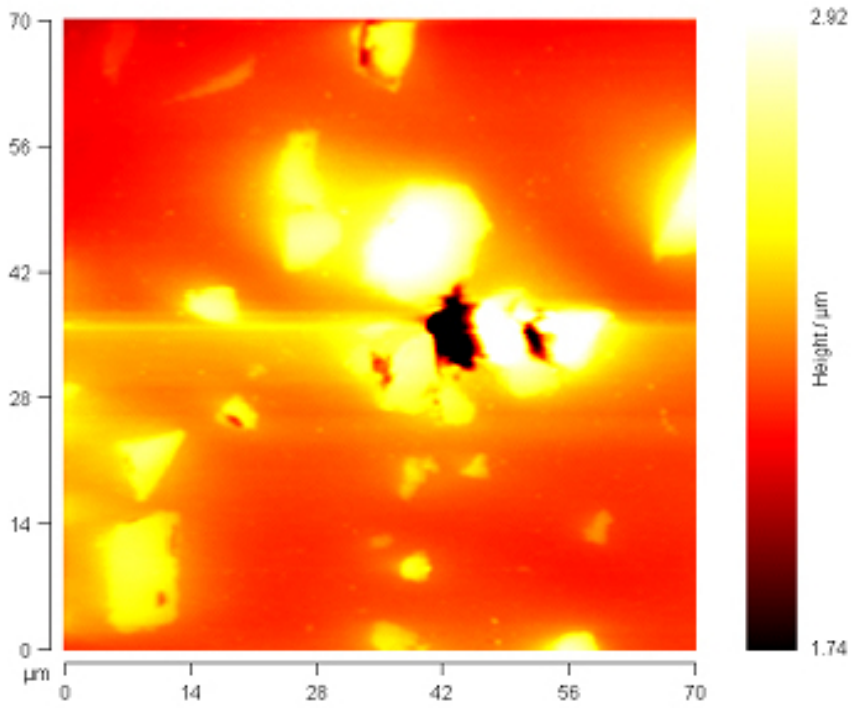

Figure 3: AFM "top view" image of uncorroded Al 6061T6/Al_2O_3p 10% cast composite sample.

T81 showed the preferential dissolution of lithium.

The aluminium matrix composite materials showed a meaningful trend to localized corrosion in seawater environments; such a phenomenon mainly comes from the dishomogeneity of the metal matrix and it is only partially affected by problems concerning the matrix reinforce particle interface.

The corrosion behaviour resulted markedly affected by the type of reinforcement because the SiC particles having a more noble potential than the aluminium matrix in comparison with the Al_2O_3 such as the silica carbon, can induce corrosion process by a galvanic effect.

Considering the marine environment as a corrosive one and the alumina particles (10% v/v) as a reinforcing agent and if we compare the results obtained with those related to the traditional Al 6061 T6 alloy (which was the composite material matrix tested) it was pointed out that the corrosion attack on the non-reinforced alloy is higher (by about 10%).

Increasing the alumina particles content rate (from 10 to 20%) a lower corrosive attack was observed (approximately analogous between the cast and extruded product), while only for 10% reinforced containing product, did the extrusion product seem to improve the corrosion resistance of the material.

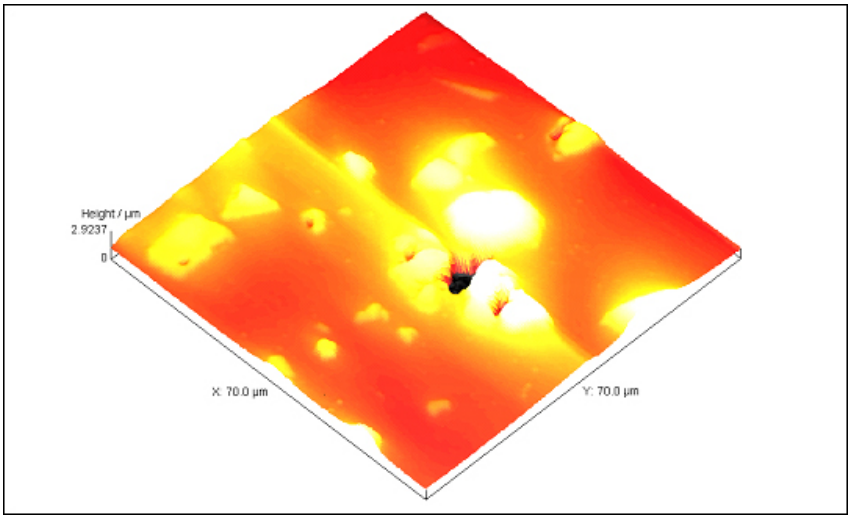

Figure 4: AFM "3D" image of uncorroded Al 6061 T6/Al_2O_3p 10% cast composite sample.

It is possible, therefore, that a higher amount of reinforcing phase reduces the localized corrosion diffusion forming a physical type barrier, while the extrusion process, making the material more homogeneous, restricts the number of graft sites.

References

[1] D. Webster and C.G. Bennet. *A d v. Mater. & Proc.* 10:49, 1989.

[2] R.J. Rioja and R.H. Graham. *A d v. Mater. & Proc.* 6:23, 1992.

[3] K.K. Sankaran and N.J. Grant. *Mat. Sci. Eng.* 44:213, 1980.

[4] E.A. Starke Jr. and T.H. Sanders Jr. *J. Metals*. 33:24, 1984.

[5] The Marine Corrosion Handbook. *Ed. T.H. Rogers - Mc Graw Hill Comp. of Canada Ltd, Canada 4*, 1960.

[6] P. Appendino and M. Montorsi. La Metallurgica Italiana. 10:743, 1986.

[7] M . Fontana, E. Gariboldi, G. Silva, and M. Vedani. La Metallurgica Italiana. 10:743, 1986.

[8] A.J. Sedriks, J.A.S. Green, and D.L. Novak. *Met. Trans.* 2:871, 1971.

[9] P.P. Trzaskoma, E. Mc Cafferty, and C.R. Crowe. *J. Electrochem. Soc.* 30:1809, 1983.

[10] Handbook of Chemistry and Physics. *CRC press, Boca Raton, Florida 61st ed.*, D:155–159, 1980-81.

[11] A.M. Beccaria, P. Traverso, and F. Gnecco. *Pitture e Vernici European Coatings*. 14:75–92, 2000.

[12] A.M. Beccaria, E. Mor, and G. Poggi. *Werkst. und Korr.* 34:236, 1983.

[13] A.M. Beccaria and P. Traverso. Atti 2° Convegno Nazionale PFT2, 29-31 Maggio 1995 Genova. 1301, 1995.

[14] M. Pourbaix. *Corros. Sci.* 14:25, 1974.

[15] A.M. Beccaria and P. Traverso. *Werkst. und Korr.* 47:261, 1996.

[16] P. Traverso and A.M. Beccaria. *Br. Corros. J.* 32:255, 1997.

[17] A.M. Beccaria, G. Poggi, D. Gingaug, and P. Castello. *Br. Corros. J.* 29:65, 1994.

[18] F. Gnecco and A.M. Beccaria. *Br. Corros.* 34:57, 1999.

[19] Z. Szklarska Smialowska and M. Janik-Czachor. *Corros. Sci*. 11:901, 1971.

[20] D. Briggs and M.P. Seah. Practical Surface Analysis. *J. Wiley & Sons, Chichester, UK*, page 487, 1984.

Coastline Extraction from SAR Images

R. Cossu, M.M. Cerimele
Institute for Applied Mathematics "Mauro Picone", CNR, Roma, Italy
r.cossu@iac.cnr.it

Abstract

The aim of this work is to develop a software tool to monitor the coastline. The implemented procedure is constituted by a set of techniques and methods for the SAR (Synthetic Aperture Radar) image segmentation, in order to investigate the state of conservation of the coastal environment. The proposed approach is based on the "level set" method applied to SAR images. In this method, an initial curve defined on the image evolves according to a PDE (Partial Differential Equation) model by means of a velocity related to the characteristics of the image to be segmented. This curve is deformed until it assumes a steady position at the boundary of the area to be extracted from the image. In our case the initial curve includes the coastal area and it moves until it reaches the line that marks the boundary between land and sea. We have pre-processed SAR images in order to remove the speckle noise, implementing an anisotropic diffusion filter. The proposed method has the advantage to extract the coastline from a single image unlike the methods, based on the classic interferometric techniques, which require two images of the same area acquired at different times or from different points of view. We used images SAR (Precise Image) PRI acquired during the ERS2 mission.

1 Introduction

Synthetic Aperture Radar (SAR) uses an active radar antenna which emits modulated microwave pulses. The amplitude and the phase of the returning signals from an Earth surface area are recorded and then combined. Since microwaves wavelength is much longer than the optical one, a huge antenna would be necessary to get acceptable resolutions. This problem has been bypassed by post-processing methods which synthesize an antenna of large dimensions with an antenna of a few meters that allows us to obtain images of up to some centimeters of resolution [1].
SAR images present advantages and disadvantages; active microwave energy penetrates clouds, thus the acquired images provide information in inclement weather, during night as well as day. Moreover the acquisition in wavelengths outside the visible and infrared regions of the electromagnetic spectrum provides information on surface roughness and moisture content of surface layers of vegetation, sand, snow and on wave properties of sea/ocean [2]. On the other hand SAR images present a granular effect due to the multiplicative noise called speckle. Because of sum the contributions of a large number of scatterers, the image pixels have different gray values and even for a single surface type. Important gray level variation may occur between adjacent pixels producing a granular effect.

The aim of this work is to develop a software tool to observe and monitor the coastline, i.e. to create a set of techniques and methodologies for the segmentation of SAR images in order to investigate the conservation status of coastal environment. It is well known that the segmentation is a partitioning of the image into disjoint regions and it is a crucial step in field of images interpretation.
In our case the developed software is based on interactive and automatic methodologies for the analysis and processing of remote sensing data [3]. The analyzed images are SAR PRI acquired during the mission ERS2 and provided by the Consortium for Informatics and Telematics "Innova" of Matera. ERS2 SAR system is capable of 25 m resolution from an altitude of 800 km, at radar wavelength of 5.7 cm.
The identification of the coastal profile in SAR images requires a complex methodology, mainly due to speckle noise, which makes the grainy image. Moreover, a further difficulty arises from the return signal measured in the areas of sea. Indeed in the case of rough sea conditions, the signal determines the intensity of SAR image similar to the land, making it difficult to distinguish the line of coast [4].
It is known that, in a planning of the coastal strip, information on the position of the coast is a key element. In this context, the realization of works related to the sea also due to man-made events can cause changes in the coastline. Hence it is fundamental to monitor the evolution of the coast with regular checks in order to examine the seasonal variability, the storms, and also changes due to human intervention.
Currently there is no typical methodology to automatically detect the coastline. This is traditionally remarked in situ by specialized operators, and it is an expensive process and prone to errors.
Recently, satellite and /or aerial images have been added to control the profile of the coast, but traditional methods of photo-interpretation and manual-tracing are affected by errors, because they are characterized by subjectivity of the result, which depends on interpretation of the operator. For this reason, in recent years, the extraction of the coastline has been the subject of research for the development of automatic or semi-automatic procedures aimed at carrying out that task.
In particular, satellite-optical images, being essentially noise-free images, are usually processed by procedures which use traditional techniques of image segmentation as thresholding and edge detection.
The processing of satellite-optical images and aerial yields results in the ascertainment of the coastline, but it should be noted that the acquisition of these images depends on sunlight and weather conditions.
In this regard, the use of images acquired by SAR provides a considerable advantage over the use of optical images. This sensor, as above written, is not dependent on sunlight, thus it produces image information at night, and also can operate in all weather conditions. This therefore allows the acquisition of image information of areas of land subject to special conditions, such as the polar areas or areas with low light constantly covered by clouds. This feature is very important because visible changes of the coast are found in the presence of inclement weather.
The proposed approach is based on the level set method [5, 6] applied to SAR images.
In this method, an initial curve defined on the image evolves according to a PDE model by means of a velocity related to the characteristics of the image to be seg-

mented. This curve is deformed until it assumes a steady position at the boundary of the area to be extracted from the image [7]. In our procedure the initial curve includes the coastal area and it moves until it reaches the line which marks the boundary between land and sea.
SAR images, due to speckle noise, require to be pre-processed by using a denoising filter. For this purpose, we have implemented an anisotropic diffusion filter[4, 8]. Finally, the proposed procedure has the advantage to extract the coastline by working on a single image unlike the classical interferometric techniques, which require two images of the same area acquired at different times or from different points of view [2]. In the future we plan to apply the proposed methodology to images obtained from the constellation of satellites Cosmo Sky-Med. These satellites are useful in monitoring changes in the Earth's surface with a very high time resolution, because they can observe the same area several times a day in all weather conditions.

2 Coastline extraction

Detecting the coastline from SAR image is a complex depending on the signal coming from water and land region. In fact when the sea is calm, we have a black region, otherwise, if the sea is slightly rough, the emitted signal is only partially reflected producing a gray region. For this reason the return signal from the sea can be frequently indistinct from one coming from the land. Moreover the presence of speckle modeled as a strong multiplicative noise makes the coastline detection even more complicated. In recent years, the "level set" method, based on the evolution of curves has been an important tool for solving image segmentation problems. In particular, this method describes the evolution of a polyline (curve), containing the interested area, until it reaches the boundary of the area to be extracted.
The main advantages of the "level set" method is that complex shaped regions can be detected and handled implicitly.
In order to obtain the governing equation of a front evolution, in [3] we have considered the contour of a region as a zero level of an implicit function defined as a distance function. So we obtained the evolution of the curve driven by a speed function depending on the image features.
In the "level set" method the choice of the speed function is fundamental to achieve a good segmentation.
In this work we propose an integrated procedure obtained by combining two different speed functions: one, called average-based speed function obtained by modelling the intensity of an image using the Gamma distribution, and an other, called gradient-based speed function, obtained by the computation of image gradient.
The SAR PRI image here analyzed has been acquired during ERS2 mission. The images are related to the sea of European coasts.
We have examined the behaviour of the algorithm by using the average-based speed. From these tests it is evident that the results depend on the initial position of the curve. In particular we have obtained a better result if the initial curve is located near the coast.
Usually the image gradient is used to identify the edges or contours; indeed if the gradient of an area is high then the related pixels correspond to edges. However, as it is known, the SAR images can look granular because they are corrupted by strong noise

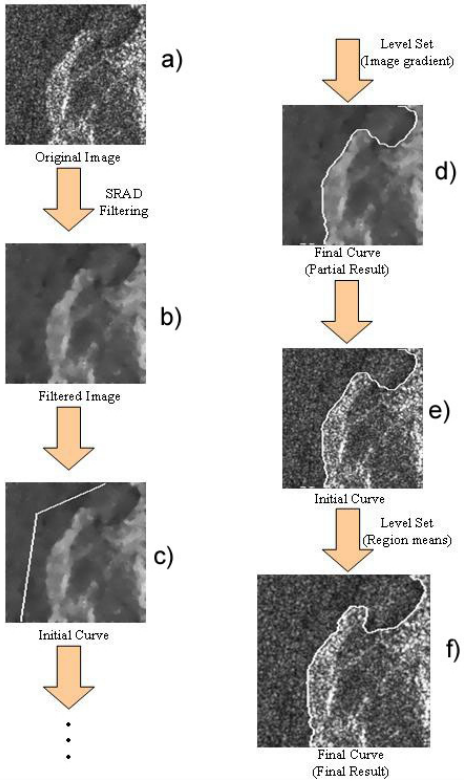

Figure 1: Integrated procedure pipeline: a) original image, b) SRAD filtered image, c) the initial curve for the gradient-based speed, d) intermediate result, e) initial curve for the average-based speed, f) final result.

speckle, and in this case the computation of the gradient could detect false edges.

For this reason in the gradient-based speed computation the images have been pre-processed by means of the SRAD (Speckle Reducing Anisotropic Diffusion) algorithm, which is an extension of Perona-Malik algorithm [8].

Unlike performed tests with average-based speed, in this case the results are independent of the position of the initial curves.

The ”level set” method, by using the average-based speed, detects the coastline with more precision in terms of pixels. In fact the image is not filtered for the noise reduction, because the average computation is already a filtering. We observed in [3] that the best result is obtained by locating the initial curve as near as possible to the coastline. This implies that the final result depends on the position of the starting curve.

The result obtained with the speed based on image gradient is less accurate in terms of pixels, because it works on the filtered image and not on the original one. However,

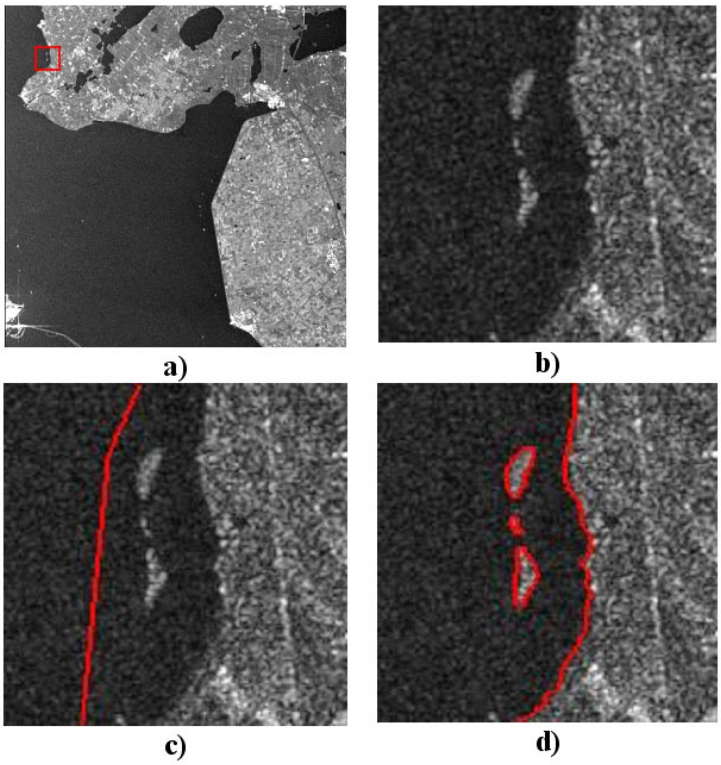

Figure 2: Example of regular coast: a) original image of Netherlands coast, b) original image included in the red square of a), c) starting contour, d) final contour.

this last approach is independent of the position of the initial curve.
The integrated procedure we developed allows the coastline to be identified automatically and independently of the initial location of the curve. In fact, it combines the two speed functions by improving the segmentation results. In the original image of 150x150 pixels (Figure 1a) SRAD filter is applied (Figure 1b). Then the initial curve (Figure 1c) evolves until it reaches the result of the "level set" method with gradient-based speed (Figure 1d). Hence the resulting contour is used as initial curve for applying the level set method (Figure 1e) to the original image by using the average-based speed, in order to obtain the final result (Figure 1f).

3 Segmentation results

In this section we show some results, obtained by using the proposed integrated procedure, combining both the average-based speed and the gradient-based speed.
The integrated procedure is applied to the regular coast of Netherlands (Figure 2). In

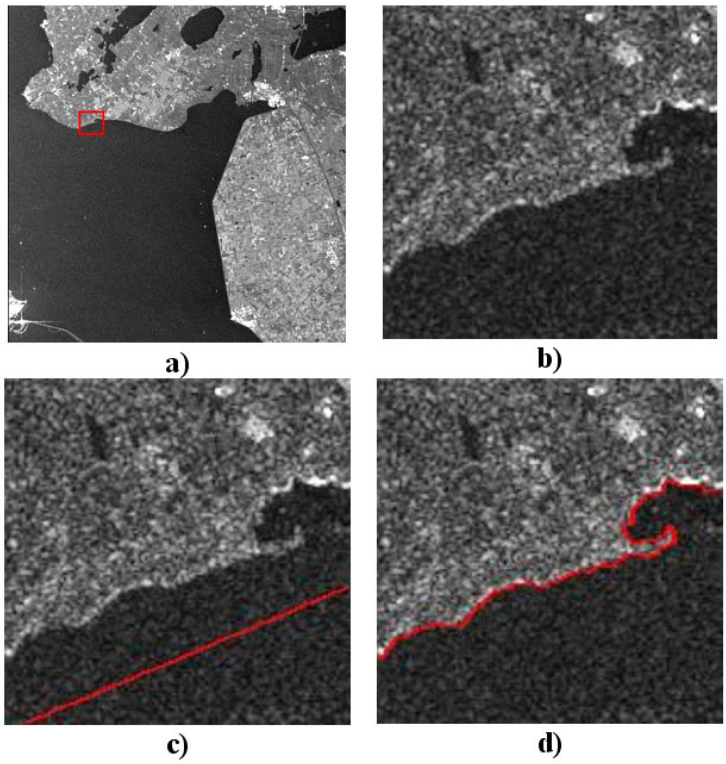

Figure 3: Example of indented coast: a) original image of Netherlands coast, b) detail included in the red square of a), c) starting contour, d) final contour.

particular, the red square in the original image of 1500 x 1500 pixels (Figure 2a) indicates the portion of 150 x 150 pixels to be segmented (Figure 2b). The initial position of the curve (Figure 2c) is modified during the evolution until the final result is reached, identifying three islands and the coast (Figure 3d).

In this example the developed technique is applied to an indented coast of Netherlands of (Figure 3). Again, the red square in the original image of 1500x1500 pixels (Figure 3a) is the portion of 150 x 150 pixels to be segmented (Figure 3b). The initial position of the curve (Figure 3c) is modified during the evolution until to reach the final contour, identifying the coast and the inlets (Figure 3d).

Finally we show the result (Figure 4) obtained in the case of an ill-defined contours coast of Balearic Islands. In this case, the red square in the original image of 1500x1500 pixels (Figure 4a) is the portion of 150x150 pixels (Figure 4b). The initial position of the curve (Figure 4c) is modified until the identification of the low contrast line between land and sea (Figure 4d). Because benchmarks of the SAR images

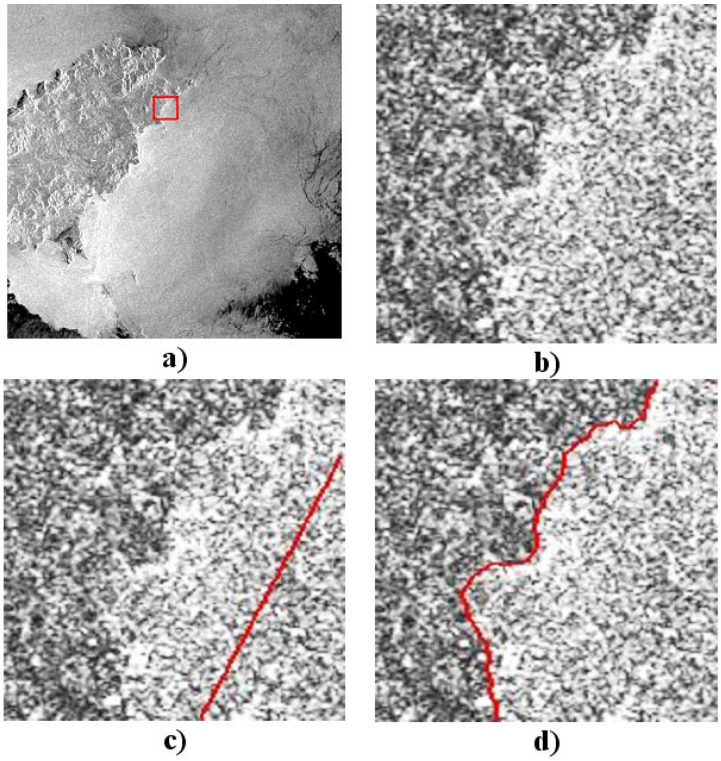

Figure 4: Example of low contrast coast: a) original image of Balearic Islands coast, b) detail included in the red square of a), c) starting contour, d) final contour.

are not known, in order to verify the accuracy of the results obtained by the proposed procedure, in [9] some tests are presented on synthetic images obtained by copying the pattern of the SAR images of two different regions (e.g. land and sea). These images were used to have the reference of the exact location of the contours.

4 Conclusions

In this work we have faced the problem to detect the coastline from SAR image by the "level set" method.

Two distinct speed evolution functions have been examined.
The former, based on the average intensities of the regions, does not need to reduce speckle noise, since the average-based speed already contains a filtering; the latter, based on the image gradient, filters speckle noise by the SRAD technique.
We proposed an innovative procedure combining the two speed functions in order to improve the two individual approaches.
The developed technique allows the segmentation results to be independent of the initial location of the curve and moreover, it automatically stops when the curve

achieves the coastline. More precisely the proposed procedure is such that any different position of the initial curve that contains the area to be segmented produces the same result.
Future development will concern the extension of the segmentation to more regions of different gray levels and the use of the CosmoSkyMed images (Constellation of Small Satellites for Mediterranean basin observation) which are a constellation of 4 satellites in order to monitor the entire globe and the Mediterranean area.

References

[1] H. Maitre. Processing of Synthetic Aperture Radar Images. 2008.

[2] S. Dellepiane, R. De Laurentiis, and F. Giordano. Coastline extraction from SAR images and a method for the evaluation of the coastline precision. *Pattern Recognition Letters*, 25:1461–1470, 2004.

[3] M.M. Cerimele, L. Cinque, R. Cossu, and R. Galiffa. Coastline detection from SAR Images by level set model. *Lecture Notes in Computer Science*, 5716:364–373, 2009.

[4] Yongjian Yu and Scott T. Acton. Speckle reducing anisotropic diffusion. *IEEE Trans. on Image Processing*, 11:1260–1270, 2002.

[5] J.A. Sethian. Evolution, implementation and application of level set and fast marching methods for advancing front. *Journal of Computational Physics*, 169:503–555, 2001.

[6] S. Osher and R. Fedkiw. Level Set Methods and Dynamic Implicit Surfaces. 2002.

[7] I. Ben Ayed, A. Mitiche, and Z. Belhadj. Multiregion level-set partitioning of synthetic aperture radar images. *IEEE Trans. Pattern Analysis and Machine Intelligence*, 27:793–800, 2005.

[8] P. Perona and J. Malik. Scale space and edge detection using anisotropic diffusion. *IEEE Trans. Pattern Analysis and Machine Intelligence*, 12:629–639, 1990.

[9] M.M. Cerimele, R. Cossu, and R. Galiffa. Level set method extension to more regions segmentation in SAR images. *IAC REport*, (190/2010), 2010.

Seafloor Exploration Using the MultiBeam Echo Sounder Technology: Some Examples

R. Tonielli[1], M. Barra[1], G. Di Martino[1], F. Foglini[2], S. Innangi[1], A. Mercorella[2], M. Rovere[2]
1, Institute for Coastal Marine Environment, CNR, Napoli, Italy
2, Institute of Marine Sciences, CNR, Bologna, Italy
renato.tonielli@iamc.cnr.it

Abstract

Until the late 70's bathymetry data of the oceans were commonly acquired by means of single beam echo sounders, along discontinue track lines with an uneven spatial distribution. More recently, the MultiBeam Echo Sounder (MBES) technology was made available to the academic research. These systems provide a full sea floor search and a high resolution imaging of the seafloor. The MBES systems provide depth values along a swath instead of a single point value by means of acoustic pulses arrays. There are several MBES models characterizing by different technical equipments in terms of frequencies, beam number and spacing. MBES systems are used in archaeological and engineering fields, where high resolution data in small areas are required, as well as in deep seafloor mapping aimed at large scale structures detection. MBES may provide also grain size information besides bathymetric data, recording the backscatter values that result from the interaction of acoustic pulses with the seafloor. This tool is particularly important to characterize the distribution of some features on the seafloor such as submarine landslides and other elements that may play an important role in the assessment of the geological hazard along the coasts. Actually some research groups are improving the backscatter analysis to generate a semi-automatic seabed classification method. This contribution will provide an overview of some recent examples studied within the framework of the CNR research projects.

1 Introduction

Over the last 30 years technological advances lead to discover and map the Earth's seafloor. The acoustic waves are today the main instrument to explore the sea bottom, being easily transmitted through the water column. Their reflection off the seafloor allows us to imagine its shape and texture. They are used underwater to detect and locate obstacles and targets, as well as to measure the characteristics of marine environment, such as seafloor topography, living organisms, currents and hydrographic structures.

Acoustic waves are the basis of *Sonar* (Sound Navigation And Ranging). A sonar is a device that uses sound in order to remotely detect and locate objects in the water. There are two basic types of sonars: the passive sonar, that is a "listening" device, i.e. it can only detect sounds emitted by a source; the active sonar, that can generate sound waves in addition to detect them [1].

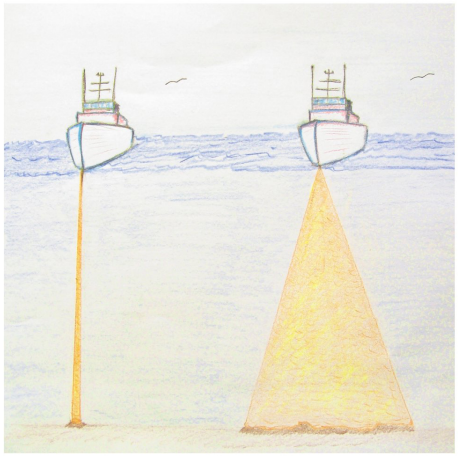

Figure 1: Difference in bottom coverage between singlebeam and multibeam systems.

The origins of sonar are old, likely in 1822, when Daniel Colloden used an underwater bell to calculate the speed of sound in Lake Geneva, Switzerland. Later on, in 1906, Lewis Nixon built the first sonar-type listening to detect icebergs. A major breakthrough came from Paul Langevin, a French physicist; he demonstrated, between 1915 and 1918, that it was possible to transmit signals, and to actively detect submarines giving both their angles and distances from receiver. Sonar technology improved considerably between the two world wars, but the period since Second World War has seen enormous advances in marine geophysics. Rapid progress came during the 1950s and 1960s, when government agencies financed multi-purpose oceanographic expeditions and gave scientists much flexibility in conducting their researches [2].

Until that time bathymetric data were collected using Singlebeam Echosounders. An echosounder is an active sonar, as it measures depth by producing an acoustic pulse and listening for the echoes returning from the seafloor. The echosounder's *projector* generates a directional pulse, so the main part of the energy is radiated within a solid angle towards the bottom, where it is reflected and finally detected by the echosounder's *receiver*. The Singlebeam provides a single measurement at the nadir depth, so data logged along transect lines cannot provide continuous coverage neither detailed information about the bottom. In 1964 a new technology, known as *Sonar Array Sounding System* (SASS), was developed for the United States Navy. The SASS received a large number of sideways reflected signals, recorded their range and bearing and, from the configuration of the transducers, computed off-track depths. This instrument was the first *Multibeam EchoSounder* (MBES) that achieved a great development during the 1970s.

A MBES emits pulses with a beam pattern that is narrow along the ship track and wide across the ship track, providing a swath of data that, depending on sensor's speci-

fication, is normally several times the water depth. A Global Positioning System (GPS), a Motion Sensor, a Sound Velocity Profiler (SVP) and a sound speed probe are used during Multibeam survey to provide vessel attitude data and sound speed in the water in order to produce accurate bathymetric record (Figure 1).
Even though Multibeams are more complex and more expensive systems than singlebeams, they are largely used within the marine sciences. In fact they are more productive, as they provide a full sea floor search and a high resolution imaging of the seafloor than Singlebeam in a short time. MBES are suitable for different applications according to their specifications; they can be installed on small vessels to perform high resolution surveys in shallow water, as well as on large ships to explore offshore deep sea areas.
Technological development leads to continuous improvements of Multibeam hardware and so to a better instrumental performance; on the other side, new software availability allows the extraction of further informations from the acoustic signal, such as backscatter intensity. In fact over the last years, great attention has been paid to backscatter analysis, that can be used to study the seafloor characteristics.

2 Multibeam EchoSounder Systems

The MBES transducer emits an acoustic pulse that travels in the water column toward the bottom and detects the reflected echo. The receive array is normal to the transmit array and the intersection between the transmit beam and the receive array forms a sequence of elliptical areas on the seafloor, called *footprints* (Figure 2).
The system performs a depth measurement for each *footprint* along a swath, computing the range along each beam to the bottom by the relation between the Two-Way Travel Time (TWTT) and the sound speed in the water.
The TWTT is measured by the maximum backscatter amplitude of inner beams, where the *footprint* is small and the echo signal has a prominent peak, and by phase detection of outer beams, where the footprint increases and the echo signal may have several peaks of comparable amplitudes [3].
There are several MBES models characterized by different technical characteristics in terms of frequencies, beam number and beam solid angle.
The following information outlines the major specifications collected from a variety of systems (Table 1).
These specifications affect the system capacity in terms of maximum operating depth and spatial resolution.
Operating frequency is the multibeam main feature: it affects the depth capabilities of the system and the vertical resolution.
Low frequency waves can travel far in the water, because they propagate along a straight line and they are not attenuated and do not lose intensity, so they can easily penetrate the medium. On the other side, high frequency waves are rapidly attenuated, but the short wavelength allow them to resolve small object providing high vertical resolution images.
The beam solid angle specifies the beam width and it can be used to estimate the across-track individual beam footprint according to the equation:

$$Footprint = Tan(beamwidth) * NadirDepth$$

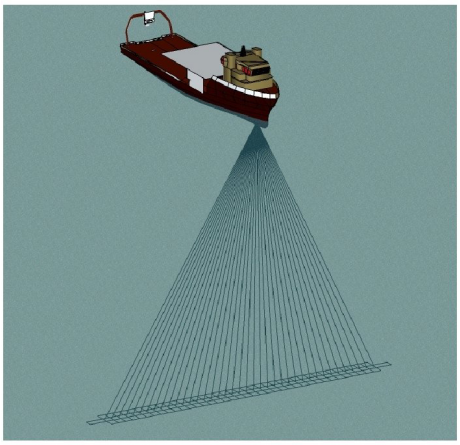

Figure 2: The intersection between total area ensonified by acoustic pulse and area covered by receive array produces the footprints.

Specifications	*Low Frequency Deep water*	*Medium Frequency Medium-depth water*	*High Frequency Shallow water*
Frequency	12 – 18 kHz	30 – 100 kHz	100 – 455 kHz
Max. operating depth	11000 m	3000 m	700 m
Beam solid angle	1 to 4 deg	1,2 to 2 deg	0,5 to 1,5 deg
Vertical Resolution	7,6 to 45 cm	1,5 to 9 cm	< 1 to 12.5 mm

Table 1: Multibeam Systems technical specifications.

So, the beamwidth defines the system horizontal resolution that is function of the vessel speed and the number of pulses per second (*ping rate*). When performing a TWTT amplitude detection method, the smaller the beam angle, the better the system is able to discern true depth and resolve small features. When performing a TWTT phase detection method, the horizontal resolution does not depend on beamwidth, because the feature detection capability may be significantly better than the physical beam opening, i.e. the system can resolve targets smaller than the *footprint* [4].
Recent low frequency MBES operate in larger depth range than in the past, thanks to the beam dynamic focusing. It reduces the distortion of the array beam pattern in the near field, so the footprint size is narrower than predicted and the system operates in shallow water without loss of resolution.
Over the last few years, some technical improvements were introduced in order to optimize system performances. MBES performing an *equi-distant* beam spacing mode, in addition to the *equi-angular mode*, were produced; systems performing the *equi-angular* mode produce an uneven distribution of beams that gradually decrease from the swath's centre to the swath's outer edges. This reduces the

system productivity by increasing the percentage of swath overlap required between survey lines. *Equi-distant beam spacing mode*, selectable by the user, provides uniform sounding density and maximizes usable outer swath, increasing system productivity [5].

Some MBES systems perform a high density processing mode to improve the horizontal resolution: they generate extra soundings so that the number of total soundings is higher than the number of acoustic beams. This technique reduces the acoustic *footprint* thus improving the system capability to detect objects and other details on the bottom.

During a bathymetric survey, a number of instruments has to be used in order to perform a real-time correction of bathymetric data for vessel position and attitude. GPS system produces vessel position and speed data by a triangulation computation founded on a satellites constellation. Positioning data may accuse errors because GPS signal propagates through the atmosphere, thus producing data accurate to a matter of meters; better accuracy is provided by other positioning systems, such as Differenzial, High Precision DGPS, Local DGPS and Real Time Kynematic DGPS. These systems provide positioning data with sub-metric to centimetric precision; RTK DGPS also provides real-time corrections for the z-axis.

Vessel movements such as roll, pitch and yaw, cause swath pointing errors and incorrect bathymetric data. The gyrocompass and the motion sensor produce very precise measurements of vessel attitude many times per second: by integrating these values with the timing of the sonar echo, an accurate bathymetric record can be produced regardless of the echo path through the water.

The water sound velocity is a basic parameter for Multibeam operations, so a sound velocity probe is mounted near the transducers; it provides a real-time sound velocity measurement in order to perform the *beam-steering*, i.e. to compute the echo arrival-time for each beam to each receiver element.

Finally, a Sound Velocity Profiler (SVP) provides the sound velocity profile in the water column. The sound speed depends on the medium density, so when the acoustic pulse propagates through a stratified water column the beam's path bends because of the refraction phenomenon. SVP data stored allow the system to compute the refraction coefficient in each water layer and to obtain the right location of the object on the seafloor relative to the sonar transducers. The SVP is lowered in the water column every 6 - 8 hours according to Intenational Hydrographic Organization [6] standards or whenever the swath bends to the bottom (*frowning*) or to the surface (*smiling*); this event can occur while surveying in coastal areas, where a fresh-water runoff is present, as well as in offshore areas, where upwelling is present. The effect of these events is an overestimated or an undervalued sound velocity profile that produce typical artifacts, such as "ripples" in logged data [7, 8].

Multibeams and associated instruments can be permanent or semi-permanent mounted on small and large ships. MBES is usually hull-mounted on ships specifically dedicated to bathymetric surveying; this is a stable configuration where the multibeam is integrated with the vessel's hull and the exact physical location of each system component and the distances between them is measured with great precision during the installation process. Pole-mounted transducers are normally used on

smaller vessels that will be temporarily dedicated to acoustic surveying. If possible, MBES is installed near the vessel centre of gravity, in order to increase the system stability and to keep it far away from vibration sources and from seafoam that affects the sound speed. Finally, MBES can be installed on Remote Operating Vessel (ROV); a shallow water instrument, normally operating at 100 meters depth, can be lowered in very deep water to perform a high resolution bottom detection. Some multibeam models are high-pressure proof and operate until 6,000 meters depth.

3 Backscatter

The primary purpose of MBES system was to obtain high-resolution bathymetry maps, but recent researches have focused on utilizing MBES backscatter data as seafloor characterization tool.

When sound waves encounter a rough boundary between two media with different impedances, waves are reflected, transmitted and scattered. The portion of energy scattered back towards the source, known as backscatter, is typically expressed in decibel value. The backscatter strength depends on: wave incidence angle with the bottom, ensonified area, absorption coefficient of water column and, most of all, bottom physical proprieties, i.e. roughness, density, acoustic impedance and coefficient reflection of sediment. In general, as the impedance contrast or roughness of a surface increases so does the intensity of backscatter; so as logarithmic parameter F of grain size decreases the acoustic impedance increases and, consequently, the scattering increases [11, 12].

Typical values of density, sound speed and resulting acoustic impedance for selected sediment types are given in Table 2. Thus, backscatter has great importance in knowing the grain size by studying differences in bottom acoustical response. Currently, there are two approaches to logging MBES's acoustic backscatter data [13]:

a) Forming two additional port and starboard wide angle receive beams to log a *sidescan-like* time series of intensities.
b) Logging a single backscatter value with each beam, either taken as the maximum intensity at bottom detect, or as average intensity centered on the bottom in the time series (called *snippet* or *footprint time series*).

The main difference between snippet and sidescan-like data is that the "sidescan" mode records the backscatter intensity from all beams and computes the average of the data, while the snippet records a range (in the time T0-Tn) of intensity values from each beam, without computing average values. This is why it is also called *footprint time series* (Figure 3).

The basic principles of measuring the seafloor backscatter strength are similar for low and high frequency systems. However, the measurement geometry and physical conditions, such as the ensonification and *footprint* areas relative to the seafloor roughness scale, Rayleigh parameter, etc., are significantly different [3].

As for now, there are a few software products available to process MBES backscatter data. Some of the most notable software packages are: SwathEd, developed by Hughes Clarke, MB systems, developed by Caress and Chayes, SonarScope, developed by the Acoustic & Seismics department of Ifremer, Geocoder, developed by Fonseca and Calder, Isis (©Triton Elics International), Hips and Sips (©2009 CARIS) and a Matlab toolbox developed by Gavrilov, Siwabessy and Parnum of the

Media	**Grain Size (F)**	**Density ($\mathbf{kg \cdot m^{-3}}$)**	**Sound Speed ($\mathbf{m \cdot s^{-1}}$)**	**Acoustic Impedance (rayls)**	**Reflection coefficient ($\mathbf{R_0}$)**
Seawater	N/A	1000	1500	$1.5*10^6$	N/A
Clay	9	1200	1470	$1.764*10^6$	0.0809
Clayey silt	7	1500	1515	$2.496*10^6$	0.2492
Very fine sand	3	1900	1680	$3.192*10^6$	0.3606
Course sand	1	2000	1800	$3.6*10^6$	0.4118
Rock	N/A	2500	3750	$9.375*10^6$	0.7241

Table 2: Typical values of density, sound speed and resulting acoustic impedance for various grades of sediment [9, 10].

Center for Marine Science and Technology (CMST).
Each of these software implements a set of steps in order to process the backscatter data that can be summarized in the following list:

1. Conversion from original acquisition data format into the software proprietary data format;
2. Calculation of XYZ position and incidence angle for each beam;
3. Calculation of XYZ position and average intensity of backscatter;
4. Removal of the system Time Variable Gain (TVG);
5. Radiometric correction (beam pattern);
6. Calculation of the surface backscatter strength.

Any software listed above has its specialization in the processing of backscatter and the choice of the most suitable software depends on what kind of output is required. For example a software like Isis is suited for processing sidescan data, but it does not allow the processing of snippet data; other software, as Caris, process the Time Series as well as the Sidescan-like; finally, there are software, as the Matlab toolbox, that implement various processing and analysis algorithms for processing MBES data.
Seafloor classification based on the analysis of MBES backscatter images often contains artifacts due to inadequate correction for angular dependence. For this purposes the correction for incidence angle is worthwhile. The relationship between backscatter strength and incidence angle can be exploited empirically, i.e. using the relative difference between angular responses to distinguish seafloor types [14]. Hughes Clarke [15] identified and used ten features of angular dependence curves, including the mean and slope from three different angular domains, that could be used for seafloor classification. In summary we can state that utilizing the angular dependence of backscatter in addition to the mean backscatter strength is a better approach to seafloor classification, because it provides more informations about morphological and physical proprieties of the seafloor [16].

4 Multibeam Echosounder applications: some examples

MBES systems are suitable for different applications according to their technical specifications. They can be used in shallow water surveys, where high resolution data in small areas are required, as well as in deep seafloor mapping aimed at large scale structures detection.
The depth range of the survey area, the required resolution and the final output affect the choice of Multibeam model and of associated instruments. An overview of some examples studied within the framework of the CNR research projects are shown.

4.1 Archaeology

Multibeam systems are used in archaeological field for different purposes, such as ancient ruins surveying or wreck searching. Very high resolution data are required for these surveys, in order to generate 20 centimeters grid cell or less, as well as high precision position system; thus, high frequency MBES and HP DGPS or Local DGPS are used. An example of an archaeological application of multibeam system is shown in Figure 4.
The bathymetric survey was carried out in 2006, on board M/N "Red Fish", a vessel 8 meters long, in order to navigate in very shallow water; a pole-mounted Reson Seabat 8125, a Landstar HP DGPS, an Ixea Octans 3000, a Reson SPV-C and a Navitronic SVP15 were used. The Tin Model shows Roman ruins of the ancient city of Baia (Naples). Some walls and a room located in very shallow water, are recognizable in the snapshot. The structures lie on the seafloor at about 6 meters depth and they are about 1 meter high; the room is included by 20 meters and 10 meters long walls.

4.2 Engineering

In engineering field very high resolution data of anthropical structures, such as docks and wharf, are required. The target of these surveys is to perform a structures monitoring as well as to plan new projects; so, high frequency MBES and sub-metric precision GPS are required for these bathymetric applications. Some examples are shown in Figure 5, Figure 6 and Figure 7).
The structure in Figure 5 is located in Bagnoli, Gulf of Naples. It is a 650 mt. long wharf aimed to goods loading and unloading operations; the wharf is included in Ex-Italsider dismissed steelwork industrial area. Supporting piers and protection blocks located at the wharf's head are visible. The bathymetric survey was carried out in 2006, on board M/N "Red Fish", using a pole-mounted Reson Seabat 8125, a Landstar DGPS, an Ixea Octans 3000, a Reson SPV-C and a Navitronic SVP15.
The shaded relief in Figure 6 is produced from very high resolution bathymetric data of Pozzuoli tourist harbour. Blocks surrounding the docks, mooring blocks and chains are visible as well as other dismissed anthropic structures such as electric lattices. The bathymetric survey was carried out using a small vessel in order to navigate around the docks; a pole-mounted Reson Seabat 8125, a Landstar DGPS, an Ixea Octans 3000, a Reson SPV-C and a Navitronic SVP15 were used. An example of high resolution data collected in Naples harbour is shown in Figure 7. Raw data are visible at the highest instrumental resolution: all correct logged beams are in fact visible showing an outer breakwater por-

tion, 30 meters long, and the blocks placed in front of it. Many processing software provide a detailed data view in order to manually remove incorrect beams. Bathymetric data were collected using a pole-mounted Reson Seabat 8125 on board M/N "Red Fish", a Landstar DGPS, an Ixea Octans 3000, a Reson SPV-C and a Navitronic SVP15.

4.3 Hydrography and Morpho-bathymetry

Many of the human activities are strictly bound to the sea. The knowledge of seafloor morphology allows optimization of these activities, especially the ship navigation. Bathymetric charts, therefore, represent an obvious resource for all the maritime activities and their development. The use of the Multibeam allows a continuous map updating, aimed to bottom variability study within the marine geohazard field.
Two examples of this application are shown. The bathymetric chart in Figure 8 was realized within the mapping project of Basilicata Region. Bathymetric data were collected from 2004 to 2007 by IAMC, during different oceanographic cruises on board R/V "Urania", R/V "Thetis" and M/N "Napoli". Different Multibeam models have been used in order to realize this chart depending on the operational depth (Seabat 8125 between 5 and 50 m depth, Seabat 8111 and Seabat 8160 between 50 and 600 m depth).
The morphological map of Straits of Messina in Figure 9 was produced from Bathymetric data collected by IAMC during different oceanographic cruises, from 2001 to 2003, using Reson Seabat 8111 (100 kHz), hull-mounted on R/V "Thetis".

4.4 Marine Geohazard

In recent years high-resolution seafloor mapping is increasingly employed for monitoring and assessing natural impact and hazard on coastal and marine areas. High-resolution multibeam bathymetry represents a fundamental tool for a first characterization of geological features that represent potential geohazards such as: volcanic vents, active faulting, submarine canyon activity, bedform migration, gas seepage, fluid escape, slope erosion and failures. Here below some examples of possible geohazards represented by a field of pockmarks in the Tyrrhenian Sea and by submarine slides affecting the continental slope of Gela Basin Sicily Channel).
The multibeam data in Figure 10 have been acquired with a Kongsberg EM12 model in 1999 by ISMAR aboard R/V Strakhov. The aim of the survey was to investigate the Tyrrhenian sea at water depths deeper than 400 m. The primary positioning sensor was the RACAL DGPS SKYFIX SPOT BEAM with a 12 channel Trimble receiver. In typical ocean depths a sounding spacing of about 50 m across and along is achievable. The data acquisition was performed to constantly match a 20 % overlap. The data were post-processed using the Kongsberg-Neptune software, with a standard procedure, including positioning and depth correction, manual and statistical cleaning of the data. The shaded relief produced from bathymetric data shows pockmarks with a diameter of 500 m.
Twin slides are shown in Figure 11. They are located along the western side of the Malta Plateau. When exposed at seafloor, failed masses show an extreme morphological complexity with massive slide blocks, pressure ridges and hummocky surface. The multibeam data have been acquired by

a Reson Seabat 8160 (50 kHz) and Konsberg EM300 (30 kHz) on board R/V Urania and R/V Odin Finder. The data acquisition was performed to constantly match a 20% overlap. The aim of the survey was to investigate the continental slope, in order to detect widespread mass failures along the Western side of the Malta plateau.

4.5 Backscatter

The MBES backscatter data provide grain size information and characterize the distribution of seafloor features such as submarine landslides and other elements that may play an important role in the assessment of the geological hazard along the coasts. Overviews of some examples of processed MBES backscatter data are in Figure 12 and in Figure 13.
A shallow water survey was performed by a Reson Seabat 8125 in order to collect high resolution morphobathymetric data along Maratea coast (Figure 12).The sidescan-like data were processed by Isis of Triton Elics: the navigation data were smoothed, TVG adjustment was performed, radiometric (beam angle and grazing angle) and geometric (slant range) corrections for each line were applied; then the lines were assembled in a mosaic. The snippet data were processed by the Matlab toolbox of CMST. This software removes all artifacts due to angular dependence and returns a file for each line, containing Easting, Northing and the decibel value of each beam. So it is possible to achieve a grid of snippet data that can be further processed (i.e. interpolation). Snippet grid contains more information about lithology than a sidescan mosaic, but there is no morphological information.
The Time Series Mosaic in Figure 13 was produced from backscatter data processed by Caris Hips and Sips. It is noteworthy that the backscatter mosaic points out the lithological facies.

5 Conclusions

Nowadays, multibeam surveys represent a basic tool for marine research projects. In this review some MBES applications, developed by CNR research scientists, were provided. The progressive improvement of multibeam echosounder systems makes these instruments suitable for a new range of applications. In particular, geological hazard, sea bottom facies characterization (including benthonic assemblages), hydrocarbon deposits acoustic response, water column acoustic imaging, quantitative studies of demersal resources, are possible application of this technology. In conclusion, it is clear that multibeam echosounder systems provide the fundamental knowledge of the seafloor for a effective development of research projects in marine environment.

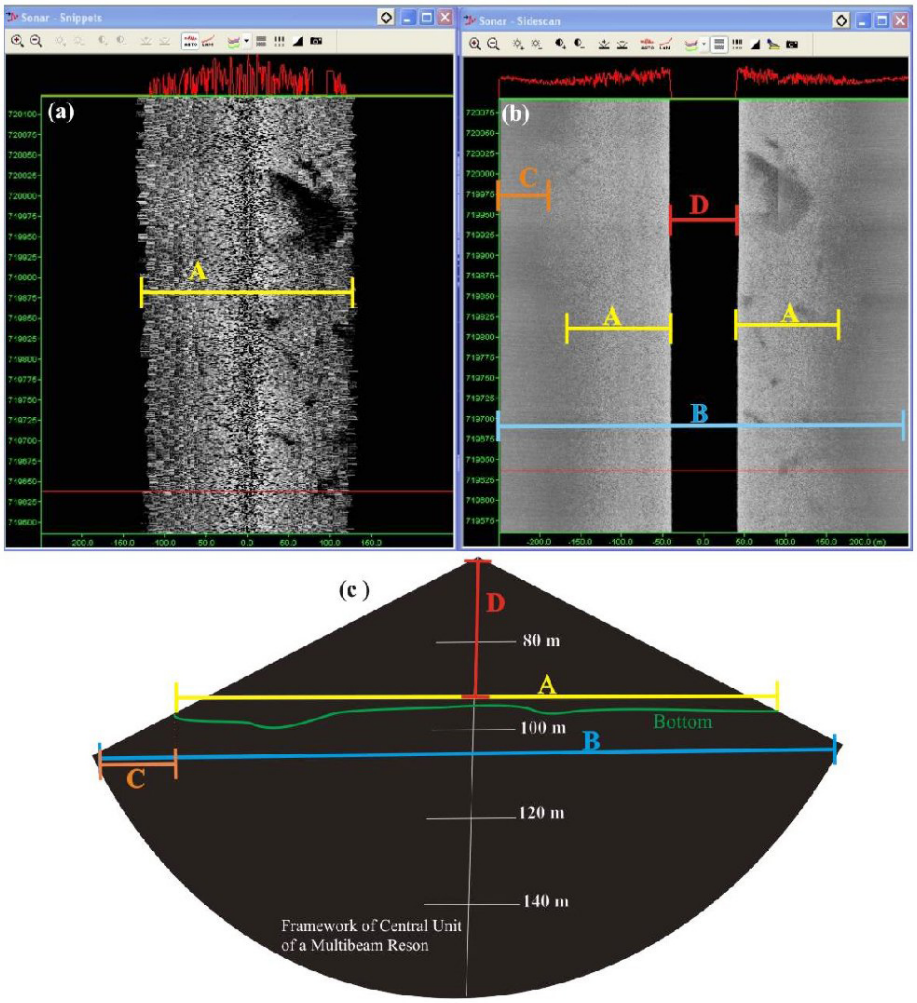

Figure 3: PDS2000 software windows of backscatter data from MBES, respectively Snippet window (3a) and Sidescan-like window (3b). Figure 3(c) - shows the Central Unit of MBES framework: the green line is the profile of the bottom ensonified by MBES. Snippet data logging horizontal range is the same as for MBES data logging (A), while Sidescan-like data logging horizontal range encloses the water column (D) and all range of acquisition (B), including null data (C).

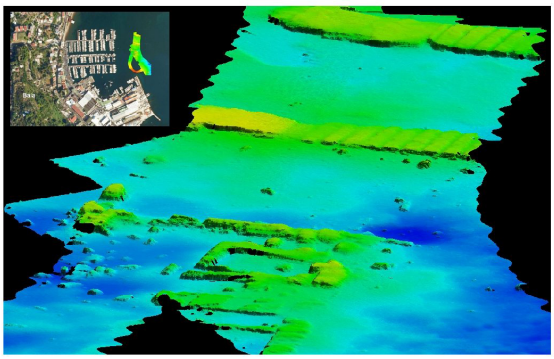

Figure 4: Archaeological structures - Tin Model, 3D view.

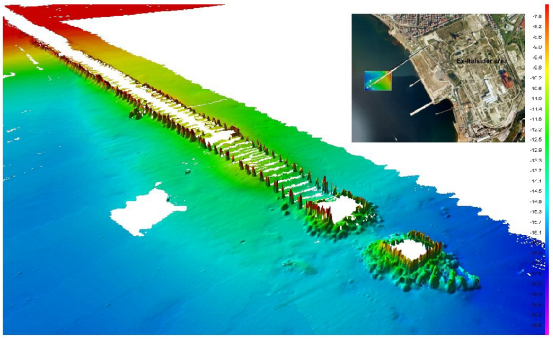

Figure 5: Wharf 3D view - Grid cell 50 cm.

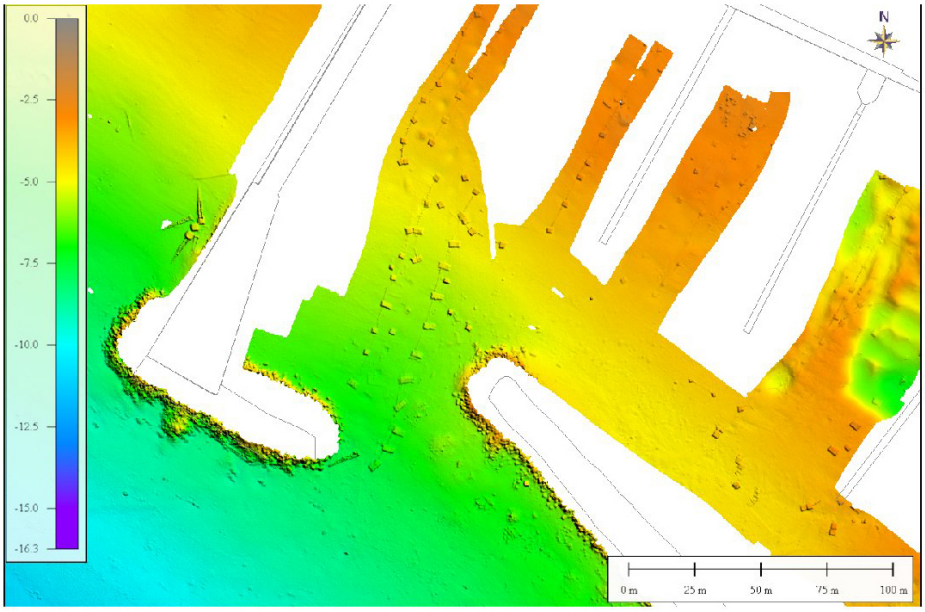

Figure 6: Pozzuoli tourist harbour 2D view Shaded relief - Grid cell 20 cm.

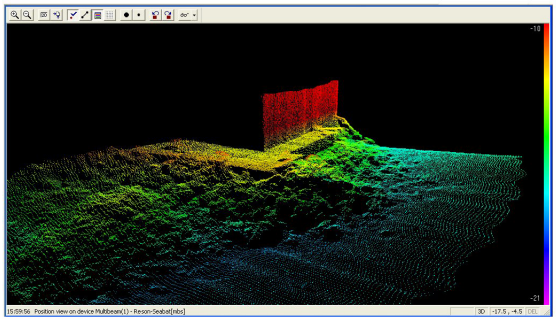

Figure 7: Naples harbour, beams 3D view - Outer breakwater.

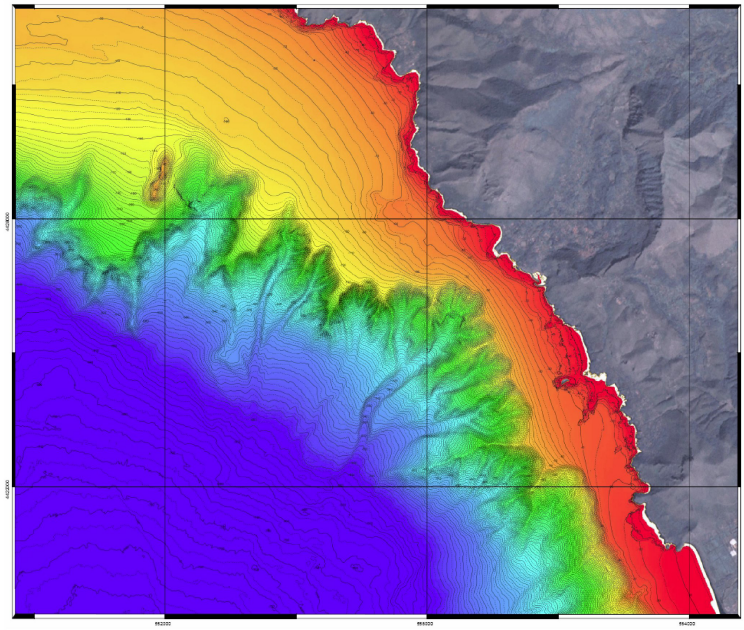

Figure 8: Bathymetric Chart and Shaded Relief of Lucania Tyrrhenian coast: Scale 1:25000, isobaths spacing 5 m, projection UTM33N, Datum WGS84, depth range 5 - 600 m.

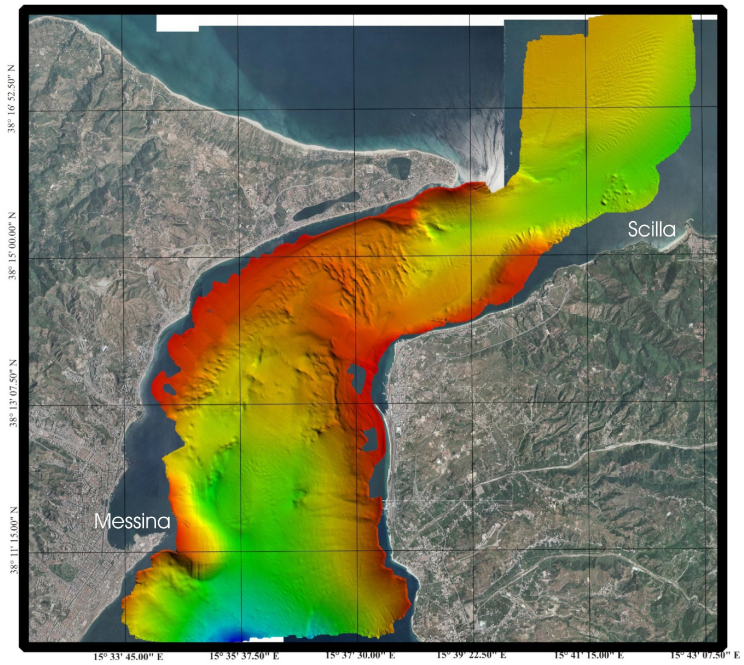

Figure 9: Straits of Messina shaded relief - Grid cell 10m - Depth range: 10 - 700 m.

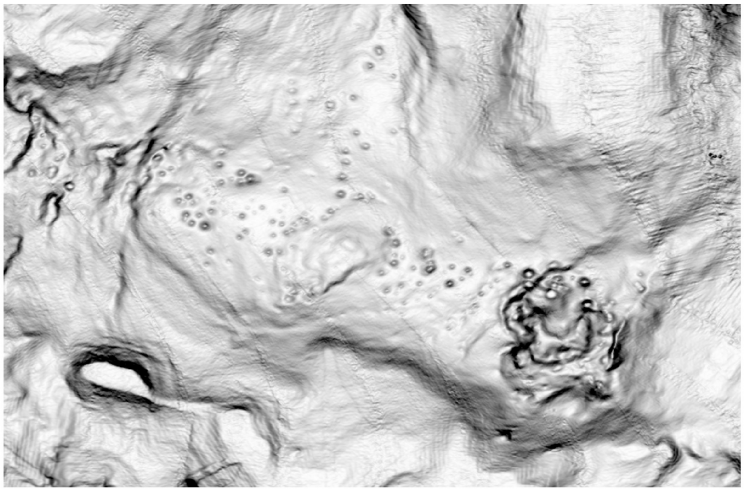

Figure 10: Pockmarks field on top a structural high in the Tyrrhenian Sea - DTM cell size: 50 m, datum WGS84. Projection Direct Mercator on 40° N.

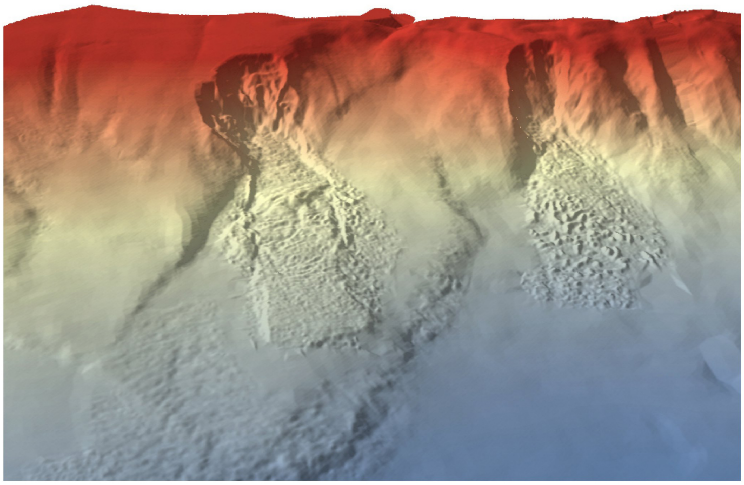

Figure 11: Twin slides on the continental slope of Gela Basin (Strait of Sicily).

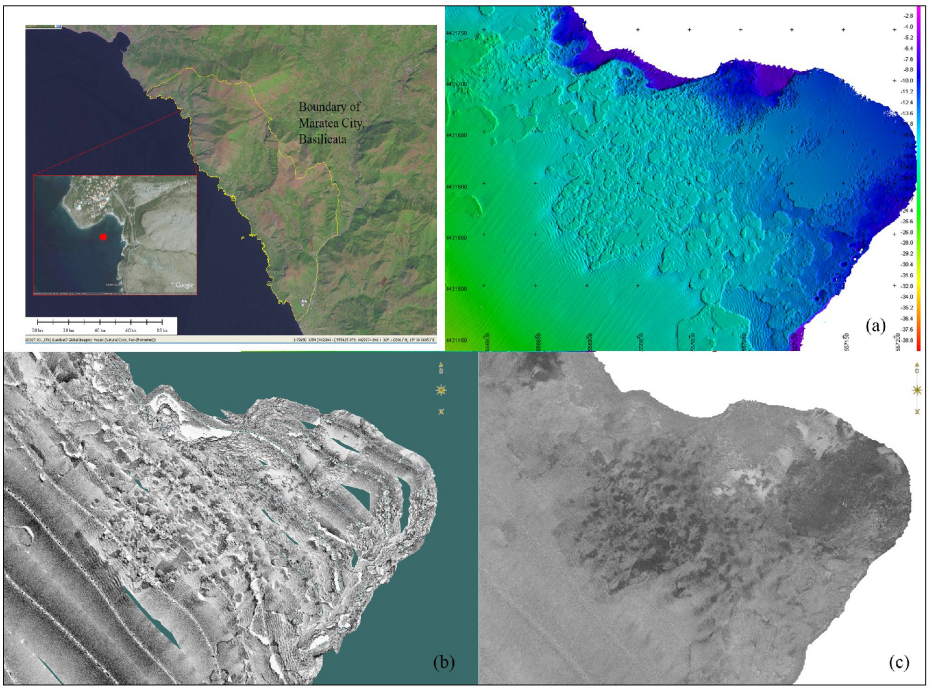

Figure 12: Bathymetric data (a), sidescan-like data (b) and snippet data (c) collected in Acquafredda's Bay (Maratea City).

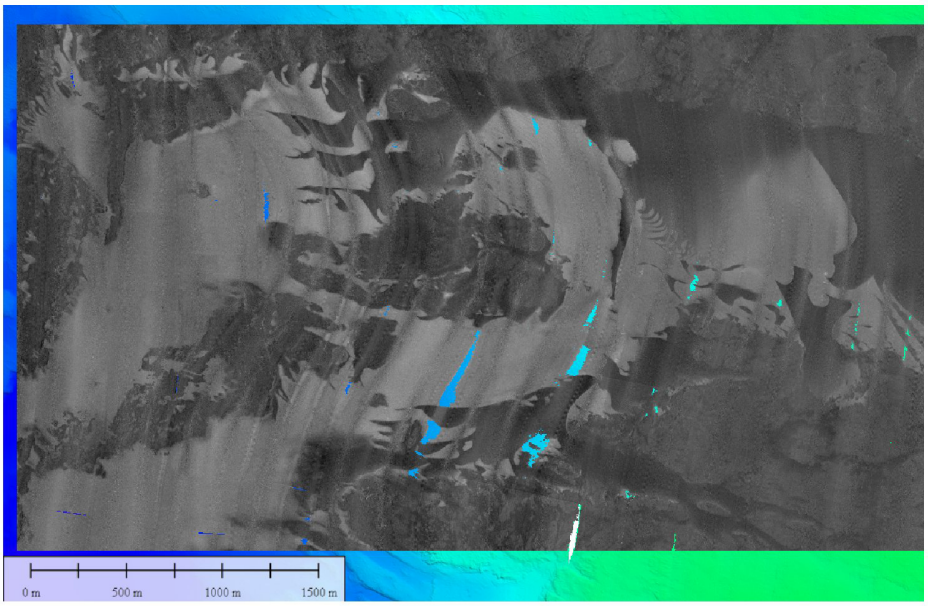

Figure 13: Time Series mosaic from Multibeam Simrad EM3002.

References

[1] L3 Communications SeaBeam Instruments. Multibeam Sonar Theory of Operation. 2000.

[2] E.J.W. Jones. Marine Geophysics. page 474, 1999.

[3] I.M. Parnum. Benthic habitat mapping using multibeam sonar systems. page 208, 2008.

[4] J. Miller, J.E. Hughes Clarke, and J. Patterson. How Effectively Have You Covered Your Bottom? *Hydrographic Journal*, (83):3–10, 1997.

[5] National Oceanic, Atmospheric Administration (NOAA), and Office of Coast Survey. Field Procedures Manual. 2010.

[6] IHO International Hydrographic Organization. IHO standard for Hydrographic Surveys - Special Publication no. 44. page 28, 2008.

[7] J.E. Hughes Clarke. Dynamic motion residuals in swath sonar data: Ironing out the creases. *International Hydrographic Review*, 4(1):6–23, 2003.

[8] G. Di Martino and R. Tonielli. Fresh water runoff effects on shallow water Multibeam surveys. *Sea Technology*, 51(5):10–13, 2010.

[9] APL. APL UW High Frequency Ocean Enviroment Acoustic Models Handbook. 1994.

[10] X. Lurton. An Introduction to underwater acoustic, Principles and Applications. page 347, 2002.

[11] I.M. Parnum, A.N. Gavrilov, P.J.W. Siwabessy, and A.J. Duncan. Analysis of multibeam data for the purposes of seafloor classification. S.P., 2007.

[12] J.A. Goff, H.C. Olson, and C.S. Duncan. Correlation of side scan backscatter intensity with grain size distribution of shelf sediments, New Jersey margin. *Geo-Marine Letters*, (20):43–49, 2000.

[13] J. Beaudoin, J.E. Hughes Clarke, E. van den Ameele, , and J. Gardner. Geometric and radiometric correction of multibeam backscatter derived from Reson 8101 systems. Canadian Hydrographic Conference Proceedings. 2002.

[14] I.M. Parnum, A.N. Gavrilov, and P.J.W. Siwabessy & A.J. Duncan. The effect of incidence angle on statistical variation of backscatter measured using a high-frequency Multibeam sonar. S.P.:433–438, 2005.

[15] J.E. Hughes Clarke. Towards remote seafloor classification using the angular response of acoustic backscatter: a case study from multiple overlapping Gloria Data. *IEEE Journal of Oceanic Engineering*, 19(1):112–127, 1994.

[16] G. De Falco, R. Tonielli, G. Di Martino, S. Innangi, S. Simeone, and I.M. Parnum. Relationships between multibeam backscatter, sediment grain size and Posidonia oceanica seagrass distribution. *Continental Shelf Research*, pages 1941–1950, 2010.

Integrating Meteo-Marine Forecast Data within Heterogeneous Earth Observation Information Services

G. Brugnoni[1,2], S. Gianfranceschi[3], F. Pasi[4,2], S. Taddei[5,2], A. Orlandi[4,2], B. Doronzo[5,2], B. Gozzini[4,2], F.P. Vaccari[2]
1, Institute for Biometeorology, CNR, Livorno, Italy
2, LaMMa Consortium, Laboratory of Monitoring and Environment Modelling for the Sustainable Development, Sesto Fiorentino (FI), Italy
3, INTECS s.p.a., Pisa, Italy
4, Institute for Biometeorology, CNR, Sesto Fiorentino, Italy
5, Institute for Biometeorology, CNR, Livorno, Italy
g.brugnoni@lamma.rete.toscana.it

Abstract

At the Consorzio LAMMA (Laboratory of Monitoring and Environmental Modelling for the sustainable development) an operational weather forecasting chain composed by numerical models, such as Weather Research and Forecasting (WRF) and the full-spectral third-generation ocean wind-wave model WaveWatch III (WW3). These models run few times a day and produce a few days forecast over the Mediterranean area. The Service Support Environment (SSE) platform created within the European Space Agency (ESA) General Support Technology Programme (GSTP) project, provides an advanced test-bed that supports service prototyping and demonstration processes, allowing the design of automatically executed workflows, with a valuable decrease of the overall development effort.
Atmosphere and wave forecast model data has been integrated in the SSE platform experiencing new weather forecast services prototyping and deliv-ery, sharing of such a data together with major European Earth Observation (EO) and geospatial data providers, fostering forecast data integration within other EO services and evaluating new business opportunities.

1 Introduction

Earth's weather and climates influence daily human events, activities, leisure, holidays, transportation, commerce, agriculture, and nearly every aspect of our lives as well as human history.
Our fascination with the weather has led to 24-hour weather networks, feature-length motion pictures, and an explosion of detailed weather data over the Internet.
Due to this great impact on human activities, the study, the observation and status prediction of weather conditions are fundamental tasks of any forecasting center. For this reason an operational meteo-marine forecasting chain for the whole Mediterranean area has been implemented at Consorzio LAMMA (Laboratory of Monitoring and Environmental Modelling for the

sustainable development). The forecasting system, operating since 2006, consists of a meteorological component, based on the WRF-ARW atmospheric model, and a marine component, based on the WW3 wind-wave model [1, 2]. The current configuration of the WRF-WW3 chain is the result of several years of study and operational activity at LAMMA, in the fields of numerical weather prediction and development of meteo-marine operational forecasting services.
The great and wide request of forecast data and the more and more appropriate and detailed forecast information availability generates a great interest in defining and providing user taylored forecast information. That means new services and new opportunities to exploit forecast data.
In recent years (2005) the European Space Agency (ESA) made operational the Service Support Environment (SSE) platform. This platform, born in 2004 from an ESA General Support Technology Programme (GSTP) project - known as Multiple Application Support Service System (MASS), provides an advanced test-bed that supports service prototyping and demonstration processes, allowing the design of automatically executed workflows, with a valuable decrease of the overall development effort. Due to the fact that SSE is a neutrally managed, open and distributed platform that offers an exclusive opportunity to integrate a wide range of heterogeneous Earth Observation (EO) and geospatial information services, including product catalogues, it has fostered the integration of different services in the EO and Geography Information Systems (GIS) domains.
In this paper the key elements of the integration of meteo-marine forecasting model data into the SSE platform are underlined. The opportunity provided by such an open platform, to share forecast data with the major European EO and geospatial providers, to easily create new services and to evaluate their business model, is also assessed.

2 Numerical models

The LAMMA meteo-marine forecasting WRF-WW3 chain runs on a cluster of Linux PCs hosted in the LAMMA facilities in Livorno.
The system performs two operational runs every day, the first initialized at 00:00 UTC and the second at 12:00 UTC. Both runs produce wave forecasts over the whole Mediterranean sea, at 0.1 degrees of resolution (namely about 10 km at 45° of latitude), for 72 hours (72 h, i.e. three days). Furthermore, the run initialized at 12:00 UTC also produces high resolution 72h forecasts (about 2 km of resolution) over a nested domain, covering the Ligurian and high Tyrrenian seas.

2.1 Meteorological model

The version 2.1.2 of the WRF-ARW model is used in the LAMMA meteo-marine forecasting chain both for scientific purposes and for the regional weather service. ARW is the dynamical nonhydrostatic solver of the Weather Research and Forecasting (WRF) system that is developed and maintened by the Mesoscale and Microscale Meteorology Division of the National Center of Atmospheric Research (NCAR). The main features of the model are: Fully compressible, Euler nonhydrostatic, Conservative for scalar variables, Terrain-following hydrostatic-pressure, Arakawa C-grid, Time-split integration using a 3rd order Runge-Kutta

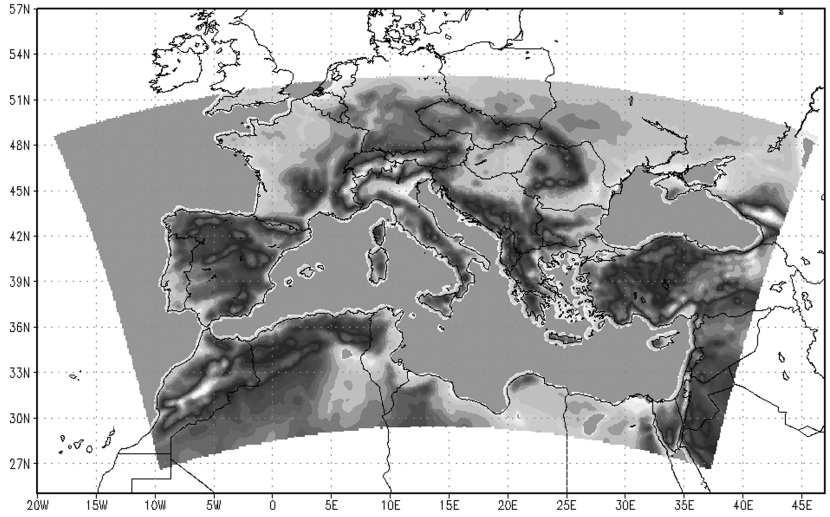

Figure 1: Meteorological model domain.

scheme with smaller time step for acoustic and gravity-wave mode.
In the LAMMA configuration, the model has an horizontal grid with a resolution of 0.2 deg (about 20 km) over a domain covering the whole Mediterranean area (224x136 points), as shown in Figure 1, and a vertical grid of 31 levels unequally spaced from ground to 100 hPa, with the first 10 levels concentrated in the boundary layer (about 1.0 km above the ground level). The model runs with a 100 s timestep.
Initial and boundary conditions, updated every six hours, are given by the NCEP - Global Forecasting System (GFS) deterministic model at the current resolution of T382L64 (about 50 km).

2.2 Wave model

The WAVEWATCH III full-spectral third-generation ocean wind-wave model used in the meteo-marine forecasting chain has been developed at NOAA/NCEP [3] in the spirit of the WAM model. In the LAMMA operational chain it is implemented the version 2.2 of WW3, with the following configuration:

- Latitude-longitude spherical grid
- Discrete interaction parametrization (DIA)
- JONSWAP bottom friction formulation
- Linear wind and current interpolation
- Seeding of high-frequency energy
- Spectral discretization on 30 frequencies in the interval 0.04-1.1 Hz and 36 directions.

The horizontal resolution of the grid over the whole Mediterranean sea is 0.1 degrees along both the meridian and zonal directions, while the resolution of the nested run (see Figure 2) is 0.02 degrees along both directions.
Wind forcing data are taken from the output of the WRF-ARW model. A scaling

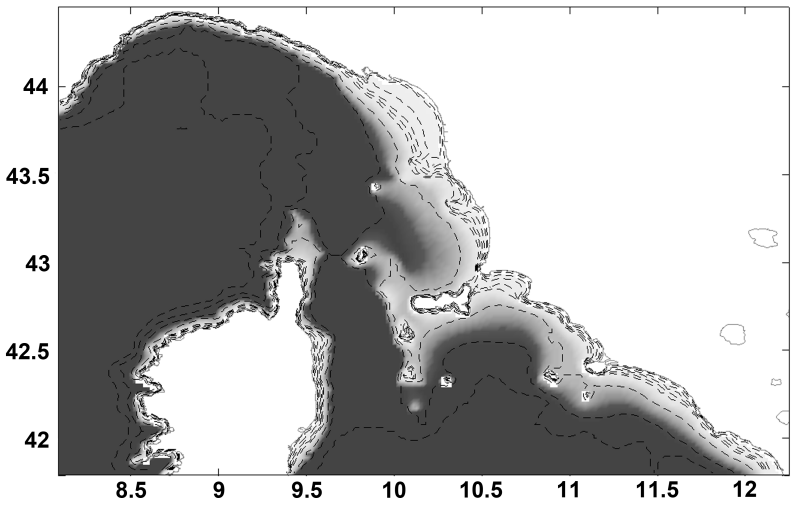

Figure 2: Domain of the WW3 high resolution grid.

factor of the WRF 10 meters wind speed is used as tuning parameter in order to optimize the WRF-WW3 (one-way) coupling.

2.3 Models output data

Both meteorological and wave models generates data for every hour of forecasts over the defined domains. The data are stored on a netcdf file. NetCDF (Network Common Data Format) is a machine-independent, self-describing, binary data format standard for exchanging scientific data. These files are stored on a local well-defined file structure.

3 SSE platform

The Service Support Environment (SSE) (SSE, 2004) (ICD, 2008) provides a reusable Service Oriented Architecture (SOA) for the integration of services in the Earth Observation and Geography Information Systems domains. A SOA is composed by a set of principles that define a loosely coupled architecture and comprises service providers and service consumers that interact according to well defined interfaces. The primary goal of SOA (thus of the SSE) is to expose application functions in a standardized way so that they can be leveraged across multiple domains (EO and GIS for the SSE). This approach greatly reduces the time, effort and cost it takes to maintain and expand solutions to meet business needs.
The main entry point of the SSE system is an Internet Portal where users, EO and GIS service providers and EO data providers are integrated in a coherent supply chain.
The main components (see Figure 3) of the SSE system are: the SSE Portal; the Area of Interest (AOI) tool which allows the users to select an area of interest in a consistent way; the SSE Toolbox which fa-

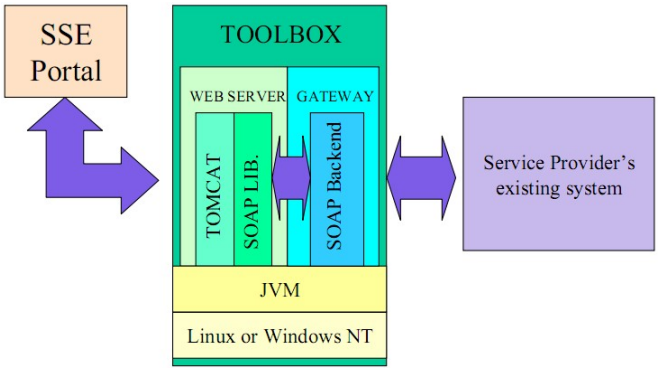

Figure 3: SSE architecture.

cilitates integration of legacy services not based on Simple Object Access Protocol (SOAP); an orchestrating workflow engine (the ORACLE BPEL PM has been selected as Commercial off-the-shelf component).
Being a SOA, the SSE is based on a non-proprietary, open, and scalable architecture for the development, implementation and deployment of services. It also supports the main OpenGis interfaces.
The environment provides various functionalities, useful for users as well as service providers. Its main functions are:

- User and Service registration,
- Service directory with browsing and search functionality,
- Request for Quotation and Order management,
- Cross catalogue searches,
- Workflow graphical editing and monitoring,
- Module for: AOI selection, layered service result visualization, integration of legacy services
- Service and company category management,
- News item management via browser and email,
- Notification by email of new service availability,
- Service subscription,
- Consultation of order list via a mobile device.

3.1 Interaction model

The SSE infrastructure does not make an assumption about the time needed by the remote service provider to generate or return a service result. Some services may require days, others such as data access may be almost instantaneous. The SSE Portal keeps results of orders (i.e. the XML message) in a database until the user accesses the Portal again. The actual data in most cases remains available a number of days on the service provider side for the user to download.
SSE supports two interaction models:

- Asynchronous operations: when an operation may take too long for a user to get the result immediately displayed in his browser, the result of the is stored in the SSE database and is available in the user's order list when he logs in the next time.

- Synchronous operations: when the service will immediately return the result, the SSE Portal visualizes it on the Web page.

3.2 Data delivery

Depending on the service, service results can be large multi-megabyte files (e.g. raster images), smaller vector images or just textual information. The SSE does not make any assumption about the format or type of a service result. The way information is presented on the Portal is defined by the service provider. The SSE support various data (i.e. service result) distribution mechanisms:

- data included in SOAP message, textual or graphical (SVG),
- data via FTP (URL in SOAP message),
- data via HTTP (URL in SOAP message),
- vector data via an OGC WFS server,
- raster data via an OGC WCS server.

Also a combination of these data delivery methods can be used.

4 Data integration

Forecast model data integration into the SSE environment has gone through different steps and phases scheduled by two projects collaboration bewteen INTECS and LAMMA. Within this projects three different services have been taylored and integrated.

4.1 Meteo-Layer

The Meteo-Layer service [4] provides the end user with a three-hour product describing atmospheric condition forecasts over a specific area of interest. Based on the AOI request by the final user the system interface with the LAMMA backend to retrieve the information necessary to fulfil the end user request. The output data, including only few out of more than hundred meteorological model variables, can be delivered in different formats according to the user input either as netcdf or grib files or as jpeg maps.

4.2 Sea State Conditions

The Sea State Condition service [5] provides the end user with data for every hour of sea state condition forecasts over its area of interest within the Mediterranean area. Based on the AOI request by the final user the system interface with the LAMMA backend to retrieve the information necessary to fulfil the end user request. The output data can be delivered in different formats according to the user input either as netcdf or grib files or as sea state conditions jpeg maps.

4.3 Weather along the route

The Weather along the route (WAtR) service [6] allow the users to define a set of location within an AOI. Given this set of points, by means of latitude, longitude and time of stay in that specific location, a meteorological bulletin is generated extracting and processing data from the latest 72 hours of forecast models data.
Moreover maps of both winds and wave data are provided to cover the area of interest of the path defined by the user.
The output data are delivered to the user via a bullettin file in pdf format.

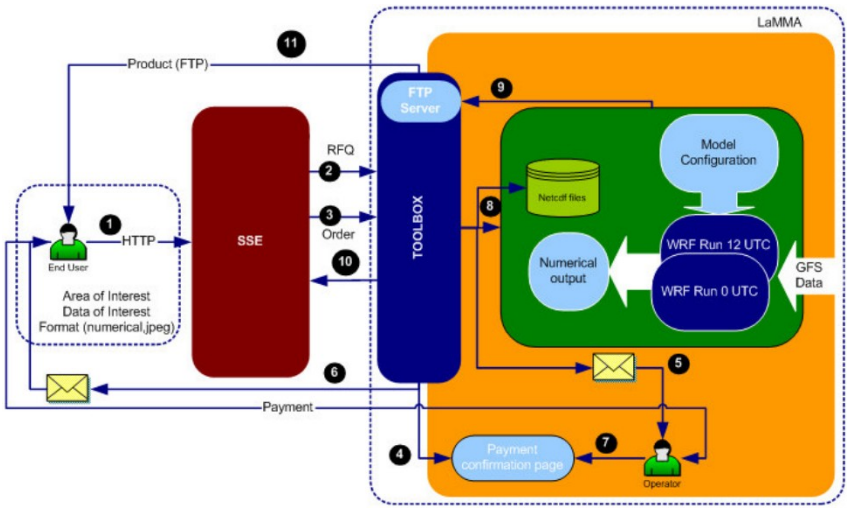

Figure 4: Interaction between users, SSE portal, TOOLBOX and LAMMA backend.

4.4 Services flow-chart

All the three services foresee a first phase to request a quotation (RFQ), even if the service if free of charge, where the user get a preview of the products. Once the RFQ has been completed the user can proceed to order the product that will be made available for download in the data format choosen by the user itself (see Figure 4).
As depicted in the Figure 4 the workflow of the services is as follow:

- The end user connects to the SSE portal, browses the service catalogue and selects the service.
- The user selects either a set of points and dates directly from the map or a set of data, depending on the related service, and decides the level of detail he wants to obtain.
- The end user sends a quotation request to the service (RFQ). The TOOLBOX installation receives the request and calculates the delivery time according to the data availability.
- The system extracts the data from the model and collect all the information needed to build the response, creates the response and sends it back to the portal.
- The results are displayed on the portal.
- The user checks the response and decides to proceeds with the order.
- The Toolbox extracts the information from the request, looks for the file matching the input criteria, invokes the netcdf processor to extract the data from the model data matching the end user input parameters, publishes the output data file on the internal FTP server and displays the forecasts symbols on the portal.
- The end user checks the results on the SSE pages and downloads the product data file.

The services previously described exposes the following SOAP interfaces via the SSE Toolbox:

- Request for Quotation (RFQ): it returns price, delivery time and payment information. Moreover it returns some pre-

view images to be displayed to the user.
- Order: it defines the Order request and Order result. The result message contains an FTP URL, with user name and password to allow the user to download the actual result file and the link to the WMS/WCS server to be linked to the Area Of Interest Tool.

In this context the Toolbox use a SOAP wrapper of Shell scripts to extract information from the model data files. Moreover it adds some logic to the service to calculate various parameters needed for the integration.

5 Conclusions

The availability of the SSE platform and all its components (e.g. TOOLBOX, AOI tool) has facilitated the prototyping and development of the three services in the web service framework.
The integration has allowed the distribution of the metereological data generated by LAMMA into a web based distributed and chainable architecture. This approach has carried out many advantages in terms of:
- direct accessibility of data according to the user needs,
- possibility to chain meteorological data with other services to easily create more and more value added services,
- easy generation of new complete services without worring of user interface, workflow definition and billing service development.

The SSE system allows an easy web enablement of manual and semi automatic services via the Toolbox and an easy user interface development via the portal and the AOI tool (by means of configuration file). Thus the SSE provides the possibility to publish prototypes and real services with a small effort and high impact on the market. This is also an opportunity for meteorological data providers to integrate their local data with major European Earth Observation and geospatial data providers.

References

[1] A. Ortolani et al. Implementing an operational chain: the Forence LaMMA laboratory. *Advances in Global Change Research*, 28, 2007.

[2] A. Orlandi et al. Implementation of a meteo-marine forecasting chain and comparison between modeled and observed data in the Ligurian and Tyrrhenian seas. 2011.

[3] H. Tolman. User manual and system documentation of WAVEWATCH-III version 2.22. *NOAA/NWS/NCEP/MMAB Technical Note*, 222, 2002.

[4] ML. Meteo Layer service. *services.eoportal.org/portal/service/ShowServiceInfo.do?serviceId=43804C89*, 2008.

[5] SSC. Sea State Conditions service. *services.eoportal.org/portal/service/ShowServiceInfo.do?serviceId=8F813580*, 2009.

[6] WR. Weather along the route service. *services.eoportal.org/portal/service/ShowServiceInfo.do?serviceId=8F814280*, 2009.

Merging Physical Oceanographic Observations and Simultaneous Seismic Reflection to Study Shelf-Slope Processes: the Example of ADRIASEISMIC-09

S. Carniel[1], J.W. Book[2], R.W. Hobbs[3], A. Bergamasco[1], M. Sclavo[1]
1, Institute of Marine Sciences, CNR, Venezia, Italy
2, NRL Stennis Space Center, Washington, USA
3, Durham University, Durham, UK
sandro.carniel@ismar.cnr.it

Abstract

During the period March 3-16, 2009 an international collaborative field experiment of Physical and Seismic Oceanography (ADRIASEISMIC-09) was carried out on board the CNR R/V Urania in the southern Adriatic Sea in order to characterize the details of the North Adriatic Dense Water (NAdDW) mass structures and test the feasibility of the seismic approach in shallow basins.
The new discipline of Seismic Oceanography is particularly well suited for study of the dynamics of bottom-trapped water masses as compared to classic techniques because it measures the full water column at 10 m horizontal resolution, it measures remotely and measurements are not hampered by a sloping bottom or concerns of instrument bottom impact, and it can operate successfully over the entire range from 100 m to 1000 m for tracking water-masses evolution down a slope.
A fast seismic data processing strategy was used, so that the seismic data were assessed for optimum locations of XBT (232), CTD and micro-structure (101) casts. These data of extremely fine detail (order of millimeters) complemented the high lateral resolution of the seismic image, allowing to track a thin bottom-boundary layer descending down the slope near Palagruza sill.

1 Introduction

Holbrook et al. [1] showed that seismic reflection profiles, adequately treated and integrated by hydrological data along the water column, are useful to provide information on the thermohaline structure of the water masses. This technique is commonly called Seismic Oceanography (SO) or Geophysical Oceanography (GO). Indeed, it is now possible to observe the oceanic dynamic and some structures (such as eddies, double diffusion, thermohaline intrusions, internal waves) at a very high detail.
In the field of the SO there exist still several problems to be solved, such as the definition of protocols to allow a better comparison of acquired data, the development of techniques to obtain optimal acquisition, especially in shallow waters, the need of development appropriate processing algorithms, etc. This will hopefully allow to obtain useful information on the ocean vertical microstructure as well.

The necessity of testing and developing these methodologies, as well as the need of improving the knowledge of the processes at the water/sediment interface, are at the basis of the ADRIASEISMIC-09 cruise carried out using the Italian CNR R/V URANIA. Indeed, the difficulty of acquiring synoptic data (e.g. classical hydrology, currentmeter and meteo data, turbulence, etc.) has until now limited the optimal use of modeling potentialities and an adequate synthesis of results. The availability of synoptic observations as those provided by the seismic oceanography technique could allow then to monitor much lager regions in a shorter time and, with the help of more classical measurements such XBTs or CTDs tow-yo, together with the support of turbulence measurements obtained via free falling probes, to depict and outline the vertical stratification in frontal regions at a very high resolution.

The interest at the origin of this proposal was also shared by several international research groups, including the Naval Research Laboratory (NRL) and the University of Durham, that took part in the campaign. In order to show the feasibility and the current state of the art in the field of the seismic oceanography, we have selected the southern Adriatic Sea region (close by the Gargano promontory and the Bari canyon, see Figure 1) for two weeks at the end of winter 2009. The reason for this choice was due to the existence of a legacy in the oceanographic and seismic databases, the presence of different oceanographic characteristics such as fronts and filaments, and the bottom topography modified by cascading and overflow processes.

The benefits resulting from the proposed activity appear to be multiple: the availability of new seismic-hydrological data that would be difficult to be collected by a purely national team; if present, the 3D mapping of the NAdDW (North Adriatic Deep Water) deep water structure when exiting from the Palagruza Sill (see again Figure 1) and starting its cascading process along the slope of the south Adriatic pit); the increase in the distributed knowledge inside the EU; the use of a large quantity of seismic data previously acquired; the foundation of a national research theme in the field of the seismic oceanography where CNR would be among the leading institutions.

2 Objectives and deliverables

The main objectives of ADRIASEISMIC-09 cruise were:

a) to test and explore benefits and limitations of state-of-the-art methods to acquire seismic data in a shallow water environment with a relatively light equipment.
b) to foster collaboration between the seismic and oceanographic community, advancing the knowledge of the water masses dynamics, such as fronts, internal waves, and of the vertical mixing processes on the shelf region, by successfully exploiting the above mentioned techniques.
c) to produce a dataset in the area in front of Bari region in the southern Adriatic, both from the oceanographic and seismic point of view.
d) to explore the feasibility of unlocking previously acquired data to make them available to the oceanographic community.
e) to contribute to building up a EU exper-

tise on these fields, allowing CNR to be better connected with Research Institutions that are making cutting-edge science.

f) to reach a detailed characterization of physical properties of the Southern Adriatic water masses, including turbulent properties, improving the performances of turbulent closure models.
g) to improve the understanding of bottom boundary layer processes in the basin.

Several types of products and deliverables are expected:

a) an observational data-set for seismic reflectivity in the Adriatic sea region.
b) an observational data set from CTD acquisitions, increasing the existing one.
c) an evaluation study of the eddy diffusivity in the southern Adriatic basin.
d) dissemination of ADRIASEISMIC-09 data in future studies.
e) joint publications dealing with: insights on the capability of seismic oceanography techniques, microstructure and turbulence measurements, water masses dynamics and distribution and cascading processes.

3 Measurements

Seismic data

A fundamental aspect of the ADRIASEISMIC-09 cruise was the tight integration of classical physical oceanography measurements with the seismic reflection images of water structure. This requires fast seismic data processing to locate at best the CTD casts. This extra processing work is partly compensated by the relatively simple average sound-speed within the water column. This was the first attempt to capture seismic images of water structure in water depths of less than 400-500 m, requiring thus testing for the most suitable seismic source-receiver configurations.

CTD casts

At all the hydrological stations, pressure, conductivity, temperature and dissolved oxygen concentration were measured with a CTD-rosette system. Salinity and potential temperature were then derived from the measured parameters. A fluoremeter and a light transmission sensor were also operating. The data were processed on board in order to correct immediately for the coarse errors.

Expendable bathy-thermographs (XBTs)

The structures in the ocean change on time scales shorter than the time required to deploy a seismic system, acquire the data and retrieve the system. Also, once the seismic system is deployed the ship can not stop for a CTD cast. The use of expendable bathy-thermograph (XBT) probes were then required to provide the background thermal structure and high vertical resolution needed to corroborate the seismic data. We deployed 240 XBTs along the seismic lines in the ADRIASEISMIC-09 experiment, of which 232 functioned properly. The XBTs were deployed at time intervals ranging from 5 to 40 minutes, depending upon the complexity of the water mass structure estimated from the last cast.

Lowered acoustic doppler current profiler (LADCP)

One Lowered Acoustic Doppler Current Profiler (LADCP) was used to measure velocity profiles. The bin size was 5 m and the range about 100 m. Ensembles are formed every second, along the down- and upcast. This allowed to obtain a vertical

profile of horizontal velocities, and to associate a velocity field to each water mass. Data were processed on board.

Vessel mounted ADCPs
The hydrographic and seismic data set have been integrated with direct current measurements. During the campaign two VM-ADCPs (75 and 300 KHz) operated along the whole ship track. The bin size was 16 m and 4 m, the depth range of the two current profilers about 700 m and 110 m respectively. Data were corrected for errors in the value of sound velocity in water, and misalignment of the instrument with respect to the axis of the ship. Data of the first part of the cruise were processed on board.

Microstructure turbolence profiler
Micro-Structure Turbulence (MST) profilers was used on the R/V URANIA and provided simultaneous microstructure and precision measurements of physical parameters. The MST profiler contained two velocity microstructure shear sensors, a microstructure temperature sensor, standard CTD sensors for precision measurements and a turbidity sensor. Measurements of microscale temperature and velocity shear allows for the estimation of several turbulence-related variables including turbulent kinetic energy and temperature variance dissipation rates, and eddy diffusivities. Measured parameters were: Pressure, CTD temperature, Conductivity, Fast temperature, Velocity shear, Turbidity. Computed parameters were: Salinity, Density, Sound velocity, Brunt Vaisala-Frequency, Seismic reflectancy, Thorpe scale (from density), Ozmidov scale, Cox number, TKE dissipation rate, Thermal dissipation rate, Eddy diffusivity from dissipation, Eddy diffusivity from Cox number and Eddy diffusivity from Thorpe scale. A total of 101 casts were acquired during the cruise.

Multibeam and chirp
During the cruise about 1600 km of CHIRP (Compressed High Intensity Radar Profile) profiles have been acquired in the Bari canyon and offshore the Gargano Promontory. Along with the CHIRP profiles, multibeam bathymetry was acquired and recorded. The multibeam system operates with frequencies between 70 and 100 kHz and owns a resolution of 1 degree by 1 degree.

Meteorological data
R/V URANIA was equipped with a full suite of meteorological sensors, acquiring wind magnitude and direction, sea surface temperature, relative humidity, incoming solar radiation and ship position.

4 Preliminary results

Previous studies demonstrated the presence of NAdDW in the southern Adriatic basin in recent years, and the mixing down to depths greater than 600 m in the Southern Adriatic Pit ([2] see Figure 1). ADRIASEISMIC-09 showed that the NAdDW was absent in the southern Adriatic basin in 2009, being the water coming from the northern basin anomalously light. From the seismic oceanographic point of view, the cruise showed how high-frequency and very high-resolution sampling is required to illuminate the mixing process dynamics, showing that a seismic profile may provide a consistent image of dT/dz of approximately 10-15s of meters. In general, while every seismic reflection corresponds to a water mass boundary, not

every water mass boundary causes a reflection. Moreover, high frequency character of water mass boundaries can change abruptly (10-20 m) and may not be interpolated or extrapolated away from point measurements.

Overall, ADRIASEISMIC-09 was the first cruise showing a successful use of SO to image water structures close to seabed in shallow water; for the first time seismic data were acquired simultaneously with turbulent (micro-structure) ones. The cruise proved also that high quality data can be obtained by using a light-weigth seismic system for SO (Source: 2 GI airguns 45/45 cu in, harmonic mode. Receiver: max offset 1200 m). Preliminary results suggest therefore that SO can provide a new and powerful tool for understanding the detailed horizontal structure of Dense Shelf Water Cascading processes.

Figure 2 presents and example of seismic acquisition along the Bari canyon. The wiggled lines imaged in the plots are related to density variations along the water column, possibly due to internal waves dynamics. Figure 3 presents an example of seismic acquisition along a different line again in the Bari canyon, with overlapped reflectivity profiles obtained via 12 concurrent XBT measurements. Note the qualitative matching between XBT (temperature) signature and the seismic patterns.

On-going work is focusing on correlating the observed ocean fine structures with internal waves dynamics detected.

5 Acknowledgements

The authors thank to G. Bortoluzzi and K. Schroeder (CNR-ISMAR) for the help in XBT data acquisition and elaboration. The scientific staff of ADRIASEISMIC-09 wishes to thank the Italian National Research Council (CNR) Ship Office, which made the R/V URANIA available for the Cruise.

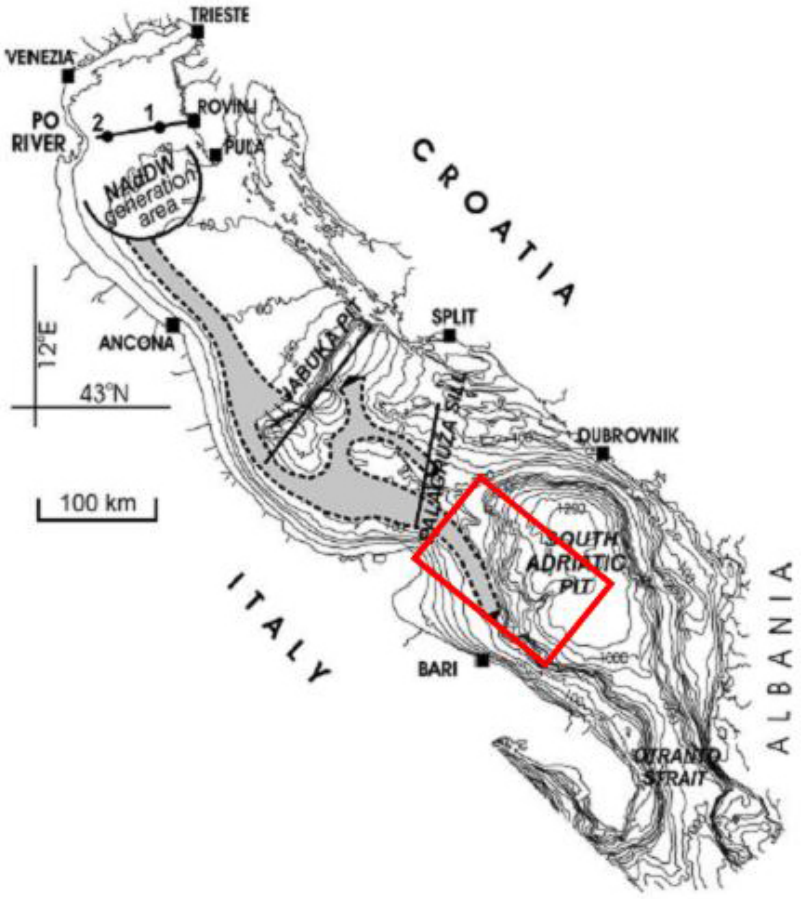

Figure 1: Dense shelf water pathways (from Vilibic and Supic, 2004). The red box includes the region of investigation of the ADRIASEISMIC-09 campaign.

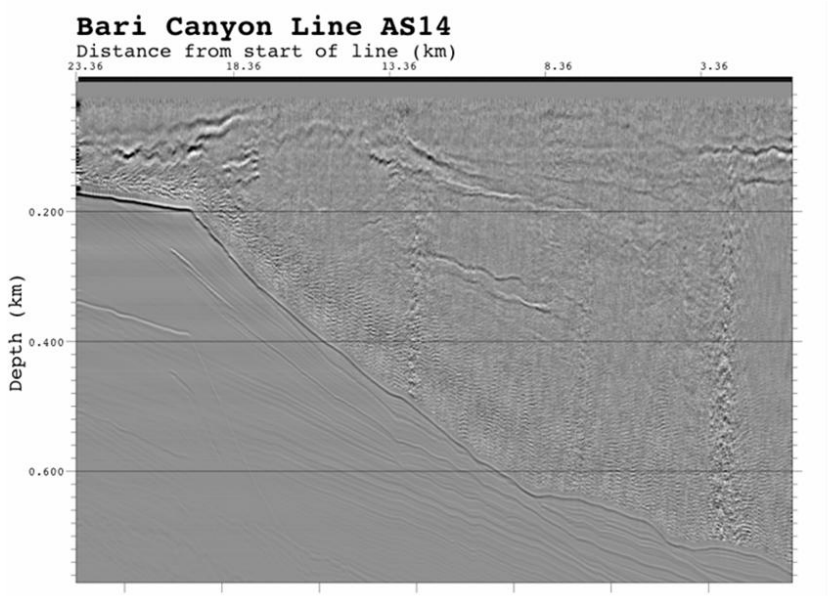

Figure 2: Example of seismic acquisition along the Bari canyon. The wiggled lines imaged in the plots are related to density variations along the water column (possibly due to internal waves).

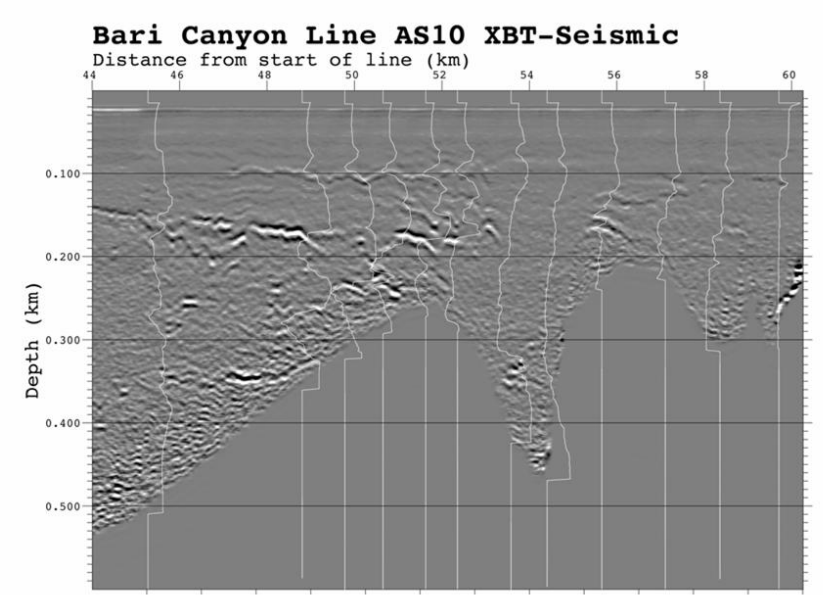

Figure 3: Example of seismic acquisition along the Bari canyon, with overlapped reflectivity profiles obtained via 12 concurrent XBT measurements. Note the matching between XBT (temperature) signature and the seismic patterns.

References

[1] W.S. Holbrook, P. Paramo, S. Pearse, and R.W. Schmitt. Thermohaline Fine Structure in an Oceanographic Front from Seismic Reflection Profiling. *Science*, 301(5634):821–824, 2003.

[2] I. Vilibic and N. Supic. Dense water generation on a shelf: the case of Adriatic Sea. *Ocean Dynamics*, 55(5-6):403–415, 2004.

The Infrastructure for Geospatial Information Interoperability in the SeaDataNet Project

S. Nativi[1], G. Manzella[2], P. Mazzetti[1], M. Santoro[1], E. Boldrini[1]
1, Institute of Methodologies for Environmental Analysis, CNR, Potenza, Italy
2, Marine Environment Research Center "S. Teresa", ENEA, Lerici, La Spezia
nativi@imaa.cnr.it

Abstract

This paper describes an interoperability solution for geospatial resources (i.e. data, services, models and applications) sharing developed in the context of the FP6 European Project SeaDataNet. It has been designed taking into account the project mission: to develop a Pan-European infrastructure for the oceanographic and marine data and products management, indexing and access.
Presently, in the framework of oceanography and marine resources, several international standards can be implemented in order to access the available resources (e.g. ISO TC211 standards, OGC specifications and INSPIRE Directive implementing rules). At the same time, there exists a number of well accepted community standards such as: THREDDS, OPeNDAP, netCDF-CF. The proposed solution is based on the "System of Systems" approach, adopting solutions to make the mentioned specifications interoperable. The resulting infrastructure implements mediation and brokering functionalities in order to provide, both scientists and decision makers, with a consistent and practical way for the discovery, evaluation, and download of heterogeneous resources needed by SeaDataNet applications. Basing on the conclusions of this work, the paper presents some recommendations for marine-oceanographic information sharing systems.

1 Introduction

The planning and implementation of research, and the efficient management of the resulting data are still two widely separated realms. Data managers consider the careful collection, management and dissemination of research data as essential for the effective use of research funds. Many researchers, on the other hand, consider data management as a technical issue assigning a low priority to that. The existing initiatives in Data Management and Information Systems are trying to bridge these two different realms.

The concept of data management has changed deeply during the last decade, moving from the idea of centralised-homogeneous systems to that of decentralised-heterogeneous ones. The costs associated with homogeneous and heterogeneous systems implementation are:

- Homogeneous system - a common data format for a common application:
  - High demands on data sharing and use
  - Low demands on system design, development, and maintenance.
  - High demands on system extension and interoperability.

• Heterogeneous system - multiple data formats for multiple applications:
- Low demands on data sharing and use
- High demands on system design, develop, and maintenance
- Low demands on system extension and interoperability.

The centralized-homogeneous data managements were important when the information system technology was based on mainframes and Internet was less developed. However, they have never been attractive to oceanography researchers for many reasons:
- they were not directly involved in systems management since the responsibility was lying on data managers only;
- it was not popular to encode data in a unique format, since this was based on the unrealistic idea that all instruments and systems have a common interface;
- data access could be time consuming.

During last decade it was also evident that data are not only coming from oceanographic 'in situ' observations, but they are also generated by different instruments and systems, such as: remote sensing sensors, numerical modelling systems, web-enabled resources, etc.

The tradition of creating formal data centres to house and distribute ocean data and products has long been shadowed by the parallel existence of direct data downloads from research groups (usually via HTML page-links and/or FTP servers). Historically, at least half of the data available to researchers has been provided outside the IODE/World Data Center System facilities (IODE, 2010) [1]. During the last decades efforts have been dedicated to create a new system of Internet communication (e.g. the Data Access Protocol [2, 3]) that would allow users to access distributed datasets directly, using a family of "middleware services" that overlay datafile caches, allowing retrieval of files in desired formats, no matter what the storage format might be.

The web has changed the way we discover and access data, and mush-up information. The simple concepts sustaining centralized information systems were overcome by emerging requirements:
- Data are heterogeneous.
- Real time data delivery is important for policy making.
- Processing is required to be done outside of the data archive (e.g. using Web or Grid computing infrastructures).
- Quick and easy access to raw data in its native format is required.
- Web-based discovery (i.e. catalogue) services are required.
- Instrument calibrations and information regarding deployment and recovery, should be digitized and made available electronically; people need to be removed from this process wherever possible.
- An architecture that supports distributed processing and archiving of higher order data products is required.

In order to implement these interoperability requirements, three types of metadata levels are needed; they support important system functionalities:
1. Discovery metadata (Directory functionality): it consists of broad descriptions of the contents of data sets used to locate data sets of potential interest.
2. Evaluation metadata (Inventory functionality): consists of a detailed list of granules (e.g., individual satellite passes, AUV dive, CTD cast) within a data set used to find the data of interest.
3. Use metadata (Data functionality): consists of the actual data objects.

To implement loosely coupled interoperability and data sharing, data and metadata

encodings should be auto-explicative and auto-consistent. This is accomplished by providing (or sharing) knowledge on:

- Syntactic and lexical encoding: information about the data types and structures used by the encoding often referred to as the data model.
- Semantics encoding: information about the data content, what the variables mean, their possible values, etc..

These general concepts are now applied in the system of systems developed by SeaDataNet [4]: an EC funded project aiming to create and operate a pan-European, marine data management infrastructure, accessible online through a unique portal. The primary goal of SeaDataNet is to develop a system which provides transparent access to marine data sets and data products from 36 countries in and around Europe. SeaDataNet aims to insures the long term archiving to the large number of multidisciplinary data (i.e. temperature, salinity current, sea level, chemical, physical and biological properties). Hence, the project is developing a standardized distributed system for managing the large and diverse datasets collected by the oceanographic fleets and the new automatic observation systems. By use of standards for communication and new developments in Information Technology (IT), the 40 insitu and satellite marine data platforms of the partnership provide metadata, data and products as a unique virtual data centre [4]. The core of the SeaDataNet infrastructure is represented by some discovery services (e.g. EDMED, EDMERP, EDMO, CSR, EDIOS) and the Common Data Index (CDI), an XML document allowing the access to data in a distributed system [5].
The middleware service adopted by SeaDataNet for discovery and query is called CDI (Common Data Index). However, the collaboration with other data management systems based on THREDDS (Thematic Realtime Environmental Distributed Data Services) [6] required the construction of a 'bridge' between the two technological solutions. In fact, these two technologies are well adopted by the information systems managed by the SeaDataNet partners.

1.1 CDI

The CDI provides an index (metadatabase) to individual data sets. Furthermore, it paves the way to direct online data access or direct online requests for data access or file downloads; in fact, the primary objective of CDI is to give users a highly detailed insight in the availability and geographical spreading of marine data across the different data centres and institutes across Europe [5]. CDI was initiated in the EU SeaSearch project [7].
Currently, it is being further developed and extended by the SeaDataNet project. All the 35 countries participating in SeaDataNet are going to utilize CDI for describing their marine data [5].

1.2 THREDDS

THREDDS is middleware to bridge the gap between data providers and data users. The goal is to simplify the discovery and use of scientific data and to allow scientific publications and educational materials to reference scientific data [6].
THREDDS initial focus was to allow data users to find datasets that are pertinent to their specific education and research needs, access the data, and use them without necessarily downloading the entire file to their local system. To achieve this, data providers must be able to publish

lists of what data are available and to describe their data enabling discovery and use: THREDDS introduced the Data Inventory Catalogs (DICs) concept [8]. They are XML documents that describe on-line datasets. These catalogs can contain arbitrary metadata; besides, a standard set of metadata to bridge to discovery centers -like GCMD, DLESE and NSDL- was defined. The THREDDS catalog service augments traditional MeteoOcean access services such as OPeNDAP [3] and netCDF [9] access via HTTP. Moreover, THREDDS implements access services to bridge the MeteoOcean and GIS communities, such the OGC Web Coverage Service interfaces.

2 Distributed Catalog Services

The interoperability solution we propose consists of utilizing a standard Distributed Catalog Service [10] to: (a) federate the THREDDS/OPeNDAP and CDI resources (i.e. services and data); (b) mediate between THREDDS/OPeNDAP and CDI resources; (c), expose THREDDS/OPeNDAP and CDI resources through a standard interface for geo-spatial information discovery and access (i.e. implementing international standards specifications for catalog and access service). Figure 1 depicts a schema of the adopted interoperability approach. This solution implements and publishes the OGC CS-W [11] standard catalog interface for resources discovery and access. It is flexible allowing the federation and mediation of other interoperability standards (i.e. international standards as well as community best practices), such as: (a) OGC access services (i.e. WMS, WCS, WFS); (b) Biodiversity community protocols (i.e. the GBIF (Global Biodiversity Information Facility) discovery and access protocols).

3 GI-cat

The deployed distributed catalog framework is based on the GI-cat technology [10]. The GI-cat supports caching and mediation capabilities; it can act as a service broker component accessing disparate (i.e. heterogeneous and distributed) resources and publishing a standard and common interface. GI-cat implements a framework to federate international standard and community service types, namely: catalog, inventory, access, and processing services. As for international standards, GI-cat supports: most of the OGC CS-W application profiles, WCS, WFS and WMS specifications. As to community services, GI-cat is able to federate: THREDDS/OPeNDAP, CDI, and GBIF services. GI-cat exposes several standard discovery interfaces, including: (a) the OGC CS-W/ISO interface [12], recommended by the European Directive INSPIRE; (b) the OGC CS-W/ebRIM-EO interface [13, 14], recommended by the GMES/ESA-HMA initiative [15]; (c) the OGC CS-W Core[11], recommended by the GEO/GEOSS [16].

4 Mediation Process: GI-cat Accessors

In the GI-cat framework, the geospatial resources heterogeneity is addressed by applying a mediation approach. Specific GI-cat components implement the mediation services required to interface heterogeneous and standard (i.e. well-known) ser-

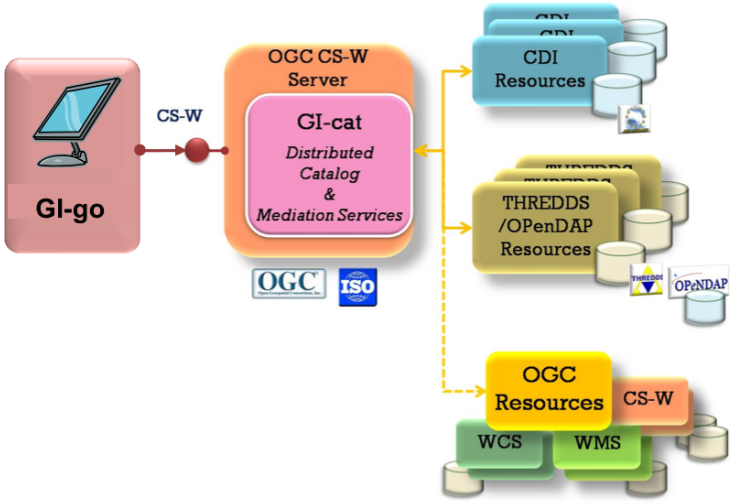

Figure 1: The adopted interoperability solution for CDI and THREDDS.

vice providers. They are called Accessors. They solve the data models multiplicity issue by mapping providers data models onto a more general resource model: the ISO 19115 Core profile [17]. The Accessors also implement a query brokering functionality by translating the query requests received by GI-cat -i.e. queries expressed according to the interface protocols exposed by GI-cat (e.g. CS-W/ISO)- into the multiple query dialects exposed by the resource providers. In the SeaDataNet system, the CDI and THHREDDS/OPeNDAP Accessors make those resource providers interoperable.

The described interoperability approach results quite general and flexible enabling to implement interoperability between CDI and THREDDS/OPeNDAP, and other provider technologies.

4.1 CDI Accessor

Figure 2 shows a UML class diagram representing a simplified version of the CDI data model. This is not a hierarchical data model. In fact, the data model only deals with low level granularity not defining high level granularity elements, such as "catalog" or dataset "aggregations". Hence, a CDI document (i.e. an XML document) describes only a dataset element formalizing its content and access metadata. To carry out CDI data model interoperability with GI-cat, the correct solution is to map a CDI resource element (i.e. a CDI dataset) onto a GI-cat "catalog" element. Clearly, this approach entails some important scalability and management issues.

Figure 2: Simplified CDI Data Model for a dataset element.

CDI element	GI-cat element
CDI document	*Catalog containing one dataset*
CDI document (with datasets aggregation)	*Catalog containing one or more datasets*

Table 1: CDI elements mapping onto GI-cat ones.

We experimented a CDI data model extension introducing a dataset aggregation level. Thus, data provider can generate and publish an aggregation document (encoded as an XML document) which aggregates existing CDI documents. For this aggregation, the CDI datasets are referenced by pointing the XML document file they are encoded by.
In this way there exists only one catalog for all the resources published by the aggregation document. GI-cat supports the CDI dataset aggregation extension. Table 1 describes the two mapping possibilities described.

4.2 Querying a CDI Resource

In general, when GI-cat receives a query request, each federated remote provider receives it through its specific Accessor which translates it, opportunately. This is not the case of CDI providers; to perform queries over CDI resources, at the beginning of each session, GI-cat harvests CDI resource (i.e. retrieves and parses the CDI XML document), maps the content onto the GI-cat data model, and caches it for subsequent queries. It is possible to perform a new harvesting during the session.

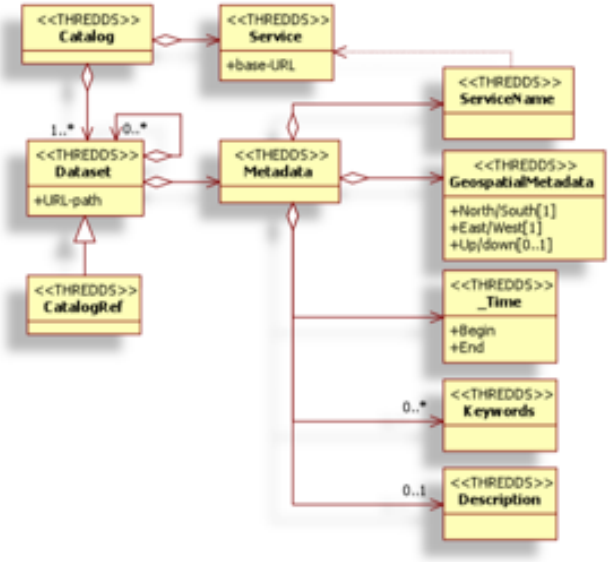

Figure 3: THREDDS data model.

4.3 THREDDS Accessor

A simplified schema of the THREDDS data model is shown in Figure 3.
The THREDDS Data Server (TDS) implements a catalog service; hence, it defines a hierarchical data model which contains a catalog element that, in turn, may contain zero or more datasets. Each dataset element may contain zero or more sub-datasets. The "catalogref" element allows a catalog to refer to other remote catalogs.
It is noteworthy that THREDDS data model supports metadata inheritance. Therefore, when an aggregated dataset (or a "CatalogRef" element) has some inheritable metadata, they propagate to the nested (or referred) datasets as well. In this way, it is possible to factor out common metadata avoiding to duplicate the same information and encouraging to publish datasets characterized by high level granularity. This feature, along with the use of "CatalogRef" element, consents to query large catalogs in an efficient way. THREDDS data model mapping on the GI-cat model is quite straightforward (see Table 2).

4.4 Querying a THREDDS Catalog

THREDDS publishes "inventory catalogs" (i.e. XML documents) over the Web.
Catalogs can reference other catalogs and can also provide links for accessing

Figure 4: THREDDS Catalog tree stategy for improving query performance.

THREDDS element	GI-cat element
Catalog	*Catalog*
CatalogRef	*DatasetCollection*
Dataset (aggregated)	*DatasetCollection*
Dataset (simple)	*Dataset*

Table 2: THREDDS elements mapping onto GI-cat ones.

datasets. THREDDS services include the Dataset Query Capabilities (DQC) which allows users to request a subset of a dataset collection. However, we preferred to harvest THREDDS inventory catalogs, following the approach already described for CDI documents. Differently from CDI, the THREDDS/OPeNDAP Accessor must deal with nested structures which make use of the "CatalogRef" element. The Accessor implements an incremental approach to avoid unnecessary network overhead and improve performances. Once a THREDDS catalog content is requested, referenced catalogs are not accessed until the content of those dataset collections is explicitly requested.

Since THREDDS data model is hierarchical, a THREDDS catalog can be represented as a tree where each internal node is either a dataset collection or a referenced catalog; each leaf is a dataset. Every tree node, and leaf, are characterized by its own metadata (which may be inheritable) plus inherited metadata. A query is performed visiting the tree with a depth first strategy, reading the metadata of each node and checking if the query clause is satisfied. When a leaf is reached and its metadata satisfy the query constraints too, the leaf (i.e. dataset) is added to the query response.

The presence of inheritable metadata allows to discard a node along with its children, if the node metadata do not satisfy the query clause. This avoids network overhead when the node to be discarded is a "CatalogRef" element.

This strategy results also efficient in order to deal with very large catalogs. In fact, it allows to discard many branches skipping

to read their metadata.

4.5 Improving Query Performance with THREDDS

Query performances depends on the matching pattern existing between the THREDDS hierarchical structure and the clause types characterizing most common queries (i.e. users common query strategy). Considering most of queries have a space-time clause, datasets should be structured according to their spatial and temporal extension, respectively. To optimize query performances with respect to spatial domain, a possible strategy consists of dividing Earth spatial domain in finite areas. A valuable example in point are the MARSDEN zones [18] or WMO zones. Following this solution, each node at the first level of the THREDDS catalog tree contains datasets belonging to the same MARSDEN area. Therefore, at the first hierarchical level, tree nodes are characterized by spatial information as inheritable metadata. While, second-level nodes inherit spatial metadata and have temporal interval metadata as inheritable one. Figure 4 shows the tree structure strategy implementing this approach. Datasets are first divided by space (i.e. MARSDEN areas), then by year, subsequently by month, and so on in accordance with the level of temporal granularity required by user queries.

4.6 Access Protocol Adaptation

Neither THREDDS nor CDI define any special access protocol; they both use standard protocols (e.g. WMS, WCS, OPeNDAP and HTTP download). When GI-cat receives a request, it performs the following actions:

a) it retrieves the available access service(s) as specified in the resource metadata;
b) in case of many available services, it selects the most flexible one -e.g. the service which supports domain and co-domain sub-settings;
c) it instantiates a correspondent Accessor component (i.e. a service client);
d) it delegates the Accessor to formulate the appropriate access request, including the sub-setting clause -if the resource provider implements the subsetting functionalities.

5 Experimentation

Several experimentations were successfully conducted using XBT (Expendable Bathythermograph) data encoded in netCDF (network Common Data Form) format [9] following the CF1 conventions [19]. The utilized CF-netCDF data model is shown in Figure 5. The CDI documents describing the XBT resources are available at: http://moon.santateresa.enea.it/SDN_CDI/ For testing the proposed CDI catalog extension supporting files aggregation, we worked out an aggregated catalog document, available at: http://zeus.pin.unifi.it/projects/cdi_registry/registry.xml. The same XBT resources encoded in CF-netCDF were also utilized to test the interoperability of THREDDS inventory catalogs. The THREDDS catalog server was configured for improving query performances applying spatial and temporal domain clauses -using the MARSDEN convention for dividing Earth in indexed areas. This catalog is available at: http://apollo.pin.unifi.it:8080/thredds/XBTdemocatalog.xml. The set up system for interoperability testing is composed of

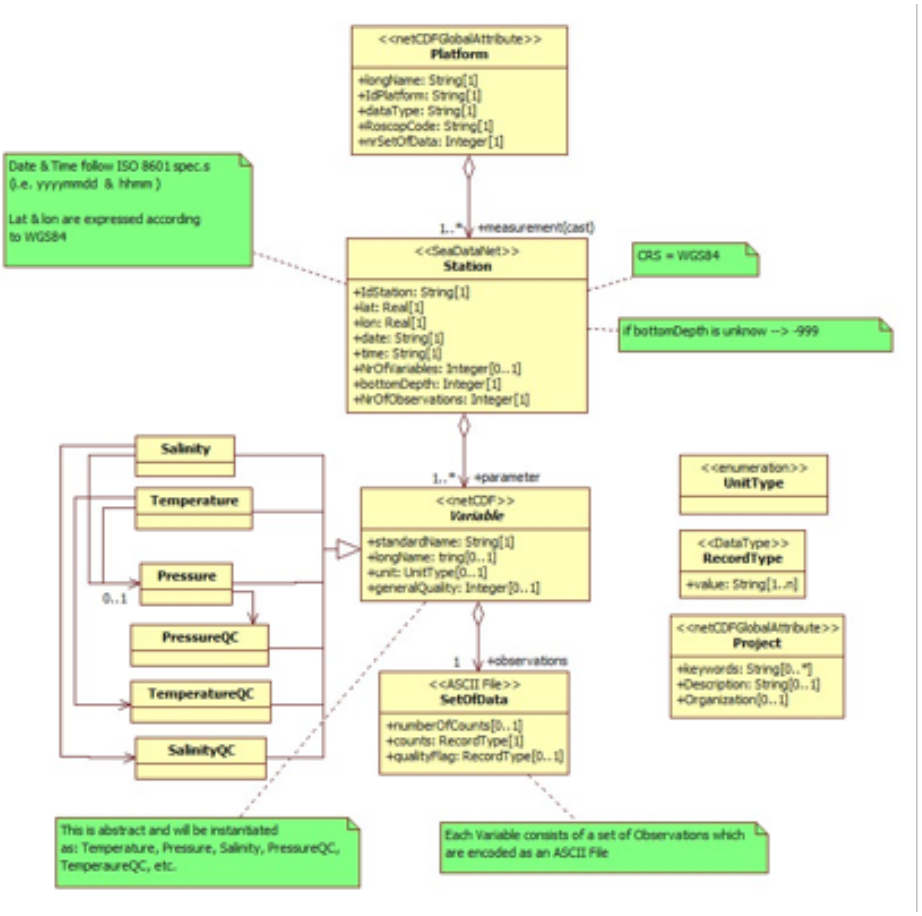

Figure 5: CF-netCDF Data Model for XBT datasets.

GI-cat catalog (http://zeus.pin.unifi.it/gi-cat-wiki) deployed in front of a CDI and a THREDDS catalog server. Besides, standard OGC Web access services were federated in order to extend the interoperability tests. To demonstrate test results, a graphical client application for GI-cat was utilized: GI-go. This is a CS-W/ISO client which is able to bind with the corresponding interface published by GI-cat. GI-go can be downloaded at: http://zeus.pin.unifi.it/gi-go. Figure 1 depicts the developed system used for the interoperability experimentations. Tests were performed querying CDI and THREDDS/OPeNDAP catalogs with combinations of spatial, temporal and keywords clauses.

6 Conclusions

To make CDI and THREDDS service providers interoperable, we propose a solution based on a distributed catalog service implementing mediation and brokering functionalities, namely GI-cat. The carried out interoperability tests were successful. They were conducted in the SeaDataNet project framework and demonstrated the effectiveness of discovering and accessing CDI and THREDDS resources through a common and standard catalog interface -the one recommended by the European Directive INSPIRE. In fact, GI-cat publishes standard CS-W interfaces. The proposed solution is flexible and allow to implement interoperability also with other standard service providers -e.g. OGC access services.

Flexibility was addressed by introducing the Accessor component: a piece of technology which addresses interoperability issues regarding a given type of service providers. By supporting asynchronous and incremental query responses, GI-cat achieves scalability as well.

The experimentations confirmed that the data model of remote service influences GI-cat query and access performances. The THREDDS model case was presented and an approach experimented for SeaDataNet was discussed.

For the SeaDataNet CDI model, a dataset aggregation element was proposed in order to improve query and access performances. This extension is very simple and is going to be adopted by the CDI specification Working Group.

CF-netCDF data access was also experimented (see Figure 5). The implementation of a common data model could improve data aggregation and interoperability. We experimented a CF-netCDF data model for describing and encoding XBT acquisitions.

7 Recommentadions

Reducing the time required to acquire, process and analyze data of known quality is a major goal that requires the development of an integrated data management and communication subsystem. The objectives are to serve data in both real-time and delayed mode and to enable users to exploit multiple data sets from many different sources. This requires a distributed network that works with common standards, reference materials and protocols for quality control to enable rapid access to and the exchange of data (e.g., metadata standards) and long-term data archival.

At Italian level, such a network will develop in an incremental way by linking and integrating existing data centers and management programs. The objective is to develop a federated data management and communications system (System of Systems) that efficiently transmits large volumes of multi-disciplinary data (in real-time, near-real-time, and delayed modes) from many sources (in situ measurements, autonomous in situ sensors, remote sensors, models' outputs, etc.) directly to users for a broad diversity of applications, including data assimilating tools, that process the measurements into maps, plots, forecasts, and environmental statistics (e.g. climatology). Resource providers should be able to transmit their products into the system with a minimum obligation to convert them to specialized encoding formats, provided that basic conditions of data quality and metadata standards are met.

While it may be possible to provide a single portal for data users for one-stop access, this will inevitably be a simplified

front end for the data management system that supports all the Italian System Of Systems (ISOS). Federated access points will tend to focus first on thematic aspects.
A centralized access point which is suitable for all types of customers, requesting data from any coast in the world, and designed to a common standard, may itself be an unattainable ideal at this stage. It is more likely that such a contact point will direct the user to other more specialized or regional product delivery centers, or would be restricted to a limited number of variables. The construction of specialized customer-related access points can then be carried out by delegated teams of experts.
The data management system will provide facilities for two data tracks, one in real-time (or near real-time) and one in the delayed mode. Both tracks are based on the same data sources and transmission systems, but the data follow different routes and are processed differently depending on user requirements. The real-time observed and generated products can also be checked after first use for up-grading and additional quality control to ensure that relevant data are preserved for final archival. Similarly, climatic data and standardised anomalies and statistics can be provided to the modelers from the archived data and time series in order to compute expected values and anomalies.
To summarize, here are some important recommendations for implementing a System of Systems approach:

1. Save all raw data in its native format.
2. Attempt to make all data available, even if it's at a crude level.
3. Archive higher-order products (including processed data files) and register their existence in a catalog.
4. Catalog these data sets. At minimum these catalogues must contain:
   - What format the file is in.
   - Which sensor captured the data.
   - What software produced this data set.
   - Who to contact regarding this data set.
   - Original capture date/time "box".
   - Latitude/Longitude(/Pressure) "box".
   - General comments about the data/file.
5. Query these catalogs (both with human interface and programmatically).
6. Digitize all records including log books (this makes the catalog more useful).
7. Distribute data archives and processing amongst people and machines.
8. Use World Wide Web to provide access.

Issues regarding calibration, validation, and metadata capacity are implied but not specifically addressed by these recommendations.

References

[1] B.B. Parker. Oceanographic Data Archeology, finding historical data for climate and global change research. *Oceanography*, 5(2), 1992.

[2] NASA Earth Science Data Systems Standards Process Group. The Data Access Protocol - DAP 2.0 [available at http://www.esdswg.org/spg/rfc/ese-rfc-004, accessed on 15 Jan 2010]. 2007.

[3] OPeNDAP. Open-source project for a network data access protocol [available at http://opendap.org, accessed on 29 Jan 2009]. 2004.

[4] SeaDataNet. SeaDataNet Home Page [available at http://www.seadatanet.org/, accessed on 15 Jan 2010]. 2010.

[5] SeaDataNet. Common Data Index [available at http://www.seadatanet.org/data_access/common_data_index_cdi, accessed on 15 Jan 2010]. 2007.

[6] B. Domenico, J. Caron, E. Davis, R. Kambic, and S. Nativi. Thematic Real-time Environmental Distributed Data Services (THREDDS): Incorporating Interactive Analysis Tools into NSDL. *Journal of Digital Information*, 2, 2002.

[7] Sea-Search. Your gateway to Oceanographic and Marine Data & Information in Europe [available at http://www.sea-search.net/, accessed on 18 JHan 2010]. 2010.

[8] UNIDATA. NetCDF Documentation [available at http://www.unidata.ucar.edu/software/netcdf/docs/, accessed on 15 Jan 2010]. 2010.

[9] UNIDATA. THREDDS Fact Sheet [available at http://www.unidata.ucar.edu/publications/factsheets/2007sheets/threddsFactSheet-1.doc, accessed on 15 Jan 2010]. 2010.

[10] S. Nativi and L. Bigagli. Discovery, Mediation, and Access Services for Earth Observation Data (in publication). *IEE Journal of Selected Topics in Applied Earth Observations & Remote Sensing*, 2009.

[11] Open Geospatial Consortium Inc. OGC® Cataloguing of ISO Metadata (CIM) Using the ebRIM profile of CS-W (0.1.8). 2007.

[12] Open Geospatial Consortium Inc. OpenGIS® Catalogue Services Specification 2.0.2 - ISO Metadata Application Profile, v. 1.0.0. 2007.

[13] Open Geospatial Consortium Inc. OpenGIS® Catalogue Services Specification v. 2.0.2 - Revision 1. 2007.

[14] Open Geospatial Consortium Inc. OGC™ Catalogue Services Specification 2.0 Extension Package for ebRIM Application Profile: Earth Observation Products (0.2.4). 2009.

[15] European Space Agency. Heterogeneous Mission Accessibility - Context [available at http://earth.esa.int/hma/context.html, accessed on 15 Jan 2010]. 2007.

[16] Group on Earth Observation. Global Earth Observation System of Systems (GEOSS) 10-Year Implementation Plan. 2005.

[17] International Organization for Standardization. Geographic information - Metadata. 2003.

[18] H.E. Sweers. An improved code to classify the location of marine and terrestrial data Limnology and oceanography. 1970.

[19] B. Eaton, J. Grogory, B. Drach, K. Taylor, and S. Hankin. NetCDF Climate and Forecast (CF) Metadat Convention v. 1.0. 2003.